



INTERNATIONAL ROADMAP FOR DEVICES AND SYSTEMS™

INTERNATIONAL  
ROADMAP  
FOR  
DEVICES AND SYSTEMS™

2021 UPDATE

CRYOGENIC ELECTRONICS AND  
QUANTUM INFORMATION PROCESSING

THE IRDS IS DEvised AND INTENDED FOR TECHNOLOGY ASSESSMENT ONLY AND IS WITHOUT REGARD TO ANY COMMERCIAL CONSIDERATIONS PERTAINING TO INDIVIDUAL PRODUCTS OR EQUIPMENT.

© 2021 IEEE. Personal use of this material is permitted. Permission from IEEE must be obtained for all other uses, in any current or future media, including reprinting/republishing this material for advertising or promotional purposes, creating new collective works, for resale or redistribution to servers or lists, or reuse of any copyrighted component of this work in other works.

All product names, trademarks and registered trademarks are property of their respective owners. All company, product and service names used in this document are for identification purposes only. Use of these names, trademarks and brands does not imply endorsement.

# TABLE OF CONTENTS

<b>Acknowledgments</b> .....	<b>vi</b>
<b>1. Introduction</b> .....	<b>1</b>
<b>2. Superconductor Electronics (SCE)</b> .....	<b>1</b>
2.1. Introduction to SCE .....	1
2.2. Applications and Market Drivers for SCE .....	3
2.2.1. Cloud (Digital Computing) .....	4
2.2.2. Measurement and Calibration Systems .....	4
2.2.3. Communications .....	6
2.2.4. Quantum Computing: Control and Readout .....	7
2.3. Present Status for SCE .....	7
2.3.1. Logic .....	7
2.3.2. Memory .....	10
2.3.3. Circuit Elements for SCE .....	14
2.3.4. Architectures and Applications .....	15
2.3.5. Fabrication for SCE .....	16
2.3.6. Electronic Design Automation (EDA) for SCE .....	21
2.3.7. Packaging and Testing for SCE .....	22
2.3.8. Interconnects for SCE .....	23
2.3.9. Refrigeration .....	23
2.4. Benchmarking and Metrics for SCE .....	25
2.4.1. Device and Circuit Benchmarking .....	25
2.4.2. Scaling of Devices and Circuits .....	28
2.4.3. System and Application Benchmarking .....	29
2.5. Active Research Questions for SCE .....	29
2.6. Roadmaps for SCE .....	32
<b>3. Cryogenic Semiconductor Electronics (Cryo-Semi)</b> .....	<b>34</b>
3.1. Introduction .....	34
3.2. Applications and Market Drivers for Cryo-Semi .....	35
3.3. Present Status for Cryo-Semi .....	35
3.3.1. Transistor Characterization and Modeling .....	35
3.3.2. Applications $\geq 10$ K .....	36
3.3.3. Applications $< 10$ K .....	36
3.4. Active Research Questions for Cryo-Semi .....	37
<b>4. Quantum Information Processing (QIP)</b> .....	<b>37</b>
4.1. Introduction .....	37
4.1.1. Quantum Computing and Simulation: Introduction .....	37
4.1.2. Quantum Communication: Introduction .....	39
4.1.3. Quantum Sensing: Introduction .....	40
4.2. Applications and Market Drivers for QIP .....	40
4.2.1. Optimization .....	40
4.2.2. Cryptanalysis .....	41
4.2.3. Quantum Simulation .....	41
4.2.4. Quantum Machine Learning .....	41
4.3. Present Status for QIP .....	42
4.3.1. Regional Efforts in QIP .....	42

4.3.2.	Analog Quantum Computing: Status .....	43
4.3.3.	Gate-Based Quantum Computing: Status .....	44
4.3.4.	Topological Quantum Computing: Status .....	47
4.3.5.	Quantum Communication and Sensing: Status.....	47
4.4.	Benchmarking and Metrics for QIP .....	48
4.5.	Active Research Questions for QIP .....	49
<b>5.</b>	<b>Challenges.....</b>	<b>50</b>
<b>6.</b>	<b>Summary .....</b>	<b>51</b>
6.1.	Superconductor Electronics (SCE) .....	51
6.2.	Cryogenic Semiconductor Electronics (Cryo-Semi).....	51
6.3.	Quantum Information Processing (QIP) .....	51
	<b>Endnotes/References .....</b>	<b>52</b>

## LIST OF FIGURES

Figure CEQIP-1	Josephson Junction Device Structures.....	2
Figure CEQIP-2	Magnetic Memory Device Structures.....	12
Figure CEQIP-3	Specific Power versus Cold Temperature for Cryogenic Refrigeration .....	25
Figure CEQIP-4	Energy versus Delay for Intrinsic Elements .....	27
Figure CEQIP-5	Energy versus Delay for Interconnects of 1 mm Length .....	28

## LIST OF TABLES

Table CEQIP-1	Initial Application and Technology Areas Considered for Superconductor Electronics (SCE).....	3
Table CEQIP-2	Matrix of Application or Technology Areas and Market Drivers for SCE .....	4
Table CEQIP-3	Typical Sensitivities of SQUID Instruments .....	5
Table CEQIP-4	Superconductor Digital Logic Families .....	7
Table CEQIP-5	Gate Sets for SCE.....	8
Table CEQIP-6	Fabrication Processes for SCE .....	17
Table CEQIP-7	Superconductor Properties for SCE .....	19
Table CEQIP-8	Superconductor EDA tools .....	22
Table CEQIP-9	Specific Power Ranges for Cryogenic Refrigeration .....	24
Table CEQIP-10	Cryogenic Refrigeration Systems for $T > 10$ K.....	24
Table CEQIP-11	Cryogenic Refrigeration Systems for $1 \text{ K} < T \leq 10 \text{ K}$ .....	24
Table CEQIP-12	Cryogenic Refrigeration Systems for $T \leq 1 \text{ K}$ .....	24
Table CEQIP-13	Energy versus Delay for Intrinsic Elements .....	27
Table CEQIP-14	Energy versus Delay for Interconnects of 1 mm Length .....	28
Table CEQIP-15	Difficult Challenges for SCE .....	29
Table CEQIP-16	Fabrication Roadmap for Superconductor Electronics (SCE) – Digital Circuits...32	
Table CEQIP-17	Fabrication Roadmap for Superconductor Electronics (SCE) — S-MCM.....	33
Table CEQIP-18	Interconnect Roadmap for Cryogenic Electronics.....	34
Table CEQIP-19	Matrix of Application Areas and Market Drivers for Cryogenic Semiconductors..35	
Table CEQIP-20	Matrix of Application Areas and Market Drivers for Quantum Information Processing (QIP).....	40

Table CEQIP-21	Quantum Computing Component Status .....	44
Table CEQIP-22	Gate-Based Quantum Computing Status Summary .....	45
Table CEQIP-23	Difficult Challenges for QIP .....	49
Table CEQIP-24	Difficult Challenges Summary .....	50

## ACKNOWLEDGMENTS

This report was prepared by the members of the Cryogenic Electronics and Quantum Information Processing (CEQIP) International Focus Team (IFT).

Name	Area	Organization
Bhushan, Manjul	SCE-Bench, -Fab	IBM, USA
Bunyk, Paul	QIP-QC	D-Wave Systems, Canada
Cuthbert, Michael	Cryo, QIP	National Quantum Computing Centre, UK
DeBenedictis, Erik	QIP-QC	Sandia National Laboratories, USA
Fagaly, Robert L.	SCE-App	Honeywell (retired), USA
Febvre, Pascal	SCE-Fab	University Savoie Mont Blanc, France
Fourie, Coenrad	SCE-EDA	Stellenbosch University, South Africa
Frank, Michael	SCE-Logic, -Roadmap	Sandia National Laboratories, USA
Gupta, Deep	SCE, Cryo-Semi	HYPRES, Inc., USA
Herr, Anna	SCE-Logic, -Roadmap	Northrop Grumman Corp., USA
Holmes, D. Scott [Chair]	SCE	Booz Allen Hamilton, USA
Humble, Travis	QIP-QC	Oak Ridge National Laboratory, USA
Leese de Escobar, Anna	SCE-Apps, SCE-Bench	Navy SPAWAR, USA
McGeoch, Catherine	QIP-QC	D-Wave Systems, Canada
Missert, Nancy	SCE-Fab	Sandia National Laboratories, USA
Mueller, Peter	QIP-QC	IBM, Switzerland
Mukhanov, Oleg	QIP-QC, SCE-Logic	Seeqc, USA
Nemoto, Kae	QIP	National Institute of Informatics (NII), Japan
Papa Rao, Satyavolu	SCE-Fab, QIP	SUNY Polytechnic, USA
Patra, Bishnu	QIP, Cryo-Semi	TU Delft, Netherlands
Plourde, Britton	QIP	Syracuse University, USA
Pugach, Nataliya	SCE-Logic, -Memory	Lomonosov Moscow State University and National Research University Higher School of Economics, Moscow, Russia
Soloviev, Igor	SCE	Lomonosov Moscow State University
Tyrrell, Brian	Cryo-Semi	MIT Lincoln Laboratory, USA
Vogelsang, Thomas	Cryo-Semi	Rambus, Inc., USA
Wilhelm-Mauch, Frank	QIP-QC	Saarland University, Germany
Noboyuki Yoshikawa	SCE-Logic, -Bench	Yokohama National University, Japan

The team thanks Paolo Gargini, An Chen, Elie Track, and the IEEE Council on Superconductivity for their encouragement and support in developing the CEQIP IFT. We also thank Linda Wilson for administrative help and support.

# CRYOGENIC ELECTRONICS AND QUANTUM INFORMATION PROCESSING

---

## 1. INTRODUCTION

The goal of this International Roadmap for Devices and Systems (IRDS) chapter is to survey, catalog, and assess the status of technologies in the areas of cryogenic electronics and quantum information processing. Application drivers are identified for sufficiently developed technologies and application needs are mapped as a function of time against projected capabilities to identify challenges requiring research and development effort.

Cryogenic electronics (also referred to as low-temperature electronics or cold electronics) is defined by operation at cryogenic temperatures (below  $-150\text{ }^{\circ}\text{C}$  or  $123.15\text{ K}$ ) and includes devices and circuits made from a variety of materials including insulators, conductors, semiconductors, superconductors, or topological materials. Existing and emerging applications are driving development of novel cryogenic electronic technologies.

Information processing refers to the input, transmission, storage, manipulation or processing, and output of data. Information processing systems to accomplish a specific function, in general, require several different interactive layers of technology. A top-down list of these layers begins with the required application or system function, leading to system architecture, micro- or nano-architecture, circuits, devices, and materials. A fundamental unit of information (e.g., a bit) is represented by a computational state variable, for example, the position of a bead in the ancient abacus calculator or the voltage (or charge) state of a node capacitance in CMOS logic. A binary computational state variable serves as the foundation for von Neumann computational system architectures that dominated conventional computing.

Quantum information processing is different in that it uses qubits, two-state quantum-mechanical systems that can be in coherent superpositions of both states at the same time, which can have computational advantages. Measurement of a qubit in a given basis causes it to collapse to one of the basis states.

Technology categories covered in this report include:

- Superconductor electronics (SCE)
- Cryogenic semiconductor electronics (Cryo-Semi)
- Quantum information processing (QIP)

*Note: In 2017, Cryogenic Electronics appeared as an emerging application within the Beyond CMOS chapter. In 2018, Cryogenic Electronics and Quantum Information Processing became an International Focus Team (IFT) responsible for preparing a separate IRDS chapter.*

## 2. SUPERCONDUCTOR ELECTRONICS (SCE)

### 2.1. INTRODUCTION TO SCE

Superconductor electronics (SCE) uses circuits and components at least some of which are in the superconducting state. Some materials become superconducting below a critical temperature,  $T_c$ . Critical temperatures of known superconductors range from near absolute zero to about  $203\text{ K}$  ( $-70\text{ }^{\circ}\text{C}$ ). The unique physics of superconductors, such as zero dc resistance for sufficiently small currents, allows construction of circuits that are otherwise difficult or impossible to realize. SCE applications tend to cluster in temperatures around the boiling point of liquid nitrogen ( $77\text{ K}$ ,  $-196\text{ }^{\circ}\text{C}$ ), the boiling point of liquid helium ( $4.2\text{ K}$ ,  $-269\text{ }^{\circ}\text{C}$ ), and the superfluid helium-4 temperature range below about  $2.17\text{ K}$ .

This report does not seek to explain the operation of superconductor electronic components or circuits except where necessary and consequential to technology roadmapping. Similarly, the focus is on applications that could benefit from technology roadmapping. Following is a very brief introduction. For those seeking to fill in the gaps, a recent and open access review of superconductor electronics is a good next step [1].

## 2 Superconductor Electronics (SCE)

Both passive (linear) and active (nonlinear) superconducting components exist. Examples of passive components are superconducting wires used as inductors, transmission lines, or resonators.

A superconducting loop with inductance  $L$  and circulating current  $I$  stores magnetic flux  $\Phi = LI$ . Unlike a loop made with normal, resistive material, the current can circulate for as long as it stays superconducting. The behavior is analogous to an ideal capacitor, but the loop stores magnetic flux instead of charge.

Only discrete values of magnetic flux are possible in a superconducting loop due to the quantum nature of the superconducting state. A simple description is that the superconducting state is associated with a wave function and that the superconducting phase change around a loop must be  $2\pi n$ , where  $n$  is the number of flux quanta in the loop. The value of the magnetic flux quantum is  $\Phi_0 = 2.07$  fWb. Expressed in practical units, 1 fWb is equivalent to 1 mA·pH or 1 mV·ps. Phase differences between points within superconductor circuits can be produced by magnetic flux, electric currents, and certain devices engineered to exhibit a strongly spatially dependent superconductor wave function. A procedure to determine the flux state in a superconducting loop is described by Fourie [2].

Josephson junctions (JJs) are active superconductor devices used for their nonlinear behavior and switching. Physically, JJs are 2-terminal devices typically made like a thin-film capacitor with superconducting plates or contacts. Common configurations are shown in Figure CEQIP-1. Quantum tunneling of Cooper pairs through the thin barrier layer allows a supercurrent to flow between the contacts with zero voltage drop. The maximum supercurrent is called the critical current,  $I_c$ .

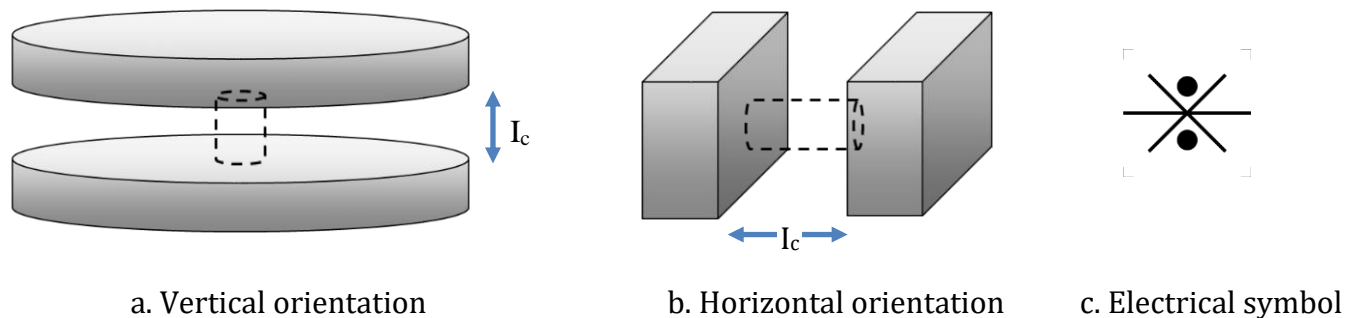


Figure CEQIP-1 Josephson Junction Device Structures

Superconductor electrodes are shown in gray. Contacts to other circuit elements are not shown. The space between the electrodes can be filled with an insulator, semiconductor, or metal. Dashed lines show an optional weak link, which can be made of the same material as the electrodes. Shown is the modern electrical symbol that includes two dots symbolizing a Cooper pair [3, 4].

When the current through a critically damped JJ exceeds the critical current, it switches (the superconducting phase difference across the junction jumps by  $2\pi$ ) and produces a single flux quantum (SFQ) output. Note that the time-dependent voltages and currents produced by the SFQ output depend on the JJ and circuit characteristics, respectively. The switching energy  $E_{sw} \sim I_c \Phi_0 = 2 \times 10^{-19}$  J = 0.2 aJ for  $I_c = 100$   $\mu$ A. Smaller values of critical current  $I_c$  are desirable for energy-efficient applications, within limits due to noise and required bit error rate or ratio (BER) [5].

Single flux quantum (SFQ) digital logic represents digital '1' and '0' by the presence, absence, polarization, or location of magnetic flux quanta within a circuit element. SFQ circuits switch magnetic flux using Josephson junctions and store flux in inductors. This is very different from semiconductor circuits, which switch electric charge using transistors and store charge in capacitors. For an explanation of how a simple SFQ gate operates, see [6]. For a review article, see [7].

Current supplied to SCE circuits is used to both compensate for energy dissipated and to shift superconducting phase differences within the circuit, biasing operation in a desired direction. Supply current type (ac or dc) and magnitude depend on the circuit or logic family. Superconductor phase engineering is an important part of SCE circuit design without analogy in CMOS circuit design [8].

Phase shift elements set or change the superconducting phase  $\varphi$  between locations in a superconducting circuit. Currents through circuit elements can be used to shift the phase. The phase difference across an inductor is given by  $\varphi_L = 2\pi IL / \Phi_0$ , where  $I$  is the current,  $L$  is the inductance, and  $\Phi_0$  is the magnetic flux quantum. Other devices such as Josephson junctions have different current–phase relationships. Achieving a given phase difference involves a tradeoff between current and inductance. Large



inductances can require too much circuit area, whereas large dc external currents can become difficult to supply without creating magnetic fields that affect circuit operation.

## 2.2. APPLICATIONS AND MARKET DRIVERS FOR SCE

Few of the application areas and market drivers considered by the IRDS Systems and Architectures (SA) and Application Benchmarking (AB) teams [9, 10] are currently relevant for superconductor electronics. The reason is that cryogenic electronics must continue to serve niche and emerging markets until it can build the capability and capacity to address larger markets.

The initial list of application areas for cryogenic electronics is shown in Table CEQIP-1 along with technology areas specific to superconductor electronics. The SCE-specific technology areas were added to enable initial tracking prior to application readiness. The matrix of application and technology areas and market drivers shown in Table CEQIP-2. The example applications and drivers included here are preliminary and require further development. Starting points include a survey of applications and markets for superconductor electronics published in 2010 [11].

Table CEQIP-1 Initial Application and Technology Areas Considered for Superconductor Electronics (SCE)

<i>Application or technology area</i>	<i>Desired metric</i>	<i>Description</i>
Optimization	Solutions per second	Integer NP-hard optimization problems
Media processing	Frames per second	Discrete processing, including the filtering, compressing, and decompressing of unknown streaming media
Cryptographic codec	Codons per second	Encrypting and decrypting of data at the edge of cryptographic science
Artificial intelligence	Accuracy, training and inference time and energy	Graphical dynamic moving image (movie) recognition of a class of targets (e.g., face, car). This can include neuromorphic or deep learning approaches such as DNNs.
Sensors *	Accuracy, resolution, rate	Sense physical quantities such as voltage, current, magnetic flux density, or magnetic flux gradient. Example sensors: superconducting quantum interference device (SQUID), superconducting nanowire single photon detector (SNSPD), transition edge sensor (TES), THz superconductor-insulator-superconductor (SIS) and superconducting hot electron bolometer (HEB) heterodyne detectors
Signal processing *	Digital clock rate, bit depth	Filters, analog to digital conversion (ADC), digital to analog conversion (DAC), digital signal processing (DSP) circuits operating either on streaming digital data or in conjunction with ADC and DAC
Sensor array readout *	Rate, multiplexed inputs	Multiplex sensor arrays
Digital computing *	Operations per second, energy per operation, circuit density	Digital computing using single flux quanta (SFQ) in superconductor circuits
Quantum computing *	Coherence time, energy per solution	Qubits, interface and control circuits for quantum computing

\* Technology areas specific to superconductor electronics

Applications can be divided into those that already require cryogenic temperatures for some part of the system and those that do not. Applications already requiring a cryogenic environment provide a much lower barrier of entry for cryogenic electronics. Examples where cryogenic environments are required include: cryogen storage and transport, superconducting magnets such as those in magnetic resonance imaging (MRI) machines and nuclear accelerators, cryogenic devices such as single photon detectors and Josephson junctions, and quantum computing. Note that Josephson junctions are key devices for superconductor electronics, metrology standards, THz detectors in radio astronomy, and for magnetic field sensors and gradiometers based on superconducting quantum interference devices (SQUIDs).

## 4 Superconductor Electronics (SCE)

Other applications do not require cryogenic temperatures; however, use of cryogenic electronics can improve metrics such as sensitivity, resolution, or energy efficiency. Examples might include: artificial intelligence, discrete event simulation, optimization, and media processing.

Following is further information about the market drivers included in Table CEQIP-2. Roadmaps will be considered to help provide the required technologies when needed by these market drivers.

Table CEQIP-2 Matrix of Application or Technology Areas and Market Drivers for SCE

Application or technology area	Market Drivers				
	Measurement & calibration systems *	Digital radio *	Quantum Computing *	Cloud	Cyber-physical systems
Optimization				G	
Media processing		X			X
Cryptographic codec				X	
Artificial intelligence		X		X	X
Sensors *	G	X			
Signal processing *	X	G	X		X
Sensor array readout *	X	X			X
Digital computing *	X	X	P	P	X
Qubit control, readout *			G		

\* Technology areas specific to SCE. X: important application; G: critical gating application; P: power-sensitive application.

### 2.2.1. CLOUD (DIGITAL COMPUTING)

Microprocessor units and memories are currently under development but not yet available as commercial products. Further in the future are large-scale computing applications that require many parallel processors for high-performance computing or data centers [12]. While the market for digital superconductor computing could be large [6], small-scale systems must be developed first and markets found. Bitcoin mining is one application under consideration that requires relatively simple processors, limited memory, and energy efficiency [13].

### 2.2.2. MEASUREMENT AND CALIBRATION SYSTEMS

Many of the systems in this section make use of quantum sensing, the use of a quantum system, quantum properties, or quantum phenomena to perform a measurement of a physical quantity [14]. Included is signal processing.

SQUID sensors utilize the Josephson and Meissner effects to create sensors [15, 16, 17] that can detect magnetic flux changes at or below the  $\mu\Phi_0$  level. The use of flux transformers can allow SQUID sensors to detect field changes at the fT level. Additional circuitry can allow SQUID sensors to detect a wide variety of electromagnetic quantities [18, 19]. SQUIDs with a flux capture area less than  $1 \mu\text{m}^2$  (nanoSQUIDs) have high spatial resolution [17, 20, 21, 22].

Table CEQIP-3 Typical Sensitivities of SQUID Instruments

Measurement	Sensitivity
Current	$10^{-12}$ A/ $\sqrt{\text{Hz}}$
Magnetic flux density	$10^{-15}$ T/ $\sqrt{\text{Hz}}$
dc voltage	$10^{-14}$ V
dc resistance	$10^{-12}$ $\Omega$
Mutual or self inductance	$10^{-12}$ H
Magnetic moment	$10^{-10}$ emu

A SQUID can also be used as a null detector in a cryogenic current comparator (CCC) [23] to achieve part-per-billion current resolution with  $< 0.1$  fA/ $\sqrt{\text{Hz}}$  sensitivity. CCCs have applications in voltage standards (§ 2.2.2.2), quantum Hall effect [24], and in particle accelerator beam diagnostics [25].

The bandwidth of commercially available electronics is typically dc to 100 kHz with flat frequency and flat phase response. Bandwidths of 10 MHz can be achieved by operating in an open loop configuration where the maximum signal does not exceed  $\Phi_0/2$ . Placing multiple Josephson loops having different loop areas in a series-parallel array [26] offers the potential to achieve  $< 0.1$  fT sensitivity levels. Known as a superconducting quantum interference filter (SQIF), these devices have already demonstrated  $> 10$  GHz bandwidths [27]. A combination of sub-fT/ $\sqrt{\text{Hz}}$  sensitivity levels and GHz bandwidths may allow SQIFs to be used a wide variety of yet to be discovered applications. While laboratory applications of SQUIDs have been the springboard for significant commercial successes in the areas of biomagnetism, magnetic property measurement systems, and geophysics, the commercial market for laboratory systems is typically at the 2 to 3 million USD level [28]. One potential use of SQUIDs with a significant commercial application is in the detection of low-field MRI signals [29].

Alternatives to SQUID sensors include the superconducting quantum interference proximity transistor (SQUIPT) [30], and possibly Josephson tunnel junctions incorporating stacked structures of normal metal and ferromagnetic layers [31, 32].

#### 2.2.2.1. BIOMAGNETISM AND MEDICAL MEASUREMENTS

The sensitivity of SQUIDs has allowed non-invasive measurements of electrophysiological activity that has led to the development of number of medical instruments [18]. The major use, responsible for over half a billion USD in sales to date, has been magnetoencephalography (MEG) for magnetic source imaging (e.g., focal epilepsy regions). Another area where SQUID-based methodologies offer diagnostic capabilities is magnetocardiography (MCG), particularly in fetal MCG to diagnose fetal heart rhythm abnormalities. Other uses of SQUID biomagnetometers include magnetoenterography (measurements of the stomach and intestines), magnetopneumography (magnetic remnance measurements of the lung), and magnetomyography and magnetoneurography (muscle and peripheral nerve studies). One disadvantage of ultra-sensitive SQUID biomagnetometers is the need for magnetically shielded rooms to reduce the effects of external electromagnetic noise.

The major drivers in the adoption of medical instrumentation are clinical acceptance, cost and safety. Clinical acceptance requires the demonstration of superior, rather than incremental, diagnostic capabilities in a modality that the physician can easily interpret. Medical equipment costing above 1 million USD is limited to medium to large hospitals. When instrument prices drop to the 250,000 USD level, the potential market expands to small hospital and medium to large clinics. Currently the per channel cost for high channel count SQUID biomagnetometers (e.g., MEG) is at or above a few thousand USD. Significant reductions in per channel cost or eliminating the need for expensive magnetically shielded rooms could significantly increase the market for SQUID biomagnetometers.

Improvements in high-temperature SQUID sensors, which are currently more expensive than low-temperature SQUID sensors, could also reduce the cryogenic requirements with a subsequent reduction in system cost.

#### 2.2.2.2. VOLTAGE STANDARDS

Voltage standard systems based on superconducting Josephson junction arrays became commercially available in 1996 and have continued development [33, 34]. An economic impact assessment of NIST's Josephson volt program performed in 2001 found a net present value of 45 million USD in the year 2000 [35]. At least 16 Josephson voltage standard systems were in operation in the United States at that time. Current information is needed about markets and market drivers for voltage standard systems.

Two complementary types of Josephson voltage standards used today are the programmable Josephson voltage standard (PJVS) and the Josephson arbitrary waveform synthesizer (JAWS, also known as the ac Josephson voltage standard or ACJVS) [34]. The

## 6 Superconductor Electronics (SCE)

main dc application for PJVS systems is the direct calibration of secondary voltage standards. With the 2019 redefinition of base units in the International System of Units (SI), both PJVS and JAWS systems will become key components for the direct realization of the unit volt.

The push to improve ac voltage standards is presently a driver for cryogenic circuit development [36, 37]. One reason is that the output voltage of a JAWS is limited by the number of Josephson junctions (JJs) that can be driven by a single pulse-generator channel. In one paper [37] the number of JJs driven by one generator channel was doubled to 51,200.

### 2.2.2.3. MAGNETIC PROPERTY MEASUREMENT SYSTEMS

Since the discovery of high-temperature superconductors, SQUID based susceptometers have been a mainstay in magnetic property measurements. Gradient detection coils surround the sample region of a variable temperature (typically 1.8 to 400+ K) insert. Surrounding the detection coils is a moderately high-homogeneity (100 ppm) superconducting magnet (0 to 9 T). The sample is moved inside the detection coils, and the resulting changes in flux are used to calculate the magnetic moment of the sample. Some systems have both axial and transverse coils. AC susceptibility can be measured by adding ac coils, although the applied fields are much smaller ( $\mu\text{T}$ ). The dynamic range can vary from  $10^{-8}$  to 2 emu. To date, over 1,300 SQUID susceptometers (from all suppliers) have been delivered generating over 250 million USD in revenues. Commercially available since the late 1970s, this market segment is the premier example that needed a SQUID-based product in quantity. Commercial manufacturers include Quantum Design and Cryogenic, Ltd.

The variable temperature platform can be expanded (without SQUID detection coils) to a variable temperature physical property measurement system allowing a wide variety of measurements to be taken from 50 mK to 800 K in fields exceeding 14 T. The variable temperature susceptometer concept can be converted to remnant field geophysical measurements (§ 2.2.2.5) by removing the dc superconducting magnet and placing three orthogonal detection coils in a magnetically shielded region. Typically placed in a horizontal orientation, nearly 150 systems have been delivered generating nearly 30 million USD in revenues. Commercial manufacturers include 2-G Enterprises and Tristan Technologies.

Nondestructive evaluation (NDE) systems using SQUID sensors have been reviewed by [38].

### 2.2.2.4. MICROSCOPY

Microscopes with SQUID or magnetic tunnel junction sensors image surface magnetic flux density with micrometer-scale resolution [39, 40, 41, 42]. Recent developments include a vector-scanning SQUID microscope [43, 44] and a system for investigation of geological samples [45]. Commercial manufacturers include Neocera Magma [46] and Tristan Technologies [47].

### 2.2.2.5. GEOPHYSICS

Magnetic field gradiometers are used to prospect for magnetic ores [18]. The value of ore deposits discovered is reported to be several billion USD, however, the cost of the cryogenic electronics is a tiny fraction of that amount. These systems require only a few Josephson junctions and can use high-temperature superconductors operating at liquid nitrogen temperatures ( $\sim 77$  K). A survey of applications affecting the environment found additional applications such as the detection of unexploded ordnance (UXO) [48].

### 2.2.2.6. ASTRONOMY

Radio and Infrared Astronomy has played an essential historical role in superconductor electronics by pulling the developments of sensitive quantum-limited superconducting SIS and HEB heterodyne detectors for millimeter, then submillimeter/THz radio telescopes and infrared telescopes like the Herschel Space Observatory or the Planck satellite. Some astronomy applications using cryogenic sensor arrays [49, 50] are growing in array size to the point that multiplexing and signal processing is needed close to the sensors. The need to go from single pixel detection at THz frequencies to array sensors with thousands or more pixels also exists for THz detectors but suffers currently from technological limitations of back-end processing.

## 2.2.3. COMMUNICATIONS

Developed communications applications are covered in the following sub-sections. Proposed communication applications include chaos encryption using a circuit with a Josephson junction in parallel with a memristor [51].

### 2.2.3.1. WIRELESS COMMUNICATIONS

High-temperature superconductor (HTS) filters are used in wireless base stations to increase base station coverage area and data throughput. Superconductor Technologies Inc. has products that operate in over 10,000 base stations [52].

### 2.2.3.2. DIGITAL RADIO

Software-defined radios perform signal processing entirely in the digital domain. By contrast, traditional radios perform signal processing in the analog domain at a single frequency. Software-defined radios require both ultra-high-speed analog-to-digital

converters (ADCs) and equally fast digital signal processing (DSP) of the converted signals, but do not require much memory. ADC and DSP circuits based on superconductor electronics have been demonstrated at speeds up to 40 GHz [53]. The commercial digital-RF receiver manufactured by HYPRES [54] performs ADC and DSP using superconductor electronics [55]. The superconducting components operate at about 4 K with a fully automated and cryogen-free refrigeration system. The application space extends beyond communications to many other uses of the radio frequency spectrum for surveillance, navigation, and spectrum management.

### 2.2.4. QUANTUM COMPUTING: CONTROL AND READOUT

Quantum computing systems operating at cryogenic temperatures below 10 K can benefit from local control and readout. Advantages include less energy dissipation in the cryogenic space and faster response times for control. Overviews of the needs are given in [597, 629, 642, 662]. The need for superconductor electronic control and readout is expected to grow with the scale of the quantum computer supported. The need for superconductors increases for systems requiring temperatures in the millikelvin range and decreases greatly for systems not requiring temperatures below about 10 K.

Current status is covered in section 2.3.4.4 and related applications of cryogenic CMOS are covered in section 3.3.3.2.

## 2.3. PRESENT STATUS FOR SCE

The integrated circuit chip with the largest Josephson junction count is the 2020 D-Wave Pegasus P16 quantum annealing processor with 1,030,000 Josephson junctions [56, 599, 600]. Considering that state-of-the-art CMOS wafer-scale chips are available with more than a trillion transistors [57], superconductor electronics is still far behind the semiconductor industry in key metrics such as integrated circuit density and complexity. Prospects remain for higher operating speeds and improved energy efficiency, especially for applications requiring operation at cryogenic temperatures.

### 2.3.1. LOGIC

The most common SCE digital logic families and some important characteristics are summarized in Table CEQIP-4 and further described below. Most of the logic families transfer one or more single flux quanta to communicate state values between gates [58]. By contrast, quantum flux parametrons (QFP) use currents between gates. Clocked (dynamic) gates can produce only one output per clock cycle, whereas combinational (static) gates have the advantage of allowing greater logic depth per clock cycle. To be identified are additional parameters for future logic family monitoring and comparison. Candidates include average number of junctions or other resources per logic gate (e.g., area, number of layers), energy per operation, or overhead for clock and power supply.

Table CEQIP-4 Superconductor Digital Logic Families

Name	References	SFQ	Power	Static Power	Dynamic power per JJ	Transformers	Static Gates	JJ count $\log_{10}(n)$
<b>RSFQ</b> : rapid single flux quantum	[59]	✓	DC	High	$\alpha I_c \Phi_0 f$	No	No	5
<b>LR-RSFQ</b> : inductor-resistor RSFQ	[60, 61]	✓	DC	Low	$\alpha I_c \Phi_0 f$	No	No	
<b>LV-RSFQ</b> : low-voltage RSFQ	[62, 63]	✓	DC	Low	$\alpha I_c \Phi_0 f$	No	No	
<b>ERSFQ</b> : energy-efficient RSFQ	[64, 65]	✓	DC	0 *	$I_b \Phi_0 f$	No	No	4
<b>eSFQ</b> : efficient SFQ	[66, 67, 68]	✓	DC	0 *	$I_b \Phi_0 f$	No	No	3
<b>Clockless SFQ, DSFQ</b>	[69, 70, 71]	✓	DC	‡	‡	No	Some	2.8
<b>RQL</b> : reciprocal quantum logic	[72, 73, 74]	✓	AC	~0	$\alpha I_c \Phi_0 f 2/3$	Yes	Some	5
<b>PML</b> : phase mode logic	[75]	✓	AC	~0	$\alpha I_c \Phi_0 f /3$	Yes	Some	
<b>AQFP</b> : adiabatic quantum flux parametron	[76]		AC	~0	$\alpha I_c \Phi_0 2 \tau_{sw} / \tau_x$	Yes	No	4.3
<b>hTron</b> : heater-cryotron nanowire	[77]	✓	DC	~0	varies	No	No	1.2

JJ count : Josephson junction count in largest circuit demonstrated as  $\text{INT}[\log_{10}(n)]$ ;  $\alpha$  : activity factor (fraction of JJs that switch in a clock cycle);  $I_c$  : average critical current;  $I_b$  : bias current;  $\tau_{sw}$  : intrinsic switching time;  $\tau_x$  : excitation rise/fall time; \* : for  $I_b$  within the energy-efficient range; ‡ depends on whether powered like RSFQ or ERSFQ, with some additional loss in reset resistors

## 8 Superconductor Electronics (SCE)

Gate set scaling trends are tracked in Table CEQIP-5. This 2021 report includes AQFP (MAJ+INV) and CMOS (NAND2) gate sets.

Table CEQIP-5 Gate Sets for SCE

### 2.3.1.1. RSFQ, LR-RSFQ, LV-RSFQ, LV-HFQ

Single flux quantum (SFQ) digital logic is described briefly in section 2.1. RSFQ circuits use resistors to distribute dc supply currents. While the use of resistors simplifies superconducting circuit design and provides steady current supply, the static power dissipated is typically between 10 and 100 times the dynamic power [66].

Several large-scale RSFQ integrated circuits have been demonstrated at high clock frequencies around 50 GHz, which include 8-bit microprocessors with memory [78, 79], single-precision floating-point units [80], FFT processors [81], and reconfigurable data paths [82]. A bit-serial microprocessor successfully operated at 106 GHz using the 200  $\mu\text{A}/\mu\text{m}^2$  process [83]. Bit-serial architectures are simpler to design but suffer from low throughput. Bit-parallel, gate-level RSFQ circuits have been developed to enhance performance. An 8-bit ALU fabricated using the Nb 9-layer, 100  $\mu\text{A}/\mu\text{m}^2$  process had a computational efficiency of 40 TOPS/W [84]. An 8-bit-wide, bit-parallel datapath composed of an arithmetic logic unit and register files operated up to 64 GHz [85].

LV-RSFQ: Low-voltage operation of RSFQ circuits can improve energy efficiency [5, 86]. An 8-bit ALU has been demonstrated at 30 GHz with energy efficiency greater than 100 TOp/J [87]. Shift register operation at 83 GHz clock frequency was demonstrated using a 200  $\mu\text{A}/\mu\text{m}^2$  JJ process [88].

LV-HFQ: Low-voltage, half flux quantum circuits incorporate  $\pi$  Josephson junctions in LV-RSFQ circuits and are expected to further improve energy efficiency, circuit density, and operating margins [89].

### 2.3.1.2. ERSFQ, ESFQ

Energy efficient RSFQ (ERSFQ) was developed by Hypres [66, 90, 91]. ERSFQ gates are similar to those in RSFQ, but bias current (power) is distributed using a current-limiting Josephson junction in series with a large bias inductor as well as a clocked feeding JTL to maintain adequate bias voltage, all of which add overhead to gate circuit area. Power distribution for energy-efficient operation adds about 30% to ERSFQ circuit overhead [92]. ERSFQ has been used to make 8-bit parallel adders with 560 and 1360 JJs [93], a decoder for RAM [94], and fast parallel counters [95]. Proposed is a superconducting magnetic FPGA based on ERSFQ logic [96].

Efficient SFQ (eSFQ) was also developed by Hypres [66, 67, 68]. In eSFQ the biasing network is designed so that in each clock period the superconducting phase at all bias injection points goes through the same change. Smaller bias inductors are required than for ERSFQ, however the gates must be designed differently. Demonstrations of eSFQ include asynchronous [97] and wave-pipelined circuits [68]. The largest eSFQ circuit demonstrated is a 184 bit shift register with  $184 \times 5 = 920$  JJs [67].

### 2.3.1.3. CLOCKLESS SFQ, DSFQ

Most logic gates in the existing dc-powered SFQ logic families like RSFQ and ERSFQ operate intrinsically as state machines, i.e., they have internal logic states and normally require a clock signal to reset them to the ground state after each clock cycle. Such explicit use of clock signals in logic networks creates significant challenges with the application of the RTL (register transfer level) design paradigm, a cornerstone of VLSI digital design methodology. RTL subdivides large digital circuits into clocked registers and clock-free, state-free logic networks called combinational logic clouds.

Dynamic SFQ was developed recently by Rylov at IBM [69, 70] and is currently at the demonstration stage. DSFQ uses a nonlinear leakage mechanism that makes the usable hold time of gate storage loops large compared to the subsequent self-reset time. This means that the hold time and hence the gate input skew tolerance become a significant portion of the clock cycle and therefore such gates can be used to build combinational logic clouds.

Kawaguchi et al. [71] developed clockless AND and NIMPLY gates consisting of NDRO and delay elements. A 4-bit CLA circuit designed with a mix of combinational (unclocked) and clocked gates has been demonstrated.

### 2.3.1.4. RQL AND PML

Reciprocal quantum logic (RQL) [98, 99, 100] and phase mode logic (PML) [75] are related logic families. RQL encodes a digital 1 using two flux quanta of opposite sense and corresponds to wave pipeline operation. PML encodes digital data as high and low states of the superconducting phase, which dissipates less dynamic power. Both use energy-efficient ac resonator-based

distribution for power and clock signals. The power is applied in parallel providing scalability to VLSI. Resonators also provide clock stability with zero jitter and skew. Both RQL and PML include combinational gates that allow 12 levels of logic per pipeline stage at 10 GHz. RQL and PML logic provide component-efficient superconducting gates with the same number of junctions as transistors in CMOS gates as well as full compatibility with standard RTL based synthesis design flow.

Design achievements include tile-based physical design to facilitate automated layout, mitigation of flux trapping, and a resonant clock network for chip-level power distribution with 50% power efficiency. A complete RTL-to-GDSII automated design flow has been developed and used to design a 16-bit CPU [101]. Circuit demonstrations include individual logic gates with a 7 dB clock margin; 3.5 GHz resonator powering a shift register with 72,800 JJs and 4 dB clock margin [102]; 16-bit ALU and 16-bit register file [103]; 0.25 MJJ resonator-based yield vehicle; and an 8-bit CPU with fully functional debug logic, register file, 8-bit CLA, and performance of write and read memory instructions [104].

### 2.3.1.5. QFP: QUANTUM FLUX PARAMETRON LOGIC

Adiabatic quantum flux parametron (AQFP) logic achieves extremely high energy efficiency by changing the potential shape adiabatically between double-well and single-well during switching [58, 105]. Unlike SFQ logic families, current polarity and magnitude communicate state values between gates. Other distinguishing features include the use of AC power and current transformers. The typical switching energy is about  $4.3 \times 10^{-22}$  J at 5 GHz clock frequency assuming unshunted junctions with critical current density of  $100 \mu\text{A}/\mu\text{m}^2$  [106]. Determining the energy dissipation of an AQFP logic gate requires accounting for the data-dependent interactions between the gate and its environment [107]. The switching energy can be further decreased in proportion to the clock frequency and perhaps even below the Landauer thermal limit by using reversible quantum-flux-parametron (RQFP) gates [108, 109, 110, 111].

Operation at high frequencies with low bit energy and low bit error rate or ratio (BER) was confirmed experimentally [112, 113]. Multi-excitation circuits (ME-AQFP) can multiply the excitation current frequency, which typically has a maximum of about 5 GHz, by a factor of 2 or 4 to allow AQFP circuit operation up to about 20 GHz [114]. AQFP logic circuits are typically clocked by four-phase AC clocks; therefore, the logic depth per clock cycle is four. The number of phases and logic depth can be increased to more than 20 for a 5 GHz clock frequency and  $100 \mu\text{A}/\mu\text{m}^2$  junction process [115]. An alternative low-latency excitation scheme based on microwave power dividers has been proposed [116].

Digital logic AQFP circuit design uses a standard cell design approach with similarities to CMOS circuit design [117]. An AQFP NAND gate requires 6 junctions, whereas the corresponding CMOS gate uses 4 transistors. Transformers for supply and signal currents also add area and are difficult to scale to small sizes. Because a majority gate is a fundamental logic gate in AQFP logic, majority-based logic synthesis is desirable [118]. Several circuits components have been designed and demonstrated by using an automated top-down design flow, which includes logic synthesis, and placement and routing [119, 120]. Functional operation has been demonstrated for 8-bit carry-lookahead (CLA) adders [121, 122] and 16-word, 1-bit register files [123]. An 8-bit CLA was demonstrated with energy dissipation of only 1.5 aJ per operation, or  $24k_B T$  per junction switching [124]. The demonstrated MANA 4-bit AQFP microprocessor with 21,460 junctions is estimated to dissipate about 30 aJ/op at 5 GHz [125].

Directly coupled quantum-flux-parametron (DQFP) is an adiabatic superconductor logic that does not require signal transformers [126, 127]. While AC power transformers are still required, the nearly 40% reduction in gate area is significant. AQFP with  $\pi$  Josephson junctions also can operate without using signal transformers [128].

### 2.3.1.6. REVERSIBLE LOGIC STYLES

There has been a long history of efforts to develop superconducting logic styles capable of approaching (logically and physically) reversible computation, starting with Likharev's work on parametric qantrons (PQ) in the 1970s [129], and reversible versions of the original 1987 quantum flux parametron (QFP) of Goto *et al.* [130]. These early efforts relied on adiabatic transformation of the potential energy function in one or more coupled SQUID loops, a theme which continues today in the recent work on negative mutual-inductance SQUIDs (nSQUIDs) [131, 132] and on reversible quantum flux parametron (RQFP) logic [109, 133, 134], a variation on AQFP logic. In addition, several groups have investigated alternative *ballistic* styles of superconducting reversible logic, including a group in Hokkaido in 2008 [135, 136], Northrop Grumman in 2010 [137], and ongoing work at the University of Maryland, [138, 139] and at Sandia National Laboratories [140, 141]. These efforts aim to surpass the energy efficiency of the existing irreversible logic styles such as those in Table CEQIP-4 and can potentially eventually push beyond the Landauer limit of  $\sim kT$  energy dissipation per operation that applies to irreversible logic.

### 2.3.1.7. OTHER SCE LOGIC

Other superconductor logic families include those based on nano-cryotrons [77, 142, 143, 144, 145, 146, 147], Josephson junction oscillators [148], and control of magnetic flux quanta using magnetic fields [149].

## 10 Superconductor Electronics (SCE)

Quantum phase slip junctions (QPSJ) are superconductor nanowire devices with a nonlinear I-V characteristic. QPSJs are a dual to Josephson junction devices, with the roles of phase and charge interchanged as well as current and voltage [150, 151, 152, 153, 154, 155, 156, 157]. Adiabatic logic circuits based on quantum charge parametrons could be made from QPSJs [158]. Advantages of QPSJs relative to JJs include voltage control, far less sensitivity to magnetic fields [151], and possibly lower switching energy. Nanowire QPSJ devices also might have some fabrication advantages over Josephson junctions, although fabrication experience with NbN nanowires indicates that challenges remain, particularly in device variability and operating temperature [153, 156, 157]. Needed is demonstration of QPSJ-based circuits with at least 100 junctions to allow evaluation of their viability for complex applications.

Spintronic superconductor electronics is a new field since about the year 2000. Like traditional spintronics, the approach is to utilize spin currents for information processing. Contrary to charge current, spin current does not conserve and is not always accompanied by charge transfer, so might be more energy efficient. Reviews of superconductor spintronics include [159, 160, 161, 162]. This new field is at the stage of development and demonstration of device concepts rather than production. It is not easy to produce spin superconducting currents; however, when produced, they persist in superconductors much better in both equilibrium [163] and nonequilibrium transport [164, 165, 166]. The use of spin currents to switch memory devices is covered in § 2.3.2.2.

### 2.3.2. MEMORY

Superconductor electronic memory can be classified by memory device technology: 1) Josephson junction logic circuits, 2) magnetic devices, or 3) nanowire superconductor devices; and by use: (a) register, (b) cache, or (c) main memory.

In JJ logic circuits and in nanowire superconductor devices, the magnetic flux in a superconducting loop in steady state is quantized and thus can be used to provide the physical basis for a digital memory element. The absence or presence of a flux quantum in the loop represents binary ‘0’ or ‘1’. Superconducting memory cells have one or more Josephson junctions in the loop to control and sense the number or location of flux quanta present.

For a review, see “16.7 Memory for Cryogenic Supercomputer” in [58].

#### 2.3.2.1. JJ MEMORY

The largest demonstrated superconducting random-access memory (RAM) is only 4 Kibit (4096 bits) [167, 168].

RQL-RAM uses pure RQL logic and is under development by Northrop Grumman [169, 170, 171]. The unit cell consists of three RQL gates, including a single NDRO gate for state and readout and two gates to implement the multiplexer. A variant called PRAM combines NDRO storage with a SQUID-based readout multiplexer. Both RQL-RAM and PRAM read and write in a single clock cycle. PRAM is expected to achieve better density, speed, and power than RQL-RAM at sizes greater than 2 Kibit. RQL-RAM has been demonstrated as 128 bit (8×16) and 1024 bit (64×16) arrays [169]. PRAM with 44  $\mu\text{m}$  × 33  $\mu\text{m}$  bit cells has been demonstrated as a complete array (drivers, unit cells, sense amps) of 512 bits (16×32) [171]. The read path shared by JMRRAM and PRAM has been demonstrated as a 16×32 array (decoders, drivers, unit cells, sense amplifiers, and test wrappers).

SFQ vortex transitional (VT) memory cells have been designed with sizes as small as 9  $\mu\text{m}$  × 11  $\mu\text{m}$ , fabricated in arrays using the MIT LL SFQ5ee process, and successfully demonstrated [172]. This demonstration was not a complete RAM as addressing and readout circuits were not included on the chip.

Lookup tables (LUT) have been demonstrated with 4 bits and designed with 16 bits using RSFQ circuits [173].

A memory cell with 3 conventional Josephson junctions (0-junctions) and a Nb/PdNi/Nb magnetic junction ( $\pi$ -junction) has been demonstrated [174]. The  $\pi$ -junction eliminates the need to provide bias current to the memory cell. Bipolar SFQ pulse trains sent over a passive transmission line are intended to perform read and write operations. Optimization of the memory cell is required for use in arrays.

#### 2.3.2.2. MAGNETIC MEMORY

Magnetic materials affect nearby superconductors and layers with aligned magnetizations have a stronger effect. The effects can be used for superconductor logic as covered in §2.3.1.7. Here the concern is only memory devices. One method to make a memory element uses two magnetic layers, one that can be switched (free) in direction and a second that is magnetically hard and serves as an unswitched reference. Switching the free layer so the two layers are either parallel or antiparallel changes the effect on nearby superconductors and can be read as memory states ‘0’ and ‘1’. Magnetic memory devices for SCE have similarities to magnetoresistive RAM (MRAM) developed for conventional electronics, however, there are also significant differences. Several types of magnetic memory devices for superconductor electronics are shown in Figure CEQIP-2.



Memory cells can be based on changes in magnetic memory device (i) Josephson critical current [175], or (ii) superconducting phase difference in the ground state [7].

#### **2.3.2.2.1. SUPERCONDUCTING SPIN VALVES (SSV)**

Figure CEQIP-2a shows an example device structure. Two magnetic layers affect a single superconductive layer, changing the superconducting critical current. A similar device type with only one magnetic layer containing multiple domains works by changing the degree of domain alignment.

Status: Superconducting spin valves with magnetic control of superconducting critical temperature ( $T_c$ ) require some effort to implement in SCE, nevertheless, they are actively developed in two main configurations: FSF [176] and SFF [177]. Parallel configuration of F-layers magnetization suppresses superconductivity and provides lower  $T_c$ , while antiparallel configuration provides higher  $T_c$  of a thin superconducting film. In the range between these two critical temperatures, the magnetization reversal of one free (F) layer switches between normal and superconducting states. Long-range triplet creation may provide an additional way to drain Cooper pairs from the superconductor, and thus produce an even larger  $T_c$  shift [178]. The use of a half-metallic ferromagnet in SFF spin valves produces a giant spin-valve effect with  $T_c$  shift  $\sim 1$  K [179]. These structures require that the  $T_c$  shift at magnetization reversal be larger than the superconducting transition width to fully switch the superconductor, a challenge that appears manageable [176, 179, 180, 181].

#### **2.3.2.2.2. SPIN VALVE JOSEPHSON JUNCTIONS (SVJJ)**

Figure CEQIP-2b shows the basic superconductor-ferromagnet-superconductor (SFS) device structure. The superconducting critical current passes directly through the magnetic layers. Adding an insulator layer (SIFS) as shown in Figure CEQIP-2c increases the normal state resistance and can provide a larger characteristic voltage  $V_c$  if the combined barrier layers are sufficiently transparent for the device to have a large critical current. The tunnel current through the insulating barrier can be increased by sandwiching it between two superconductor layers (SISFS) as shown in Figure CEQIP-2d. While spin valve JJs can be made using either spin-singlet or spin-triplet supercurrents [182], spin triplet devices are covered separately in section 2.3.2.2.4.

Challenges include sensitivity to magnetic layer thicknesses and quality, and the need to switch the free layer using magnetic fields produced by external control circuits.

Status: Spin valve Josephson junctions are under development by Northrop Grumman in collaboration with Michigan State University [183, 184], Hypres/SeeQC (USA) [185], University of Leeds [186], Lomonosov Moscow State University [175], Institute of Solid State Physics RAS (Russia), and others. Northrop Grumman is developing Josephson magnetic random-access memory (JMRAM) using a spin valve Josephson junction for state and a SQUID-based readout multiplexer. Unit cell size, set by the readout multiplexer, scales to 32 Mibit/cm<sup>2</sup> with 90 nm feature size. The projected read and write energies per 64-bit word at 4 K are 10 aJ and 50 fJ, respectively. Advantages of JMRAM are high density and reads that are fast and low energy. Writes are expected to take longer than 1 ns but could be tolerable using memory latency hiding techniques. The JMRAM unit cell and its write drivers have been demonstrated as stand-alone devices [187].

SISFS junctions with a single ferromagnetic layer are under development experimentally [220, 221, 188] and theoretically [222, 189]. These junctions include a soft ferromagnetic layer of PdFe with about 1% iron that changes magnetic state in a weak external field, thereby shifting the Josephson current Fraunhofer pattern and thus the current-phase relationship (CPR).

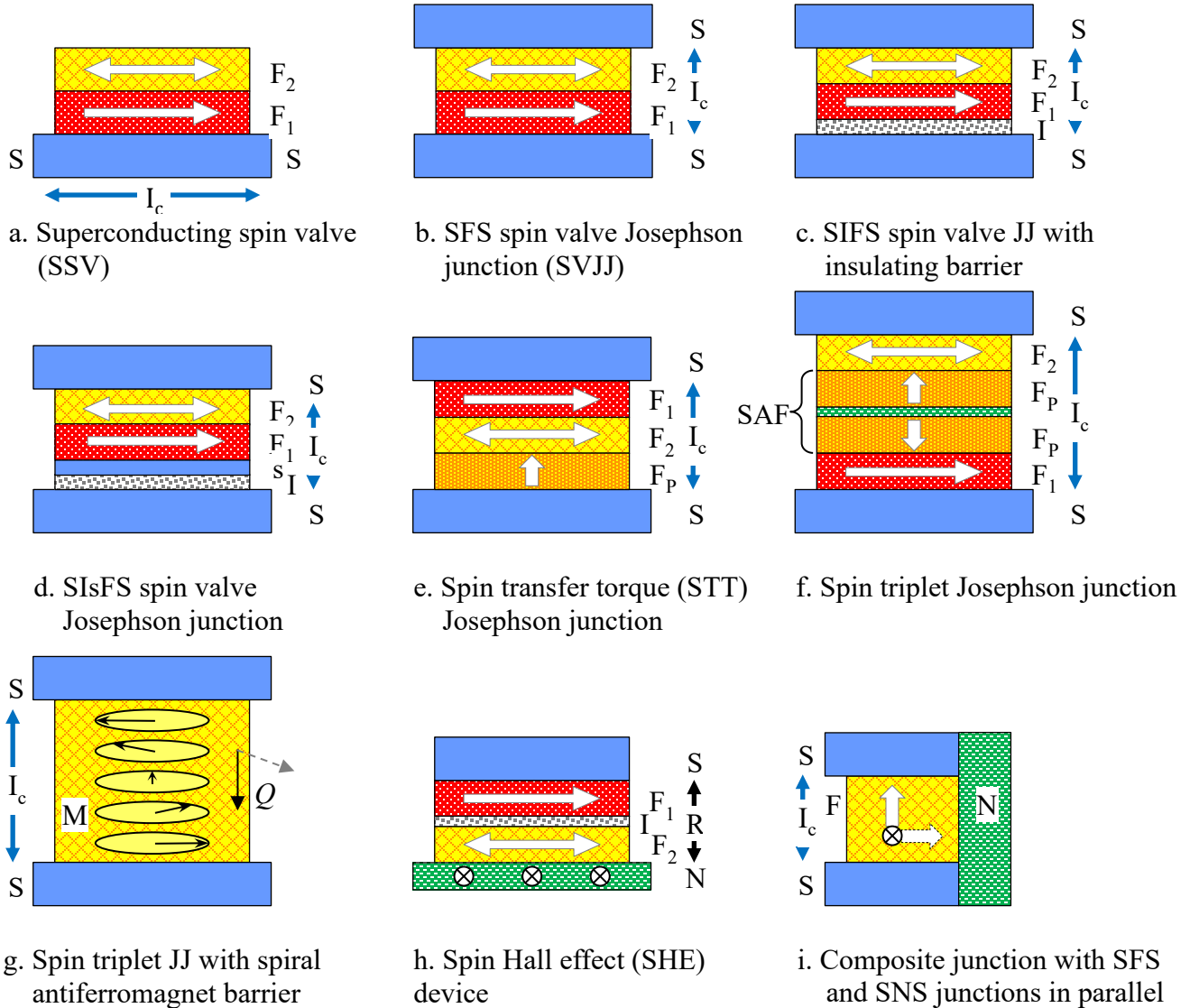


Figure CEQIP-2 Magnetic Memory Device Structures

Superconductors (S) are shown in solid blue. Ferromagnetic materials (F) are shown with magnetization direction either fixed (hard) or bidirectional (soft). Insulators (I) are speckled gray. Normal metals (N) are checkered green. Buffer layers are not shown except within a SAF.

**2.3.2.2.3. SPIN TRANSFER TORQUE JOSEPHSON JUNCTIONS (STTJJ)**

Figure CEQIP-2e shows an example device structure. Spin transfer torque (STT) devices use spin-polarized currents to switch the magnetization direction in one layer within the device. Switching the free layer is performed by passing current through a spin polarizing layer  $F_p$ . The resulting spin current produces a torque on the free layer that depends on current direction. Spin current production is covered in § 2.3.1.7. STT junctions might scale to smaller sizes than SVJJs as they do not rely on magnetic fields produced by nearby control wires. Challenges include the need for bi-directional write currents, high current density required for switching, and difficulty fabricating the polarizing layer.

Status: STT switching has been observed in Josephson junctions with pseudo-spin-valve barriers  $\text{Ni}_{0.8}\text{Fe}_{0.2}/\text{Cu}/\text{Ni}$ , although the switching currents were high [190]. Spin-valve nanopillars with in-plane magnetized dilute permalloy demonstrated switching times  $\sim 0.5$  ns and energies of 18–36 fJ, depending on direction [191]. CoFeB/MgO-based perpendicular magnetic tunnel junctions (pMTJs) have magnetoresistance  $>120\%$  at 9 K [192]. Orthogonal spin-transfer (OST) devices with orthogonally magnetized layers have been demonstrated with switching times well below 1 ns; however, devices with greater magnetoresistance will be required to allow readout by superconductor circuits [193].

#### 2.3.2.2.4. SPIN TRIPLET JOSEPHSON JUNCTIONS (S3JJ)

Figure CEQIP-2f shows an example device structure. The synthetic antiferromagnet (SAF) in the structure shown serves to fix the  $F_p$  layers in a perpendicular orientation. Noncollinear magnetization of the magnetic layers can create spin triplet Cooper pairs, which have a longer range than the ordinary spin singlet Cooper pairs [161, 194, 195]. Also required are nonmagnetic spacer layers to decouple magnetic layers while promoting high magnetic quality in the subsequent layer. An advantage is that the  $0-\pi$  switching is caused by spin rotations rather than phase accumulation as in SVJJs, so device behavior is less sensitive to the exact thicknesses of the  $F_1$  and  $F_2$  layers. Challenges include getting sufficiently high critical current density in a structure with so many layers.

Status: Birge's group at Michigan State University is developing memory devices based on Josephson junctions with spin triplet supercurrent [182, 195, 196, 197]. The most recent work demonstrated controlled switching of the ground-state phase difference between 0 and  $\pi$ , but the critical currents were less than 10  $\mu\text{A}$ .

Spiral (helical) antiferromagnets have been proposed as an alternative barrier material for superconducting spin triplet spin valves [198, 199, 200, 201] and spin triplet Josephson junctions [202]. Figure CEQIP-2g shows an example device structure that replaces multiple barrier layers with a single layer with spiral magnetization. Switching the spiral magnetization vector  $Q$  between stable states can change both  $I_c$  and the ground state (zero current) superconducting phase difference  $\phi_0$ . MnSi develops helical magnetic order below a transition temperature of 29.5 K and might be a suitable material that could produce  $0-\pi$  junctions with layer thickness in the range of 3.2 to 4.0 nm. The potential barrier separating spiral magnetic orientations might make these devices less susceptible to half-select problems. Challenges include demonstration of memory elements.

#### 2.3.2.2.5. SPIN HALL EFFECT (SHE) DEVICES

Figure CEQIP-2h shows an example device structure with current  $\otimes$  going into the normal metal layer at the bottom. Spin-orbit torque (SOT) from the spin Hall effect in heavy metals can rapidly and reliably switch an adjacent ferromagnet (F) free layer of a nanoscale magnetic tunnel junction in a three-terminal configuration. Challenges include the need for bi-directional write currents and write voltages difficult to provide with SFQ circuits.

Status: Raytheon BBN (USA) together with Buhrman's group at Cornell University have demonstrated cryogenic spin Hall effect magnetic tunnel junction (SHE-MTJ) memory devices in a  $4 \times 4$  array [203]. Heater-cryotron bit select devices were used to achieve writing times of a few nanoseconds, write energies  $\sim 8$  pJ, and BER  $\sim 10^{-6}$ . Prospects for decreasing the bit energies include improved spin Hall materials, device structures, or lithography [203, 204]. Challenges include memory arrays with thousands of bits and lower read and write energies.

#### 2.3.2.2.6. COMPOSITE JUNCTIONS

Figure CEQIP-2i shows an example composite junction consisting of two parallel regions with different characteristics. In the structure shown, the SNS portion functions as a Josephson junction with 0 phase difference at zero current and the SFS portion can function as a  $\pi$ -phase junction. The composite junction functions as a SQUID consisting of the two junctions in parallel. The readout time of such memory elements is estimated as 10s of picoseconds. Writing by magnetization reversal requires times on the order of 10 ns [7]. Composite junctions with a non-single-valued current-phase relationship (CPR) might be able to switch between two logic states by changing the current through the device, which could occur on the picosecond timescale. Some of these theoretical predictions were based on nonuniform SF-FNS junctions with different structures [205, 206]. Recent theoretical work indicates that the structure shown in Figure CEQIP-2i is most suitable for practical realization among those considered [207]. Challenges are likely to include fabrication, scalability to small sizes, and incorporation into accessible memories.

#### 2.3.2.2.7. OTHER MAGNETIC MEMORY DEVICES

Josephson junctions with Si barriers containing Mn magnetic nanoclusters have been demonstrated to function as memristive elements capable of synaptic weight training using electrical pulses with energies as small as 3 aJ [208]. Proposed is a memory element containing a magnetic EuS magnetic film on top of a NbN nanowire [209]. Proposed is a hybrid memory using Josephson junctions and Toggle MRAM [210].

## 14 Superconductor Electronics (SCE)

### 2.3.2.3. OTHER CRYOGENIC MEMORY

Hybrid superconductor-CMOS memories are covered in section 3.3. Nanowire-based memory devices are under investigation by a few groups [77, 211]. A memory array of 8 cells (2 bits  $\times$  4 words) has been demonstrated using heater-cryotrons [77]. Proposed but not yet demonstrated devices include ternary memory cells using Josephson junctions [212, 213], superconducting memristors [214, 215] and meminductors [216].

### 2.3.3. CIRCUIT ELEMENTS FOR SCE

#### 2.3.3.1. SWITCHING DEVICES

Weak-link nanobridges are being investigated as scalable alternatives to SIS Josephson junctions [17, 145, 146, 217, 218].

Magnetic elements are incorporated in switching devices such as SFIS junctions [219], SIsFS junctions [220, 221, 222], and superconducting ferromagnetic transistors with SISFIFS structures [223]. SIsFS junctions are promising due to their high- $I_c R_n$  product, up to about 2 mV, that determines the maximum switching frequency of the device. Such junctions have non-single-valued current-phase relationships (CPR) as discussed in §2.3.2.2.

High-temperature superconductors (HTS) have a critical temperature  $T_c$  greater than 30 K. Josephson junctions produced in  $\text{YBa}_2\text{Cu}_3\text{O}_{7-\delta}$  (YBCO) films by helium-ion beam irradiation have been fabricated with junction widths down to 50 nm [224]. A step-edge HTS Josephson-junction mixer operated at 600 GHz and temperatures of 20–40 K with superior performance [225]. Progress on applications of high-temperature superconducting microwave filters has been reviewed [226]. Still, the large spreads typical in HTS device characteristics are problematic for SFQ logic. The small coherence lengths typical of HTS materials cause junctions made of these materials to be very sensitive to fabrication variations. So, requirements for Josephson nanostructures must be even stronger than for low  $T_c$  systems, while the accuracy of HTS junction fabrication is much more difficult to achieve.

#### 2.3.3.2. CURRENT SUPPLY

SFQ circuits require DC bias currents to switching Josephson junctions of about  $0.7I_c$ , or roughly 100  $\mu\text{A}$  per junction. Large supply currents are undesirable as they can exceed the current carrying capacity of thin film lines and also produce magnetic flux that can affect circuit operation. DC powered circuits are thus limited to a few thousand junctions per supply pad on the chip. A technique called current recycling allows a smaller DC bias current to cascade through multiple circuit blocks and thus reduce the required supply current [227, 228]. Disadvantages of current recycling include more difficult design and greater variation in bias currents.

AC power can supply current to many more junctions using transformers in series, with each transformer providing AC bias current to a single junction or subcircuit. AC power is used for RQL [73], PML, and QFP circuits [116]. Rectifying circuits can be used to provide local DC currents using AC power distribution networks [229].

#### 2.3.3.3. PHASE SHIFT ELEMENTS

As introduced in section 2.1, phase shift elements set or change the superconducting phase  $\varphi$  between locations in a superconducting circuit. Currents through circuit elements can be used to shift the phase. The phase difference across an inductor is given by  $\varphi_L = 2\pi IL / \Phi_0$ , where  $I$  is the current,  $L$  is the inductance, and  $\Phi_0$  is the magnetic flux quantum. Other devices such as Josephson junctions have different current–phase relationships. Achieving a given phase difference involves a tradeoff between current and inductance. Large inductances can require too much circuit area, whereas large dc external currents can become difficult to supply without creating magnetic fields that affect circuit operation.

Wires that produce magnetic fields are the simplest inductive devices. Note that magnetic inductance can depend significantly on the full geometry of the circuit, including ground planes that carry current return paths, which can reduce calculation accuracy [230]. Wire inductors are also susceptible to interference between inductors and from the external environment.

High kinetic inductance superconductors such as  $\text{MoN}_x$  or  $\text{NbN}$  can be used to fabricate smaller inductors [231]. The kinetic inductance in thin films of these materials can be many times larger than the inductance produced magnetically. Advantages of kinetic inductors include less dependence on nearby circuits, which makes design easier. Kinetic inductors are also less sensitive than magnetic inductors to interference from external currents and magnetic fields.

Stacks of Josephson junctions can provide sufficient inductance to replace thin-film inductors [232]. Josephson junctions used to provide inductance must operate well below their critical current to avoid switching and to avoid the large inductance variation that occurs near the critical current. Stacks of 3 to 4 junctions can be fabricated as pillars with heights less than 200 nm. If fabricated with the same critical current density as the switching junctions, the stacked JJ inductors must be of larger diameter to avoid switching. Using different fabrication processes for switching and inductor junctions can provide denser circuits at the expense of greater process complexity. Tolpygo et al. [231] argue that fabrication of thin-film inductors is much simpler and expected to have a higher yield than stacked junctions, thus favoring the high kinetic inductance approach.

Magnetic junctions can provide non-zero phase shift without an applied bias current. Josephson junctions can be characterized by their current-phase relationships, particularly the ground state phase shift [233]. Junctions with zero phase shift in their ground state, like those typically used for switching, are called 0 JJs. Pi junctions ( $\pi$  JJs) have  $\pm\pi$  phase shift in the ground state and can be used to create circuits that require little or no external bias current [89, 233, 234, 235, 236, 237]. Junctions with other ground state phase shift are known to exist (e.g.  $0-\pi$ ,  $\varphi$ ,  $2\varphi$ ) and might be fabricable [207, 238]. Advantages of using magnetic junction phase shifters can include reduction in bias current required, reduction in junction count, improvements in energy efficiency, increased circuit density, and increased operating margins [89]. Magnetic junctions not intended to switch do not require large  $IcRn$  products, so are relatively simple to fabricate.

Phase shift elements needing near-term development include manufacturable high kinetic inductors, stacked junction inductors, and  $\pi$ -JJs.

#### **2.3.3.4. TRANSFORMERS**

Current transformers rely on magnetic coupling between inductors, which seems difficult to scale to very small dimensions. Shielding to prevent interference from external signals can also add to the difficulty in scaling transformers [228]. Transformers are most important in AC-powered logic families such as RQL, PML, and all forms of QFP. DC current recycling can also use transformers to couple signals between circuit blocks.

Miniaturization of transformers is addressed in [172]. Needed are transformer alternatives or scaling approaches that allow significantly higher logic gate and memory cell density.

#### **2.3.3.5. TRANSMISSION LINES**

On-chip data interconnects can be either Josephson transmission lines (JTLs) or passive transmission lines (PTLs) [239, 240, 241, 242, 243]. JTL cells include 2 JJs, both of which switch when transmitting a digital ‘1’. Long JTLs consume too much energy and result in too much time delay and jitter, so PTLs are often preferred for distances longer than a few gate lengths.

Passive transmission lines transmit SFQ pulses over a stripline or microstrip. SFQ signals travel ballistically on PTLs at roughly one third the speed of light and can travel several millimeters before regeneration is required. The impedance of a PTL should closely match the driver circuit output impedance and the receiver circuit input impedance to minimize reflections. A challenge is that matching the stripline impedance to a Josephson junction driver, which typically has low impedance, can require a stripline with signal line width of 1  $\mu\text{m}$  to 10  $\mu\text{m}$ . The effective output impedance of a Josephson junction is the resistance including any shunt. Stripline and microstrip impedance scaling and matching are discussed in [239, 242]. Losses in Nb striplines of 250 nm width were found to be dominated by losses in the dielectric at low power and in the superconductor at high power [244]. Another challenge for scaling is that electromagnetic wave propagation can slow down significantly as Nb linewidth decreases below 1  $\mu\text{m}$  due to increasing kinetic inductance and fringing capacitance [245].

#### **2.3.3.6. FLUX TRAPS AND MOATS**

Magnetic flux trapped within superconducting circuits causes circulating currents that can cause the circuits to malfunction. Flux traps or moats attract magnetic flux during cooldown through the transition from normal to superconducting states and provide a location where the flux can be held without seriously affecting nearby circuits [246, 247, 248].

### **2.3.4. ARCHITECTURES AND APPLICATIONS**

#### **2.3.4.1. TRADITIONAL COMPUTING ARCHITECTURES**

Von Neumann microarchitectures typical in CMOS microprocessors are also common in superconductor processors using SFQ logic. Recent examples include 8-bit microprocessors with memory [78, 79], a 16-bit bit-slice ALU for 32- or 64-bit RSFQ microprocessors [249], and design of a 16-bit RQL CPU [101]. Gate-level deep pipelining with bit-parallel architecture can be disadvantageous for CMOS due to pipeline register overhead but appears promising for SFQ processor designs [250]. The MANA 4-bit AQFP microprocessor was developed with a hybrid RISC-dataflow architecture using 21,460 junctions and is estimated to dissipate about 30 aJ/op at 5 GHz [125, 251].

#### **2.3.4.2. RECONFIGURABLE COMPUTING ARCHITECTURES**

The small amount of SFQ-compatible memory available for microprocessors has driven alternative architectures such as reconfigurable data-path processors [82].

Superconductor field-programmable gate arrays (SFPGAs) were first proposed in 2007 using RSFQ logic circuits and RSFQ NDROs as memory elements [252]. Proposed is an RSFQ SFPGA using magnetic Josephson junctions (MJJs) for implementation of area-efficient switches [96]. An all-SFQ FPGA design that allows both combinational and sequential logic is analyzed for chip sizes from 5 mm  $\times$  5 mm to 50 mm  $\times$  50 mm [253]. An AQFP SFPGA with a cryo-CMOS memory has been designed and a 2 $\times$ 2

## 16 Superconductor Electronics (SCE)

unit system demonstrated [254]. FPGAs can provide significant benefits to users in flexibility and reconfigurability, but at a cost of significant circuit overhead. Challenges for superconductor FPGAs include switch matrix overhead using SFQ logic and the low density of superconductor circuits, which does not yet allow sufficient functionality in a single-chip SFGA. Still, work is needed to prepare for the time when sufficient circuit density and complexity is available.

### 2.3.4.3. NEUROMORPHIC ARCHITECTURES

Neuromorphic approaches to computing and artificial intelligence using superconductor electronics are under investigation. In the fields of machine learning and artificial intelligence, superconductor electronics is one of many emerging device technologies [255]. As intrinsically nonlinear elements, Josephson junctions might have advantages for artificial neural networks due to behavioral similarities to biological neural circuits, high speed, and energy efficiency. For example, an artificial synapse based on ferromagnetic Josephson junctions demonstrated a spiking energy per pulse less than 1 aJ [208]. Neuromorphic approaches include those based on switching Josephson junctions [256, 257, 258, 259, 260, 261, 262, 263], AQFP circuits [264, 265, 266], magnetic Josephson junctions [208, 267, 268, 269], nanowires [145, 146, 153, 270, 271], quantum phase slip junctions (QPSJs) [155], optoelectronic approaches using photons for communication and superconductor electronics for computation [272, 273], and superconducting qubits [274]. To date, only small neuromorphic circuits have been demonstrated.

### 2.3.4.4. QUANTUM COMPUTING: CONTROL AND READOUT

The D-Wave 2000Q released in 2017 includes a superconducting chip with 128,472 Josephson junctions, of which 75% are in classical SFQ digital control circuitry to program the processor and read out the results and the remainder are either directly in qubits or in the analog coupling elements that allow qubits to interact in a programmable way. The D-Wave Pegasus P16 chip in the Advantage QA system released in 2020 includes a superconducting chip with 1,030,000 Josephson junctions, 40,484 couplers, and a maximum of 5,640 qubits [556].

SFQ pulses have been demonstrated to control a superconducting transmon qubit [275]. A Josephson arbitrary waveform synthesizer (JAWS) using an array of 102 Nb/Nb-Si/Nb JJs successfully generated control signals at 4 K [276].

AQFP appears promising for qubit control circuits due to its extremely low energy dissipation [277].

### 2.3.4.5. OTHER COMPUTING ARCHITECTURES

So-called MAGIC (Memory And loGIC) cells perform the functions of both memory and logic [278, 279].

An amoeba-inspired problem solver for a small-scale Boolean satisfiability problem (SAT) has been demonstrated using stochastic AQFP gates in a scalable architecture [280].

Memcomputing uses logic elements containing memory. Digital memcomputing machines with self-organizing logic gates have been simulated with promising results [281, 282, 283]. Needed is replication of the results reported.

### 2.3.4.6. SENSOR READOUT APPLICATIONS

A high-sensitivity and energy-efficient AQFP readout interface has been developed for an array of NbTiN superconducting nanowire single-photon detectors (SNSPDs) [284]. Improved timing information is possible with hybrid AQFP-RSFQ circuits [285].

## 2.3.5. FABRICATION FOR SCE

Josephson junctions are typically made by forming a barrier layer sandwiched between two superconducting electrodes, a structure like a thin-film capacitor shown in Figure CEQIP-1a. A variety of materials can be used, but most common for SFQ logic operating in the 4 K temperature range are junctions made with niobium electrodes separated by a thin aluminum oxide barrier layer (for details, see §2.3.5.1). The horizontal orientation shown in Figure CEQIP-1b is also possible, although less common as the barrier is more difficult to fabricate.

Weak link or nanobridge junctions consist of a small filament of superconductor or normal metal between larger electrodes. The diameter and length of the weak link need to be around the superconducting coherence length, which is about 38 nm for Nb and 5 nm for NbN (see Table CEQIP-7). Such dimensional control was difficult until recently and sandwich junctions were easy to produce, so processes for making weak link junctions have not been refined to the extent necessary for fabrication of complex circuits. Prospects for weak link junctions are explored, for example, in [20, 217, 218].

Acceptable process variations are typically tighter for Josephson junctions than for CMOS transistors, which presents fabrication challenges, especially as the push for greater energy efficiency drives designers toward smaller junctions. On the positive side, superconductor electronics has less need to reduce device sizes as Josephson junction switching speed does not depend directly on device size and superconducting interconnects reduce the penalty for sending signals over a distance. Still, there are significant advantages to increasing the number of devices on a chip, so the push to smaller device and feature sizes continues.

Table CEQIP-6 *Fabrication Processes for SCE*

Organization	Process	Wafer sizes	F [nm]		Wire material, layers	Barrier material	J <sub>c</sub> [ $\mu\text{A}/\mu\text{m}^2$ ]
			JJ	Wire			
AIST, Japan	ADP2	3 inch	□ 1000*	1000	Nb, 9	Al-AIO <sub>x</sub>	100
AIST, Japan	DGP	3 inch	□ 1000*	1000	Nb, 7	Al-AIO <sub>x</sub>	(2x) 100
AIST, Japan	HSTP	3 inch	□ 1000*	1000	Nb, 4	Al-AIO <sub>x</sub>	100
AIST, Japan	STP2	3 inch	□ 2000	1500	Nb, 4	Al-AIO <sub>x</sub>	25
D-Wave Systems, USA/Canada	SFQ	200 mm	○ 600	250	Nb, 6	Al-AIO <sub>x</sub>	100
Leibniz-IPHT, Germany	RSFQ1H	100 mm	● 3800	2500	Nb, 3	Al-AIO <sub>x</sub>	10
Leibniz-IPHT, Germany	SQUID	100 mm	● 3800	2500	Nb, 2	Al-AIO <sub>x</sub>	0.7–3.5
MIT LL, USA	SC2	200 mm	○ 600	150	Nb, 8	Al-AIO <sub>x</sub>	100, 200, 600
MIT LL, USA	PSE2 (2 JJ layers)	200 mm	○ 600 ○ 500	350	Nb, 8	Al-AIO <sub>x</sub> , Ni	100, 200, 600 > 3000
MIT LL, USA	SC1	200 mm	○ 600	250	Nb, 8; MoN <sub>x</sub> , 1	Al-AIO <sub>x</sub>	100, 200
MIT LL, USA	SFQ5ee	200 mm	○ 600	350	Nb, 8; MoN <sub>x</sub> , 1	Al-AIO <sub>x</sub>	100
MIT LL, USA	SFQ4ee	200 mm	○ 700	500	Nb, 8	Al-AIO <sub>x</sub>	100
NGC, USA	RQL25	150 mm	○ 600	250	Nb, 7	Al-AIO <sub>x</sub>	100
NIST, USA	SFQ	3 inch	○ 1500	1000	Nb, 4	Nb <sub>x</sub> Si <sub>1-x</sub>	40
NIST, USA	SQUID	3 inch, 150 mm	○ 1500	600	Nb, 3	Al-AIO <sub>x</sub>	10
NIST, USA	Voltage std	3 inch, 150 mm	○ 1500	600	Nb, 2	Nb <sub>x</sub> Si <sub>1-x</sub>	200
PTB, Germany	Voltage std	3 inch	○ 250	500	Nb, 4-5	Nb <sub>x</sub> Si <sub>1-x</sub>	40–200
SeeQC, USA	SeeQC-C2SL.d	150 mm	–	250	Nb, 2; AlMn, 1	–	–
SeeQC, USA	SeeQC-C4SL	150 mm	○ 600	250	Nb, 4, 5	Al-AIO <sub>x</sub>	1, 10, 45, 100
SeeQC, USA	SeeQC-Q5SL, -C6SL, -9SL	150 mm	○ 600	250	Nb, 4, 5, 8; NbN <sub>x</sub> , 1	Al-AIO <sub>x</sub>	10, 45, 100
SIMIT, China	Nb03	100 mm	○ 1400	1600	Nb, 3	Al-AIO <sub>x</sub>	60
SkyWater Technology, USA		200 mm	○ 600	250	Nb, 6	SiO <sub>2</sub>	10
STAR Cryo-electronics, USA	Delta-1000	150 mm	○ 3500	1000	Nb, 3	Al-AIO <sub>x</sub>	1
SUNY Polytechnic, USA	Qubit Rev.0	300 mm	○ 140	140	Al, 2	Al-AIO <sub>x</sub>	0.2–2

F : feature size, minimum; J<sub>c</sub> : JJ critical current density; □●○ : JJ layout shapes; \* 700 for AQFP

Planarized processes for superconductor integrated circuit fabrication have been developed by AIST [286, 287, 288, 289, 290, 291], MIT Lincoln Laboratory [292, 293, 294, 295, 296], NIST [297], and SeeQC, which spun out of Hypres in 2019 [298, 299]. Unplanarized processes are in use at IPHT, Star Cryoelectronics, and SIMIT [300, 301, 302]. The only 300 mm fabrication is at

## 18 Superconductor Electronics (SCE)

SUNY Polytechnic and is still exploratory [303, 304]. A few processes include MoN<sub>x</sub> superconductor layers with high kinetic inductance [231], self-shunted Josephson junctions [296, 305, 306], or  $\pi$  junctions [295].

SCE fabrication processes are summarized in Table CEQIP-6, with additional information available in the linked spreadsheet. The barrier material Al-AIO<sub>x</sub> indicates formation by thermal oxidation of an aluminum layer that is only partially consumed. To be identified are key process parameters for future monitoring. Candidates include variability of  $I_c$  and  $J_c$ ,  $R_n$  and  $I_c R_n$  product, sub-gap resistance  $R_{sg}$  or  $R_{sg}/R_n$  ratio, inductance per square, metal layer thickness, dielectric thickness, and yield.

### 2.3.5.1. NIOBIUM-BASED JUNCTION FABRICATION

Josephson junction fabrication for non-quantum applications ( $T > 1$  K) typically involves formation of the junction layer stack, commonly called the trilayer, followed by junction definition. The layer stack is typically formed as a series of steps without exposure to atmosphere. Key layers include base superconductor, barrier, and top superconductor (or counter electrode). While the barrier can be any non-superconductor or weak link, most common for superconductor electronics are insulator or semiconductor barriers as they produce higher switching voltages and speeds. The critical current through a Josephson junction depends on the quality of the superconducting electrodes, especially near the barrier layer.

#### 2.3.5.1.1. BASE SUPERCONDUCTOR FORMATION

Nb (niobium) has a critical temperature  $T_c$  of about 9.2 K and is the most common superconductor for electronic applications at liquid helium temperature, near 4 K.

The superconductive properties of Nb are strongly dependent on purity [307]. Degradation of Nb films can occur by exposure to hydrogen [308, 309] or oxygen [310]. Properties can also change over time by diffusion through the Nb and between adjacent materials such as Ti [311]. Good superconducting properties favor Nb films with a columnar grain structure and large grains, however a rough surface under thin barrier layers can cause problems. A smooth Nb surface is desired as junctions fabricated on rough surfaces show increased variation [312]. One way to reduce Nb surface roughness is to deposit the base electrode using Nb/Al/Nb multilayers [313]. Nb surface morphology also can be controlled by bias target ion beam deposition (BTIBD) [314]. Other factors affecting Nb quality include residual stress in sputtered Nb films, film thicknesses, surface morphology, deposition rate, substrate temperature during deposition, and substrate preparation [315, 316].

#### 2.3.5.1.2. BARRIER LAYER FORMATION, ALO<sub>x</sub>

As seen in Table CEQIP-6, aluminum oxide is the most common barrier for SCE with Nb electrodes. The usual process involves deposition of 5 to 10 nm of Al on the base Nb layer, exposure to oxygen gas to form ~ 1 nm of AlO<sub>x</sub> on top of the Al, and deposition of the Nb top electrode [317, 293]. The Al layer wets Nb well, smooths out roughness in the underlying Nb surface, and provides a relatively flat surface for growth of the oxide layer. The Al layer is only partially consumed during oxidation. Formation of the Al/AlO<sub>x</sub> barrier is a complex process and conduction through the barrier can depend on many factors. Simulations are providing insight into the relationships between barrier processing, structures, and properties [318, 319, 320, 321]. Plots of critical current density  $J_c$  as a function of oxygen exposure show regions with different slopes at low and high  $J_c$  [293]. Very thin barriers with high  $J_c$  shows evidence of conduction through numerous, small channels, perhaps related to defects or impurities in the oxide. As the oxide thickness increases, the number of high-conductivity channels decreases and conduction transitions to percolation between high-conductivity regions. Thicker oxide layers are dominated by tunneling of Cooper pairs (supercurrent).

Although remarkable progress has been achieved using Al/AlO<sub>x</sub> barriers, several challenges will need to be addressed for scaling circuits to higher complexity, integration density, or speed. Perhaps the most serious challenge is the thermal stability of the amorphous aluminum oxide barrier, often designated AlO<sub>x</sub> as it is not necessarily Al<sub>2</sub>O<sub>3</sub>. Many groups have observed a significant degradation of junction properties when processing temperatures exceed 200 °C. The necessity to keep processing temperatures low limits the temperature allowed for the interlayer dielectric deposition (typically SiO<sub>2</sub>), which has been optimized for Si-based microelectronics above 200 °C. The low processing temperature limit for AlO<sub>x</sub> also complicates integration of these junctions with other circuit components such as magnetic memory elements and CMOS devices.

Variation in high critical current density, self-shunted junctions is another concern. The properties of junctions are expected to be exponentially dependent on the thickness of the oxide layer, so that as the oxide thickness is reduced below 1 nm, high yield requires limiting thickness variations to less than a monolayer across large wafers, which is extremely challenging. Double-barrier junctions were proposed as a way to reduce variations across a junction and achieve self-shunted behavior at modest critical current densities but have so far yielded devices with unfavorable characteristics for high speed operation [322]. Recent fabrication improvements have dramatically reduced the number of junctions with properties outside the design range (“outliers”), but the mechanism responsible for the remaining outliers is not yet completely understood. If related to non-uniform oxide thickness or the presence of a non-uniform defect population, new approaches will be needed to achieve high yield upon further



scaling [323]. Barrier formation by atomic layer deposition (ALD) shows promise but needs to be demonstrated in a production process [324, 325, 326].

Self-shunted junctions for use in SFQ circuits can be made by various methods reviewed in [327]. Methods with  $\text{AlO}_x$  barriers include very thin barrier layers [293] or increasing the Al thickness so that the barrier includes a thicker normal metal layer in series with the insulating oxide layer [328].

### 2.3.5.1.3. BARRIER LAYER FORMATION, ALTERNATIVES TO $\text{AlO}_x$

Nb-Si barriers are deposited as amorphous silicon with niobium in solid solution. Other designations for this barrier material include  $\text{Nb}_x\text{Si}_{1-x}$  and a-Si-Nb. Nb-Si films of interest for SFQ circuits are on the insulating side of the metal-insulator transition, which means less than about 11% niobium [329]. Nb-Si has lower resistivity than  $\text{AlO}_x$ , so greater thickness is required. Nb-Si barrier Josephson junctions have been used for several years in commercial voltage standard chips containing many thousands of Josephson junctions (see § 2.2.2.2). The potential for application of Nb-Si barriers in SFQ circuits that operate at higher clock frequencies is under active investigation [305, 306, 330]. Advantages include a thicker barrier layer and thus less sensitivity to small changes in thickness. Disadvantages include low thermal stability [331], high dielectric constant [305], and difficulty in achieving uniformity across a wafer by co-sputtering [332].

Si-W barriers are deposited as amorphous silicon with tungsten in solid solution [333].

Aluminum nitride ( $\text{AlN}_x$ ) tunnel barriers have good characteristics up to high current densities, although formation by plasma nitridation of an Al layer is more difficult than the formation of  $\text{AlO}_x$  barriers [334]. Although nitride barriers are expected to have higher thermal stability than  $\text{AlO}_x$  above 200 °C, statistical studies on the stability of junction properties fabricated with higher processing temperatures have not yet been performed.

Halfniium oxide ( $\text{HfO}_x$ ) was investigated as an insulating barrier material, but fabrication of good junctions was found to be difficult [335]. Hf-Ti self-shunted resistive barriers have been made with critical voltages up to 70  $\mu\text{A}$  and  $J_c$  from 500 to 6000  $\mu\text{A}/\mu\text{m}^2$  [20]. Graphene barriers have been demonstrated using CVD compatible with wafer-scale fabrication [336].

Needed are further studies of alternative barriers to determine whether they have significant advantages over  $\text{AlO}_x$ .

### 2.3.5.1.4. TOP SUPERCONDUCTOR FORMATION

The top Nb layer is typically deposited directly on top of the  $\text{AlO}_x$  barrier using the same deposition parameters for other Nb layers. There is some concern that the thin  $\text{AlO}_x$  layer could be damaged by energetic deposition of Nb atoms or that chemical reactions could occur at the  $\text{AlO}_x/\text{Nb}$  interface. A thin layer of Al deposited on top of the barrier and under the Nb top layer can improve junction properties [337].

### 2.3.5.1.5. JUNCTION PATTERNING AND DEFINITION

After deposition of the junction trilayer, individual junctions are defined by photolithography, historically followed by wet anodization of exposed Nb and Al [338]. Note that wet anodization is not a common process in semiconductor foundries, and that processes have been developed that do not use anodization [300, 315].

### 2.3.5.2. ALTERNATIVE SUPERCONDUCTORS

While a variety of materials exhibit superconductivity [339], only a few are used in electronic circuits due to property, fabricability, and compatibility requirements. Superconductor materials and properties most relevant to superconductor electronics are included in Table CEQIP-7. The status of superconductor electronics based on materials other than Nb is summarized in following subsections.

Table CEQIP-7 Superconductor Properties for SCE

Material	$T_c$ [K] Bulk	$T_c$ [K] Thin Film (thickness)	Band gap $2\Delta_0$ [meV]	Coherence length, $\xi$ [nm]	Mag. Pen. Depth, $\lambda_L$ [nm]	$J_c$ [GA/m <sup>2</sup> ]	Crystal structure	$T_{\text{melt}}$ [K]
Al	1.18		0.34	1600	16		fcc, Al	933
In	3.41		1.0				tetragonal	430
MgB <sub>2</sub>	39	close to bulk	1.8-7.5	3.7-12 ab 1.6-3.6 c	85-180		C32	1100
MoGe	7.4	4.4 (7.5 nm) [340]	2.2			12 (250 mK)	amorphous	

Material	$T_c$ [K] Bulk	$T_c$ [K] Thin Film (thickness)	Band gap $2\Delta_0$ [meV]	Coherence length, $\xi$ [nm]	Mag. Pen. Depth, $\lambda_L$ [nm]	$J_c$ [GA/m <sup>2</sup> ]	Crystal structure	$T_{melt}$ [K]
MoN	12						hexagonal	
Mo <sub>0.6</sub> Re <sub>0.4</sub>	15	12 (20 nm) [341]					A15	
MoSi	7.5	4.2 (4 nm) [340]				11–25 (1.7 K)	amorphous	
Nb	9.2		3.0	30–38	90		bcc, A2	2750
NbN	16	8.6 (3 nm) [340]	4.9	5	270	20–40 (4.2 K)	cubic, B1	2846
NbTiN	12–16	10–14 (50 nm) [342]				9.7–20.8 (2.5 K)	cubic, B1	
NbSi	3.1	2 (10 nm) [340]	0.94			0.14 (300 mK)	amorphous	
Nb <sub>3</sub> Sn	18.3		7	4	30		A15	
NbTi	9.0		3	5	150			
Pb	7.2						fcc, A1	601
TiN	5.5						cubic, B1	3200
WSi	5	3.7 (4.5 nm) [340]	1.52			8 (250 mK)	amorphous	
Yba <sub>2</sub> Cu <sub>3</sub> O <sub>7</sub>	92		50-60	1.5 ab ~0.3 c	140 $\perp$ 700 $\parallel$		perovskite	> 1270

$\perp$  : magnetic field perpendicular to the layers;  $\parallel$  : magnetic field parallel to the layers; Strukturbericht symbols for crystal structures

Note: Blank entries do not necessarily indicate lack of available information.

### 2.3.5.2.1. NBN AND NBTiN

NbN (niobium nitride) and NbTiN (niobium titanium nitride) each have bulk  $T_c$  of about 17 K, which can be approached for films thicker than about 100 nm. Both materials have a crystal structure that does not match well with Si or SiO<sub>x</sub>, but the superconducting properties can be improved by using buffer layers [343] or III-nitride substrates [344]. NbTiN films just 4 nm thick have been fabricated with a  $T_c$  of about 10 K [345]. NbN and NbTiN films can be deposited at room temperature by reactive magnetron sputtering or by reactive bias target ion beam deposition (RBTIBD) for lower surface roughness [346].

Josephson junctions have been fabricated with insulating barriers of deposited AlN [347, 348, 349, 350], AlN formed by nitridation of an Al layer [351], thermally oxidized Al [352], deposited MgO [353, 354, 355, 356, 357], deposited MgO-AlN-MgO [358], and thermally oxidized HfO<sub>x</sub> [359]. Self-shunted junctions can be made using conductive barrier materials such as Ti-N [360] or Ta<sub>x</sub>N [358, 361, 362, 363, 364]. Note that pure Al is far more difficult to nitridize than to oxidize, which is one reason that directly deposited barriers are more common on NbN and NbTiN. Another reason is that pure Al pulls N from adjacent NbN or NbTiN, which degrades the superconducting properties of both layers. Using a Hf diffusion barrier along with tunnel junction barriers of either HfO<sub>x</sub> or Al-AlO<sub>x</sub> showed limited success and sensitivity to the thickness of the Hf layer [365].

Fabrication processes for integrated circuits have been developed [348].

Ferromagnetic Josephson junctions using NbN have been fabricated [366, 367]. GdN can function as a spin filter in NbN junctions [368].

Needed is work on magnetic shielding and flux trapping in NbN and NbTiN circuits. The magnetic penetration depth of these materials ( $\lambda_L > 200$  nm) is large, which means that much greater thickness might be required for shielding than in pure Nb ( $\lambda_L \sim 90$  nm). Nb layers might be used for shielding.

### 2.3.5.2.2. MgB<sub>2</sub>

Magnesium diboride (MgB<sub>2</sub>) has a critical temperature  $T_c$  of about 39 K and exhibits s-wave superconductivity, which implies that it can be used to make three-dimensional materials and devices more easily than with the d-wave, planar superconductors. MgB<sub>2</sub> films of good quality have been fabricated using hybrid physical-chemical vapor deposition (HPCVD) on Si wafers coated with a boron buffer layer to prevent chemical reactions between Mg vapor and the Si substrate, however deposition and growth temperatures are high (~700 °C) [369]. Josephson junctions fabricated in sandwich geometry with MgO barriers have some attractive properties, but also unacceptably large critical current distributions [370, 371]. In-plane Josephson junctions with

barriers formed by helium ion beam irradiation show reduced parameter spreads, but work is needed to increase the  $I_c R_n$  product of the junctions [371, 372, 373]. Additional challenges include lack of multi-layer interconnects and degradation of  $\text{MgB}_2$  on exposure to atmosphere, which makes patterning more difficult.

### 2.3.5.2.3. YBCO

Yttrium barium copper oxide (YBCO) is a family of crystalline compounds with a defect perovskite structure consisting of layers.  $\text{YBa}_2\text{Cu}_3\text{O}_{7-x}$  (Y123) can have a superconducting critical temperature around 90 K, although the superconducting properties are much better in the a-b plane than in the c direction. The small coherence length ( $\xi \sim 1.5$  nm in the ab plane) makes YBCO sensitive to grain boundaries and makes fabrication of Josephson junctions difficult. Challenges include high-synthesis temperatures ( $> 700$  °C), poor conductivity across high-angle grain boundaries, brittleness, lack of multi-layer interconnects, and large scatter in Josephson junction critical currents.

Grain boundary junctions in YBCO have been used to make small RSFQ circuits [374]. Large numbers of step-edge junctions have been fabricated by argon ion milling steps into an MgO substrate before deposition of the YBCO film, although  $I_c$  variation was high ( $1\sigma = 20$  to 30%) [375]. In-plane Josephson junctions with barriers formed by helium ion beam irradiation show promise [224]. Applications tolerant of Josephson junction variation seem most promising, including junction arrays for magnetic sensors and amplifiers, microwave generators, and vortex-flow transistors [376]. Applications without junctions might include superconducting interconnects between environments below 10 K and intermediate temperatures in the 20 to 80 K range where semiconductor circuits can operate with less refrigeration penalty.

### 2.3.5.2.4. OTHER SUPERCONDUCTORS

Re (rhenium) is a superconductor with a relatively weak tendency to oxidize, which is advantageous in superconducting quantum circuit and qubit applications. Re/Al-AIO<sub>x</sub>/Re Josephson tunnel junctions have been fabricated with a  $T_c$  of 4.8 K [377].

Mo–Re (molybdenum–rhenium) alloys exhibit superconducting transition temperatures up to 15 K in bulk and up to about 9 K in thin films [341]. Mo–Re thin films can be sputter deposited at room temperature and are stable even under typical carbon nanotube CVD growth conditions that require a hydrogen-methane atmosphere at 900 °C. Josephson junctions have been fabricated with barriers of Si(W) that form tungsten nanorod or nanocluster weak links in Si [378, 379, 380, 381, 382, 383, 384, 385], and graphene [386]. Challenges include the cost of Re, which is roughly 100 times that of Nb.

TiN (titanium nitride) with a  $T_c$  of 5 K has been used to make TiN/AlN/TiN junctions for use as photon detectors [387].

High-temperature superconductors (HTS) have a critical temperature  $T_c$  greater than 30 K, which includes  $\text{MgB}_2$  (section 2.3.5.2.2) and YBCO (section 2.3.5.2.3). As noted in section 2.3.3.1 Switching Devices, HTS Josephson junctions have not proven fabricable with the uniformity necessary for large scale circuits. Without adequate switching devices, HTS applications are limited to passive RF components and interconnects to higher temperatures.

Other superconducting materials (e.g., high-  $T_c$  oxides, 2D, topological) could have applications in novel devices [388].

### 2.3.5.3. FABRICATION FACILITIES AND EQUIPMENT

The IC Insights forecast for 2018 is that 300 mm wafers represented about 70% of worldwide integrated circuit capacity, 200 mm wafers represent about 25% of capacity, and almost all the remainder is for wafers of 150 mm or smaller diameter [389]. The choice of wafer size is important for SCE fabrication as fabrication processes and yield depend on the tooling available. Processes developed for one wafer size can require significant changes when migrated to a different wafer size. SCE fabrication on 300 mm wafers has begun and should help inform when or whether the benefits justify the cost [303, 304].

Magnetic layers in superconductor circuits can be fabricated using equipment developed for the general electronics and MRAM industries [390].

## 2.3.6. ELECTRONIC DESIGN AUTOMATION (EDA) FOR SCE

EDA tools developed for semiconductor circuits require modifications to be useful for designing superconducting circuits. For example, inductance—whether self or mutual—is critical in superconducting circuits. Connecting wires must have inductance values within a specified range to allow either pulse transmission or quantized flux storage. Mutual inductance within tight margins is required for the successful operation of logic gates that contain transformers, such as AQFP and RQL, while parasitic inductance and coupling must be minimized to maintain acceptable circuit operating margins. Standard EDA tools have poor inductance extraction capability, ignore the kinetic inductance important in superconductors, and cannot route wiring subject to inductance limits. Numerical inductance solvers are needed, and InductEx [391] is one three-dimensional inductance extraction tool developed for superconductor integrated circuit structures such as logic gates [392].

## 22 Superconductor Electronics (SCE)

Further, SFQ circuits use pulse-based logic, not the voltage-state logic for which most EDA tools have been developed, so that timing definitions differ. Timing parameters in SFQ circuits are state-dependent, and critical timings can exist between any pair of inputs that may exclude the clock [2, 393]. EDA tools for SCE must thus include timing extraction and HDL model generation tools that handle state-dependent pulse-based timing characteristics.

Quantum flux parametron (QFP) logic circuits have slightly different EDA requirements and tools. One difference is the need for equal currents at the inputs to a gate, which requires path balancing. A semi-custom EDA flow has been developed for QFP logic circuits [394] and a fully-automated flow is under development [395].

EDA for SCE must also address phenomena that do not affect semiconductor circuits. Device-level design and simulation, part of what is traditionally called technology computer-aided design (TCAD), has focused on Josephson junctions [396, 397]. Flux trapping analysis and mitigation is another important area. Moats in the ground planes of superconductor circuits provide low-energy locations for magnetic flux to trap during cool-down, but flux trapping analysis tools are required to calculate optimal moat positions and analyze the detrimental effects of persistent currents in superconducting loops induced by nearby trapped flux [246]. There has been recent progress on developing the basics of flux trapping analysis tools [398] and the compact model extraction required to incorporate phenomena such as flux trapping and external magnetic fields into simulation and verification tools [247].

The status of EDA for SCE has been reviewed [399, 400, 401] and recent work includes [230, 402, 403, 404, 405, 406, 407]. The ongoing IARPA SuperTools program seeks to develop a complete EDA tool chain for SCE [401, 408, 409, 410] that includes back-end capabilities for device and gate design, and front-end capabilities for behavioral-to-logic and clock tree synthesis and automated placement-and-route methods. Models for Josephson junctions are fundamental to circuit simulation. The RCSJ model is easy to implement in circuit simulators like SPICE, but the accuracy can be inadequate for high- $J_c$ , self-shunted JJs [411]. The more accurate Werthamer model is easiest to implement in simulators based on superconducting phase like PSCAN2 [412] rather than in simulators based on voltage levels like SPICE, which has resulted in the rise of dual-capability superconductor circuit simulators such as JoSIM that allows both voltage and phase-based simulation [413]. Phase-based simulation is unique to superconductor electronic circuits and is required for specific simulations such as trapped flux and the coupling thereof to superconductor circuit structures.

The superconductor EDA tools most used for analog and digital integrated circuit design today are listed in Table CEQIP-8.

Table CEQIP-8 Superconductor EDA tools

Domain/level	Application	Tool name	Highest maturity and scale	References
Physical	Technology CAD	FLOOXs	Academic – 1 device, 2D	[409, 396, 397]
Physical	Parameter/compact model extraction	InductEx, TetraHenry, lmeter, 3D-MLSI	Commercial – 1,000 devices	[391, 247]
Physical	Electrical simulation	JSIM, JoSIM, WRSpice, HSPICE	Commercial – 100,000 devices	[413]
Physical	Layout-versus-schematic verification	SpiRA	Academic – 1,000 devices	
Digital system	Logic simulation	iVerilog		
Digital system	Synthesis, place and route	qPALACE, unnamed tools for AQFP	Academic – 10,000 logic cells	[394, 404, 409]

### 2.3.7. PACKAGING AND TESTING FOR SCE

Superconductive multichip module (S-MCM) technology has been developed for superconductor chips [414, 415, 416]. The most advanced process can make S-MCMs up to 96 mm × 96 mm using interposers with 4 layers of Nb and 0.8 μm to 1 μm minimum linewidth fabricated on 200 mm silicon wafers [416]. The S-MCM roadmap is summarized in Table CEQIP-17.

Packaging for cryogenic optoelectronic devices is reviewed by [417].

Semiconductor chips are typically tested before wafer dicing and packaging of good die. Systems capable of wafer testing at cryogenic temperatures can greatly reduce testing time while increasing throughput [418]. Thermally induced voltage alteration (TIVA) is a room-temperature failure analysis technique recently found useful with SCE circuits [419, 420]. Needed is research on the extent to which TIVA at room temperature can take the place of circuit testing at cryogenic temperatures.

Failure analysis (FA) techniques for SCE are largely similar to those for other nanoelectronic technologies, but with some different materials and concerns [421].

### 2.3.8. INTERCONNECTS FOR SCE

Transmission lines, including Josephson transmission lines (JTLs) and passive transmission lines (PTLs), are covered in section 2.3.3.5.

Chip-to-chip communication using SFQ pulses has been demonstrated at data rates up to 117 Gbit/s over microstrip lines 6.4 mm long [422] and up to 82 Gbit/s over microstrip lines almost 20 mm long [415]. Double-flux-quantum pulses can be used for longer distances or improved signal-to-noise [423]. ERSFQ circuits for 16-bit parallel data transmission have been demonstrated [424].

Within the cryogenic environment, superconductors can be used for both power and data. Niobium has a superconducting critical temperature  $T_c$  of about 9 K and has been used to make coaxial cables [425] as well as flexible ribbon cable transmission lines on thin film polyimide [426]. NbTi has a similar critical temperature, but lower thermal conductivity, and has also been used to make coaxial cables [427] and microstrip ribbon cables [428]. Electroplated rhenium (Re) in multilayers with noble metals has an enhanced critical temperature of about 6 K and could have fabrication advantages [429].

Power and data need to move between the cryogenic and room temperature environments with very low heat load to the cryogenic environment. Most challenging is movement of data from a cryogenic environment due to the small energy in an SFQ pulse and the refrigeration penalty on any energy dissipated in amplifying or converting signals at cryogenic temperatures [430]. Placing signal amplifiers at multiple temperature stages can reduce total power dissipation [431, 432, 433, 434]. Electro-optical approaches proposed or under development include direct conversion [435, 436] and modulation [437, 438]. Nanowire cryotrons can produce electrical signals at the  $\sim 1$  V level necessary to drive conventional semiconductor electronics [439].

The interconnect roadmap is summarized in Table CEQIP-18.

### 2.3.9. REFRIGERATION

Cryogenic cooling technologies have developed steadily over the past few decades based on various well documented thermodynamic heat engine cycles [440] moving the industry away from a reliance on liquid cryogenics towards new cryogen-free closed cycle apparatus. This has been beneficial for the research community and is increasingly being adopted for industrial and medical applications. It is estimated that helium usage for low-temperature physics is  $\sim 4\%$  of global helium consumption and declining [441]. Not only does this enable greater access to cooling technologies through reduced operating costs, ease of use, reduced safety considerations and reduced reliance on access to liquefiers and gas supply chain it has also introduced a change in design considerations. Gone are the constraints placed on vessel size and shape considerations due to optimal cryogenic consumption performance such as neck diameter for services, cabling, cryoelectronics thermalization and staging. New considerations are available cooling powers at intermediate temperatures, the interdependence of the available cooling power at these stages, mechanical vibrations, electrical & acoustic noise, and utility & power requirements. Furthermore, applications with ‘ride through’ or ‘duty cycle’ requirements such as MRI and gyrotron beamline injection magnets have already demonstrated that hybrid structures utilizing a helium bath with integrated closed cycle cooler continuously recondensing the boiling liquid can maintain steady state operation for long term continuous operation.

Cryogenic technologies require refrigeration, unlike most other beyond CMOS technologies. Comparison at room temperature, taken as 300 K, requires accounting for the power cost of cryogenic refrigeration. The specific power of a refrigerator is defined as the input power divided by the cooling power. Note that specific power is the inverse of the coefficient of performance (COP). The specific power of an ideal Carnot refrigerator varies with temperature as  $(T_H - T_L)/(T_L)$  where  $T_H$  is the high temperature at which heat is rejected and  $T_L$  is the low temperature at which cooling takes place. Cryogenic refrigeration system efficiency, and thus specific power, varies depending on cold-end temperature, refrigeration capacity and design [442, 443].

*The approach taken is to use box plot statistics for specific cooling powers of commercial refrigeration systems at cold-end temperatures of interest. The effect of refrigeration can be presented using a simple whisker plot using only the minimum, median, and maximum specific power values rather than a full box plot. Specific powers for benchmarking and metrics use are summarized in Table CEQIP-9 and plotted in Figure CEQIP-3. The empirical fit shown in the figure (specific power  $\sim T_{cold}^{-2}$ ) has no known basis, but does show that refrigeration cost tends to*

## 24 Superconductor Electronics (SCE)

grow rapidly as the operating temperature decreases. Details are in Table CEQIP-10 through Cryogenic Refrigeration Systems for  $1\text{ K} < T \leq 10\text{ K}$

Table CEQIP-12. Note that refrigeration at  $T \sim 4\text{ K}$  is split into high- and low-power groups as their performance characteristics too different to combine. Low-power refrigerators for  $T \sim 4\text{ K}$  are often called cryocoolers.

Cryogenic refrigeration systems for  $T \leq 1\text{ K}$  are listed in Cryogenic Refrigeration Systems for  $1\text{ K} < T \leq 10\text{ K}$  Table CEQIP-12 and are typically dilution refrigerators [444].

Needed is a model for specific power values at other temperatures, perhaps using cryogenic refrigeration performance models [445, 446]. Such a model might be used to produce nominal values that are less sensitive to the collection of existing refrigerators. Improvements in efficiency are desirable and seem possible, although higher efficiency approaches are likely to cost more [447].

Table CEQIP-9 Specific Power Ranges for Cryogenic Refrigeration

$T_{\text{cold}}$	Cooling Power Range	Specific Power * [W/W]			
		Average	Low	Median	High
80 K	1.4 W to 190 kW	5.19E+01	7.18E+00	3.67E+01	1.50E+02
40 K	1.1 W to 52.7 kW	1.85E+02	2.17E+01	<b>8.63E+01</b>	7.50E+02
20 K	2 W to 100 W	4.85E+02	1.17E+02	<b>4.23E+02</b>	1.30E+03
4.5 K	( $\geq 10\text{ W}$ ) 130 W to 1000 W	4.03E+02	3.15E+02	<b>3.91E+02</b>	5.77E+02
4.2 K	(< 10 W) 0.08 W to 2.0 W	1.07E+04	4.00E+03	<b>8.30E+03</b>	3.75E+04
100 mK	0.1 mW to 1.0 mW	3.72E+07	1.27E+07	<b>2.95E+07</b>	1.07E+08
20 mK	6 $\mu\text{W}$ to 30 $\mu\text{W}$	1.13E+09	4.56E+08	<b>9.75E+08</b>	2.08E+09

\* Specific power: (W at 300 K)/(W at T cold)

Table CEQIP-10 Cryogenic Refrigeration Systems for  $T > 10\text{ K}$

Table CEQIP-11 Cryogenic Refrigeration Systems for  $1\text{ K} < T \leq 10\text{ K}$

Table CEQIP-12 Cryogenic Refrigeration Systems for  $T \leq 1\text{ K}$

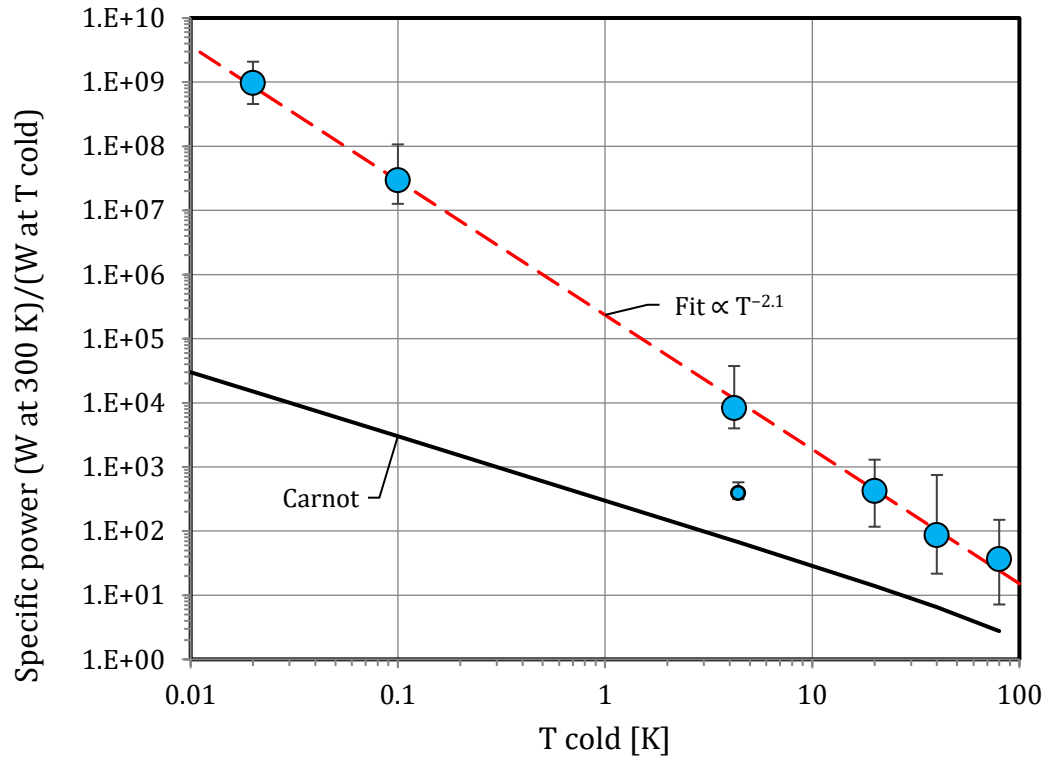


Figure CEQIP-3 Specific Power versus Cold Temperature for Cryogenic Refrigeration

At  $T \sim 4$  K,  $\circ$  is for large systems ( $>10$  W cooling power) and  $\bullet$  is for small systems.

## 2.4. BENCHMARKING AND METRICS FOR SCE

Beyond-CMOS electronics must consider new devices, circuits, and architectures. Determining which emerging or novel technologies are most promising and thus most deserving of development effort can be difficult, especially for significantly non-conventional technologies such as cryogenic electronics. Fair and effective metrics and figures of merit are needed for comparison.

### 2.4.1. DEVICE AND CIRCUIT BENCHMARKING

Recently, there have been efforts to benchmark a variety of beyond-CMOS technologies [448, 449, 450, 451]. Nikonov and Young [448] included in traditional energy-delay comparisons some state variables other than voltage (e.g., magnetization, polarization, spin current, orbital state) and extended comparisons from switching devices alone to logic circuits as large as an arithmetic logic unit (ALU). Still, the existing benchmarks and metrics did not consider superconductor electronics, and are limited as computing also requires interconnects and memories, not just logic circuits.

First, consider intrinsic device switching energy versus switching time (delay) and how to add superconductor electronics to existing comparisons. Nikonov and Young include data for beyond-CMOS devices fabricated at the 15 nm scale in Table 5 of their supplemental material [448]. For Josephson junctions in RQL technology with critical current density  $J_c = 100 \mu\text{A}/\mu\text{m}^2$  and device current  $I_c = 100 \mu\text{A}$ , the intrinsic switching energy  $E_{sw} = I_c \Phi_0 / 3 = 69 \text{ zJ}$  [98, 106]. The intrinsic switching time is taken as the SFQ pulse width, roughly FWHM [452, 453],  $t_{sw} = (\pi \Phi_0 C_s / 2J_c)^{1/2} = 1.5 \text{ ps}$  with specific capacitance  $C_s = 70 \text{ fF}/\mu\text{m}^2$  typical of junctions with this  $J_c$ .

AQFP-based logic is a benchmarking challenge as the switching device is a circuit that moves between two states semi-adiabatically. The switching energy depends on ramp rate as  $E_{sw} = 2I_c \Phi_0 t_{sw}/t_x$ , where  $t_x$  is the excitation time [106, 108]. The intrinsic switching time is  $t_{sw} = (2\pi \Phi_0 C_s / \beta_c J_c)^{1/2} = 0.21 \text{ ps}$  for the AIST, Japan ADP2 junction fabrication technology with  $J_c = 100 \mu\text{A}/\mu\text{m}^2$ , specific capacitance  $C_s = 63 \text{ fF}/\mu\text{m}^2$ , and unshunted junctions with damping parameter  $\beta_c = 190$ . For a 5 GHz clock frequency with  $t_x = 100 \text{ ps}$  and  $I_c = 50 \mu\text{A}$ ,  $E_{sw} = 0.43 \text{ zJ}$ . For AQFP gates, the delay is given not by the intrinsic junction

## 26 Superconductor Electronics (SCE)

switching time  $t_{sw}$  or by the excitation time  $t_x$ , but by the clock period divided by the number of phases. For 4-phase clocking at 5 GHz, the delay is 50 ps. Multi-excitation AQFP (ME-AQFP) [114] could increase clock frequency to 20 GHz and reduce the delay to 12.5 ps, however the energy-delay product remains constant, so the energy would increase by a factor of 4 to 1.7 zJ.

Figure CEQIP-4 shows the energy versus delay for several switching devices including RQL and AQFP. The energy-delay product for these superconducting logic technologies is seen to be competitive, even including the cost of cryogenic refrigeration. This is due to the fact that the energy-delay product is the ratio of the consumed power by the square of the speed (clock frequency) of the circuits. Since the power is fixed by external constraints (cost, volume, mass, etc.) this factor is fixed for a given application, independently from the technology that is used. Then speed, hence superconductors, come into play.

Next, consider interconnects. The energy versus delay for beyond-CMOS interconnects of 10  $\mu\text{m}$  length is plotted in Figures 7 and 8 of Pan and Naeemi [451]. For RQL, Dorjjevets, et al. [454] give data transfer energies for 32-bit Josephson transmission lines (JTL) and passive transmission lines (PTL) with  $I_c = 38 \mu\text{A}$  in their Figure 1. On a per-bit basis and removing the refrigeration allowance, the transmission energies for a 1 mm distance are  $(6.3 \text{ fJ})(1000 \mu\text{m})/[(50 \mu\text{m})(96 \text{ bit})(1000 \text{ W/W})] = 1300 \text{ zJ/bit}$  for 100  $\mu\text{m}$  by JTL and  $(12.5 \text{ fJ})/[(96 \text{ bit})(1000 \text{ W/W})] = 130 \text{ zJ/bit}$  for up to 20 mm by PTL. The delay for a JTL is about an SFQ pulse width times the number of JTL cells  $t_{JTL} = (1.5 \text{ ps})(1000 \mu\text{m})/(25 \mu\text{m}) = 60 \text{ ps}$ . A PTL consists of 2 JTL cells on each end of a ballistic transmission line, so the delay for a PTL is  $t_{PTL} = (4)(1.5 \text{ ps}) + (1000 \mu\text{m})/(100 \mu\text{m/ps}) = 16 \text{ ps}$ , where  $c/3 \approx 100 \mu\text{m/ps}$  is the approximate speed of propagation on the PTL. Note that JTLs and PTLs have different characteristics beyond energy and delay. For example, the repeater distances are 25  $\mu\text{m}$  for JTL versus 20 mm for PTL, and area is required from different layers. For JTLs and PTLs in the RSFQ logic family, see [240].

AQFP gates output currents, not SFQ pulses, and have different interconnect characteristics. Buffer (repeater) cells have the energy and delay of a single AQFP gate with a maximum drive distance of about 1 mm [455]. AQFP (5 GHz) interconnect energy and delay are thus 0.43 zJ and 50 ps for distances of 0 to 1 mm. For 20 GHz operation the delay decreases to 12.5 ps, and the energy increases to 1.7 zJ.

Figure CEQIP-5 shows the energy versus delay for interconnects of 1 mm length including RQL and AQFP. The energy-delay product for these superconducting logic technologies is seen to be better than the alternatives, even including the cost of cryogenic refrigeration. This plot for interconnects of a single length does not show that the energy remains the same for AQFP out to 1 mm and for PTL (RQL) out to 20 mm. Note that an error was made in the equivalent 2017 figure (BC4.1b) that made the differences appear smaller: the alternative technologies were plotted for 10  $\mu\text{m}$  length and the superconductor technologies for 100  $\mu\text{m}$  length, 10 times longer.

Some applications require the electronics to operate at cryogenic temperatures. Examples include some digital-RF receivers, focal plane arrays for astronomy, quantum computing, and magnetic resonance imaging (MRI). For operation at 4 K, all technologies would require refrigeration, in which case RQL and AQFP have a clear advantage.

A generalized methodology for comparing superconductor electronics with other technologies will require several developments. To avoid the effort of full-circuit simulations, performed in [454], models must be developed for energy, delay, and circuit area for a variety of superconductor technologies. The effort can start from previous work such as [106, 456, 457], but will need to be extended considerably. Metrics are needed that allow comparison of technologies at very different feature sizes. Interconnect benchmarking is needed as a function of transmission distance. Clocking delay must be included for logic families such as RSFQ that require clocking of each gate.



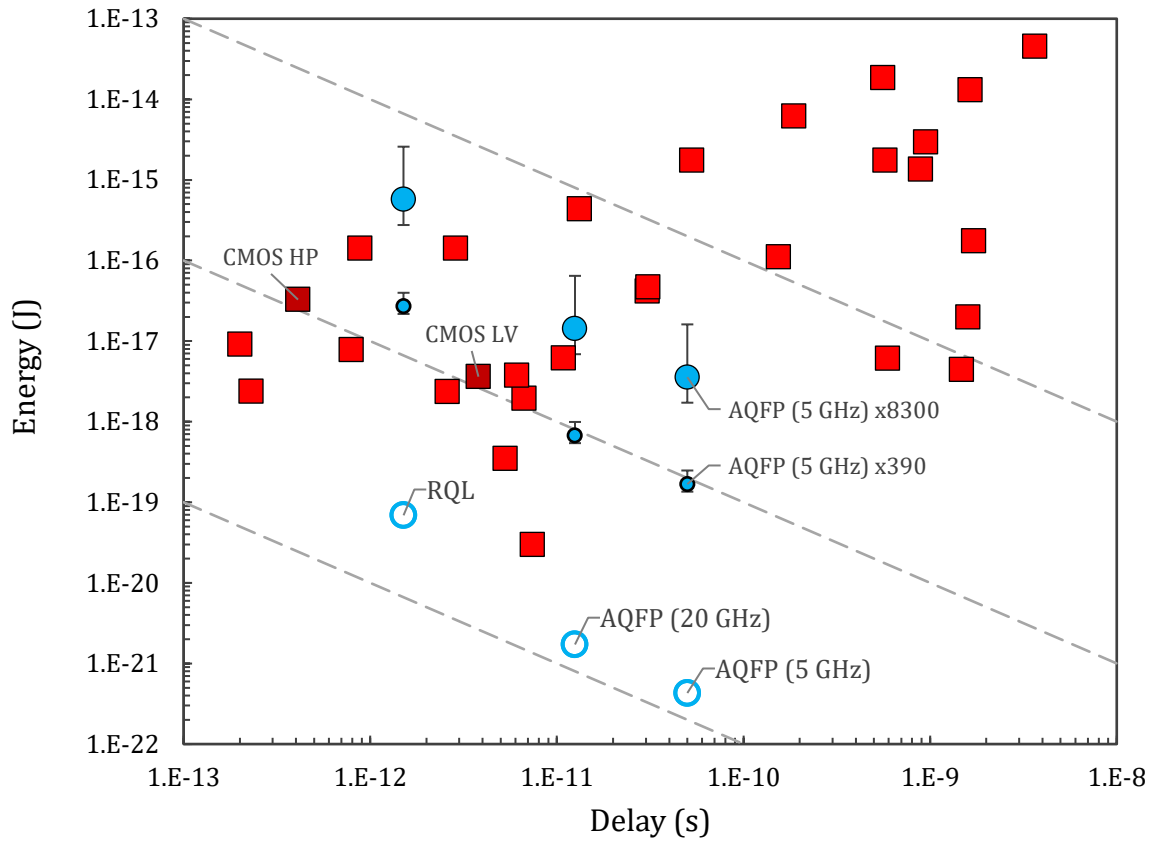


Figure CEQIP-4 Energy versus Delay for Intrinsic Elements

Note: Superconductor devices (AQFP, RQL) have open circles  $\circ$  for operation at  $\sim 4$  K and solid circles with whiskers showing ranges including refrigeration power from Table CEQIP-9. The  $\bullet$  is for large refrigeration systems ( $>10$  W cooling power) and  $\odot$  is for small systems (cryocoolers). All other devices are from [451]. Dashed lines show constant energy-delay products.

Table CEQIP-13 Energy versus Delay for Intrinsic Elements

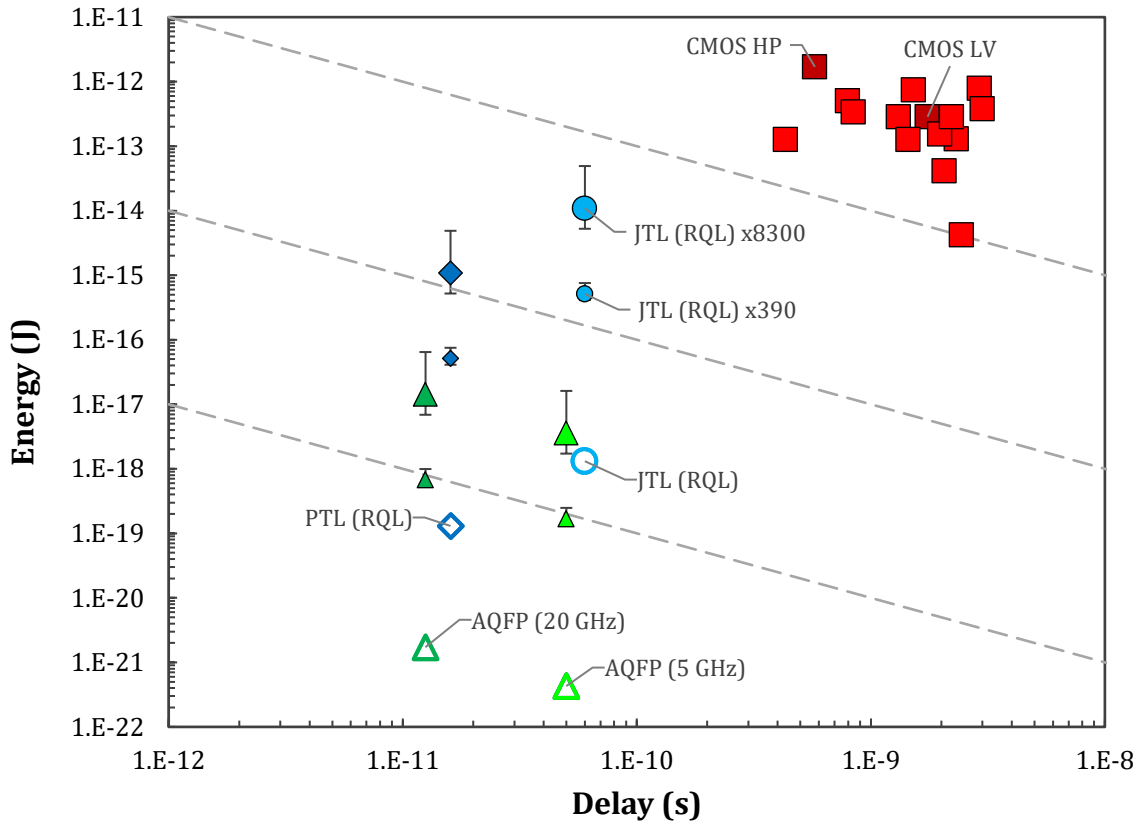


Figure CEQIP-5 Energy versus Delay for Interconnects of 1 mm Length

Note: Superconductor devices (AQFP, RQL) have open symbols (e.g.,  $\circ$ ) for operation at  $\sim 4$  K and solid symbols with whiskers showing ranges including refrigeration power from Table CEQIP-9. Small, solid symbols (e.g.,  $\bullet$ ) are for large refrigeration systems ( $>10$  W cooling power) and large, solid symbols (e.g.,  $\bullet$ ) are for small systems (cryocoolers). All other devices are from [451]. Dashed lines show constant energy-delay products.

Table CEQIP-14 Energy versus Delay for Interconnects of 1 mm Length

Table CEQIP-14b Energy versus Delay for Interconnects of 0.01 to 1 mm Length

### 2.4.2. SCALING OF DEVICES AND CIRCUITS

As introduced in section 2.1, single flux quantum (SFQ) digital circuits use superconducting loops. The superconducting phase must be continuous and single valued at any point around the loop, which requires that the phase change around the loop must be an integer multiple of  $2\pi$ . For a superconducting loop with inductance  $L$  and circulating current  $I$ , the requirement is that the loop contain magnetic flux  $n_{fj} \Phi_0 = LI$ , where  $n_{fj}$  is an integer and  $\Phi_0$  is the magnetic flux quantum. Josephson junctions in the loops limit the circulating supercurrent to  $I_c$ , thus the required inductance is  $L = n_{fj} I_c / \Phi_0$ , where the value of  $n_{fj}$  is between about 0.5 and 1.5, depending on whether a loop is intended to store a flux quantum ( $n_{fj} > 1$ ) or not ( $< 1$ ). Scaling the loops to smaller sizes depends on scaling both the inductive elements and Josephson junctions. Phase shift can be provided by devices other than inductors, as noted in section 2.3.3.3.

Scaling of phase shift elements should consider system-wide effects. For example, the bias current supply network can more than double the power, energy, or area required by the functional portion of the circuit. A study of phase shift element scaling, costs, and benefits is needed to construct a technology roadmap.

### 2.4.3. SYSTEM AND APPLICATION BENCHMARKING

Pan and Naeemi [450] make the case that some beyond-CMOS devices offer fundamentally different or unique characteristics best suited to novel circuit implementations not well evaluated by traditional metrics and benchmarks. Needed are methods to more accurately predict the performance of computing systems based on emerging technologies or approaches to computing. Metrics for cryogenic electronics are expected to start with figures of merit comparing performance (e.g., computation, data movement, memory capacity) against required resources such as chip area.

## 2.5. ACTIVE RESEARCH QUESTIONS FOR SCE

Difficult challenges for SCE are described in Table CEQIP-15. Future work includes identification of key challenges and tracking of active research.

Table CEQIP-15 Difficult Challenges for SCE

<i>Near-Term Challenges: 2020-2027</i>	<i>Description</i>
Integrated circuit fabrication	Foundries for commercial production now process 200 mm or smaller wafers using equipment lacking state-of-the-art capability. Achieving the yield and throughput for large-scale applications will require process improvements and, possibly, a move to 300 mm wafers. Planarization and thickness control are challenging in stacks of multiple superconductor layers when the layer thicknesses remain the same, rather than increasing with layer number as in CMOS back-end processes.
Device variability	Variation in device parameters reduces the operating margins of circuits. Needed is better process control, better device designs, or circuit designs that tolerate or compensate for device variability.
High critical current density junctions ( $J_c > 100 \mu\text{A}/\mu\text{m}^2$ )	The $\text{AlO}_x$ barrier in Josephson junctions with $J_c = 100 \mu\text{A}/\mu\text{m}^2$ is now approximately 1 nm thick. Thinner barriers increase $J_c$ , allowing smaller and faster JJs. For $J_c > 500 \mu\text{A}/\mu\text{m}^2$ the sub-gap resistance can be sufficiently low to eliminate the need for shunt resistors. Uniformity control will be challenging as defects typically dominate conduction through thinner barrier layers and thickness control is also difficult. Materials and process development is needed to improve uniformity and control of devices with high $J_c$ .
Superconducting materials with higher critical temperature ( $T_c$ )	Higher $T_c$ materials would allow operation at higher temperatures, which would significantly reduce the required cooling power, or would make circuits less sensitive to self heating at temperatures well below $T_c$ . Niobium (Nb) is the superconducting material most common for 4 K applications. Changing the superconducting material would require significant development and might also require changes in the junction barrier. Processes for large-scale integrated circuit fabrication require multiple superconductor layers, vias, and high-uniformity junctions. Changes in other materials-dependent properties such as magnetic penetration depth $\lambda$ , superconducting coherence length $\xi$ , and kinetic inductance would require redesign of devices and circuits.

### 30 Superconductor Electronics (SCE)

<i>Near-Term Challenges: 2020-2027</i>	<i>Description</i>
Magnetic materials fabrication process integration	<p>Magnetic materials are desired to make both memory and passive devices and can enable compact high-value inductors and high-coupling factor mutual inductances. Integrating magnetic materials into foundry processes will be difficult.</p> <p>Materials and device geometries with lower magnetization are needed to reduce switching energy. Magnetic properties at room and cryogenic temperatures do not seem to correlate, so measurement is required until adequate theory can be developed.</p> <p>Better fixed magnetic layer materials are needed as nickel has problems that will prevent scaling to small sizes.</p> <p>Interface roughness and morphology must be controlled for good magnetic properties.</p>
Electronic design automation (EDA) tools	<p>EDA tools for CMOS are not adequate for SCE. Inductance is critical in superconducting circuits and connecting wires must have inductance values within a specified range. Circuit simulators and timing analysis must be modified for pulse-based logic. Flux trapping analysis—both for trapping probability and the coupling of trapped flux in moats to circuits—is required, while analysis of the coupling of bias current and ground plane return currents to circuit structures are also important and difficult at chip level.</p> <p>The modeling of Josephson junction dynamics for EDA simulation tools is currently not sufficiently accurate for self-shunted junctions, and the extraction of more complete simulation models with the aid of technology CAD (TCAD) methods will become important as device size shrinks.</p>
Switching devices	<p>Fan-in or fan-out greater than one requires additional circuitry due to the low gain and low isolation provided by Josephson junctions (in contrast to semiconductor transistors). SFQ-compatible devices with greater gain and isolation are under development, but not yet proven in large-scale fabrication.</p>
Transformer miniaturization or replacement	<p>Current transformers rely on magnetic coupling between inductors, which seems difficult to scale to very small dimensions. Needed are transformer alternatives or scaling approaches that allow significantly higher logic gate and memory cell density.</p>
Shrinking devices and interconnects at dimensions of tens of nanometers	<p>The state of the art for complex superconducting circuits deal with Josephson junctions with sizes down to 200 nm and passive circuitry with linewidth down to about 90 nm (for nanowire-based detectors for instance). These dimensions are of the order of the London penetration depth but higher than the superconductor coherence length in most of cases and really much higher than CMOS typical scales.</p> <p>What happens in practical electronic circuits when 1, 2 or even the 3 dimensions of a superconducting object reach or go even below the coherence length? Can we make nanodevices of the same dimensions of semiconductor circuits?</p>
Interconnects, on-chip and chip-to-chip	<p>Superconducting passive transmission lines (PTLs) used for ballistic transport of SFQ pulses must have low impedance to match the low impedance available from Josephson junction drivers. Grounded shields are also required to avoid crosstalk, which require more area and reduce circuit density. Also needed are higher-impedance Josephson junctions or methods for making smaller transmission lines with lower impedance.</p>
Interconnects between cryogenic and room temperature environments	<p>Interconnects for both digital and analog signals require careful optimization to balance electrical and thermal properties. Use of cryogenic semiconductor and photonic components in data links require further development.</p>

<i>Near-Term Challenges: 2020-2027</i>	<i>Description</i>
Packaging for SCE	<p>Operation at cryogenic temperatures requires different materials, packaging, testing, and cooling systems, much of which will require new development. State-of-the art systems package a few superconductor ICs in a commercial cryostat. Scaling up to systems with higher complexity chips and multi-chip modules will require further reduction of power consumption by all components.</p> <p>Josephson junctions are extremely sensitive to magnetic fields and require shielding, which becomes more challenging as system volumes grow.</p>

<i>Long-Term Challenges: 2028-2034</i>	<i>Description</i>
Temperature limits compatible with CMOS fabrication processes	<p>Nb/Al-AlO<sub>x</sub>/Nb Josephson junctions are sensitive to temperature. Fabrication processing temperatures are currently limited to less than 200 °C, which requires different processes than those used in CMOS technology, which has a limit of 400 °C. A different barrier to allow use of standard CMOS processes would allow access to existing processes used to make fine features and reduce process development costs, but requires new barrier development.</p>
Cryogenic refrigeration	<p>The cost of refrigeration can be prohibitive for small systems that do not require a cryogenic environment for some other reason. Cryogenic refrigerators have improved immensely, driven in part by the requirement for the trouble-free operation of MRI systems in hospitals. Still, improvements in the efficiency of small refrigerators (less than 1 W at 4 K) would reduce the system size for which superconducting computing becomes competitive.</p> <p>More efficient or lower cost refrigeration systems for temperatures below 10 K would help to reduce operating costs.</p>
Optical input/output (I/O)	<p>Communication with room-temperature systems and networks will require a high-data-rate I/O, but interconnection cannot introduce significant heat into a low-temperature environment. Optical fiber digital links would be ideal, but efficient SFQ-to-optical converters must be developed.</p>
Cost	<p>Costs of superconductor electronic devices, circuits, and systems are presently high, partly due to low fabrication volumes.</p>
Higher temperature ( $T_c$ ) superconductors	<p>The energy-delay product of a digital gate is given by the power consumption divided by the square of the speed. It gives a good advantage to superconductors, counterbalanced by the fact that the integration density is currently much smaller than for CMOS. Moreover, interconnects are necessary for complex multi-chips systems and their limitations between chips and between temperature stages will dominate the ultimate system performances. The use of self-shunted Josephson junctions <b>with <math>T_c</math> above 30 K and with <math>R_n I_c</math> products in the 5-10 mV range is very challenging</b>, but would open the range of applications and increase circuit performance significantly, for example: clock frequencies close to 1 THz, reduced need for signal amplification for transmission to room temperature environments, much more energy-efficient refrigeration above 20 K, and higher circuit density in absence of external shunt resistors.</p>

## 2.6. ROADMAPS FOR SCE

Of the areas in cryogenic electronics (SCE, cryo-semi, QC), the largest market potential and need for improved capability are in the SCE and QC areas. A roadmap for SCE will be developed first as the technology and needs are better understood. Past SCE roadmapping efforts provide a base for future efforts [11, 399, 453, 458, 459, 460, 461, 462, 463, 464].

The roadmap for fabrication of digital SCE circuits is summarized in Table CEQIP-16, with additional information in the linked spreadsheet.

Foundry and fabrication are key technology areas for SCE and face some challenging decisions. Foremost is identification of suitable foundries. Of the facilities currently capable of producing complex superconductor circuits (> 100,000 Josephson junctions), MIT Lincoln Laboratory is not allowed to produce commercial products, and D-Wave Systems has limited access. At least one foundry that can handle the materials specific to SCE and produce commercial products with sufficient yield is needed. Multi-project wafer (MPW) service is desirable and will require well-characterized processes and more complete process design kits (PDKs) than currently available.

New materials, processes, and devices will need to be developed. Approaches to increase circuit density and complexity include: smaller feature sizes, stud vias, high sheet resistance layer, increase critical current density  $J_c$ , self-shunted JJs, increase wiring layers, multiple JJ layers, high kinetic inductance layers, magnetic JJs, stacked JJ inductors, or ac-to-dc rectifiers. How these will be developed and incorporated into the foundries is an open question. The achievable rate of progress must be considered.

Table CEQIP-16 *Fabrication Roadmap for Superconductor Electronics (SCE) – Digital Circuits*

Year	2019	2020	2022	2024	2026	2028	2030
<b>Digital SCE Fabrication</b>							
"Node Range" label	"250"	"250"	"150"	"150"	"90"	"90"	"65"
Substrate material, maximum size (mm)	Si, 200	Si, 200	Si, 200	Si, 200	Si, 300	Si, 300	Si, 300
<b>Wiring</b>							
Superconductor	Nb	Nb	Nb	Nb	Nb	Nb	Nb
Supercond. layers	8	8	10	10	12	12	14
Linewidth, min. (nm)	250	250	150	150	90	90	65
I <sub>c</sub> , minimum (μA)	200	200, 1200	100, 580	100, 580	50, 290	50, 290	20, 110
<b>Junctions, Switching</b>							
Junction materials	Al/AIOx	Al/AIOx	Al/AIOx	Al/AIOx	Al/AIOx	Al/AIOx	Al/AIOx
Junction layers	1	2	2	2	2	2	2
Junction critical current densities, J <sub>c</sub> (μA/μm <sup>2</sup> )	100	100, 600	100, 600	100, 600	100, 600	100, 600	100, 600
Minimum junction diameter (nm)	500	500	350	350	250	250	150
Min. junction critical current, I <sub>c</sub> (μA)	20	20, 118	10, 58	10, 58	5, 29	5, 29	2, 11
Killer defect density per layer (1/cm <sup>2</sup> )	< 0.1	< 0.1	< 0.1	< 0.1	< 0.1	< 0.1	< 0.1
J <sub>c</sub> wafer-to-wafer variation	10%	3%	3%	3%	3%	3%	3%
Maximum relative spread (σ/I <sub>c</sub> ) at minimum I <sub>c</sub>	3%	3%	3%	3%	3%	3%	3%

Year	2019	2020	2022	2024	2026	2028	2030
<b>Junctions, Magnetic (Pi)</b>							
Junction materials		Ni	Ni	Ni	Ni	Ni	Ni
Junction layers	0	1	1	1	1	1	1
Junction critical current densities ( $\mu\text{A}/\mu\text{m}^2$ )		3000	3000	3000	3000	3000	3000
Junction diameter, minimum (nm)	500	500	350	350	250	250	250
<b>Resistors</b>							
Resistor material	Mo, MoNx	Mo, MoNx	Mo, MoNx	Mo, MoNx	Mo, MoNx	Mo, MoNx	Mo, MoNx
Resistor layers	1	1	1	1	1	1	1
Resistor sheet resistance ( $\Omega/\square$ )	2, 6, 10	2, 6, 10	2, 6, 10	2, 6, 10	2, 6, 10	2, 6, 10	2, 6, 10
<b>HKI (high kinetic inductance) Layers</b>							
HKI material	MoNx	NbNx	NbNx	NbNx	NbNx	NbNx	NbNx
HKI layers	1	1	1	1	1	1	1

The superconductor multi-chip module (S-MCM) roadmap is summarized in Table CEQIP-17. Future packaging and integration roadmaps might include parameters such as contact count and layout, or memory interface specifications. A goal of this roadmap is to avoid duplication of roadmaps for conventional electronics and to maintain compatibility where possible [465].

Table CEQIP-17 *Fabrication Roadmap for Superconductor Electronics (SCE) — S-MCM*

Year	2019	2020	2022	2024	2026	2028	2030
<b>MCM Substrate Fabrication</b>							
Substrate material, maximum size (mm)	Si, 48x48	Si, 48x48	Si, 96x96	Si, 200	Si, 300	Si, 300	Si, 300
Superconductor	Nb	Nb	Nb	Nb	Nb	Nb	Nb
Superconductor layers	4	4	6	6	8	8	8
Linewidth, minimum (nm)	800	800	800	800	800	800	800
Superconductor	Nb	Nb	Nb	Nb	Nb	Nb	Nb
Impedance, single-ended ( $\Omega$ )	50	50	50	50	50	50	50
Loss (dB/m), crosstalk (dB)	< 2, < -40	< 2, < -40	< 2, < -40	< 2, < -40	< 2, < -40	< 2, < -40	< 2, < -40

The interconnect roadmap is summarized in Table CEQIP-18, with additional information in the linked spreadsheet. Interconnects can be in forms such as wires or ribbon cables and the materials can be superconducting, normal metal, or optical.

Table CEQIP-18 *Interconnect Roadmap for Cryogenic Electronics*

Year	2019	2020	2022	2024	2026	2028	2030
<b>Cables, Superconducting, &lt; 5 K</b>							
Cable type	Coaxial, Single	Coaxial, Single	Flex Cable, Microstrip	Flex Cable, Microstrip	Flex Cable, Stripline	Flex Cable, Stripline	Flex Cable, Stripline
Superconducting material, T <sub>c</sub> (K)	NbTi, 9	NbTi, 9	NbTi, 9	NbTi, 9	NbTi, 9	NbTi, 9	NbTi, 9
Data rate per lane (Gb/s)	25	25	15	15	30	30	50
Lanes per cable	1	1	10	10	20	20	40
Pitch (mm)							
Edge data rate (Gb/s-mm)	25	25	100	100	400	400	1000
Impedance ( $\Omega$ )	5 to 50	5 to 50	5 to 50	5 to 50	5 to 50	5 to 50	5 to 50
Loss (dB/m), crosstalk (dB)	< 2, < -40	< 2, < -40	< 2, < -40	< 2, < -40	< 2, < -40	< 2, < -40	< 2, < -40
Connector type							
<b>Cables, 4 to 60 K</b>							
Cable type	Coaxial, Single	Coaxial, Single	Flex Cable, Microstrip	Flex Cable, Microstrip	Flex Cable, Stripline	Flex Cable, Stripline	Flex Cable, Stripline
Superconducting?	No	No	Partial	Partial	Yes	Yes	Yes
Superconductor	-	-	ReBCO	ReBCO	ReBCO	ReBCO	ReBCO
Data rate per lane (Gb/s)	50	50	15	15	30	30	50
Edge data rate (Gb/s-mm)	40	40	100	100	400	400	1000
Impedance, single-ended ( $\Omega$ )	50	50	50	50	50	50	50
Loss (dB/m), crosstalk (dB)	< 2, < -40	< 2, < -40	< 2, < -40	< 2, < -40	< 2, < -40	< 2, < -40	< 2, < -40

### 3. CRYOGENIC SEMICONDUCTOR ELECTRONICS (CRYO-SEMI)

#### 3.1. INTRODUCTION

Reasons for operating semiconductor electronics at cryogenic temperatures include: 1) performance improvement (e.g., lower noise, higher speed, increased efficiency) or 2) to support a sensor, actuator, or other device in a cryogenic environment. For a brief introduction, see [466].

In the 1980s ETA Corporation built several computers with as many as 2000 CMOS chips operating in liquid nitrogen [467]. More recently, commercial cryogenic electronic components were evaluated for suitability at 4.2 K and used successfully to build a complete digital to analog multiplexer [468].

In addition to cryogenic CMOS circuits, bipolar technologies (e.g., SiGe heterojunction bipolar transistors) offer advantages in higher operating speeds when cooled to lower temperatures. While standalone cryogenic semiconductor circuits may not offer a compelling advantage over their room-temperature counterparts due to the higher power consumption required for cryogenic refrigeration, they might in applications requiring cryogenic devices and circuits. Since cryogenic semiconductor devices operate over a wide range of temperatures, one can optimize the overall power consumption of a hybrid-temperature system by selecting the appropriate operating temperature of different cryogenic semiconductor circuits and subsystems. In combination with superconductor electronics, a wide range of cryogenic semiconductor circuits have potential use. These include memory, processor, and amplifiers for digital data links [431, 432, 433], as well as microwave analog signals.

General references include [469, 470]. A review by Valentine and McCluskey covers cryogenic semiconductor devices and packaging [471].



### 3.2. APPLICATIONS AND MARKET DRIVERS FOR CRYO-SEMI

Advances in cryogenic semiconductor capabilities historically have been driven by the needs of sensors such as low-bandgap semiconductor detectors operated at cryogenic temperatures. Applications tended to be in the medical, scientific and aerospace/defense markets. In recent decades, the rapid improvement of semiconductor performance following to Moore's law and Dennard scaling made development of cryogenic semiconductors for higher performance too difficult to justify. However, as Moore's law nears its end and new paradigms are being explored for high-performance computing, cryogenic semiconductors could play an enabling role.

Quantum computing research and development is driving increased investment in cryogenic electronics, including cryogenic semiconductors. Quantum computers that operate at cryogenic temperatures, typically in the millikelvin temperature range, require communication with and control by classical (non-quantum) electronic systems. The closer the classical systems can operate, both in distance and temperature, the better. Cryogenic semiconductor electronics developed for quantum computing is also finding applications elsewhere. For example, Rambus initially started development of cryogenic semiconductor memory in support of quantum computing efforts at Microsoft, but more recently has been pursuing broader applications that benefit in power/performance metrics [472].

Application areas and market drivers considered by the IRDS Systems and Architectures (SA) and Application Benchmarking (AB) teams [10] are shown in Table CEQIP-19. Current status of applications in operating temperature ranges above and below 10 K are covered in § 3.3.2 and § 3.3.3, respectively.

Table CEQIP-19 Matrix of Application Areas and Market Drivers for Cryogenic Semiconductors

Application Areas	Market Drivers			
	Aerospace/Defense	Cloud	Scientific	Medical
Sensors & Sensor Interfaces	G		G	G
ADC/Mixed Signal	G		X	X
Digital Logic	X	P	X	
Memory	X	X, P		

X: important application; G: critical gating application; P: power-sensitive application.

### 3.3. PRESENT STATUS FOR CRYO-SEMI

#### 3.3.1. TRANSISTOR CHARACTERIZATION AND MODELING

While some semiconductor devices and circuits have been found to function at cryogenic temperatures, design and optimization specifically for cryogenic operation will require further device characterization and model development.

Early work showed that MOSFET models covering a large temperature range from cryogenic to room temperatures need to consider incomplete ionization in addition to the usual expressions for temperature dependence in compact models [473, 474]. As a first step to a full compact model ranging from 4.2 K to 300 K, long channel equations covering the full temperature range were developed and verified against experiment [475]. Recent work includes [476].

Transistor characterization was extended over time to more modern technologies, either down to 77 K [477, 478, 479] or to near 4 K [480, 481, 482, 483]. One publication studies behavior at 4 K and at 100 mK and discusses compact modeling, while showing that the region both < 40 nm and < 4 K remained unexplored [484]. On-chip microwave passive components have been characterized and modeled in 40 nm CMOS up to 30 GHz at 4 K [485]. Advanced semiconductor device physics and performance down to 20 K has been reviewed, including fully depleted ultrathin film SOI devices, tri-gate, FinFETs, omega-gate nanowire FETs, and 3D-stacked SiGe nanowire FETs [486].

Research needs for high-energy physics applications presented in 2013 included cryogenic CMOS device models for technology nodes 130 nm and below [487]. Since that time, considerable advances have been made in cryogenic modeling, driven by both digital and sensing applications. Compact models supporting 4 K operation have been developed and validated nanometer scale technologies (160 nm, 40 nm, 28 nm) [484, 488]. It has been experimentally demonstrated for a 40 nm CMOS process that variability increases at cryogenic temperatures, and that the conventionally-used Pelgrom and Croom models for mismatch

## 36 Cryogenic Semiconductor Electronics (Cryo-Semi)

continue to apply at higher temperatures [483]. A study of 28 nm FDSOI MOSFETs at cryogenic temperatures down to 100 mK found that they outperformed 40 nm bulk MOSFETs in all aspects, including variability [489].

Development of unified models that offer accuracy across the deep cryogenic to room temperature range is an area of active research [475, 490, 491]. Reliability studies for cryogenic CMOS have focused on hot carrier degradation, which is generally accepted as the dominant failure mechanism at low temperatures [492]. Nevertheless, bias temperature instability (BTI) stress could play a role at cryogenic conditions, especially in modern CMOS devices, and should be addressed.

### 3.3.2. APPLICATIONS $\geq 10$ K

In the late 1980s DRAM at 77 K was evaluated for performance improvement giving the shortest access latencies at the time [493, 494]. More recently, DRAM at 77 K was proposed as a memory system for computers using superconducting electronics [495]. Several commercial DRAM chips have been found to work at temperatures as low as 77 K [496] and their retention behavior between 77 K and 360 K was studied [497]. Evaluation of a cache architecture with SRAM and DRAM caches operating at 77 K shows 2 times faster cache access and 2 times larger capacity compared to conventional caches running at the room temperature [498]. CryoCore, a core microarchitecture optimized to maximize performance and area efficiency while minimizing the cooling cost at 77 K, is projected to achieve 41% higher single-thread performance for the same power budget and 2 $\times$  higher multi-thread performance for the same die area [499].

Charge-trapping memory (CTM), recognized as one of the most promising non-volatile memories in the industry, has good retention and endurance performance, low power consumption, and compatibility with standard CMOS processes. Silicon–oxide–nitride–oxide–silicon (SONOS) is one of the most representative and widely studied CTMs. Recently, CTM has been developed and characterized in the 300 K to 10 K temperature range [500].

### 3.3.3. APPLICATIONS $< 10$ K

#### 3.3.3.1. SENSORS AND SYSTEMS

Cryogenic multi-channel readout systems using gallium arsenide junction field-effect transistor (GaAs JFET) integrated circuits (ICs) were developed for a multipixel camera for astronomical observation [501].

#### 3.3.3.2. QUANTUM COMPUTING: CONTROL AND READOUT

Quantum computing applications of cryogenic CMOS have been under development recently. Overviews of the needs for cryogenic CMOS in quantum computing are given in [502, 503]. Further work includes FPGA based approaches [504, 505, 506] and CMOS-based circuit designs of cryogenic low noise amplifiers and oscillators [507]. CMOS control chips have been demonstrated to operate at  $T \sim 4$  K for superconducting transmon qubits [508] and for spin qubits [509]. Specially-developed CMOS chips with digitally multiplexed input lines can operate at mK temperatures to reduce the number of control lines coming from higher temperatures [510, 511, 512].

#### 3.3.3.3. HYBRID SEMICONDUCTOR – SUPERCONDUCTOR CIRCUITS

Hybrid circuits combining semiconductor and superconductor elements operating at cryogenic temperatures have been developed [513, 514, 515]. Van Duzer et al. [516] demonstrated a hybrid RSFQ-CMOS memory operated at 4 K. The 64 Kibit CMOS memory chip was fabricated by TSMC using 65 nm technology. The power dissipation of 12 mW at 1 GHz operation at 4 K is acceptable for small to medium circuits. Konno, et al., [517] improved the design, reducing the power by 54%. Proposed is an even more energy-efficient hybrid memory using superconducting nanocryotron (nTron) drivers and CMOS memory arrays [518].

A superconductive field-effect transistor might be useful as an interface between CMOS and SFQ circuits [519].

Hybrid superconductor-semiconductor digital data links using cryogenic SiGe heterojunction bipolar transistors (HBTs) are being developed. In these links the gain and the corresponding power consumption are distributed over the 4 K to 300 K temperature range for overall optimization of the link figure of merit (energy per bit) [431, 432, 433, 434].

Optoelectronic devices combining superconductors with semiconductors are under development and might have applications in quantum information processing or interfaces between cryogenic electrical and optical communications [520]. Packaging for cryogenic optoelectronics is reviewed in [521]. Proposed are hybrid semiconductor-superconductor neural networks for neuromorphic computing [272].

Superconductive multichip module (S-MCM) technology has been developed to support integration of superconductor and semiconductor circuits [416].

### 3.4. ACTIVE RESEARCH QUESTIONS FOR CRYO-SEMI

One critical impediment to effective utilization of these cryogenic models is the lack of integration into foundry process design kits. This has historically been a captive effort within the organization performing circuit design activities, and hence has been a barrier to entry for newer design teams.

A review paper has recently been published by IMEP-LAHC comparing the physics and performance of various nanoscale devices at cryogenic temperatures [486]. In addition to research oriented towards the cryogenic utilization of semiconductor devices, observation of cryogenic operation also has general utility in understanding and measuring the physics of carrier transport [522].

## 4. QUANTUM INFORMATION PROCESSING (QIP)

### 4.1. INTRODUCTION

Quantum information is the information of the state of a quantum system. While quantum effects tend to become important at the scale of atoms, they also can affect the behavior of macroscopic systems such as superconducting circuits at extremely low temperatures, typically below 0.1 K. Quantum information processing (QIP) involves encoding, transforming, and decoding quantum information.

Areas of QIP covered in this section include quantum computing and simulation, quantum communication, and quantum sensing. Each is introduced briefly in the following subsections.

#### 4.1.1. QUANTUM COMPUTING AND SIMULATION: INTRODUCTION

Quantum computing and simulation use quantum phenomena of superposition (existence in multiple states at once) and entanglement (correlation between qubits) to solve problems. For a deeper introduction to quantum computing than provided here, material is available spanning the range from basic and easy to follow [523, 524, 525, 526] to suitable for those undertaking serious study [527, 528].

Whereas conventional digital computing uses bits with values of either '0' or '1', quantum computing uses qubits that can have a quantum-mechanical *superposition* of '0' and '1' at the same time. The probability of being in either state can range from 0 to 1 (100%), but the probabilities always sum to 1 for a truly two-state system. *Entanglement* of multiple qubits allows the computational power to grow exponentially with the number of qubits, rather than linearly with the number of bits as in a conventional digital computer. A quantum computer performs a series of operations (a quantum algorithm) to modify qubit superpositions (probability of being in a particular state) and entanglements to increase some probabilities and to reduce others. Measurement of a qubit causes its state, and the states of entangled qubits, to collapse to either '0' or '1' with a probability dependent on the state of the qubit at the time of measurement. The goal is to maximize the probability of measuring the correct answer.

The way quantum computers use superposition, entanglement, and probabilities makes them very different from classical computers. For example, digital computers are deterministic and cannot generate truly random results. Randomness is inherent in quantum computing, so could have advantages in modeling systems in which randomness is important. Another fundamental difference is that an unknown quantum state cannot be copied perfectly, a consequence of what is called the no-cloning theorem. Transferring a quantum state from one qubit to another is possible, but only with destruction of the state in the initial qubit. The only way to create multiple copies of the same data is to perform the state preparation multiple times on separate qubits.

[Frameworks or models for quantum computing](#) [529] are varied and include the following approaches of practical importance.

- Analog or [adiabatic](#) quantum computation, typically based on quantum annealing, which performs processing by initialization of the system followed by slow, global control of the qubits towards a final state and readout.
- [Gate-based](#) quantum computation uses a sequence of few-qubit quantum gates performing logical operations, followed by measurement.
- [Measurement-based or one-way](#) quantum computation [530] first prepares a highly-entangled resource state and then performs single qubit measurements in a specific order to perform an algorithm. The computation is "one-way" because the measurements consume the resource state.
- [Topological](#) quantum computation performed by physical braiding of non-Abelian anyons, which are quasiparticles that occur only in two-dimensional systems and have less restricted properties than fermions and bosons.

## 38 Quantum Information Processing (QIP)

Physical implementations for quantum computing [531] are also varied and include the following approaches of greatest relevance.

- Superconducting qubits are made from superconducting circuits with Josephson junctions as nonlinear elements.
- Trapped ion qubits use atomic transitions of ions trapped by electromagnetic fields.
- Neutral atom qubits trapped in an optical lattice formed by counter-propagating laser beams.
- Quantum dot qubits based on spin states of electrons trapped on nanometer-scale semiconductor islands.
- Double quantum dot qubits based on the location of electrons that can move between tiny semiconductor islands.
- Nitrogen-vacancy (N-V) center qubits in diamond.
- Photons.

Quantum computers will serve as accelerators within larger computer systems for the foreseeable future. Reasons include the large overhead to implement fault-tolerant quantum computation and the fact that quantum computation has not shown any advantages over classical digital computation for many applications.

Making a quantum computer is challenging because qubits face requirements pulling in opposite directions. On the one hand, qubits require isolation from the environment to avoid unintentional changes to their quantum states. Whereas digital circuits have only two states with a significant energy difference between the two, qubits have an infinite number of states with infinitesimal energy differences, thus the state is easily changed. On the other hand, interaction between components is required for qubit manipulation and readout. Some systems can adjust the coupling between components as needed, increasing the coupling only when needed and decreased to provide isolation at all other times.

Hardware components for a quantum computer generally consist of 4 layers [532]: 1) the “quantum data plane,” where the qubits reside; 2) the “control and measurement plane,” responsible for carrying out operations and measurements on the qubits as required; 3) the “control processor plane,” which determines the sequence of operations and measurements that the algorithm requires, potentially using measurement outcomes to inform subsequent quantum operations; and 4) the “host processor,” a classical computer that handles access to networks, large storage arrays, and user interfaces. This host processor has a high data rate connection to the control processor and runs a conventional operating system, which facilitates user interactions.

Components in the first two layers need to satisfy the 5 DiVincenzo criteria [533] for a physical implementation of quantum computing (scalable array of qubits, initialization, universal gate set, low error rate, qubit-specific readout). Later added were 2 criteria relating to the communication of quantum information (ability to convert between stationary and mobile qubits, and ability to transmit mobile qubits between specified locations). Moving quantum information using mobile or “flying” qubits is called *quantum teleportation*. Modern quantum computer architectures do not necessarily satisfy all 7 conditions. Even if all 7 conditions were satisfied, achieving either noisy intermediate-scale quantum (NISQ) or fault tolerant quantum computing would require further development.

Following are introductions to the main frameworks or models for quantum computing.

### 4.1.1.1. ANALOG QUANTUM COMPUTING: INTRODUCTION

Analog quantum computers directly manipulate the interactions between qubits without breaking actions into individual gate operations. Hamiltonian-based quantum computation is another term for analog approaches including universal adiabatic quantum computing, quantum simulation, and quantum annealing.

In physics terminology, the Hamiltonian, or energy state, of a quantum system is used to encode or model a problem. In Hamiltonian-based approaches, the energy landscape starts flat and changes slowly and continuously to a final state with the energy peaks and valleys representing the problem to be solved. In adiabatic quantum computation (AQC), the system evolves adiabatically, i.e. without exchanging energy with its environment. Quantum annealing refers to systems that are not completely adiabatic.

Quantum annealing can model some problems using a set of qubits with programmable states and interactions. The system of qubits is initialized in a simple ground state, commonly by adjusting all qubits and all interactions to be the same and then applying a sufficiently strong effective magnetic field perpendicular to the problem basis, to randomize their quantum states into an equiprobable superposition of ‘0’ and ‘1’. In ideal AQC, turning off the effective magnetic field sufficiently slowly while simultaneously adjusting the qubit weights and interactions toward the model values allows the system to remain in ground state as it evolves. Quantum tunneling through energy barriers helps the system to stay in the lowest energy state. The final state of the

system at zero effective magnetic field represents the solution for the problem modeled. For implementation details in a superconducting system, see [534, 535].

The probability of finding the optimal solution using quantum annealing depends on factors such as qubit quality, rate of change of the applied magnetic field, and interactions with the environment. If the magnetic field changes too rapidly, the quantum system might not be able to track the lowest state as it moves. If the magnetic field changes too slowly relative to the characteristic qubit coherence time, too many qubits lose coherence and thus the ability to tunnel through energy barriers to stay in the lowest energy state. Always ending in the optimal (lowest energy) state is not critical because the computation can be repeated multiple times to find an optimal result.

The complexity or scale of problems solvable using quantum annealing depends on factors such as the number of qubits and their connectivity. Applications include optimization (§ 4.2.1), quantum simulation (§ 4.2.3), and quantum machine learning (§ 4.2.4).

Qubit quality factors such as coherence times are believed to be less important for quantum annealing than for gate-model quantum computing. For the status of quantum annealing, see § 4.3.2.

#### **4.1.1.2. GATE-BASED QUANTUM COMPUTING: INTRODUCTION**

Another approach to quantum computing, the quantum gate model, uses a series of quantum logic gates to perform computations [536, 537]. The process begins with a state initialized to the computational basis, i.e. ‘0’ or ‘1’, applies a sequence of quantum logic gates, and measures the qubits on the computation basis to read out the result. Unlike many classical logic gates, quantum logic gates are reversible. A complete, or universal, set of quantum gates is needed to achieve the full capability of quantum computation [525]. Different physical implementation used to make quantum gates can have different gates that are natural or easiest to implement [538].

Qubit manipulations performed in the lowest hardware levels include initialization, universal gates, and readout. For fault-tolerant quantum computation, the error rates for qubit manipulations must be below threshold error rates that depend on the error correction approach used. Noisy intermediate-scale quantum (NISQ) computers make use of qubits without quantum error correction, and while not fully fault-tolerant, are expected to be realizable in the near term and to have some applications [539, 540].

Potential applications include classically challenging computational problems, such as factoring large numbers. Recent advancements include a theoretical proof that the number of steps needed to solve certain linear algebra problems using parallel quantum circuits is independent of the problem size, whereas the number of steps grows logarithmically with problem size for classical circuits [541]. Further applications include simulation of physical systems, database search, portfolio optimization, machine learning, artificial intelligence, and combinatorial optimization [542]. This so-called quantum advantage comes from the quantum correlations present in quantum circuits, but not in classical circuits. Known classical supercomputers cannot simulate quantum computers more than about 50 sufficiently coherent qubits.

For the status of gate-based quantum computing, see § 4.3.3.

#### **4.1.1.3. TOPOLOGICAL QUANTUM COMPUTING: INTRODUCTION**

Topological quantum computation with non-Abelian anyons in the ideal conditions of zero temperature and infinite anyon separation would heavily suppress errors at the hardware level, avoiding the need for resource intensive quantum error correction [543, 544, 545]. Ideal conditions cannot be met in reality, resulting in some decoherence of the encoded information [546], although the requirements for error correction could be far less than for other qubits [547]. An accurate assessment of the scalability of topological quantum computing requires the development and characterization of actual topological qubits, which has not yet been achieved.

#### **4.1.2. QUANTUM COMMUNICATION: INTRODUCTION**

Quantum communication involves the generation and use of quantum states and resources for communication protocols and is inherently distributed in nature with separation between nodes ranging from micrometer to planetary scales. Its main applications are in provably secure communication, long-term secure storage, cloud computing and other cryptography-related tasks, as well as in the future, a secure “quantum web” distributing quantum resources like entanglement, nonlocality, randomness and connecting remote devices and systems.

Quantum key distribution, which is a quantum communication protocol for two parties, involves a sender (Alice) and a receiver (Bob), who share one-time pad material (a shared classical random bit string). The simplest implementation requires only the superposition state of a photonic qubit with no entanglement required at all. This advanced technology has reached the stage where successful field trials have been performed and left running for several years. Future applications will be determined by the distance at which secure keys can be established. Current QKD implementations have a limitation on both the distance and

rate at which shared keys can be established, for instance the best performance currently is ~ 1 Mbit/s over 50 km. As the communication distance increases further, the rate rapidly decreases, and a few hundred kilometers is considered the limit. To go farther and maintain the level of key security, the current QKD implementations require quantum repeaters to be added, which is also the key technology needed to distribute quantum entanglement over long distances.

**4.1.3. QUANTUM SENSING: INTRODUCTION**

Quantum sensing is the use of a quantum system, quantum properties, or quantum phenomena to perform a measurement of a physical quantity [14]. Quantum sensors enable measuring a physical quantity to a precision beyond the quantum standard limit (shot noise limit) possible with classical technology. Intermediate sensing applications to exploit quantum effects are also possible.

Quantum-enabled sensing that cannot achieve sensitivities beyond the standard quantum limit (SQL) nonetheless can provide advantages in comparison to conventional sensing by manipulating a sensor’s quantum nature. Examples include functional NMR and non-classical light spectroscopy and sensing. It is the most relevant approach for commercial development at the current stage.

Quantum sensing beyond the SQL requires the manipulation of quantum information on the probe state. Hence it requires control of quantum-phase information and the ability to read it out. One of the most advanced technologies utilizes quantum correlated light. Matter-based sensors are under development using NV centers in diamond and hybrid quantum systems.

Quantum imaging is based on similar technology; however, this focuses on a different aspect of sensing. Using quantum-mechanically correlated light, imaging is possible with limited probing of the object under consideration. Important applications are in medical and biological applications where avoiding damage caused by the sensing is regarded as a vital factor.

Quantum global sensing uses quantum coherence to measure large-scale global properties with high accuracy. Application examples include natural-resource searching and crustal-movement imaging. The core technologies required for global sensing are quantum sensors combined with quantum repeater networks.

**4.2. APPLICATIONS AND MARKET DRIVERS FOR QIP**

Quantum computing applications include secure computation, trusted data storage, and efficient applications [548, 549].

The publications of Shor’s algorithm providing an exponential speed-up for factorizing a number [550] and Grover’s algorithm providing polynomial speedup for unstructured search [551] gave theoretical grounding to the concept of using quantum mechanics to enhance computing performance. Many algorithms are currently available [552, 553]. Proposed are algorithms on machine learning, optimization based on the quantum approximate optimization algorithm (QAOA), and notably applications in theoretical chemistry and materials science [554].

Application areas and market drivers considered by the IRDS Systems and Architectures (SA) and Application Benchmarking (AB) teams [10] are shown in Table CEQIP-20 and described in following subsections.

*Table CEQIP-20 Matrix of Application Areas and Market Drivers for Quantum Information Processing (QIP)*

Application Areas	Market Drivers		
	Cloud	Communications	Sensing
Optimization	G		
Cryptographic codec	X	X	
Physical system simulation – Quantum simulation	X		
Artificial intelligence	X		X

\* Technology areas specific to QIP. X: important application; G: critical gating application; P: power-sensitive application.

**4.2.1. OPTIMIZATION**

Optimization involves selection of a best choice among many and is important for solving a variety of practical problems in fields such as engineering design, logistics, manufacturing, and finance [555]. The difficulty of solving optimization problems increases

with the number of elements, possible interactions, and constraints. Quantum computers are expected to provide the greatest benefit with complex optimization problems.

Quantum-annealing processors are designed to solve NP-hard logistics and scheduling problems with applications in industry, military, government, and science. Optimization is a core subproblem in machine learning applications and requires many samples of optimal and near-optimal solutions. Quantum-annealing processors based on superconducting flux qubits are commercially available from D-Wave Systems [556]. For details, see § 4.3.2. Systems have been commercially available since 2011 at a cost of about 10 million USD each [557]. These systems can also be accessed online in a cloud computing model. Quantum computing approaches that require cryogenic temperatures are likely to need RF signal processing and control as well as digital computation within the cryogenic space.

Note that no general physical computing method (including analog and quantum approaches) has yet been clearly demonstrated to be capable of solving NP-hard problems without requiring exponential physical resources (energy or time) to be invested in the physical process performing the computation. The prevailing view among computational complexity theorists [558] is that solving NP-hard problems in polynomial time would require uncovering new physics (i.e., beyond standard quantum mechanics).

Quantum algorithms are known for gate model quantum systems and could be applied to problems in optimization and machine learning on sufficiently large systems.

#### **4.2.2. CRYPTANALYSIS**

It is conjectured that quantum computers (gate model and/or annealing-based processors) of sufficient size could be used to break current cryptographic protocols (notably RSA encryption). Quantum devices for secure key exchange have been developed that would be necessary to support certain post-RSA cryptographic methods.

Quantum communications has applications in secure communications and also has applications for movement of quantum information [559].

#### **4.2.3. QUANTUM SIMULATION**

Simulators model systems to give information about their behavior. Quantum simulators use quantum effects and are expected to scale better than classical simulators and thus to allow simulation of systems beyond the capabilities of classical simulators [560, 561]. Research and Markets projects that the global simulation software market will grow from USD 6.26 billion in 2017 to USD 13.45 billion by 2022 [562]. Quantum simulation is currently a tiny fraction of the overall simulation market.

Quantum simulators can be classified as analog and digital simulators [563]. In analog simulators, a controlled physical system described by the model to be investigated is built and investigated. In the context of cryoelectronics, this has a long tradition from the Josephson junction arrays studied since the 1990s to modern cavity areas. In digital simulators, the model to be simulated is encoded into a quantum computer algorithm that allows to extract the desired property. The required compilation is often very economical, making these the first expected applications of quantum computers.

Digital quantum simulation can have a major impact on the investigations of molecules and materials, allowing their electronic structure to be simulated even in the case of strong correlations. Techniques to take this to disruptive levels on gate-based quantum computers are known [564, 565, 566] and small instances have been demonstrated [561, 567, 568]. A long-term goal of this activity is the simulation of nitrogenase [569].

Quantum annealing can be applied to problems in quantum simulation by querying the qubit superposition states mid-anneal. Quantum annealing processors have been applied to problems in quantum simulation and materials simulation, e.g., for spin systems [570, 571, 572]. In 2019 a photonic quantum information processor was used to experimentally simulate a stochastic process with 16 possible outcomes [573]. Quantum simulators with 1D interactions have been demonstrated with up to 51 neutral atoms in Rydberg states [574] and up to 53 ions in linear traps [575]. Desired for simulations are multi-dimensional quantum interactions [576].

#### **4.2.4. QUANTUM MACHINE LEARNING**

Machine learning assisted or enhanced by quantum computing is a relatively new application area under evaluation and development [577, 578, 579, 580]. Quantum annealing can be useful in discrete optimization and sampling, in particular Boltzmann sampling, which is a core technique in machine learning. Known applications contain image recognition and pattern inference for vehicles and healthcare, neural networks, and recommendation systems. Advances in algorithms for quantum machine learning have also resulted in improvements to classical algorithms, which has reduced the potential benefits [581]. The Journal Quantum Machine Intelligence began publication in 2019 [582].

### 4.3. PRESENT STATUS FOR QIP

For a list of companies worldwide engaged in the development of quantum computing or quantum communication, see [583, 584]. While there are few commercial products or services based on quantum information processing, research and development activity continues to ramp up. A striking development during recent years has been an informal competition to produce circuits for quantum computing with the highest qubit count. The competition shows tantalizing improvement, although the results are announced by press releases without independent verification and benchmark results are not comparable from one qubit type to another.

Quantum communications requires different technological elements such as quantum memory and quantum optical interface. These fundamental elements for quantum communications are still under development. The most matured quantum communication application is quantum key distribution (QKD), which is still limited to relatively short distances. Implementing QKD on a network over practical distances still requires a quantum repeater, which has not been demonstrated to date.

#### 4.3.1. REGIONAL EFFORTS IN QIP

Announcements of additional funding for quantum computing or QIP have been made by Australia, Canada, China, the EU, Germany, India [585], the Netherlands, Singapore, the UK, and the USA.

##### 4.3.1.1. AUSTRALIA

A CSIRO roadmap report released in 2020 outlines Australian and global opportunities in QIP [549].

##### 4.3.1.2. CHINA

China is building a new multi-location quantum information laboratory and investing over 100 billion RMB in QIP [586]. Commercial projects of large scale are also underway [587].

##### 4.3.1.3. EUROPE

European quantum technologies roadmap reports have been published since 2005 [554, 588]. The European Commission started a quantum technologies flagship program and will begin selection of research and innovation projects in 2018 [589, 590, 591]. Initial quantum computing grants funded two of the leading approaches: superconducting circuits and trapped ions.

Next to this EC-wide effort, there are notable national programs. These include Germany having committed 650 M€ for quantum technologies [592]. The UK Quantum Technology Hubs are going into their second round, and the Netherlands published a National Agenda for Quantum Technology in 2019 [593].

##### 4.3.1.4. JAPAN

Quantum computation in Japan is focused almost entirely on superconducting implementations. Examples of this emphasis include a flagship project within Q-LEAP (2018–2027) funded by MEXT as well as the ERATO project (JST 2016–2021, 1.5 billion yen) for macroscopic quantum machines. The architecture is based on the topological surface code. The goal of this effort is to implement a quantum computer using 100 qubits by 2028. Architectural development is quite advanced in Japan with architectures also being developed for distributed, optical-based and ion-trap based quantum computing systems. Hardware development has started for those approaches where the current focus is on realization of the necessary hardware building blocks.

Japan has also been putting significant effort into quantum annealing systems with AIST being the core research institute involved. The hardware is based on superconducting qubits hardware using double-bonding technique. The current coherence time is on the nanosecond scale, which is three orders of magnitude smaller than the computational time. The software development in this area has focused on mappings between the problem to be solved and the chip design.

The unique situation in Japan for computation is the development of non-quantum unconventional computers. These are often referred as quantum stimulated computers. These are in effect dedicated single purpose machines using conventional technology, and hence there is no quantum coherence involved during the computation. These developments are mainly done in industry sector with government funding. (Example projects: ImPact 2014–2018, 3 billion yen; NEDO 2016–)

Japan has two further strengths in quantum communications research. One is quantum key distribution (QKD) and the second is quantum repeaters. Japan has a long history in QKD development, centered at NICT. After 20 years of fundamental research development, the project has involved industries to run field experiments for a trusted node based QKD network and has now reached an implementation stage where it will be used for commercial purposes. A national project funded by MIC for satellite based QKD has recently started in 2018 which aims to integrate the satellite and trusted node approaches together to explore the feasibility of physical layer security. (Projects: MIC 2018–, satellite, 5 years; SIP 2018–, commercial development, 2.5 billion yen)



Quantum repeater research has been led by theory development and combined with optical and CQED technologies. The architectural designs are advanced in nature, though their implementation is still in the fundamental research phase. The key technology to be developed is the light matter interface. As the architectural design is well established, a breakthrough would provide a scalable growth for quantum communication networks.

The current implementations within the quantum sensing arena are mostly a quantum enhanced technology. The sensitivity is still within that achievable with conventional approaches, however these new technologies show several real advantages. These technologies are based on variety of quantum systems including nitrogen vacancy (NV) centers in diamond, nuclear spin ensembles, low-dimensional quantum systems and nano- or opto-mechanical systems to highlight a few main examples. Hybridization of these systems is also quite popular to control those systems as well as to generate new applications and physical phenomena. (Projects: MEXT 2015–2019, 1 billion yen; JST-CREST 2016–2023, 4.5 billion yen; a Flagship Q-LEAP 2018–2027)

Quantum sensing beyond the standard quantum limit and current sensitivities is still a challenge to realize. The main obstacle is the noise effect on the probe. Error control mechanisms and applications are currently investigated. Further, the principle of a number of these schemes has been demonstrated; however, it will take more time to realize true sensing prototypes.

#### 4.3.1.5. USA

US gate-type quantum computers lead the world in qubit count, with benchmarked results of Google at 53 qubits for their quantum supremacy experiment described below, IBM at 53, and an announcement of Intel at 49. For ion trap qubits, IonQ has announced 160 qubits, of which 79 are functional and the others are for storage. These are all US companies, although Intel had a non-US partner. While these systems were top-in-class worldwide when announced, qubit count is widely regarded as only being one component of a more complete metric.

The latest new US activity is the National Quantum Initiative Act (NQI), passed by the US government in December 2018 (1.2 billion USD over 5 years). While the new NQI funding is substantial, overall US government investments are even larger. US industrial investments are difficult to assess exactly, but a speaker in the NQI Senate hearing estimated them to be in the billions but probably less than 10 billion USD [594].

The NQI includes the expected funding for science and engineering research, but additionally includes government support for an industry-government consortium intended to increase the efficiency of the human enterprise that will develop quantum computing. The consortium is called the Quantum Economic Development Consortium (QED-C) and currently includes over 60 voting member companies and a board including large companies, small companies, and key government agencies [595]. QED-C is like the semiconductor consortium SEMATECH when it was started in the 1980s. QED-C will identify common needs and communicate them to the US government with the intent of better aligning government R&D with industrial needs. These needs include research funding for the most crucial science and technology, yet also include indirect albeit crucial areas such as workforce development, the supply chain, and standards.

The US Department of Energy (DoE) is establishing several centers for quantum computing. Of those, both [Berkeley Quantum](#) and the [Chicago Quantum Exchange](#) include programs of cryoelectronic qubits. The DOE Office of Science has established a Quantum Computing User Program at Oak Ridge National Laboratory. This program provides access to commercially available quantum computing resources through the Oak Ridge Leadership Computing Facility. In 2020, the DOE Office of Science announced a Funding Opportunity Announcement for National Centers for Quantum Information Science as part of the NQI. Up to five centers are expected to be established under this funding opportunity. In 2020, the DOE Office of Science announced a Quantum Internet Blueprint as part of a planned effort to connect all 17 DOE national laboratories by a quantum network.

While quantum computing is still very much in the research stage, US companies are beginning to offer access via the Internet as well as offering machines for purchase [583]. Access typically includes software that abstracts the underlying qubit operations into a form more easily learned by programmers—or in some cases into an application-specific framework that offers a “turnkey” solution within a limited problem domain.

#### 4.3.2. ANALOG QUANTUM COMPUTING: STATUS

Quantum-annealing processors based on superconducting flux qubits have been developed by and are commercially available from D-Wave Systems [6, 556, 596, 597, 598]. The D-Wave 2000Q released in 2017 includes a superconducting chip with 128,472 Josephson junctions, of which 75% are in classical SFQ digital control circuitry to program the processor and read out the results and the remainder are either directly in qubits or in the analog coupling elements that allow qubits to interact in a programmable way. The D-Wave Pegasus P16 chip in the Advantage QA system released in 2020 includes a superconducting chip with 1,030,000 Josephson junctions, 40,484 couplers, and a maximum of 5,640 qubits [599, 600]. Differences between the 2000Q and Advantage systems include an upgrade from Chimera to Pegasus hardware graph topology [601].

## 44 Quantum Information Processing (QIP)

Quantum annealing algorithms are reviewed in [602] and evidence for advantages are presented in [603]. A method to factorize integers using quantum annealing was developed and demonstrated using the D-Wave 2000Q [604]. An error suppression and correction scheme known as quantum annealing correction (QAC) has been used with D-Wave systems [605]. Portfolio optimization has been used as a case study to benchmark quantum annealing controls and their relative effects on computational accuracy [606]. Benchmarking results remain generally controversial.

Theoretically, any algorithm for gate-based quantum computing can be performed by error-free AQC [607, 608]; however, as with all quantum computing models, achieving perfect error-free operation in practical systems is not possible [609]. Many theoretical questions about efficient computation in the AQC model are open; for a survey of current status see [603]. Quantum annealing systems with up to 2000 qubits have been implemented and deployed, and hundreds of different problems have been demonstrated to work on these systems. In terms of performance, existing quantum annealing systems has been shown to break even with, and sometimes outperform, classical alternatives in some use scenarios [610, 611, 612].

### 4.3.3. GATE-BASED QUANTUM COMPUTING: STATUS

Many types of qubits have been proposed or demonstrated for use in quantum computing, including trapped ions, cold atoms in optical lattices, liquid and solid-state spin resonance, photons, quantum dots, nanowires, superconducting circuits, and NV centers. Reviews include [560, 613, 614, 615]. Following subsections cover status of qubits and associated hardware most relevant to gate-based quantum computing.

Quantum architectures based on quantum gates and circuits are in active research. Architectures and considerations specific to qubit type are covered in the following subsections. All platforms suffer to different degrees from errors including decoherence. Scaling to large systems will require the application of error correction techniques such as surface codes [616]. The classical electronic controllers used to manipulate and read out qubits also must be designed to minimize the introduction of errors [617] and will likely need a quantum-specific instruction set architecture (ISA) [618, 619]. Qubit control using cryogenic semiconductors or superconductor electronics is also covered in sections 3.3.3.2 and 2.2.4. Quantum computers will be used as accelerators or co-processors within larger computing systems, and the architecture for such systems is under development [620].

Table CEQIP-21 gives details of quantum computing component status. Table CEQIP-22 summarizes the status of major quantum computing development approaches. Computing capability grows exponentially with qubit count. Qubit connectivity is the average number of qubits that can be made to interact with a given qubit, with higher connectivity being advantageous [621]. The 2-qubit gate depth is an indication of the number of logic gates that can be performed before loss of coherence significantly increases the error. Quantum teleportation is useful for moving quantum information around larger systems. Qubit function and system scalability are subjective ratings. Note that while some aspects of quantum dot and topological approaches seem favorable to scaling, the difficulty in making reproducible qubits and 2-qubit gates gives cause for doubt.

Industry has started to integrate quantum devices and to scale up towards computing systems. For a list of companies worldwide engaged in the development of quantum computing or quantum communication, see [583, 584]. Several cloud-based quantum computing platforms are now available to users [622, 623].

Notably, Google has reported a demonstration of quantum supremacy, i.e., the claim to outperform the largest currently known supercomputers in one task [624]. The devices consist of a 9 by 6 array of nearest-neighbor coupled superconducting qubits, of which one was not used. The task was the execution of a random algorithm whose output, in the quantum case, is described by the Porter-Thomas distribution and it was certified that the device worked well enough to approach this result. A key factor in this achievement is two-qubit gate error ratios less than 1% across the chip. There is a debate on literature about the computational claim [625, 626], which does not detract from the hardware achievement.

The overall picture is that no approach has emerged as most likely to scale to the millions of qubits needed. One possibility is that a hybrid approach using different qubit types could best satisfy the range of requirements for a large-scale gate model quantum computer.

*Table CEQIP-21 Quantum Computing Component Status*

Table CEQIP-22 Gate-Based Quantum Computing Status Summary

Qubit type	Quantum volume [627]	Qubit count	Qubit connectivity	2-qubit gate depth	Quantum teleportation	Qubit function	System scalability
Superconducting	64	53	3.25	667	yes	fair	fair
Trapped ion	512	11	10	> 100 000	yes	fair	fair
Quantum dot	–	4	1	104	–	poor–fair	fair–good
Photonic	–	4			yes	poor	fair

2-qubit gate depth: ratio of coherence time divided by 2-qubit gate time ( $T_2^*/t_{2q}$ )

#### 4.3.3.1. SUPERCONDUCTING QUBITS AND DEVICES

Superconducting qubits are artificial atoms of macroscopic size made from thin-film inductors, capacitors and Josephson junctions. There are many ways to implement, control, couple, and read out superconducting qubits [614, 628, 629]. Common materials used to build superconducting qubits are niobium, aluminum and aluminum oxide [630]. Controlling devices with voltages rather than currents has advantages in some cases and has motivated development of a voltage-tunable transmon qubit with graphene-based Josephson junctions, although the coherence time needs improvement [631]. Other voltage-controlled devices include the gatemon qubit [632] and a superconducting quantum bus [633]. For current status of superconducting qubits, see [634].

One- and two-qubits gates can be implemented in various ways. A common method applies microwave pulses tuned to specific frequencies for driving the needed actions [628, 635]. A general issue in the required control and readout processes are the decoherence effects on the qubit. Qubit decoherence is caused by interactions between the qubit and its surrounding environment [636, 637, 638]. To mitigate errors caused by various decoherence sources, including fluctuations of magnetic and electric fields, various low-level strategies such as optimum working points are applied, with the goal of reaching the error correction threshold.

Error corrected superconducting qubit devices will allow systems with higher complexity, which is required for future quantum information processing architectures [536, 639, 640, 641, 642, 643, 644, 645].

System achievements include demonstration of quantum volume 64 [646].

**Superconducting Devices:** Superconducting quantum computing systems are built from modules containing qubits and other superconducting components or devices. In the circuit quantum electrodynamics (cQED) architecture pioneered in 2004 [647], the qubits, which are inherently nonlinear devices, are coupled to linear resonant structures, which can be used for coupling between qubits, as well as the measurement of qubits for transferring readout results to the outside classical world [648]. Commonly these linear resonators are formed from thin-film coplanar waveguide (CPW) resonators, which are straightforward to fabricate with quite low microwave losses [649], although to obtain the proper resonance frequencies for integrating with qubits, these CPW resonators must be rather long, typically several mm, posing a challenge for reducing device areas. Inserting a Josephson junction in such a CPW resonator allows one to tune or modulate its resonance frequency [650]. Alternatively, lumped-element linear resonators offer the ability to form significantly more compact structures for coupling and measuring qubits. However, fabricating lumped-element resonators with sufficiently low microwave loss can be challenging [651]. Fully superconducting indium-bump interconnects have been demonstrated that allow for the three-dimensional integration of quantum circuits without introducing lossy amorphous dielectrics [652]. Superconducting through-silicon vias (TSVs) enable higher levels of chip stacking and have been demonstrated using TiN [653].

Measuring the state of a quantum system in general requires more care than detecting a classical bit due to subtleties of the fundamental quantum measurement process. For superconducting qubits in a cQED environment, measurement is typically done with extremely weak microwave signals that must then be amplified by another class of superconducting devices that work very close to the quantum limit [654]. This includes Josephson parametric converters [655], Josephson parametric amplifiers [656, 657] and traveling wave amplifiers [658]. This amplifier-based measurement approach requires strong microwave pump tones for driving the parametric nonlinearity of the amplifier. In order to prevent these pump tones or other noise processes in the amplifier from perturbing the qubit, it is necessary to include significant amounts of non-reciprocal elements, such as microwave isolators or circulators, between the amplifiers and qubits and resonator circuits. Conventional cryogenic microwave isolators and circulators are bulky, magnetic, and difficult to thermalize at millikelvin temperatures, posing a challenge for scaling to large systems. Alternative approaches to forming non-reciprocal elements are currently being developed using superconducting circuitry and parametric active devices [659].

## 46 Quantum Information Processing (QIP)

An alternative to amplifier-based qubit measurement involves the use of a microwave photon detector, the Josephson photomultiplier (JPM) [660], which can provide a digital result from qubit measurement at the millikelvin stage of the cryostat [661] for interfacing with a cryogenic digital coprocessor in the low-temperature environment [662]. In addition, because no parametric pump tone is needed, JPMs can be coupled to superconducting qubits and resonators without the need for intervening isolators or circulators [661].

The conventional approach to the control of superconducting qubits and the implementation of quantum gates involves the use of resonant microwave pulses with carefully controlled amplitude and phase. Microwave-based gates have been refined to the point where gate errors are less than 0.1% [663], exceeding the fault-tolerant threshold for implementing quantum error correction. However, the generation of microwave signals for qubit gates requires a significant hardware overhead of room-temperature equipment outside of the cryostat, including microwave sources, arbitrary waveform generators, mixers, and amplifiers. An alternative approach currently being explored involves the use of SFQ-based superconducting digital electronics to drive quantum gates using resonant trains of SFQ pulses [664, 665, 666], thus greatly reducing the requirements for room-temperature hardware and moving much of the control elements into the low-temperature environment [662].

Communication of entangled qubit states through a one-meter-long superconducting cable has been demonstrated [667]. Use of photonic quantum interconnects for longer distance communication requires efficient transducers. Recent developments include [668, 669, 670].

### 4.3.3.2. TRAPPED ION QUBITS

Trapped ion qubits encode quantum information in the electronic energy levels of ions such as  $\text{Ca}^+$  or  $\text{Yb}^+$ . The ions are suspended in ultra-high vacuum using electromagnetic fields and two-qubit gate operations can be performed between nearby ions. Lasers and photon detectors are typically used for qubit control and readout. Operation at cryogenic temperatures helps to achieve the necessary vacuum conditions and reduces electronic noise. Operation at 50 to 100 K provides significant benefits; however, operation in the 1 to 10 K range might prove necessary, especially for early systems. For reviews, see [576, 614, 671].

An 11-qubit quantum computer has been demonstrated with all-to-all qubit connectivity [672]. Coherence times of trapped ion qubits is typically long ( $> 1$  s), but gate times have also tended to be long ( $\sim 50$   $\mu\text{s}$ ). Fast ( $\sim 1$   $\mu\text{s}$ ) and high-fidelity two-qubit logic gates have been demonstrated by using amplitude-shaped laser pulses [673]. Quantum teleportation has been demonstrated using the ability to move individual ions [674].

Linear ion traps have worked well and allow all-to-all entanglement of 10 to 20 qubits. Current efforts are focused on scaling up to the range of 50 to 100 qubits [675]. Scaling to significantly larger numbers of qubits requires physical movement of ions between linear traps or some other method for transporting quantum information between modules [671, 676]. Challenges include the scalability of systems with multiple linear traps.

### 4.3.3.3. QUANTUM DOT QUBITS

Quantum dots confine one or more electrons or holes within a region of host material both small enough that quantum effects are significant and large enough to allow control. Semiconductors are commonly used as the host material. Electrodes can be used to control the electron number or spin state in the quantum dot [677]. Other names for quantum dot qubits include spin, silicon, or semiconductor qubits.

Several types of quantum dot qubits are under investigation [678, 696, 697]. Spin-based quantum dot qubits have demonstrated long coherence times due to their relative insensitivity to charge fluctuations; however, their gate times have been slower than desired because an oscillating current applied to the electrodes is used to produce an oscillating magnetic field to interact with the electron's spin. Charge-based quantum dot qubits allow much more rapid manipulation using electric fields; however, they suffer from rapid decoherence due to sensitivity to charge noise. A balance of desired characteristics might be achievable with hybrid qubits [698].

Nuclear spin can also be used in quantum dots qubits, although these are considered to be hybrids with the nuclear magnetic resonance (NMR) approach to quantum computing. Nuclear spin qubits have potential advantages but are still in early stages of development [679, 680].

Semiconductor materials: GaAs was used initially as it can make high quality quantum wells for trapping electrons; however, both Ga and As have a net nuclear spin that interacts with and causes the electron spin to rapidly lose quantum phase coherence. Currently favored semiconductor materials include Si, Ge, SiGe, and isotopically purified  $^{28}\text{Si}$  [681, 682, 683]. Challenges for quantum dot qubits in silicon include control over location of quantum dots, control of 2-qubit coupling strength, and lack of significant spin-orbit coupling for electrons, which can result in relatively long interaction times.

One- and two-quantum-bit gates for quantum computation can be implemented using the spin states of coupled single-electron quantum dots [684, 685] and have recently been demonstrated with error ratios approaching the threshold for error correction and system scaling [686, 687]. The fastest demonstrated 2-qubit gates with Si qubits are 800 ps with error ratio  $< 1e-3$  [688]. Coupling of quantum dot qubits over distances much longer than the size of a single quantum dot has been demonstrated using a superconducting microwave resonator [689, 690, 691]. A device with 4 interacting quantum dot qubits has been demonstrated [692].

Architectures for quantum computers based on quantum dots are an active area of research [693, 694, 695, 696, 697, 698]. Quantum dots both require and benefit from advanced semiconductor manufacturing processes [418, 694, 699]. Operating temperatures for quantum dot qubits could be as high as the 1 K range [700] and could allow integration with control electronics on the same chip [701]. Systems capable of controlling many quantum dot qubits have been demonstrated [509, 511, 512] or proposed [702, 703] and seem scalable to thousands of qubits. Together, these characteristics might enable the construction of more complex processing architectures.

#### **4.3.3.4. PHOTONIC QUBITS**

Photons have some advantages as qubits, including stability at room temperature and long quantum coherence time. A significant problem has been the lack of a natural two-qubit gate due to the fact that photons do not interact with each other. Groups are working to develop non-linear elements necessary for two-qubit photonic gates, but progress had been slow [613, 704]. Multi-photon entanglement in silicon devices and chip-to-chip quantum teleportation was reported in 2020 [705] and might provide a scalable platform for quantum computing or for more general quantum information processing [706]. A quantum sampling algorithm demonstrated in 2021 [707] on a programmable photonic chip using highly squeezed states is promising, yet the quality of the qubits needs to be improved considerably and photon losses reduced if the technology is ever to scale to practical problems [708].

#### **4.3.4. TOPOLOGICAL QUANTUM COMPUTING: STATUS**

Majorana zero modes are expected to be the simplest and most controllable types of anyons, although they do not provide the full power of topologically protected quantum computation. One approach to creating Majorana zero modes involves fabricating superconductors on top of 2D or 1D semiconductors that exhibit the quantum Hall effect. Efforts to develop topological qubits using Majorana zero modes in topological superconductors have not yet succeeded but show some promise [709, 710]. Getting the required physical properties together in one device has been challenging. Alternative designs for topologically protected qubits are also being pursued [544, 711, 712].

Scalable architectures based on topological qubits are in the early research stage [545, 547].

#### **4.3.5. QUANTUM COMMUNICATION AND SENSING: STATUS**

Quantum communication technologically ranges from point-to-point quantum key distribution to fully quantum networks [713, 714]. The most important applications of cryoelectronics in this field are single photon detectors based on superconducting nanowires [715]. A cryogenic microwave-based quantum communication scheme has been proposed and is being researched in the EU [716].

Technologies for quantum communication relevant to current quantum information technology developments include quantum key distribution, quantum interconnects, and quantum repeaters; each covered in following sub-sections along with quantum sensing.

##### **4.3.5.1. QUANTUM KEY DISTRIBUTION**

Quantum key distribution has moved from the research arena now to the product development phase where market alignment is highly essential. Further technology developments to higher generation rates over long distance are important and necessary. For long distance QKD systems, there are two directions currently being investigated: trusted relay optical-fiber-based networks and satellite communications which could be combined in the future. These technologies are in principle only based on the superposition of quantum states and do not rely on quantum entanglement. The challenge is to go beyond 10 Mbit/s for 50 km, and 1 kbit/s for satellite communications. To eliminate trusted nodes, which inherently severely compromise key security, the move to quantum repeater technology is needed.

Quantum key distribution utilizing quantum repeaters naturally allows extending the communication distance significantly without compromising key security. The challenge is to develop the key technology necessary in quantum repeaters. Limiting the use of quantum repeaters to only QKD allows elimination of several components including technologically difficult quantum memories with long storage times. Another possible quantum communication approach including QKD is a quantum sneakernet, a system based on physical movement of quantum memory [717]. This is a quantum-memory-based quantum communication system whereas quantum repeaters are communication-channel-based system. Quantum sneakers require an extremely long-

## 48 Quantum Information Processing (QIP)

lived quantum memory with coherence time sufficient for a quantum signal to be physically delivered from the sender to the receiver. This necessitates either a fault-tolerant quantum error corrected qubit (composed of many physical qubits) or an exceptionally long coherence for the quantum memory (possibly weeks).

### 4.3.5.2. QUANTUM REPEATERS

Quantum repeaters are a core technology for quantum communication. Any direct quantum communication between two parties has a distance limitation as the success rate decreases exponentially with the communication distance. To overcome this fundamental limitation, waystations are required in the communication channel, similar to amplifiers in classical communication channels. However, unlike amplifiers used for classical signals, it is impossible to amplify a quantum signal due to the no-cloning theorem. Hence quantum repeaters work by generating and then swapping entanglement between waystations to extend the range of quantum correlations. Quantum repeaters allows the generation of entanglement over the entire communication network. The deterioration of the fidelity of entanglement can be recovered by distillation (purification) of the quantum state.

Quantum relays are a precursor technology to full quantum repeaters. They are in a sense quantum pre-repeaters or primitive quantum repeaters with limited functionality. It does not show the scalability that a true quantum repeater-based network would exhibit (polynomial resource usage with the quality of the entangled resource not scaling exponentially with overall communication distance) but it can scale polynomially if the quantum memory has an infinite coherence time. Typical technological requirements for the relays are single photon sources, single photon detectors, quantum memories, and an interface between the matter-based qubit and photon. The requirements include optical cavity developments, control of matter qubits with optical transitions as such as NV centers in diamond, and lossless fiber-cavity coupling. Quantum relays and quantum repeaters share many of the basic hardware technology components, though the architectures of the communication systems are vastly different.

Quantum repeaters need to have at most a polynomial scaling in terms of resources required while at the same time establishing entangled states whose quality does not scale down exponentially with the number of repeater nodes in the network. A quantum repeater system consists of three distinct operations: entanglement distribution, entanglement swapping, and entanglement distillation (purification) and error correction. Although quantum repeaters employ error correction, the implementation is much simpler than in quantum computation and fault tolerance is not necessary.

### 4.3.5.3. QUANTUM INTERCONNECTS

Quantum interconnects are components of quantum communications systems used to transport entanglement between quantum devices. In particular, they can be used to fundamentally change the connectivity for quantum adiabatic computation, quantum annealing, and quantum simulation, providing significant benefits in this era of noisy intermediate-scale quantum (NISQ) computing [539]. In the longer term, quantum interconnects allow distributed quantum computation. For a review and roadmap of quantum interconnects, see [718].

Quantum interconnects can be implemented on chip and between chips for short distances that do not require quantum repeaters. For example, entangled superconducting qubit states have been communicated through a one-meter-long superconducting cable [667]. Long distance quantum interconnects are expected to use photons. Use of photonic quantum interconnects by non-photonic qubits requires efficient transducers.

The quantum internet is a network of quantum computers connected by quantum communication channels. On the quantum internet, quantum computers are connected coherently and one can distribute quantum correlations and consume them in a global fashion. Such a network of coherently connected quantum computers would allow global distribution and consumption of quantum correlations.

### 4.3.5.4. QUANTUM SENSING

Quantum sensing is an area of active research [14, 719].

## 4.4. BENCHMARKING AND METRICS FOR QIP

Quantum information processing is rapidly progressing through an exploratory stage of engineering research, and there is widespread consensus that significant development across many different technologies remains necessary to meet the long-term expectation of fault-tolerant, universal quantum devices. Recent experimental demonstrations have passed significant milestones in the design, fabrication, and operation of noisy intermediate-scale quantum (NISQ) computing devices [539]. These efforts have been highlighted by the recent public announcement of an experimental demonstration comparing the time and power performance of a 53-qubit superconducting processor to the world's fastest supercomputer [624] as well as the doubling of a device-specific benchmarks for another 20-qubit processor [720]. Quantum engineering advances underscore the importance of tracking the rapid technical progress in quantum information processing and to forecast future developments in quantum

engineering research. These insights are necessary to monitor the overall growth in sophistication of quantum engineering. A five-layer system to that end has been proposed in Germany [613].

Methods for tracking the development of quantum information processing are under active development by the research community [672, 721, 722, 723, 724, 725, 726, 727, 728, 729, 730]. Those methods seek to evaluate the salient features and behaviors of quantum information devices as well as the performance for their expected usage. Many metrics and benchmarks for quantum information processing are intended to be representative of device growth and device performance by building on techniques used for device characterization, verification, and validation. In addition, metrics tailored to device usage draw from monitoring conventional notions of time, accuracy, and precision. More broadly, metrics for quantum information processing have been defined at different levels of abstraction including the physical, logical, and system levels. These metrics represent the concerns of information processing as well as the concerns that are unique to quantum information. The IEEE has engaged in several efforts to build a structured community for discussing these points and building scientific consensus [731].

Presently, the global community is debating the metrics and benchmarks designed around the expected use cases and technology layers for quantum information processing devices. In this description, use cases represent a category that identifies a designed purpose for a quantum computing device or system. Common examples include noisy, intermediate-scale quantum devices, quantum annealers, and quantum simulators. Technology layers identify the levels of design complexity in a quantum computing device or system. These layers include the low-level physical registers storing quantum states, the integrated control systems expressing quantum operations, and the system-level performance concerns for specific applications.

Existing metrics for quantum devices characterize the noise in the physical register and the errors observed from low-level physical gate operations. Methods for characterizing noise are generally device dependent and the results tailored to the specific device instance. The aggregate effects of sources of errors also have been proposed for evaluating device performance, but outstanding questions remain on how to connect these metrics to application performance. In the context of application performance, time-to-solution has been used as a device-agnostic method of comparison across solution methods. However, current devices are too small to enable broad ranges in problem evaluation and the comparison of quantum technologies against conventional devices is complicated by vastly different levels of technology maturity. While all leading demonstrations focus on advancing a chosen metric, there remains a lack of direct connection between experimental achievements and the forecasting of fault-tolerant quantum information processing [732]. The related topics of device verification and validation have also emerged as important to quantum engineering research [733].

#### 4.5. ACTIVE RESEARCH QUESTIONS FOR QIP

Superconducting quantum computing requires further development, lower error rates, and scale (number of qubits) to clearly demonstrate the improved performance of important applications. Integrated circuit technologies are required that are scalable and address the special needs of quantum circuits [734]. More work is needed to explore potential applications for quantum algorithms and to develop suitable quantum processor architectures. As mentioned above, the integration of superconducting digital electronics with superconducting qubits for control and readout holds promise for scaling to significantly larger systems than is possible with present state-of-the-art approaches [662].

*Table CEQIP-23 Difficult Challenges for QIP*

<i>Near-Term Challenges: 2020-2027</i>	<i>Summary of Issues and Opportunities</i>
Physical qubits	Design and fabrication of qubit devices with enhanced qubit coherence times and gate fidelities
Logical qubits	Implementation of fully error-corrected logical qubits and protected gate operations
Readout of qubits	Development of scalable, cryogenic qubit readout hardware
Interconnects, cryogenic to room temperature	Development of low thermal conductance and high bandwidth interconnects between different temperature stages of cryogenic- and room-temperature electronics

## 5. CHALLENGES

The top near term challenges for superconductor electronics (SCE) and quantum information processing (QIP) are given in the table below. These are a very high-level summary of challenges that the industry needs to address for this IFT.

Table CEQIP-24 Difficult Challenges Summary

Near-Term Challenges: 2020-2027	Summary of Issues and Opportunities
SCE: Integrated circuit fabrication	<p>Foundries for commercial production now process 200 mm or smaller wafers using equipment lacking state-of-the-art capability. Achieving the yield and throughput for large-scale applications will require process improvements and, possibly, a move to 300 mm wafers.</p> <p>Planarization and thickness control is challenging in stacks of multiple superconductor layers when the layer thicknesses remain the same, rather than increasing with layer number as in CMOS back-end processes.</p>
SCE: Device variability	<p>Variation in device parameters reduces the operating margins of circuits. Needed is better process control, better device designs, or circuit designs that tolerate or compensate for device variability.</p>
SCE: High critical current density junctions ( $J_c > 100 \mu\text{A}/\mu\text{m}^2$ )	<p>The <math>\text{AlO}_x</math> barrier in Josephson junctions with <math>J_c = 100 \mu\text{A}/\mu\text{m}^2</math> is now approximately 1 nm thick. Thinner barriers increase <math>J_c</math>, allowing smaller and faster JJs. For <math>J_c &gt; 500 \mu\text{A}/\mu\text{m}^2</math> the sub-gap resistance can be sufficiently low to eliminate the need for shunt resistors. Uniformity control will be challenging as defects typically dominate conduction through thinner barrier layers and thickness control is also difficult. Materials and process development is needed to improve uniformity and control of devices with high <math>J_c</math>.</p>
SCE: Electronic design automation (EDA) tools	<p>EDA tools for CMOS are not adequate for SCE. Inductance is critical in superconducting circuits and connecting wires must have inductance values within a specified range. Circuit simulators and timing analysis must be modified for pulse-based logic. Flux trapping analysis—both for trapping probability and the coupling of trapped flux in moats to circuits—is required, while analysis of the coupling of bias current and ground plane return currents to circuit structures are also important and difficult at chip level.</p>
SCE: Packaging	<p>Operation at cryogenic temperatures requires different materials, packaging, testing, and cooling systems, much of which will require new development. State-of-the-art systems package a few superconductor ICs in a commercial cryostat. Scaling up to systems with higher complexity chips and multi-chip modules will require further reduction of power consumption by all components.</p> <p>Josephson junctions are extremely sensitive to magnetic fields and require shielding, which becomes more challenging as system volumes grow.</p>
QIP: Qubit, physical	<p>Identify qubit technology with the best overall characteristics for use in quantum computing.</p>
QIP: Qubit, logical	<p>Demonstrate logical qubits and error correction sufficient for scaling to larger systems.</p>



## 6. SUMMARY

This IRDS chapter surveys Cryogenic Electronics (sections 2 and 3), and Quantum Information Processing (section 4), which include alternatives to conventional CMOS technologies. Although novel functionalities and applications have been a primary objective of cryogenic electronics and quantum information processing, high performance, large system energy efficiency, or low power dissipation at cryogenic temperatures could become important as well.

### 6.1. SUPERCONDUCTOR ELECTRONICS (SCE)

Logic families continue to develop with very different characteristics. The maximum number of Josephson junction switching elements in a circuit is around 1 million.

Cryogenic random-access memory (RAM) with sufficient density and capacity continues to be the most important need for superconductor electronics. Memory based on logic-style Josephson junctions is most developed but has not yet achieved 1 Mibit capacity.

Roadmaps for various aspects of SCE technology were introduced in the 2020 edition.

### 6.2. CRYOGENIC SEMICONDUCTOR ELECTRONICS (CRYO-SEMI)

Monitoring of applications, drivers, and technologies will continue. No areas seem ready for roadmapping at this time.

### 6.3. QUANTUM INFORMATION PROCESSING (QIP)

Monitoring of applications, drivers, and technologies will continue. No areas seem ready for roadmapping at this time, although some are close.

## ENDNOTES/REFERENCES

---

- 1 A. I. Braginski, “Superconductor electronics: Status and outlook,” *J. Supercond. Nov. Magn.*, vol. 32, pp. 23–44, Jan. 2019, doi: [10.1007/s10948-018-4884-4](https://doi.org/10.1007/s10948-018-4884-4).
- 2 C. J. Fourie, “Extraction of dc-biased SFQ circuit Verilog models,” *IEEE Trans. Appl. Supercond.*, vol. 28, no. 6, p. 1300811, Sep. 2018, doi: [10.1109/TASC.2018.2829776](https://doi.org/10.1109/TASC.2018.2829776).
- 3 “IEC 60417 - 6371, Josephson junction,” 2016-09-17. [Online]. Available: <https://www.iso.org/obp/ui#iec:grs:60417:6371>, accessed 2020-03-15.
- 4 International Electrotechnical Commission: IEC 61788-22-1 standard on “Superconductivity—part 22-1: superconducting electronic devices—generic specification for sensors and detectors”: <https://webstore.iec.ch/publication/26674>; IEC 60617—graphical symbols for diagrams: superconducting region, one superconducting connection (S01924), normal-superconducting boundary (S01925), and Josephson junction (S01926), <https://webstore.iec.ch/publication/2723>. Free access: [http://snf.ieeeecsc.org/sites/ieeeecsc.org/files/documents/snf/abstracts/edOhkuboM\\_Report\\_of\\_IEC-IEEE\\_joint\\_IWSSD20160129-final-4\\_040617.pdf](http://snf.ieeeecsc.org/sites/ieeeecsc.org/files/documents/snf/abstracts/edOhkuboM_Report_of_IEC-IEEE_joint_IWSSD20160129-final-4_040617.pdf)
- 5 M. Kuniyoshi *et al.*, “Investigation of timing parameters in single-flux-quantum circuits using low critical-current junctions and low bias voltages,” *IEEE Trans. Appl. Supercond.*, 2021, doi: [10.1109/TASC.2021.3067827](https://doi.org/10.1109/TASC.2021.3067827).
- 6 D. S. Holmes, A. M. Kadin, and M. W. Johnson, “Superconducting computing in large-scale hybrid systems,” *Computer*, vol. 48, no. 12, pp. 34–42, Dec. 2015, doi: [10.1109/MC.2015.375](https://doi.org/10.1109/MC.2015.375).
- 7 I. I. Soloviev, N. V. Klenov, S. V. Bakurskiy, M. Y. Kupriyanov, A. L. Gudkov, and A. S. Sidorenko, “Beyond Moore’s technologies: Operation principles of a superconductor alternative,” *Beilstein J. Nanotech.*, vol. 8, no. 1, pp. 2689–2710, Dec. 2017, doi: [10.3762/bjnano.8.269](https://doi.org/10.3762/bjnano.8.269).
- 8 T. Yamashita, “Phase shift and control in superconducting hybrid structures,” *IEICE Trans. Electron.*, vol. E101.C, no. 5, pp. 378–384, May 2018, doi: [10.1587/transele.E101.C.378](https://doi.org/10.1587/transele.E101.C.378).
- 9 T. M. Conte, E. P. DeBenedictis, P. A. Gargini, and E. Track, “Rebooting computing: The road ahead,” *Computer*, vol. 50, no. 1, pp. 20–29, Jan. 2017, doi: [10.1109/MC.2017.8](https://doi.org/10.1109/MC.2017.8).
- 10 “IRDS 2018 Reports - IEEE International Roadmap for Devices and Systems,” May 2019. [Online]. Available: <https://irds.ieee.org>.
- 11 S. Anders *et al.*, “European roadmap on superconductive electronics – status and perspectives,” *Physica C*, vol. 470, no. 23–24, pp. 2079–2126, Dec. 2010, doi: [10.1016/j.physc.2010.07.005](https://doi.org/10.1016/j.physc.2010.07.005).
- 12 D. S. Holmes, A. L. Ripple, and M. A. Manheimer, “Energy-efficient superconducting computing—power budgets and requirements,” *IEEE Trans. Appl. Supercond.*, vol. 23, no. 3, p. 1701610, June 2013, doi: [10.1109/TASC.2013.2244634](https://doi.org/10.1109/TASC.2013.2244634).
- 13 S. S. Tannu, P. Das, M. L. Lewis, R. Krick, D. M. Carmean, and M. K. Qureshi, “A case for superconducting accelerators,” in *Proc. 16th ACM Int.l Conf. Computing Frontiers*, New York, NY, USA, 2019, pp. 67–75, doi: [10.1145/3310273.3321561](https://doi.org/10.1145/3310273.3321561).
- 14 C. L. Degen, F. Reinhard, and P. Cappellaro, “Quantum sensing,” *Rev. Mod. Phys.*, vol. 89, no. 3, p. 035002, Jul. 2017, doi: [10.1103/RevModPhys.89.035002](https://doi.org/10.1103/RevModPhys.89.035002).
- 15 J. Clarke and A. I. Braginski, Eds., *The SQUID Handbook: Fundamentals and Technology of SQUIDS and SQUID Systems*, vol. I, Weinheim, FRG: Wiley-VCH Verlag GmbH & Co. KGaA, 2004, doi: [10.1002/3527603646](https://doi.org/10.1002/3527603646).
- 16 C. Granata and A. Vettoliere, “Nano superconducting quantum interference device: A powerful tool for nanoscale investigations,” *Physics Reports*, vol. 614, pp. 1–69, Feb. 2016, doi: [10.1016/j.physrep.2015.12.001](https://doi.org/10.1016/j.physrep.2015.12.001).
- 17 M. J. Martínez-Pérez and D. Koelle, “NanoSQUIDS: Basics & recent advances,” *Physical Sciences Reviews*, vol. 2, no. 8, 2017, doi: [10.1515/psr-2017-5001](https://doi.org/10.1515/psr-2017-5001).
- 18 R. L. Fagaly, “Superconducting quantum interference device instruments and applications,” *Rev. Sci. Instrum.*, vol. 77, no. 10, p. 101101, Oct. 2006, doi: [10.1063/1.2354545](https://doi.org/10.1063/1.2354545).
- 19 J. Clarke and A. I. Braginski, Eds., *The SQUID Handbook. Vol. 2. Applications of SQUIDS and SQUID Systems*. Weinheim, Germany: Wiley-VCH, 2006.

- 20 S. Bechstein *et al.*, “Investigation of nanoSQUID designs for practical applications,” *Supercond. Sci. Technol.*, vol. 30, no. 3, p. 034007, Feb. 2017, doi: [10.1088/1361-6668/aa557f](https://doi.org/10.1088/1361-6668/aa557f).
- 21 L. Hao and C. Granata, “Recent trends and perspectives of nanoSQUIDs: Introduction to ‘Focus on nanoSQUIDs and their applications’,” *Supercond. Sci. Technol.*, vol. 30, no. 5, p. 050301, Apr. 2017, doi: [10.1088/1361-6668/aa68d6](https://doi.org/10.1088/1361-6668/aa68d6).
- 22 C. Granata, P. Silvestrini, B. Ruggiero, and A. Vettoliere, “Modelled Spin Sensitivity of nanoSQUIDs in Different Configurations,” *IEEE Trans. Appl. Supercond.*, vol. 28, no. 4, p. 1600705, June 2018, doi: [10.1109/TASC.2018.2799701](https://doi.org/10.1109/TASC.2018.2799701).
- 23 I. K. Harvey, “A precise low temperature dc ratio transformer,” *Rev. Sci. Instrum.*, vol. 43, pp. 1626–1639, 1972, doi: [10.1063/1.1685508](https://doi.org/10.1063/1.1685508).
- 24 F. Raso, R. Hernandez, A. Mendez, L. Matias, and M. Anguas, “Proposal of a new method of measurement of the quantized hall resistance with a binary Josephson array in a bridge configuration,” in *2008 Conference on Precision Electromagnetic Measurements Digest*, 2008, pp. 162–163, doi: [10.1109/CPEM.2008.4574703](https://doi.org/10.1109/CPEM.2008.4574703).
- 25 L. Hao, J. C. Gallop, J. C. Macfarlane, and C. Carr, “HTS cryogenic current comparator for non-invasive sensing of charged particle beams,” *IEEE Trans. Instrum. Meas.*, vol. 52, no. 2, pp. 617–620, Apr. 2003, doi: [10.1109/TIM.2003.810456](https://doi.org/10.1109/TIM.2003.810456).
- 26 J. Oppenlaender *et al.*, “Superconducting quantum interference filters operated in commercial miniature cryocoolers,” *IEEE Trans. Appl. Supercond.*, vol. 15, no. 2, pp. 936–939, June 2005, doi: [10.1109/TASC.2005.850128](https://doi.org/10.1109/TASC.2005.850128).
- 27 G. V. Prokopenko ; O.A. Mukhanov and R. R. Romanofsky, “SQIF antenna measurement in near field”, *2015 15th International Superconductive Electronics Conference (ISEC)*, Jul. 2015, doi: [10.1109/ISEC.2015.7383482](https://doi.org/10.1109/ISEC.2015.7383482).
- 28 R. L. Fagaly, “The commercialization of SQUIDs,” *IEEE Trans. Appl. Supercond.*, vol. 25, no. 3, p. 1601507, June 2015, doi: [10.1109/TASC.2014.2364212](https://doi.org/10.1109/TASC.2014.2364212).
- 29 M. Mossle *et al.*, “SQUID-detected in vivo MRI at microtesla magnetic fields,” *IEEE Trans. Appl. Supercond.*, vol. 15, no. 2, pp. 757–760, June 2005, doi: [10.1109/TASC.2005.850043](https://doi.org/10.1109/TASC.2005.850043).
- 30 R. N. Jabdaraghi, D. S. Golubev, J. P. Pekola, and J. T. Peltonen, “Noise of a superconducting magnetic flux sensor based on a proximity Josephson junction,” *Sci. Rep.*, vol. 7, no. 1, p. 8011, Aug. 2017, doi: [10.1038/s41598-017-08710-7](https://doi.org/10.1038/s41598-017-08710-7).
- 31 I. P. Nevirkovets and O. A. Mukhanov, “Peculiar interference pattern of Josephson junctions involving periodic ferromagnet-normal metal structure,” *Supercond. Sci. Technol.*, vol. 31, no. 3, p. 03LT01, 2018, doi: [10.1088/1361-6668/aaa6b6](https://doi.org/10.1088/1361-6668/aaa6b6).
- 32 E. Romans, “Out of the loop—a superconducting tunnel junction that behaves like a SQUID,” *Supercond. Sci. Technol.*, vol. 31, no. 6, p. 060501, June 2018, doi: [10.1088/1361-6668/aac0e6](https://doi.org/10.1088/1361-6668/aac0e6).
- 33 J. Kohlmann and R. Behr, “Development of Josephson voltage standards,” Chapter 11 in: *Superconductivity – Theory and Applications*, Adir Moyses Luiz, Ed., Jul. 2011, doi: [10.5772/17031](https://doi.org/10.5772/17031).
- 34 A. Rüfenacht, N. E. Flowers-Jacobs, and S. P. Benz, “Impact of the latest generation of Josephson voltage standards in ac and dc electric metrology,” *Metrologia*, vol. 55, no. 5, p. S152, 2018, doi: [10.1088/1681-7575/aad41a](https://doi.org/10.1088/1681-7575/aad41a).
- 35 D. P. Leech, “Economic Impact Assessment of the NIST’s Josephson Volt Standard Program,” TASC for The National Institute of Standards and Technology, *Planning Report* 01-1, Jul. 2001. Available online: <https://www.nist.gov/tpo/nist-economic-impact-studies-0>, accessed 2020-03-15.
- 36 N. E. Flowers-Jacobs, A. E. Fox, P. D. Dresselhaus, R. E. Schwall, and S. P. Benz, “Two-volt Josephson arbitrary waveform synthesizer using Wilkinson dividers,” *IEEE Trans. Appl. Supercond.*, vol. 26, no. 6, p. 1400207, Sep. 2016, doi: [10.1109/TASC.2016.2532798](https://doi.org/10.1109/TASC.2016.2532798).
- 37 N. E. Flowers-Jacobs, S. B. Waltman, A. E. Fox, P. D. Dresselhaus, and S. P. Benz, “Josephson arbitrary waveform synthesizer with two layers of Wilkinson dividers and an FIR filter,” *IEEE Trans. Appl. Supercond.*, vol. 26, no. 6, p. 1400307, Sep. 2016, doi: [10.1109/TASC.2016.2582800](https://doi.org/10.1109/TASC.2016.2582800).
- 38 M. I. Faley, E. A. Kostyurina, K. V. Kalashnikov, Y. V. Maslennikov, V. P. Koshelets, and R. E. Dunin-Borkowski, “Superconducting quantum interferometers for nondestructive evaluation,” *Sensors*, vol. 17, no. 12, p. 2798, Dec. 2017, doi: [10.3390/s17122798](https://doi.org/10.3390/s17122798).
- 39 J. R. Kirtley and J. P. Wikswo, “Scanning SQUID microscopy,” *Annu. Rev. Mater. Sci.*, vol. 29, no. 1, pp. 117–148, Aug. 1999, doi: [10.1146/annurev.matsci.29.1.117](https://doi.org/10.1146/annurev.matsci.29.1.117).

- 
- 40 L. A. Knauss *et al.*, “Scanning SQUID microscopy for current imaging,” *Microelectron. Reliab.*, vol. 41, no. 8, pp. 1211–1229, Aug. 2001, doi: [10.1016/S0026-2714\(01\)00108-1](https://doi.org/10.1016/S0026-2714(01)00108-1).
- 41 R. L. Fagaly, “The commercialization of SQUIDs,” *IEEE Trans. Appl. Supercond.*, vol. 25, no. 3, p. 1601507, June 2015, doi: [10.1109/TASC.2014.2364212](https://doi.org/10.1109/TASC.2014.2364212).
- 42 P. Reith, X. R. Wang, and H. Hilgenkamp, “Analysing magnetism using scanning SQUID microscopy,” *Rev. Sci. Instrum.*, vol. 88, no. 12, p. 123706, Dec. 2017, doi: [10.1063/1.5001390](https://doi.org/10.1063/1.5001390).
- 43 T. D. Vu *et al.*, “Constructing a vector scanning SQUID system,” *J. Phys.: Conf. Ser.*, vol. 1054, no. 1, p. 012059, 2018, doi: [10.1088/1742-6596/1054/1/012059](https://doi.org/10.1088/1742-6596/1054/1/012059).
- 44 T. D. Vu *et al.*, “Scanning SQUID microscopy for sensing vector magnetic field,” *IEEE Trans. Appl. Supercond.*, vol. 28, no. 4, p. 1601105, June 2018, doi: [10.1109/TASC.2018.2808765](https://doi.org/10.1109/TASC.2018.2808765).
- 45 H. Oda *et al.*, “Scanning SQUID microscope system for geological samples: System integration and initial evaluation,” *Earth, Planets and Space*, vol. 68, no. 1, p. 179, Nov. 2016, doi: [10.1186/s40623-016-0549-3](https://doi.org/10.1186/s40623-016-0549-3).
- 46 Neocera Magma, LLC. [Online]. Available: <https://neoceramagma.com/products/magma-ssm/>, accessed 2021-03-30.
- 47 Tristan Technologies, Inc. [Online]. Available: [tristantech.com](http://tristantech.com), accessed 2021-03-30.
- 48 S. Nishijima *et al.*, “Superconductivity and the environment: A roadmap,” *Supercond. Sci. Technol.*, vol. 26, no. 11, p. 113001, Sep. 2013, doi: [10.1088/0953-2048/26/11/113001](https://doi.org/10.1088/0953-2048/26/11/113001).
- 49 Powerful Supercomputer Makes ALMA a Telescope, <https://www.nrao.edu/pr/2012/almacorrelator/>, accessed 2021-03-30.
- 50 The Square Kilometre Array Project, <https://www.skatelescope.org/the-ska-project/>, accessed 2021-03-30.
- 51 G. Zhang, J. Ma, A. Alsaedi, B. Ahmad, and F. Alzahrani, “Dynamical behavior and application in Josephson Junction coupled by memristor,” *Appl. Math. Comput.*, vol. 321, pp. 290–299, Mar. 2018, doi: [10.1016/j.amc.2017.10.054](https://doi.org/10.1016/j.amc.2017.10.054).
- 52 Superconductor Technologies Inc., Commercial Wireless Solutions, <https://www.suptech.com/legacy-wireless-products/>, accessed 2021-03-30.
- 53 D. K. Brock, E. K. Track, and J. M. Rowell, “Superconductor ICs: The 100-GHz second generation,” *IEEE Spectrum*, vol. 37, no. 12, pp. 40–46, Dec. 2000, doi: [10.1109/6.887595](https://doi.org/10.1109/6.887595).
- 54 HYPRES, Inc., Advanced Digital-RF Receiver. [Online]. Available: <https://www.hypres.com/products/advanced-digital-rf-receiver/>, accessed 2021-03-30.
- 55 D. Gupta *et al.*, “Modular, multi-function digital-RF receiver systems,” *IEEE Trans. Appl. Supercond.*, vol. 21, no. 3, pp. 883–890, June 2011, doi: [10.1109/TASC.2010.2095399](https://doi.org/10.1109/TASC.2010.2095399).
- 56 Josephson junction count, [https://en.wikipedia.org/wiki/Josephson\\_junction\\_count](https://en.wikipedia.org/wiki/Josephson_junction_count), accessed 2021-03-22.
- 57 As of 2020, the highest transistor count in any IC chip is the Wafer Scale Engine 2 by Cerebras with 2.6 trillion MOSFETs, [https://en.wikipedia.org/wiki/Transistor\\_count](https://en.wikipedia.org/wiki/Transistor_count), accessed 2021-03-30.
- 58 O. Mukhanov, N. Yoshikawa, I. P. Nevirkovets, and M. Hidaka, “Josephson Junctions for Digital Applications,” in *Fundamentals and Frontiers of the Josephson Effect*, F. Tafuri, Ed. Cham: Springer International Publishing, 2019, pp. 611–701, doi: [10.1007/978-3-030-20726-7\\_16](https://doi.org/10.1007/978-3-030-20726-7_16).
- 59 K. K. Likharev and V. K. Semenov, “RSFQ logic/memory family: A new Josephson-junction technology for sub-terahertz-clock-frequency digital systems,” *IEEE Trans. Appl. Supercond.*, vol. 1, no. 1, pp. 3–28, Mar. 1991, doi: [10.1109/77.80745](https://doi.org/10.1109/77.80745).
- 60 Y. Yamanashi, T. Nishigai, and N. Yoshikawa, “Study of LR-loading technique for low-power single flux quantum circuits,” *IEEE Trans. Appl. Supercond.*, vol. 17, no. 2, pp. 150–153, June 2007, doi: [10.1109/TASC.2007.898608](https://doi.org/10.1109/TASC.2007.898608).
- 61 T. Orllepp, O. Wetzstein, S. Engert, J. Kunert, and H. Toepfer, “Reduced power consumption in superconducting electronics,” *IEEE Trans. Appl. Supercond.*, vol. 21, no. 3, pp. 770–775, June 2011, doi: [10.1109/TASC.2011.2117410](https://doi.org/10.1109/TASC.2011.2117410).
- 62 M. Tanaka, M. Ito, A. Kitayama, T. Kouketsu, and A. Fujimaki, “18-GHz, 4.0-aJ/bit operation of ultra-low-energy rapid single-flux-quantum shift registers,” *Jpn. J. Appl. Phys.*, vol. 51, no. 5, p. 053102, May 2012, doi: [10.1143/JJAP.51.053102](https://doi.org/10.1143/JJAP.51.053102).
- 63 M. Tanaka, A. Kitayama, T. Koketsu, M. Ito, and A. Fujimaki, “Low-energy consumption RSFQ circuits driven by low voltages,” *IEEE Trans. Appl. Supercond.*, vol. 23, no. 3, p. 1701104, June 2013, doi: [10.1109/TASC.2013.2240555](https://doi.org/10.1109/TASC.2013.2240555).

- 64 O. A. Mukhanov, "Energy-efficient single flux quantum technology," *IEEE Trans. Appl. Supercond.*, vol. 21, no. 3, pp. 760–769, June 2011, doi: [10.1109/TASC.2010.2096792](https://doi.org/10.1109/TASC.2010.2096792).
- 65 D. E. Kirichenko, S. Sarwana, and A. F. Kirichenko, "Zero static power dissipation biasing of RSFQ circuits," *IEEE Trans. Appl. Supercond.*, vol. 21, no. 3, pp. 776–779, June 2011, doi: [10.1109/TASC.2010.2098432](https://doi.org/10.1109/TASC.2010.2098432).
- 66 M. Volkmann, A. Sahu, C. Fourie, and O. Mukhanov, "Implementation of energy efficient single flux quantum digital circuits with sub-aJ/bit operation," *Supercond. Sci. Technol.*, vol. 26, no. 1, p. 015002, Jan. 2013, doi: [10.1088/0953-2048/26/1/015002](https://doi.org/10.1088/0953-2048/26/1/015002).
- 67 M. H. Volkmann, A. Sahu, A. V. Dotsenko, and O. A. Mukhanov, "Operation of practical eSFQ circuits," in *2013 IEEE 14th International Superconductive Electronics Conference (ISEC)*, Jul. 2013, doi: [10.1109/ISEC.2013.6604279](https://doi.org/10.1109/ISEC.2013.6604279). (184 bit eSFQ shift register with  $184 \times 5 = 920$  JJs)
- 68 M. H. Volkmann, I. V. Vernik, and O. A. Mukhanov, "Wave-pipelined eSFQ circuits," *IEEE Trans. Appl. Supercond.*, vol. 25, no. 3, p. 1301005, June 2015, doi: [10.1109/TASC.2014.2379191](https://doi.org/10.1109/TASC.2014.2379191).
- 69 S. Rylov, "Clockless dynamic SFQ AND gate with high input skew tolerance," *IEEE Trans. Appl. Supercond.*, vol. 29, no. 5, Art. no. 1300805, Aug. 2019, doi: [10.1109/TASC.2019.2896137](https://doi.org/10.1109/TASC.2019.2896137).
- 70 S. Rylov, "Direct current powered clockless superconducting logic family using dynamic internal state," *United States Patent 10680617B2*, June 2020.
- 71 T. Kawaguchi, K. Takagi, and N. Takagi, "Rapid single-flux-quantum logic circuits using clockless gates," *IEEE Trans. Appl. Supercond.*, 2021, doi: [10.1109/TASC.2021.3068960](https://doi.org/10.1109/TASC.2021.3068960).
- 72 Q. P. Herr, A. Y. Herr, O. T. Oberg, and A. G. Ioannidis, "Ultra-low-power superconductor logic," *J. Appl. Phys.*, vol. 109, no. 10, p. 103903, May 2011, doi: [10.1063/1.3585849](https://doi.org/10.1063/1.3585849).
- 73 O. T. Oberg, Q. P. Herr, A. G. Ioannidis, and A. Y. Herr, "Integrated power divider for superconducting digital circuits," *IEEE Trans. Appl. Supercond.*, vol. 21, no. 3, pp. 571–574, June 2011, doi: [10.1109/TASC.2010.2086415](https://doi.org/10.1109/TASC.2010.2086415).
- 74 A. Y. Herr, Q. P. Herr, O. T. Oberg, O. Naaman, J. X. Przybysz, P. Borodulin, and S. B. Shauck, "An 8-bit carry look-ahead adder with 150 ps latency and sub-microwatt power dissipation at 10 GHz," *J. Appl. Phys.*, vol. 113, no. 3, p. 033911, Jan. 2013, doi: [10.1063/1.4776713](https://doi.org/10.1063/1.4776713).
- 75 D. Carmean, A. Braun, A. Y. Herr, and Q. P. Herr, "Phase-mode based superconducting logic," *United States Patent 9887700B2*, Feb. 2018.
- 76 N. Takeuchi, D. Ozawa, Y. Yamanashi, and N. Yoshikawa, "An adiabatic quantum flux parametron as an ultra-low-power logic device," *Supercond. Sci. Tech.*, vol. 26, 035010, Mar. 2013, doi: [10.1088/0953-2048/26/3/035010](https://doi.org/10.1088/0953-2048/26/3/035010).
- 77 B. A. Butters, R. Baghdadi, M. Onen, E. A. Toomey, O. Medeiros, and K. K. Berggren, "A scalable superconducting nanowire memory cell and preliminary array test," *Supercond. Sci. Technol.*, vol. 34, no. 3, p. 035003, Jan. 2021, doi: [10.1088/1361-6668/abd14e](https://doi.org/10.1088/1361-6668/abd14e).
- 78 Y. Ando, R. Sato, M. Tanaka, K. Takagi, N. Takagi, and A. Fujimaki, "Design and demonstration of an 8-bit bit-serial RSFQ microprocessor: CORE e4," *IEEE Trans. Appl. Supercond.*, vol. 26, no. 5, p. 1301205, Aug. 2016, doi: [10.1109/TASC.2016.2565609](https://doi.org/10.1109/TASC.2016.2565609).
- 79 R. Sato *et al.*, "High-speed operation of random-access-memory-embedded microprocessor with minimal instruction set architecture based on rapid single-flux-quantum logic," *IEEE Trans. Appl. Supercond.*, vol. 27, no. 4, p. 1300505, June 2017, doi: [10.1109/TASC.2016.2642049](https://doi.org/10.1109/TASC.2016.2642049).
- 80 X. Peng, Q. Xu, T. Kato, Y. Yamanashi, N. Yoshikawa, A. Fujimaki, N. Takagi, K. Takagi and M. Hidaka, "High-speed demonstration of bit-serial floating-point adders and multipliers using single-flux-quantum circuits," *IEEE Trans. Appl. Supercond.*, vol. 25, p. 1301106, June 2015, doi: [10.1109/TASC.2014.2382973](https://doi.org/10.1109/TASC.2014.2382973).
- 81 F. Ke, O. Chen, Y. Wang, and N. Yoshikawa, "Demonstration of a 47.8 GHz high-speed FFT processor using single-flux-quantum technology," *IEEE Trans. Appl. Supercond.*, vol. 31, no. 5, Art. no. 1300905, Aug. 2021, doi: [10.1109/TASC.2021.3059984](https://doi.org/10.1109/TASC.2021.3059984).
- 82 A. Fujimaki *et al.*, "Large-scale integrated circuit design based on a Nb nine-layer structure for reconfigurable data-path processors," *IEICE Trans. Electron.*, vol. E97–C, no. 3, pp. 157–165, Mar. 2014, doi: [10.1587/transele.E97.C.157](https://doi.org/10.1587/transele.E97.C.157).
- 83 S. Nagasawa, T. Satoh, and M. Hidaka, "Uniformity and reproducibility of submicron 20 kA/cm<sup>2</sup> Nb/AlO<sub>x</sub>/Nb Josephson junction process," in *15th Int. Supercond. Electron. Conf. (ISEC 2015)*, Nagoya, Japan, 2015, doi: [10.1109/ISEC.2015.7383488](https://doi.org/10.1109/ISEC.2015.7383488).

- 84 M. Tanaka *et al.*, “High-throughput bit-parallel arithmetic logic unit using rapid single-flux-quantum logic,” *16th Int. Supercond. Electron. Conf. (ISEC 2017)*, Sorrento, Italy, 2017.
- 85 R. Kashima, I. Nagaoka, M. Tanaka, T. Yamashita, and A. Fujimaki, “64-GHz datapath demonstration for bit-parallel SFQ microprocessors based on a gate-level-pipeline structure,” *IEEE Trans. Appl. Supercond.*, vol. 31, no. 5, Art. no. 1301006, Aug. 2021, doi: [10.1109/TASC.2021.3061353](https://doi.org/10.1109/TASC.2021.3061353).
- 86 M. Tanaka, M. Ito, A. Kitayama, T. Kouketsu, and A. Fujimaki, “18-GHz, 4.0-aJ/bit operation of ultra-low-energy rapid single-flux-quantum shift registers,” *Jpn. J. Appl. Phys.*, vol. 51, no. 5, p. 053102, May 2012, doi: [10.1143/JJAP.51.053102](https://doi.org/10.1143/JJAP.51.053102).
- 87 I. Nagaoka, M. Tanaka, K. Sano, T. Yamashita, A. Fujimaki, and K. Inoue, “Demonstration of an energy-efficient, gate-level-pipelined 100 TOPS/W arithmetic logic unit based on low-voltage rapid single-flux-quantum logic,” *ISEC 2019*, Riverside, CA, USA, Jul. 2019, doi: [10.1109/ISEC46533.2019.8990905](https://doi.org/10.1109/ISEC46533.2019.8990905).
- 88 M. Tanaka, M. Kozaka, Y. Kita, A. Fujimaki, S. Nagasawa, and M. Hidaka, “Rapid single-flux-quantum circuits fabricated using 20-kA/cm<sup>2</sup> Nb/AlO<sub>x</sub>/Nb process,” *IEEE Trans. Appl. Supercond.*, vol. 25, no. 3, p. 1100304, June 2015, doi: [10.1109/TASC.2014.2365100](https://doi.org/10.1109/TASC.2014.2365100).
- 89 F. Li, Y. Takeshita, D. Hasegawa, M. Tanaka, T. Yamashita, and A. Fujimaki, “Low-power high-speed half-flux-quantum circuits driven by low bias voltages,” *Supercond. Sci. Technol.*, vol. 34, no. 2, p. 025013, Feb. 2021, doi: [10.1088/1361-6668/abcaac](https://doi.org/10.1088/1361-6668/abcaac).
- 90 O. A. Mukhanov, “Energy-efficient single flux quantum technology,” *IEEE Trans. Appl. Supercond.*, vol. 21, no. 3, pp. 760–769, June 2011, doi: [10.1109/TASC.2010.2096792](https://doi.org/10.1109/TASC.2010.2096792).
- 91 D. E. Kirichenko, S. Sarwana, and A. F. Kirichenko, “Zero static power dissipation biasing of RSFQ circuits,” *IEEE Trans. Appl. Supercond.*, vol. 21, no. 3, pp. 776–779, June 2011, doi: [10.1109/TASC.2010.2098432](https://doi.org/10.1109/TASC.2010.2098432).
- 92 C. Shawawreh *et al.*, “Effects of adaptive DC biasing on operational margins in ERSFQ circuits,” *IEEE Trans. Appl. Supercond.*, vol. 27, no. 4, pp. 1–6, June 2017, doi: [10.1109/TASC.2017.2669581](https://doi.org/10.1109/TASC.2017.2669581).
- 93 A. F. Kirichenko, I. V. Vernik, J. A. Vivalda, R. T. Hunt, and D. T. Yohannes, “ERSFQ 8-bit parallel adders as a process benchmark,” *IEEE Trans. Appl. Supercond.*, vol. 25, no. 3, p. 1300505, June 2015, doi: [10.1109/TASC.2014.2371875](https://doi.org/10.1109/TASC.2014.2371875).
- 94 I. V. Vernik, A. F. Kirichenko, O. A. Mukhanov, and T. A. Ohki, “Energy-efficient and compact ERSFQ decoder for cryogenic RAM,” *IEEE Trans. Appl. Supercond.*, vol. 27, no. 4, p. 1301205, Dec. 2016, doi: [10.1109/TASC.2016.2646926](https://doi.org/10.1109/TASC.2016.2646926).
- 95 M. E. Çelik *et al.*, “Fast RSFQ and ERSFQ parallel counters,” *IEEE Trans. Appl. Supercond.*, vol. 30, no. 7, p. 1302404, Oct. 2020, doi: [10.1109/TASC.2020.3010692](https://doi.org/10.1109/TASC.2020.3010692).
- 96 N. K. Katam, O. A. Mukhanov, and M. Pedram, “Superconducting magnetic field programmable gate array,” *IEEE Trans. Appl. Supercond.*, vol. 28, no. 2, p. 1300212, Jan. 2018, doi: [10.1109/TASC.2018.2797262](https://doi.org/10.1109/TASC.2018.2797262).
- 97 I. V. Vernik, S. B. Kaplan, M. H. Volkmann, A. V. Dotsenko, C. J. Fourie, and O. A. Mukhanov, “Design and test of asynchronous eSFQ circuits,” *Supercond. Sci. Technol.*, vol. 27, no. 4, p. 044030, Apr. 2014, doi: [10.1088/0953-2048/27/4/044030](https://doi.org/10.1088/0953-2048/27/4/044030).
- 98 Q. P. Herr, A. Y. Herr, O. T. Oberg, and A. G. Ioannidis, “Ultra-low-power superconductor logic,” *J. Appl. Phys.*, vol. 109, no. 10, p. 103903, May 2011, doi: [10.1063/1.3585849](https://doi.org/10.1063/1.3585849).
- 99 O. T. Oberg, Q. P. Herr, A. G. Ioannidis, and A. Y. Herr, “Integrated power divider for superconducting digital circuits,” *IEEE Trans. Appl. Supercond.*, vol. 21, no. 3, pp. 571–574, June 2011, doi: [10.1109/TASC.2010.2086415](https://doi.org/10.1109/TASC.2010.2086415).
- 100 A. Y. Herr, Q. P. Herr, O. T. Oberg, O. Naaman, J. X. Przybysz, P. Borodulin, and S. B. Shauck, “An 8-bit carry look-ahead adder with 150 ps latency and sub-microwatt power dissipation at 10 GHz,” *J. Appl. Phys.*, vol. 113, no. 3, p. 033911, Jan. 2013, doi: [10.1063/1.4776713](https://doi.org/10.1063/1.4776713).
- 101 M. Vesely Jr. *et al.*, “An 8-bit and 16-bit ALU for superconducting reciprocal quantum logic (RQL) CPUs,” presentation 1EPo2E-09 [E29], Applied Superconductivity Conference, Seattle, WA, USA, Oct. 28 – Nov. 2, 2018.
- 102 Q. P. Herr *et al.*, “Reproducible operating margins on a 72 800-device digital superconducting chip,” *Supercond. Sci. Technol.*, vol. 28, no. 12, p. 124003, Dec. 2015, doi: [10.1088/0953-2048/28/12/124003](https://doi.org/10.1088/0953-2048/28/12/124003).
- 103 R. Clarke *et al.*, “Demonstrations of RQL memories for a 16-bit CPU,” presentation 3EOr2C-01, Applied Superconductivity Conference, Seattle, WA, USA, Oct. 28 – Nov. 2, 2018.

- 
- 104 P. Farrell *et al.*, “A superconducting 8-bit CPU design,” presentation 1EOr1C-03, Applied Superconductivity Conference, Seattle, WA, USA, Oct. 28 – Nov. 2, 2018.
- 105 N. Takeuchi, D. Ozawa, Y. Yamanashi, and N. Yoshikawa, “An adiabatic quantum flux parametron as an ultra-low-power logic device,” *Supercond. Sci. Tech.*, vol. 26, 035010, Mar. 2013, doi: [10.1088/0953-2048/26/3/035010](https://doi.org/10.1088/0953-2048/26/3/035010).
- 106 N. Takeuchi, Y. Yamanashi, N. Yoshikawa, “Energy efficiency of adiabatic superconductor logic,” *Supercond. Sci. Technol.*, vol. 28, 015003, Jan. 2015, doi: [10.1088/0953-2048/28/1/015003](https://doi.org/10.1088/0953-2048/28/1/015003).
- 107 T. Yamae, N. Takeuchi, and N. Yoshikawa, “Systematic method to evaluate energy dissipation in adiabatic quantum-flux-parametron logic,” *J. Appl. Phys.*, vol. 126, no. 17, p. 173903, Nov. 2019, doi: [10.1063/1.5119306](https://doi.org/10.1063/1.5119306).
- 108 N. Takeuchi, Y. Yamanashi, and N. Yoshikawa, “Simulation of sub- $k_B T$  bit-energy operation of adiabatic quantum-flux-parametron logic with low bit-error-rate,” *Appl. Phys. Lett.*, vol. 103, 62602, Aug. 2013, doi: [10.1063/1.4817974](https://doi.org/10.1063/1.4817974).
- 109 N. Takeuchi, Y. Yamanashi, and N. Yoshikawa, “Reversible logic gate using adiabatic superconducting devices,” *Sci. Rep.*, vol. 4, 6354, Sep. 2014, doi: [10.1038/srep06354](https://doi.org/10.1038/srep06354).
- 110 N. Takeuchi, Y. Yamanashi, and N. Yoshikawa, “Reversibility and energy dissipation in adiabatic superconductor logic,” *Sci. Rep.*, vol. 7, no. 1, p. 75, Mar. 2017, doi: [10.1038/s41598-017-00089-9](https://doi.org/10.1038/s41598-017-00089-9).
- 111 N. Takeuchi and N. Yoshikawa, “Minimum energy dissipation required for a logically irreversible operation,” *Phys. Rev. E*, vol. 97, no. 1, p. 012124, Jan. 2018, doi: [10.1103/PhysRevE.97.012124](https://doi.org/10.1103/PhysRevE.97.012124).
- 112 N. Takeuchi, Y. Yamanashi, and N. Yoshikawa, “Measurement of 10 zJ energy dissipation of adiabatic quantum-flux-parametron logic using a superconducting resonator,” *Appl. Phys. Lett.*, vol. 102, 052602, Feb. 2013, doi: [10.1063/1.4790276](https://doi.org/10.1063/1.4790276).
- 113 N. Takeuchi, H. Suzuki, N. Yoshikawa, “Measurement of low bit-error-rates of adiabatic quantum-flux-parametron logic using a superconductor voltage driver,” *Appl. Phys. Lett.*, vol. 110, 202601, May 2017, doi: [10.1063/1.4983351](https://doi.org/10.1063/1.4983351).
- 114 K. Fang, N. Takeuchi, T. Ando, Y. Yamanashi, and N. Yoshikawa, “Multi-excitation adiabatic quantum-flux-parametron,” *J. Appl. Phys.*, vol. 121, p. 143901, 2017, doi: [10.1063/1.4979856](https://doi.org/10.1063/1.4979856).
- 115 M.N. Takeuchi, M. Nozoe, Y. He, and N. Yoshikawa, “Low-latency adiabatic superconductor logic using delay-line clocking,” *Appl. Phys. Lett.*, vol. 115, no. 7, p. 072601, Aug. 2019, doi: [10.1063/1.5111599](https://doi.org/10.1063/1.5111599).
- 116 Y. He, N. Takeuchi, and N. Yoshikawa, “Low-latency power-dividing clocking scheme for adiabatic quantum-flux-parametron logic,” *Appl. Phys. Lett.*, vol. 116, no. 18, p. 182602, May 2020, doi: [10.1063/5.0005612](https://doi.org/10.1063/5.0005612).
- 117 Y. He *et al.*, “A Compact AQFP Logic Cell Design Using an 8-Metal Layer Superconductor Process,” *Supercond. Sci. Technol.*, vol. 33, Art. no. 035010, Feb. 2020, doi: [10.1088/1361-6668/ab6feb](https://doi.org/10.1088/1361-6668/ab6feb).
- 118 O. Chen *et al.*, “Adiabatic quantum-flux-parametron: Towards building extremely energy-efficient circuits and systems,” *Sci. Rep.*, vol. 9, no. 1, p. 10514, Jul. 2019, doi: [10.1038/s41598-019-46595-w](https://doi.org/10.1038/s41598-019-46595-w).
- 119 O. Chen, T. Tanaka, R. Saito, C. L. Ayala, N. Takeuchi, and N. Yoshikawa, “Design of adiabatic quantum-flux-parametron register files using a top-down design flow,” *IEEE Trans. Appl. Supercond.*, 2019, doi: [10.1109/TASC.2019.2908277](https://doi.org/10.1109/TASC.2019.2908277).
- 120 T. Tanaka, C. L. Ayala, Q. Xu, R. Saito, and N. Yoshikawa, “Fabrication of adiabatic quantum-flux-parametron integrated circuits using an automatic placement tool based on genetic algorithms,” *IEEE Trans. Appl. Supercond.*, vol. 29, no. 5, p. 1301706, Aug. 2019, doi: [10.1109/TASC.2019.2900220](https://doi.org/10.1109/TASC.2019.2900220).
- 121 N. Takeuchi, Y. Yamanashi, and N. Yoshikawa, “Adiabatic quantum-flux-parametron cell library adopting minimalist design,” *J. Appl. Phys.*, vol. 117, 173912, May 2015, doi: [10.1063/1.4919838](https://doi.org/10.1063/1.4919838).
- 122 C. L. Ayala, N. Takeuchi, Y. Yamanashi, T. Ortlev, and N. Yoshikawa, “Majority-logic-optimized parallel prefix carry look-ahead adder families using adiabatic quantum-flux-parametron logic,” *IEEE Trans. Appl. Supercond.*, vol. 27, 1300407, June 2017, doi: [10.1109/TASC.2016.2642041](https://doi.org/10.1109/TASC.2016.2642041).
- 123 N. Tsuji, C. L. Ayala, N. Takeuchi, T. Ortlev, Y. Yamanashi, and N. Yoshikawa, “Design and implementation of a 16-word by 1-bit register file using adiabatic quantum flux parametron logic,” *IEEE Trans. Appl. Supercond.*, vol. 27, 1300904, June 2017, doi: [10.1109/TASC.2016.2642041](https://doi.org/10.1109/TASC.2016.2642041).
- 124 N. Takeuchi, T. Yamae, C. L. Ayala, H. Suzuki, and N. Yoshikawa, “An adiabatic superconductor 8-bit adder with 24kBT energy dissipation per junction,” *Appl. Phys. Lett.*, vol. 114, no. 4, p. 042602, Jan. 2019, doi: [10.1063/1.5080753](https://doi.org/10.1063/1.5080753).

- 125 C. L. Ayala, T. Tanaka, R. Saito, M. Nozoe, N. Takeuchi, and N. Yoshikawa, "MANA: A monolithic adiabatic integration architecture microprocessor using 1.4zJ/op unshunted superconductor Josephson junction devices," *IEEE J. Solid-State Circuits*, Dec. 2020, doi: [10.1109/JSSC.2020.3041338](https://doi.org/10.1109/JSSC.2020.3041338).
- 126 N. Takeuchi, K. Arai, and N. Yoshikawa, "Directly coupled adiabatic superconductor logic," *Supercond. Sci. Technol.*, vol. 33, no. 6, p. 065002, May 2020, doi: [10.1088/1361-6668/ab87ad](https://doi.org/10.1088/1361-6668/ab87ad).
- 127 R. Ishida, N. Takeuchi, T. Yamae, and N. Yoshikawa, "Design and demonstration of directly coupled quantum-flux-parametron circuits with optimized parameters," *IEEE Trans. Appl. Supercond.*, vol. 31, no. 5, Art. no. 1100505, Aug. 2021, doi: [10.1109/TASC.2021.3059723](https://doi.org/10.1109/TASC.2021.3059723).
- 128 K. Arai, N. Takeuchi, T. Yamashita, and N. Yoshikawa, "Adiabatic quantum-flux-parametron with  $\pi$  Josephson junctions," *J. Appl. Phys.*, vol. 125, no. 9, p. 093901, Mar. 2019, doi: [10.1063/1.5080467](https://doi.org/10.1063/1.5080467).
- 129 K. Likharev, "Dynamics of some single flux quantum devices: I. Parametric quantron," *IEEE Trans. Magn.*, vol. 13, no. 1, pp. 242–244, Jan. 1977, doi: [10.1109/TMAG.1977.1059351](https://doi.org/10.1109/TMAG.1977.1059351).
- 130 Y. Harada, E. Goto, and N. Miyamoto, "Quantum flux parametron," in *1987 International Electron Devices Meeting*, 1987, pp. 389–392, doi: [10.1109/IEDM.1987.191439](https://doi.org/10.1109/IEDM.1987.191439).
- 131 J. Ren and V. K. Semenov, "Progress with physically and logically reversible superconducting digital circuits," *IEEE Trans. Appl. Supercond.*, vol. 21, no. 3, pp. 780–786, June 2011, doi: [10.1109/TASC.2011.2104352](https://doi.org/10.1109/TASC.2011.2104352).
- 132 M. Lucci *et al.*, "Low-power digital gates in ERSFQ and nSQUID technology," *IEEE Trans. Appl. Supercond.*, vol. 26, no. 3, pp. 1–5, Apr. 2016, doi: [10.1109/TASC.2016.2535146](https://doi.org/10.1109/TASC.2016.2535146).
- 133 N. Takeuchi, Y. Yamanashi, and N. Yoshikawa, "Recent progress on reversible quantum-flux-parametron for superconductor reversible computing," *IEICE Trans. Electron.*, vol. E101.C, no. 5, pp. 352–358, May 2018, doi: [10.1587/transele.E101.C.352](https://doi.org/10.1587/transele.E101.C.352).
- 134 T. Yamae, N. Takeuchi, and N. Yoshikawa, "A reversible full adder using adiabatic superconductor logic," *Supercond. Sci. Technol.*, vol. 32, no. 3, p. 035005, Jan. 2019, doi: [10.1088/1361-6668/aaf8c9](https://doi.org/10.1088/1361-6668/aaf8c9).
- 135 T. Asai, K. Yamada, and Y. Amemiya, "Single-flux-quantum logic circuits exploiting collision-based fusion gates," *Physica C*, vol. 468, no. 15, pp. 1983–1986, Sep. 2008, doi: [10.1016/j.physc.2008.05.273](https://doi.org/10.1016/j.physc.2008.05.273).
- 136 K. Yamada, T. Asai, and Y. Amemiya, "Combinational logic computing for single-flux quantum circuits with asynchronous collision-based fusion gates," in *23rd Intl. Tech. Conf. Circuits/Systems, Computers, and Communications (ITC-CSCC 2008)*, pp. 445–448, 2008, doi: [10.34385/proc.39.H3-5](https://doi.org/10.34385/proc.39.H3-5).
- 137 Q. P. Herr, J. E. Baumgardner, and A. Y. Herr, "Method and apparatus for ballistic single flux quantum logic," *United States Patent 7868645B2*, Jan. 2011.
- 138 K. D. Osborn and W. Wustmann, "Ballistic reversible gates matched to bit storage: Plans for an efficient CNOT gate using fluxons," *Reversible Computation*, 2018, pp. 189–204, doi: [10.1007/978-3-319-99498-7\\_13](https://doi.org/10.1007/978-3-319-99498-7_13).
- 139 W. Wustmann and K. D. Osborn, "Reversible fluxon logic: Topological particles allow ballistic gates along one-dimensional paths," *Phys. Rev. B*, vol. 101, no. 1, p. 014516, Jan. 2020, doi: [10.1103/PhysRevB.101.014516](https://doi.org/10.1103/PhysRevB.101.014516).
- 140 M. P. Frank, "Asynchronous ballistic reversible computing," in *2017 IEEE International Conference on Rebooting Computing (ICRC)*, 2017, doi: [10.1109/ICRC.2017.8123659](https://doi.org/10.1109/ICRC.2017.8123659).
- 141 M. P. Frank, R. M. Lewis, N. A. Missert, M. A. Wolak, and M. D. Henry, "Asynchronous ballistic reversible fluxon logic," *IEEE Trans. Appl. Supercond.*, vol. 29, no. 5, p. 1302007, Aug. 2019, doi: [10.1109/TASC.2019.2904962](https://doi.org/10.1109/TASC.2019.2904962).
- 142 A. N. McCaughan, N. S. Abebe, Q.-Y. Zhao, and K. K. Berggren, "Using geometry to sense current," *Nano Lett.*, vol. 16, no. 12, pp. 7626–7631, Nov. 2016, doi: [10.1021/acs.nanolett.6b03593](https://doi.org/10.1021/acs.nanolett.6b03593).
- 143 Q.-Y. Zhao, A. N. McCaughan, A. E. Dane, K. K. Berggren, and T. Ortlev, "A nanocryotron comparator can connect single-flux-quantum circuits to conventional electronics," *Supercond. Sci. Technol.*, vol. 30, no. 4, p. 044002, 2017, doi: [10.1088/1361-6668/aa5f33](https://doi.org/10.1088/1361-6668/aa5f33).
- 144 K. Sano *et al.*, "Thermally assisted superconductor transistors for Josephson-CMOS hybrid memories," *IEICE Trans. Electron.*, vol. E101.C, no. 5, pp. 370–377, May 2018, doi: [10.1587/transele.E101.C.370](https://doi.org/10.1587/transele.E101.C.370).
- 145 E. Toomey, M. Onen, M. Colangelo, B. A. Butters, A. N. McCaughan, and K. K. Berggren, "Bridging the gap between nanowires and Josephson junctions: A superconducting device based on controlled fluxon transfer," *Phys. Rev. Applied*, vol. 11, no. 3, p. 034006, Mar. 2019, doi: [10.1103/PhysRevApplied.11.034006](https://doi.org/10.1103/PhysRevApplied.11.034006).



- 146 M. Onen, B. A. Butters, E. Toomey, T. Gokmen, and K. K. Berggren, "Design and characterization of superconducting nanowire-based processors for acceleration of deep neural network training," *Nanotechnology*, vol. 31, no. 2, p. 025204, Oct. 2019, doi: [10.1088/1361-6528/ab47bc](https://doi.org/10.1088/1361-6528/ab47bc).
- 147 K. Zheng *et al.*, "A superconducting binary encoder with multigate nanowire cryotrons," *Nano Lett.*, Apr. 2020, doi: [10.1021/acs.nanolett.0c00498](https://doi.org/10.1021/acs.nanolett.0c00498).
- 148 S. Lynch, J. Borresen, and K. Latham, "Josephson junction binary oscillator computing," in *2013 IEEE 14th International Superconductive Electronics Conference (ISEC)*, 2013, doi: [10.1109/ISEC.2013.6604275](https://doi.org/10.1109/ISEC.2013.6604275).
- 149 V. K. Vlasko-Vlasov, F. Colauto, T. Benseman, D. Rosenmann, and W.-K. Kwok, "Triode for magnetic flux quanta," *Sci. Rep.*, vol. 6, p. 36847, Nov. 2016, doi: [10.1038/srep36847](https://doi.org/10.1038/srep36847).
- 150 J. E. Mooij *et al.*, "Superconductor-insulator transition in nanowires and nanowire arrays," *New J. Phys.*, vol. 17, no. 3, p. 033006, 2015, doi: [10.1088/1367-2630/17/3/033006](https://doi.org/10.1088/1367-2630/17/3/033006).
- 151 S. E. de Graaf *et al.*, "Charge quantum interference device," *Nat. Phys.*, vol. 14, no. 6, pp. 590–594, June 2018, doi: [10.1038/s41567-018-0097-9](https://doi.org/10.1038/s41567-018-0097-9).
- 152 U. S. Goteti and M. C. Hamilton, "Charge-based superconducting digital logic family using quantum phase-slip junctions," *IEEE Trans. Appl. Supercond.*, vol. 28, no. 4, p. 1300504, June 2018, doi: [10.1109/TASC.2018.2803123](https://doi.org/10.1109/TASC.2018.2803123).
- 153 N. G. N. Constantino, M. S. Anwar, O. W. Kennedy, M. Dang, P. A. Warburton, and J. C. Fenton, "Emergence of quantum phase-slip behaviour in superconducting NbN nanowires: DC electrical transport and fabrication technologies," *Nanomaterials (Basel)*, vol. 8, no. 6, June 2018, doi: [10.3390/nano8060442](https://doi.org/10.3390/nano8060442).
- 154 R. Cheng, U. S. Goteti, and M. C. Hamilton, "Spiking neuron circuits using superconducting quantum phase-slip junctions," *J. Appl. Phys.*, vol. 124, no. 15, p. 152126, Oct. 2018, doi: [10.1063/1.5042421](https://doi.org/10.1063/1.5042421).
- 155 R. Cheng, U. S. Goteti, and M. C. Hamilton, "Superconducting neuromorphic computing using quantum phase-slip junctions," *IEEE Trans. Appl. Supercond.*, vol. 29, no. 5, p. 1300505, Aug. 2019, doi: [10.1109/TASC.2019.2892111](https://doi.org/10.1109/TASC.2019.2892111).
- 156 U. S. Goteti and M. C. Hamilton, "Complementary quantum logic family using Josephson junctions and quantum phase-slip junctions," *IEEE Trans. Appl. Supercond.*, vol. 29, no. 5, p. 1302206, Aug. 2019, doi: [10.1109/TASC.2019.2904695](https://doi.org/10.1109/TASC.2019.2904695).
- 157 M. Lyatti *et al.*, "Energy-level quantization and single-photon control of phase slips in YBa<sub>2</sub>Cu<sub>3</sub>O<sub>7-x</sub> nanowires," *Nat. Commun.*, vol. 11, no. 1, p. 763, Feb. 2020, doi: [10.1038/s41467-020-14548-x](https://doi.org/10.1038/s41467-020-14548-x).
- 158 M. C. Hamilton and U. S. Goteti, "Quantum phase slip junction based adiabatic logic circuits and applications of same," *US10879906B2*, Dec. 29, 2020.
- 159 M. Eschrig, "Spin-polarized supercurrents for spintronics," *Phys. Today*, vol. 64, no. 1, p. 43, 2011, doi: [10.1063/1.3541944](https://doi.org/10.1063/1.3541944).
- 160 M. G. Blamire and J. W. A. Robinson, "The interface between superconductivity and magnetism: Understanding and device prospects," *J. Phys.: Condens. Matter*, vol. 26, no. 45, p. 453201, 2014, doi: [10.1088/0953-8984/26/45/453201](https://doi.org/10.1088/0953-8984/26/45/453201).
- 161 M. Eschrig, "Spin-polarized supercurrents for spintronics: A review of current progress," *Rep. Prog. Phys.*, vol. 78, no. 10, p. 104501, 2015, doi: [10.1088/0034-4885/78/10/104501](https://doi.org/10.1088/0034-4885/78/10/104501).
- 162 J. Linder and J. W. A. Robinson, "Superconducting spintronics," *Nat. Phys.*, vol. 11, no. 4, pp. 307–315, Apr. 2015, doi: [10.1038/nphys3242](https://doi.org/10.1038/nphys3242).
- 163 J. A. Ouassou, S. H. Jacobsen, and J. Linder, "Conservation of spin supercurrents in superconductors," *Phys. Rev. B*, vol. 96, no. 9, p. 094505, Sep. 2017, doi: [10.1103/PhysRevB.96.094505](https://doi.org/10.1103/PhysRevB.96.094505).
- 164 H. Yang, S.-H. Yang, S. Takahashi, S. Maekawa, and S. S. P. Parkin, "Extremely long quasiparticle spin lifetimes in superconducting aluminium using MgO tunnel spin injectors," *Nat. Mater.*, vol. 9, no. 7, pp. 586–593, Jul. 2010, doi: [10.1038/nmat2781](https://doi.org/10.1038/nmat2781).
- 165 C. H. L. Quay, D. Chevallier, C. Bena, and M. Aprili, "Spin imbalance and spin-charge separation in a mesoscopic superconductor," *Nat. Phys.*, vol. 9, no. 2, pp. 84–88, Feb. 2013, doi: [10.1038/nphys2518](https://doi.org/10.1038/nphys2518).
- 166 J. A. Ouassou, J. W. A. Robinson, and J. Linder, "Controlling spin supercurrents via nonequilibrium spin injection," *Sci. Rep.*, vol. 9, no. 1, Art. no. 12731, Sep. 2019, doi: [10.1038/s41598-019-48945-0](https://doi.org/10.1038/s41598-019-48945-0).

- 167 S. Nagasawa, K. Hinode, T. Satoh, Y. Kitagawa, and M. Hidaka, "Design of all-dc-powered high-speed single flux quantum random access memory based on a pipeline structure for memory cell arrays," *Supercond. Sci. Technol.*, vol. 19, no. 5, pp. S325–S330, May 2006, doi: [10.1088/0953-2048/19/5/S34](https://doi.org/10.1088/0953-2048/19/5/S34).
- 168 S. Nagasawa, T. Satoh, K. Hinode, Y. Kitagawa, and M. Hidaka, "Yield evaluation of 10-kA/cm<sup>2</sup> Nb multi-layer fabrication process using conventional superconducting RAMs," *IEEE Trans. Appl. Supercond.*, vol. 17, no. 2, pp. 177–180, June 2007, doi: [10.1109/TASC.2007.898050](https://doi.org/10.1109/TASC.2007.898050).
- 169 R. Burnett *et al.*, "Demonstration of superconducting memory for an RQL CPU," in *MEMSYS '18: Proc. Int. Symp. Memory Systems*, Oct. 2018, pp. 321–323, doi: [10.1145/3240302.3270313](https://doi.org/10.1145/3240302.3270313).
- 170 R. Posey, R. Burnett, Q. Herr, and D. Miller, "Demonstration of superconducting memory with passive transmission line-based reads," in *MEMSYS '19: Proc. Int. Symp. Memory Systems*, Sep. 2019, pp. 531–533, doi: [10.1145/3357526.3357577](https://doi.org/10.1145/3357526.3357577).
- 171 R. Posey, R. Burnett, D. Miller, and Q. Herr, "Demonstration of superconducting PRAM memory," presentation Wk1EOr2B-01 at the 2020 Applied Superconductivity Conference, Oct. 28, 2020.
- 172 V. K. Semenov, Y. A. Polyakov, and S. K. Tolpygo, "Very large scale integration of Josephson-junction-based superconductor random access memories," *IEEE Trans. Appl. Supercond.*, vol. 29, no. 5, p. 1302809, Aug. 2019, doi: [10.1109/TASC.2019.2904971](https://doi.org/10.1109/TASC.2019.2904971).
- 173 T. Hosoya, Y. Yamanashi, and N. Yoshikawa, "Compact superconducting lookup table composed of two-dimensional memory cell array reconfigured by external DC control currents," *IEEE Trans. Appl. Supercond.*, vol. 31, no. 3, p. 1300406, Apr. 2021, doi: [10.1109/TASC.2021.3049771](https://doi.org/10.1109/TASC.2021.3049771).
- 174 Y. Takeshita *et al.*, "High-speed memory based on 0- $\pi$  SQUIDs with passive transmission lines," *IEEE Trans. Appl. Supercond.*, vol. 31, no. 5, Art. no. 1100906, 2021, doi: [10.1109/TASC.2021.3060351](https://doi.org/10.1109/TASC.2021.3060351).
- 175 A. Vedyayev, C. Lacroix, N. Pugach, and N. Ryzhanova, "Spin-valve magnetic sandwich in a Josephson junction," *Europhys. Lett.*, vol. 71, no. 4, p. 679, Jul. 2005, doi: [10.1209/epl/i2005-10118-y](https://doi.org/10.1209/epl/i2005-10118-y).
- 176 D. Lenk *et al.*, "Full-switching FSF-type superconducting spin-triplet magnetic random access memory element," *Phys. Rev. B*, vol. 96, no. 18, p. 184521, Nov. 2017, doi: [10.1103/PhysRevB.96.184521](https://doi.org/10.1103/PhysRevB.96.184521).
- 177 Z. Feng, J. W. A. Robinson, and M. G. Blamire, "Out of plane superconducting Nb/Cu/Ni/Cu/Co triplet spin-valves," *Appl. Phys. Lett.*, vol. 111, no. 4, p. 042602, Jul. 2017, doi: [10.1063/1.4995434](https://doi.org/10.1063/1.4995434).
- 178 M. G. Flokstra *et al.*, "Controlled suppression of superconductivity by the generation of polarized Cooper pairs in spin-valve structures," *Phys. Rev. B*, vol. 91, no. 6, p. 060501, Feb. 2015, doi: [10.1103/PhysRevB.91.060501](https://doi.org/10.1103/PhysRevB.91.060501).
- 179 A. Singh, S. Voltan, K. Lahabi, and J. Aarts, "Colossal proximity effect in a superconducting triplet spin valve based on the half-metallic ferromagnet CrO<sub>2</sub>," *Phys. Rev. X*, vol. 5, no. 2, p. 021019, May 2015, doi: [10.1103/PhysRevX.5.021019](https://doi.org/10.1103/PhysRevX.5.021019).
- 180 A. A. Kamashev *et al.*, "Increasing the performance of a superconducting spin valve using a Heusler alloy," *Beilstein J. Nanotech.*, vol. 9, pp. 1764–1769, June 2018, doi: [10.3762/bjnano.9.167](https://doi.org/10.3762/bjnano.9.167).
- 181 X. L. Wang *et al.*, "Giant triplet proximity effect in superconducting pseudo spin valves with engineered anisotropy," *Phys. Rev. B*, vol. 89, no. 14, p. 140508, Apr. 2014, doi: [10.1103/PhysRevB.89.140508](https://doi.org/10.1103/PhysRevB.89.140508).
- 182 N. O. Birge and M. Houzet, "Spin-singlet and spin-triplet Josephson junctions for cryogenic memory," *IEEE Magnetics Letters*, vol. 10, p. 4509605, Oct. 2019, doi: [10.1109/LMAG.2019.2955419](https://doi.org/10.1109/LMAG.2019.2955419).
- 183 E. C. Gingrich *et al.*, "Controllable 0- $\pi$  Josephson junctions containing a ferromagnetic spin valve," *Nat Phys*, vol. 12, no. 6, pp. 564–567, June 2016, doi: [10.1038/nphys3681](https://doi.org/10.1038/nphys3681).
- 184 B. M. Niedzielski, T. J. Bertus, J. A. Glick, R. Loloee, W. P. Pratt, and N. O. Birge, "Spin-valve Josephson junctions for cryogenic memory," *Phys. Rev. B*, vol. 97, no. 2, p. 024517, Jan. 2018, doi: [10.1103/PhysRevB.97.024517](https://doi.org/10.1103/PhysRevB.97.024517).
- 185 S. E. Shafraniuk, I. P. Nevirkovets, and O. A. Mukhanov, "Modeling computer memory based on ferromagnetic/superconductor multilayers," *Phys. Rev. Applied*, vol. 11, no. 6, p. 064018, June 2019, doi: [10.1103/PhysRevApplied.11.064018](https://doi.org/10.1103/PhysRevApplied.11.064018).
- 186 N. Satchell *et al.*, "Spin-valve Josephson junctions with perpendicular magnetic anisotropy for cryogenic memory," *Appl. Phys. Lett.*, vol. 116, no. 2, p. 022601, Jan. 2020, doi: [10.1063/1.5140095](https://doi.org/10.1063/1.5140095).

- 187 I. M. Dayton *et al.*, “Experimental demonstration of a Josephson magnetic memory cell with a programmable pi-junction,” *IEEE Magn. Lett.*, vol. 9, p. 3301905, 2018, doi: [10.1109/LMAG.2018.2801820](https://doi.org/10.1109/LMAG.2018.2801820).
- 188 I. P. Nevirkovets and O. A. Mukhanov, “Memory cell for high-density arrays based on a multiterminal superconducting-ferromagnetic device,” *Phys. Rev. Appl.*, vol. 10, no. 3, p. 034013, Sep. 2018, doi: [10.1103/PhysRevApplied.10.034013](https://doi.org/10.1103/PhysRevApplied.10.034013).
- 189 S. V. Bakurskiy *et al.*, “Current-phase relations in SISFS junctions in the vicinity of  $0-\pi$  transition,” *Phys. Rev. B*, vol. 95, no. 9, p. 094522, Mar. 2017, doi: [10.1103/PhysRevB.95.094522](https://doi.org/10.1103/PhysRevB.95.094522).
- 190 B. Baek *et al.*, “Spin-transfer torque switching in nanopillar superconducting-magnetic hybrid Josephson junctions,” *Phys. Rev. Appl.*, vol. 3, no. 1, p. 011001, 2015, doi: [10.1103/PhysRevApplied.3.011001](https://doi.org/10.1103/PhysRevApplied.3.011001).
- 191 L. Rehm, V. Sluka, G. E. Rowlands, M.-H. Nguyen, T. A. Ohki, and A. D. Kent, “Sub-nanosecond switching in a cryogenic spin-torque spin-valve memory element with a dilute permalloy free layer,” *Appl. Phys. Lett.*, vol. 114, no. 21, p. 212402, May 2019, doi: [10.1063/1.5094924](https://doi.org/10.1063/1.5094924).
- 192 L. Lang *et al.*, “A low temperature functioning CoFeB/MgO-based perpendicular magnetic tunnel junction for cryogenic nonvolatile random access memory,” *Appl. Phys. Lett.*, vol. 116, no. 2, p. 022409, Jan. 2020, doi: [10.1063/1.5129553](https://doi.org/10.1063/1.5129553).
- 193 G. E. Rowlands *et al.*, “A cryogenic spin-torque memory element with precessional magnetization dynamics,” *Sci. Rep.*, vol. 9, no. 1, Art. no. 803, Jan. 2019, doi: [10.1038/s41598-018-37204-3](https://doi.org/10.1038/s41598-018-37204-3).
- 194 A. Iovan and V. M. Krasnov, “Signatures of the spin-triplet current in a Josephson spin valve: A micromagnetic analysis,” *Phys. Rev. B*, vol. 96, no. 1, p. 014511, Jul. 2017, doi: [10.1103/PhysRevB.96.014511](https://doi.org/10.1103/PhysRevB.96.014511).
- 195 N. O. Birge, “Spin-triplet supercurrents in Josephson junctions containing strong ferromagnetic materials,” *Phil. Trans. R. Soc. A*, vol. 376, no. 2125, p. 20150150, Aug. 2018, doi: [10.1098/rsta.2015.0150](https://doi.org/10.1098/rsta.2015.0150).
- 196 J. A. Glick *et al.*, “Spin-triplet supercurrent in Josephson junctions containing a synthetic antiferromagnet with perpendicular magnetic anisotropy,” *Phys. Rev. B*, vol. 96, no. 22, p. 224515, Dec. 2017, doi: [10.1103/PhysRevB.96.224515](https://doi.org/10.1103/PhysRevB.96.224515).
- 197 J. A. Glick *et al.*, “Phase control in a spin-triplet SQUID,” *Sci. Adv.*, vol. 4, no. 7, p. eaat9457, Jul. 2018, doi: [10.1126/sciadv.aat9457](https://doi.org/10.1126/sciadv.aat9457).
- 198 F. Chiodi *et al.*, “Supra-oscillatory critical temperature dependence of Nb-Ho bilayers,” *Europhys. Lett.*, vol. 101, no. 3, p. 37002, 2013, doi: [10.1209/0295-5075/101/37002](https://doi.org/10.1209/0295-5075/101/37002).
- 199 N. Satchell *et al.*, “Control of superconductivity with a single ferromagnetic layer in niobium/erbium bilayers,” *Phys. Rev. Appl.*, vol. 7, no. 4, p. 044031, Apr. 2017, doi: [10.1103/PhysRevApplied.7.044031](https://doi.org/10.1103/PhysRevApplied.7.044031).
- 200 N. G. Pugach *et al.*, “Superconducting spin valves controlled by spiral re-orientation in B20-family magnets,” *Appl. Phys. Lett.*, vol. 111, no. 16, p. 162601, Oct. 2017, doi: [10.1063/1.5000315](https://doi.org/10.1063/1.5000315).
- 201 N. G. Pugach and M. O. Safonchik, “Increase in the critical temperature of the superconducting transition of a hybrid structure upon the magnetization of spiral antiferromagnets,” *JETP Lett.*, vol. 107, no. 5, pp. 302–306, Mar. 2018, doi: [10.1134/S0021364018050119](https://doi.org/10.1134/S0021364018050119).
- 202 N. Pugach, M. Safonchik, D. Heim, and V. O. Yagovtsev, “Superconducting spin valves based on spiral magnets,” *Phys. Solid State*, vol. 60, no. 11, pp. 2237–2243, 2018, doi: [10.1134/S1063783418110276](https://doi.org/10.1134/S1063783418110276).
- 203 M.-H. Nguyen *et al.*, “Cryogenic memory architecture integrating spin Hall effect based magnetic memory and superconductive cryotron devices,” *Sci. Rep.*, vol. 10, no. 1, p. 248, Jan. 2020, doi: [10.1038/s41598-019-57137-9](https://doi.org/10.1038/s41598-019-57137-9).
- 204 G. E. Rowlands *et al.*, “Nanosecond reversal of three-terminal spin-Hall-effect memories sustained at cryogenic temperatures,” *Phys. Rev. Applied*, vol. 15, no. 2, p. L021004, Feb. 2021, doi: [10.1103/PhysRevApplied.15.L021004](https://doi.org/10.1103/PhysRevApplied.15.L021004).
- 205 D. M. Heim *et al.*, “The effect of normal and insulating layers on  $0-\pi$  transitions in Josephson junctions with a ferromagnetic barrier,” *New J. Phys.*, vol. 17, no. 11, p. 113022, 2015, doi: [10.1088/1367-2630/17/11/113022](https://doi.org/10.1088/1367-2630/17/11/113022).
- 206 S. V. Bakurskiy, N. V. Klenov, I. I. Soloviev, M. Y. Kupriyanov, and A. A. Golubov, “Superconducting phase domains for memory applications,” *Appl. Phys. Lett.*, vol. 108, no. 4, p. 042602, Jan. 2016, doi: [10.1063/1.4940440](https://doi.org/10.1063/1.4940440).
- 207 S. V. Bakurskiy, N. V. Klenov, I. I. Soloviev, A. Sidorenko, M. Y. Kupriyanov, and A. A. Golubov, “Compact Josephson  $\phi$ -junctions,” in *Functional Nanostructures and Metamaterials for Superconducting Spintronics: From Superconducting Qubits to Self-Organized Nanostructures*, A. Sidorenko, Ed. Cham: Springer International Publishing, 2018, pp. 49–71, doi: [10.1007/978-3-319-90481-8\\_3](https://doi.org/10.1007/978-3-319-90481-8_3).

- 208 M. L. Schneider *et al.*, “Ultralow power artificial synapses using nanotextured magnetic Josephson junctions,” *Sci. Adv.*, vol. 4, no. 1, p. e1701329, Jan. 2018, doi: [10.1126/sciadv.1701329](https://doi.org/10.1126/sciadv.1701329).
- 209 S. Pagano *et al.*, “Proposal for a nanoscale superconductive memory,” *IEEE Trans. Appl. Supercond.*, vol. 27, no. 4, p. 1801004, Jan. 2017, doi: [10.1109/TASC.2017.2647903](https://doi.org/10.1109/TASC.2017.2647903).
- 210 J. Yau, Y. Fung, and G. W. Gibson, “Hybrid cryogenic memory cells for superconducting computing applications,” in *IEEE International Conference on Rebooting Computing (ICRC)*, Nov. 2017, doi: [10.1109/ICRC.2017.8123684](https://doi.org/10.1109/ICRC.2017.8123684).
- 211 A. Murphy, D. V. Averin, and A. Bezryadin, “Nanoscale superconducting memory based on the kinetic inductance of asymmetric nanowire loops,” *New J. Phys.*, vol. 19, no. 6, p. 063015, 2017, doi: [10.1088/1367-2630/aa7331](https://doi.org/10.1088/1367-2630/aa7331).
- 212 N. S. Nair, “Theoretical Studies on Control and Synchronization of Coupled Nonlinear Systems,” Ph.D., University of Tennessee, 2018. [Online]. Available: [https://trace.tennessee.edu/utk\\_graddiss/5029](https://trace.tennessee.edu/utk_graddiss/5029).
- 213 N. Nair and Y. Braiman, “A ternary memory cell using small Josephson junction arrays,” *Supercond. Sci. Technol.*, vol. 31, no. 11, p. 115012, 2018, doi: [10.1088/1361-6668/aae2a9](https://doi.org/10.1088/1361-6668/aae2a9).
- 214 S. Peotta and M. Di Ventra, “Superconducting memristors,” *Phys. Rev. Appl.*, vol. 2, no. 3, p. 034011, Sep. 2014, doi: [10.1103/PhysRevApplied.2.034011](https://doi.org/10.1103/PhysRevApplied.2.034011).
- 215 J. Salmilehto, F. Deppe, M. Di Ventra, M. Sanz, and E. Solano, “Quantum memristors with superconducting circuits,” *Sci. Rep.*, vol. 7, no. 1, Dec. 2017, doi: [10.1038/srep42044](https://doi.org/10.1038/srep42044).
- 216 C. Guarcello, P. Solinas, M. DiVentra, and F. Giazotto, “Solitonic Josephson-based meminductive systems,” *Sci. Rep.*, vol. 7, p. 46736, 2017, doi: [10.1038/srep46736](https://doi.org/10.1038/srep46736).
- 217 Y.-P. Shim and C. Tahan, “Bottom-up superconducting and Josephson junction devices inside a group-IV semiconductor,” *Nat. Commun.*, vol. 5, no. May, p. 4225, Jul. 2014, doi: [10.1038/ncomms5225](https://doi.org/10.1038/ncomms5225).
- 218 C. D. Shelly, P. See, J. Ireland, E. J. Romans, and J. M. Williams, “Weak link nanobridges as single flux quantum elements,” *Supercond. Sci. Technol.*, vol. 30, no. 9, p. 095013, Sep. 2017, doi: [10.1088/1361-6668/aa80cd](https://doi.org/10.1088/1361-6668/aa80cd).
- 219 H. Ito, S. Taniguchi, K. Ishikawa, H. Akaike, and A. Fujimaki, “Fabrication of superconductor–ferromagnet–insulator–superconductor Josephson junctions with critical current uniformity applicable to integrated circuits,” *Appl. Phys. Express*, vol. 10, no. 3, p. 033101, Feb. 2017, doi: [10.7567/APEX.10.033101](https://doi.org/10.7567/APEX.10.033101).
- 220 R. Caruso *et al.*, “Properties of ferromagnetic Josephson junctions for memory applications,” *IEEE Trans. Appl. Supercond.*, vol. 28, no. 7, p. 1800606, Oct. 2018, doi: [10.1109/TASC.2018.2836979](https://doi.org/10.1109/TASC.2018.2836979).
- 221 R. Caruso *et al.*, “RF assisted switching in magnetic Josephson junctions,” *J. Appl. Phys.*, vol. 123, no. 13, p. 133901, Apr. 2018, doi: [10.1063/1.5018854](https://doi.org/10.1063/1.5018854) (erratum: doi:[10.1063/1.5037275](https://doi.org/10.1063/1.5037275)).
- 222 S. V. Bakurskiy, N. V. Klenov, I. I. Soloviev, N. G. Pugach, M. Y. Kupriyanov, and A. A. Golubov, “Protected  $0-\pi$  states in SIsFS junctions for Josephson memory and logic,” *Appl. Phys. Lett.*, vol. 113, no. 8, p. 082602, Aug. 2018, doi: [10.1063/1.5045490](https://doi.org/10.1063/1.5045490).
- 223 I. P. Nevirkovets, S. E. Shafraniuk, O. Chernyashvskyy, D. T. Yohannes, O. A. Mukhanov, and J. B. Ketterson, “Investigation of current gain in superconducting-ferromagnetic transistors with high- $J_c$  acceptor,” *IEEE Trans. Appl. Supercond.*, vol. 27, no. 4, p. 1800804, June 2017, doi: [10.1109/TASC.2016.2637864](https://doi.org/10.1109/TASC.2016.2637864).
- 224 E. Y. Cho, Y. W. Zhou, J. Y. Cho, and S. A. Cybart, “Superconducting nano Josephson junctions patterned with a focused helium ion beam,” *Appl. Phys. Lett.*, vol. 113, no. 2, p. 022604, Jul. 2018, doi: [10.1063/1.5042105](https://doi.org/10.1063/1.5042105).
- 225 X. Gao, J. Du, T. Zhang, and Y. J. Guo, “Noise and conversion performance of a high- $T_c$  superconducting Josephson junction mixer at 0.6 THz,” *Appl. Phys. Lett.*, vol. 111, no. 19, p. 192603, Nov. 2017, doi: [10.1063/1.5004733](https://doi.org/10.1063/1.5004733).
- 226 L. Chunguang, W. Xu, W. Jia, S. Liang, and H. Yusheng, “Progress on applications of high temperature superconducting microwave filters,” *Supercond. Sci. Technol.*, vol. 30, no. 7, p. 073001, 2017, doi: [10.1088/1361-6668/aa69f1](https://doi.org/10.1088/1361-6668/aa69f1).
- 227 K. Sano *et al.*, “Reduction of the supply current of single-flux-quantum time-to-digital converters by current recycling techniques,” *IEEE Trans. Appl. Supercond.*, vol. 27, no. 4, p. 1300305, June 2017, doi: [10.1109/TASC.2016.2646916](https://doi.org/10.1109/TASC.2016.2646916).
- 228 V. K. Semenov and Y. Polyakov, “Current recycling: New results,” *IEEE Trans. Appl. Supercond.*, vol. 29, no. 5, p. 1302304, Aug. 2019, doi: [10.1109/TASC.2019.2904961](https://doi.org/10.1109/TASC.2019.2904961).
- 229 V. Semenov, E. Golden, and S. K. Tolpygo, “SFQ bias for SFQ digital circuits,” *IEEE Trans. Appl. Supercond.*, 2021, doi: [10.1109/TASC.2021.3067231](https://doi.org/10.1109/TASC.2021.3067231).

- 230 K. Jackman and C. J. Fourie, "Tetrahedral modeling method for inductance extraction of complex 3-D superconducting structures," *IEEE Trans. Appl. Supercond.*, vol. 26, no. 3, p. 0602305, Apr. 2016, doi: [10.1109/TASC.2016.2522299](https://doi.org/10.1109/TASC.2016.2522299).
- 231 S. K. Tolpygo *et al.*, "Superconductor electronics fabrication process with MoN<sub>x</sub> kinetic inductors and self-shunted Josephson junctions," *IEEE Trans. Appl. Supercond.*, vol. 28, no. 4, p. 1100212, June 2018, doi: [10.1109/TASC.2018.2809442](https://doi.org/10.1109/TASC.2018.2809442).
- 232 M. A. Castellanos-Beltran, D. I. Olaya, A. J. Sirois, P. D. Dresselhaus, S. P. Benz, and P. F. Hopkins, "Stacked Josephson junctions as inductors for single flux quantum circuits," *IEEE Trans. Appl. Supercond.*, vol. 29, no. 5, p. 1300705, Aug. 2019, doi: [10.1109/TASC.2019.2898406](https://doi.org/10.1109/TASC.2019.2898406).
- 233 I. I. Soloviev *et al.*, "Superconducting digital circuits without inductors based on bistable Josephson junctions," *arXiv:2011.05856 [cond-mat.supr-con]*, Feb. 2021.
- 234 A. Andreski, "Superconducting Circuits with  $\pi$ -shift Elements," Ph.D., University of Twente, 2011. Available online: <https://research.utwente.nl/en/publications/superconducting-circuits-with-pi-shift-elements>.
- 235 V. V. Bolginov, A. N. Rossolenko, A. B. Shkarin, V. A. Oboznov, and V. V. Ryazanov, "Fabrication of optimized superconducting phase inverters based on superconductor-ferromagnet-superconductor  $\pi$ -junctions," *J. Low Temp. Phys.*, vol. 190, no. 5–6, pp. 302–314, Mar. 2018, doi: [10.1007/s10909-017-1843-6](https://doi.org/10.1007/s10909-017-1843-6).
- 236 Y. Yamanashi, S. Nakaiishi, A. Sugiyama, N. Takeuchi, and N. Yoshikawa, "Design methodology of single-flux-quantum flip-flops composed of both 0- and  $\pi$ -shifted Josephson junctions," *Supercond. Sci. Technol.*, Aug. 2018, doi: [10.1088/1361-6668/aad78d](https://doi.org/10.1088/1361-6668/aad78d).
- 237 D. Hasegawa, Y. Takeshita, K. Sano, M. Tanaka, A. Fujimaki, and T. Yamashita, "Magnetic Josephson junctions on Nb four-layer structure for half flux quantum circuits," IEEE ISEC 2019, Jul. 2019, doi: [10.1109/ISEC46533.2019.8990908](https://doi.org/10.1109/ISEC46533.2019.8990908).
- 238 E. Strambini *et al.*, "A Josephson phase battery," *Nat. Nanotechnol.*, vol. 15, pp. 656–660, Aug. 2020, doi: [10.1038/s41565-020-0712-7](https://doi.org/10.1038/s41565-020-0712-7).
- 239 S. Razmkhah and A. Bozbey, "Design of the passive transmission lines for different stripline widths and impedances," *IEEE Trans. Appl. Supercond.*, vol. 26, no. 8, pp. 1–6, Dec. 2016, doi: [10.1109/TASC.2016.2598769](https://doi.org/10.1109/TASC.2016.2598769).
- 240 T. Jabbari, G. Krylov, S. Whiteley, E. Mlinar, J. Kawa, and E. G. Friedman, "Interconnect routing for large scale RSFQ circuits," *IEEE Trans. Appl. Supercond.*, vol. 29, no. 5, p. 1102805, Aug. 2019, doi: [10.1109/TASC.2019.2903023](https://doi.org/10.1109/TASC.2019.2903023).
- 241 P. Le Roux, K. Jackman, J. A. Delpont, and C. J. Fourie, "Modeling of superconducting passive transmission lines," *IEEE Trans. Appl. Supercond.*, vol. 29, no. 5, p. 1101605, Aug. 2019, doi: [10.1109/TASC.2019.2902476](https://doi.org/10.1109/TASC.2019.2902476).
- 242 L. Schindler, P. le Roux, and C. J. Fourie, "Impedance matching of passive transmission line receivers to improve reflections between RSFQ logic cells," *IEEE Trans. Appl. Supercond.*, vol. 30, no. 2, p. 1300607, Mar. 2020, doi: [10.1109/TASC.2020.2964542](https://doi.org/10.1109/TASC.2020.2964542).
- 243 T. Jabbari and E. G. Friedman, "Global interconnects in VLSI complexity single flux quantum systems," SLIP '20, San Diego, CA, USA, Nov. 2020, doi: [10.1145/3414622.3431911](https://doi.org/10.1145/3414622.3431911).
- 244 D. E. Oates, S. K. Tolpygo, and V. Bolkhovskiy, "Submicron Nb microwave transmission lines and components for single-flux-quantum and analog large-scale superconducting integrated circuits," *IEEE Trans. Appl. Supercond.*, vol. 27, no. 4, p. 1501505, June 2017, doi: [10.1109/TASC.2017.2649842](https://doi.org/10.1109/TASC.2017.2649842).
- 245 S. K. Tolpygo, E. B. Golden, T. J. Weir, and V. Bolkhovskiy, "Inductance and mutual inductance of superconductor integrated circuit features with sizes down to 120 nm. Part I," *arXiv:2101.07457 [cond-mat]*, Jan. 2021.
- 246 V. K. Semenov and M. M. Khapaev, "How moats protect superconductor films from flux trapping," *IEEE Trans. Appl. Supercond.*, vol. 26, no. 3, p. 1300710, Apr. 2016, doi: [10.1109/TASC.2016.2547218](https://doi.org/10.1109/TASC.2016.2547218).
- 247 C. J. Fourie and K. Jackman, "Software tools for flux trapping and magnetic field analysis in superconducting circuits," *IEEE Trans. Appl. Supercond.*, vol. 29, no. 5, Art no, Aug. 2019. 1301004, doi: [10.1109/TASC.2019.2899333](https://doi.org/10.1109/TASC.2019.2899333).
- 248 A. Y. Herr, V. V. Talanov, and Q. P. Herr, "Superconductor ground plane patterning geometries that attract magnetic flux," *United States Patent 20200287118A1*, Sep. 10, 2020.
- 249 G. Tang, P. Qu, X. Ye, and D. Fan, "Logic design of a 16-bit bit-slice arithmetic logic unit for 32-/64-bit RSFQ microprocessors," *IEEE Trans. Appl. Supercond.*, vol. 28, no. 4, June 2018, doi: [10.1109/TASC.2018.2799994](https://doi.org/10.1109/TASC.2018.2799994).
- 250 K. Ishida, M. Tanaka, T. Ono, and K. Inoue, "Towards ultra-high-speed cryogenic single-flux-quantum computing," *IEICE Trans. Electron.*, vol. E101.C, no. 5, pp. 359–369, May 2018, doi: [10.1587/transle.E101.C.359](https://doi.org/10.1587/transle.E101.C.359).

- 251 C. L. Ayala, N. Takeuchi, Q. Xu, Y. Yamanashi, T. Ortlev, N. Yoshikawa, “Adiabatic quantum-flux-parametron-based microprocessor: Architecture, logic design, modeling, and design tools,” The 11th Superconducting SFQ VLSI Workshop (SSV 2018), Tsukuba, Japan, February 7-8, 2018.
- 252 C. J. Fourie and H. van Heerden, “An RSFQ superconductive programmable gate array,” *IEEE Trans. Appl. Supercond.*, vol. 17, no. 2, pp. 538–541, June 2007, doi: [10.1109/TASC.2007.897387](https://doi.org/10.1109/TASC.2007.897387).
- 253 C. C. Maree and C. J. Fourie, “Development of an All-SFQ Superconducting Field-Programmable Gate Array,” *IEEE Trans. Appl. Supercond.*, vol. 29, no. 4, p. 1300212, June 2019, doi: [10.1109/TASC.2018.2886208](https://doi.org/10.1109/TASC.2018.2886208).
- 254 Y. Okuma, N. Takeuchi, Y. Yamanashi, and N. Yoshikawa, “Design and demonstration of an adiabatic-quantum-flux-parametron field-programmable gate array using Josephson-CMOS hybrid memories,” *IEEE Trans. Appl. Supercond.*, vol. 29, no. 8, Art. no. 1103606, Dec. 2019, doi: [10.1109/TASC.2019.2938577](https://doi.org/10.1109/TASC.2019.2938577).
- 255 K. Berggren *et al.*, “Roadmap on emerging hardware and technology for machine learning,” *Nanotechnology*, vol. 32, no. 1, p. 012002, Jan. 2021, doi: [10.1088/1361-6528/aba70f](https://doi.org/10.1088/1361-6528/aba70f).
- 256 T. Onomi and K. Nakajima, “An improved superconducting neural circuit and its application for a neural network solving a combinatorial optimization problem,” *J. Phys.: Conf. Ser.*, vol. 507, no. 4, p. 042029, 2014, doi: [10.1088/1742-6596/507/4/042029](https://doi.org/10.1088/1742-6596/507/4/042029).
- 257 K. Segall *et al.*, “Synchronization dynamics on the picosecond time scale in coupled Josephson junction neurons,” *Phys. Rev. E*, vol. 95, no. 3, p. 032220, Mar. 2017, doi: [10.1103/PhysRevE.95.032220](https://doi.org/10.1103/PhysRevE.95.032220).
- 258 G. Tzimpragos *et al.*, “A computational temporal logic for superconducting accelerators,” in *Proc. 25th Int. Conf. Architectural Support for Programming Languages and Operating Systems (ASPLoS)*, Lausanne, Switzerland, Mar. 2020, pp. 435–448, doi: [10.1145/3373376.3378517](https://doi.org/10.1145/3373376.3378517).
- 259 A. Bozbey, M. A. Karamuftuoglu, S. Razmkhah, and M. Ozbayoglu, “Single flux quantum based ultrahigh speed spiking neuromorphic processor architecture,” *arXiv:1812.10354 [physics]*, Jul. 2020.
- 260 K. Ishida *et al.*, “SuperNPU: An extremely fast neural processing unit using superconducting logic devices,” in *2020 53rd Annual IEEE/ACM International Symposium on Microarchitecture (MICRO)*, Athens, Greece, Oct. 2020, pp. 58–72, doi: [10.1109/MICRO50266.2020.00018](https://doi.org/10.1109/MICRO50266.2020.00018).
- 261 M. L. Schneider and K. Segall, “Fan-out and fan-in properties of superconducting neuromorphic circuits,” *J. Appl. Phys.*, vol. 128, no. 21, Art. no. 214903, Dec. 2020, doi: [10.1063/5.0025168](https://doi.org/10.1063/5.0025168).
- 262 U. S. Goteti and R. C. Dynes, “Superconducting neural networks with disordered Josephson junction array synaptic networks and leaky integrate-and-fire loop neurons,” *J. Appl. Phys.*, vol. 129, no. 7, p. 073901, Feb. 2021, doi: [10.1063/5.0027997](https://doi.org/10.1063/5.0027997).
- 263 G. Tzimpragos *et al.*, “Temporal computing with superconductors,” *IEEE Micro*, 2021, doi: [10.1109/MM.2021.3066377](https://doi.org/10.1109/MM.2021.3066377).
- 264 I. I. Soloviev *et al.*, “Adiabatic superconducting artificial neural network: Basic cells,” *J. Appl. Phys.*, vol. 124, no. 15, Art. no. 152113, Sep. 2018, doi: [10.1063/1.5042147](https://doi.org/10.1063/1.5042147).
- 265 N. V. Klenov, A. E. Schegolev, I. I. Soloviev, S. V. Bakurskiy, and M. V. Tereshonok, “Energy efficient superconducting neural networks for high-speed intellectual data processing systems,” *IEEE Trans. Appl. Supercond.*, vol. 28, no. 7, Art. no. 1301006, Oct. 2018, doi: [10.1109/TASC.2018.2836903](https://doi.org/10.1109/TASC.2018.2836903).
- 266 R. Cai *et al.*, “A stochastic-computing based deep learning framework using adiabatic quantum-flux-parametron superconducting technology,” in *Proceedings of the 46th International Symposium on Computer Architecture - ISCA '19*, Phoenix, Arizona, 2019, pp. 567–578, doi: [10.1145/3307650.3322270](https://doi.org/10.1145/3307650.3322270).
- 267 M. L. Schneider *et al.*, “Energy-efficient single-flux-quantum based neuromorphic computing,” in 2017 IEEE International Conference on Rebooting Computing (ICRC), 2017, doi: [10.1109/ICRC.2017.8123634](https://doi.org/10.1109/ICRC.2017.8123634) (video presentation: <https://ieeetv.ieee.org/conference-highlights/energy-efficient-single-flux-quantum-based-neuromorphic-computing-ieee-rebooting-computing-2017?rf=channels|104&>, accessed 2020-03-15).
- 268 M. L. Schneider, C. A. Donnelly, and S. E. Russek, “Tutorial: High-speed low-power neuromorphic systems based on magnetic Josephson junctions,” *J. Appl. Phys.*, vol. 124, no. 16, p. 161102, Oct. 2018, doi: [10.1063/1.5042425](https://doi.org/10.1063/1.5042425).
- 269 M. L. Schneider *et al.*, “Synaptic weighting in single flux quantum neuromorphic computing,” *Sci. Rep.*, vol. 10, no. 1, Art. no. 934, Jan. 2020, doi: [10.1038/s41598-020-57892-0](https://doi.org/10.1038/s41598-020-57892-0).

- 270 E. Toomey, K. Segall, and K. K. Berggren, “Design of a power efficient artificial neuron using superconducting nanowires,” *Front. Neurosci.*, vol. 13, Art. no. 933, Sep. 2019, doi: [10.3389/fnins.2019.00933](https://doi.org/10.3389/fnins.2019.00933).
- 271 E. Toomey, K. Segall, M. Castellani, M. Colangelo, N. Lynch, and K. K. Berggren, “Superconducting Nanowire Spiking Element for Neural Networks,” *Nano Lett.*, vol. 20, no. 11, pp. 8059–8066, Nov. 2020, doi: [10.1021/acs.nanolett.0c03057](https://doi.org/10.1021/acs.nanolett.0c03057).
- 272 J. M. Shainline *et al.*, “Superconducting optoelectronic loop neurons,” *J. Appl. Phys.*, vol. 126, no. 4, p. 044902, Jul. 2019, doi: [10.1063/1.5096403](https://doi.org/10.1063/1.5096403).
- 273 J. M. Shainline, “Fluxonic Processing of Photonic Synapse Events,” *IEEE J. Sel. Topics Quantum Electron.*, vol. 26, no. 1, p. 7700315, Jan. 2020, doi: [10.1109/JSTQE.2019.2927473](https://doi.org/10.1109/JSTQE.2019.2927473).
- 274 N. V. Klenov *et al.*, “A neuron based on a single flux qubit,” *Low Temp. Phys.*, vol. 45, no. 7, pp. 769–775, Jul. 2019, doi: [10.1063/1.5111305](https://doi.org/10.1063/1.5111305).
- 275 E. Leonard *et al.*, “Digital coherent control of a superconducting qubit,” *Phys. Rev. Appl.*, vol. 11, no. 1, p. 014009, Jan. 2019, doi: [10.1103/PhysRevApplied.11.014009](https://doi.org/10.1103/PhysRevApplied.11.014009).
- 276 A. J. Sirois, M. Castellanos-Beltran, A. E. Fox, S. P. Benz, and P. F. Hopkins, “Josephson microwave sources applied to quantum information systems,” *IEEE Trans. Quantum Eng.*, vol. 1, p. 6002807, 2020, doi: [10.1109/TQE.2020.3045682](https://doi.org/10.1109/TQE.2020.3045682).
- 277 N. Yoshikawa, “Superconducting digital electronics for controlling quantum computing systems,” *IEICE Trans. Electron.*, vol. E102-C, no. 3, pp. 217–223, Mar. 2019, doi: [10.1587/transele.2018SDI0003](https://doi.org/10.1587/transele.2018SDI0003).
- 278 V. K. Semenov, “Magic cells and circuits: New convergence of memory and logic functions in superconductor devices,” *IEEE Trans. Appl. Supercond.*, vol. 23, no. 3, Art. no. 1700908, June 2013, doi: [10.1109/TASC.2012.2237214](https://doi.org/10.1109/TASC.2012.2237214).
- 279 V. K. Semenov, “Erasing logic-memory boundaries in superconductor electronics,” in *2016 IEEE International Conference on Rebooting Computing (ICRC)*, San Diego, CA, USA, 2016, doi: [10.1109/ICRC.2016.7738711](https://doi.org/10.1109/ICRC.2016.7738711).
- 280 N. Takeuchi, M. Aono, and N. Yoshikawa, “Superconductor amoeba-inspired problem solvers for combinatorial optimization,” *Phys. Rev. Appl.*, vol. 11, no. 4, p. 044069, Apr. 2019, doi: [10.1103/PhysRevApplied.11.044069](https://doi.org/10.1103/PhysRevApplied.11.044069).
- 281 S. R. B. Bearden, H. Manukian, F. L. Traversa, and M. Di Ventra, “Instantons in self-organizing logic gates,” *Phys. Rev. Appl.*, vol. 9, no. 3, p. 034029, Mar. 2018, doi: [10.1103/PhysRevApplied.9.034029](https://doi.org/10.1103/PhysRevApplied.9.034029).
- 282 M. Di Ventra and F. L. Traversa, “Perspective: Memcomputing: Leveraging memory and physics to compute efficiently,” *J. Appl. Phys.*, vol. 123, no. 18, p. 180901, May 2018, doi: [10.1063/1.5026506](https://doi.org/10.1063/1.5026506).
- 283 F. L. Traversa, P. Cicotti, F. Sheldon, and M. Di Ventra, “Evidence of exponential speed-up in the solution of hard optimization problems,” *Complexity*, p. 7982851, 2018, doi: [10.1155/2018/7982851](https://doi.org/10.1155/2018/7982851).
- 284 F. China, N. Takeuchi, S. Miki, M. Yabuno, S. Miyajima, and H. Terai, “Cryogenic readout of superconducting nanowire single-photon detectors using high-sensitivity adiabatic quantum-flux-parametron circuits,” *Supercond. Sci. Technol.*, vol. 34, no. 4, p. 044003, Apr. 2021, doi: [10.1088/1361-6668/abe7ac](https://doi.org/10.1088/1361-6668/abe7ac).
- 285 N. Takeuchi *et al.*, “Scalable readout interface for superconducting nanowire single-photon detectors using AQFP and RSFQ logic families,” *Opt. Express, OE*, vol. 28, no. 11, pp. 15824–15834, May 2020, doi: [10.1364/OE.392507](https://doi.org/10.1364/OE.392507).
- 286 M. Hidaka, S. Nagasawa, K. Hinode, and T. Satoh, “Improvements in fabrication process for Nb-based single flux quantum circuits in Japan,” *IEICE Trans. Electron.*, vol. E91-C, no. 3, pp. 318–324, Mar. 2008, doi: [10.1093/ietele/e91-c.3.318](https://doi.org/10.1093/ietele/e91-c.3.318).
- 287 S. Nagasawa *et al.*, “New Nb multi-layer fabrication process for large-scale SFQ circuits,” *Physica C*, vol. 469, no. 15–20, pp. 1578–1584, 2009, doi: [10.1016/j.physc.2009.05.219](https://doi.org/10.1016/j.physc.2009.05.219).
- 288 S. Nagasawa, T. Satoh, and M. Hidaka, “Uniformity and reproducibility of submicron 20 kA/cm<sup>2</sup> Nb/AlO<sub>x</sub>/Nb Josephson junction process,” in *15th International Superconductive Electronics Conference (ISEC)*, Nagoya, Japan, 2015, doi: [10.1109/ISEC.2015.7383488](https://doi.org/10.1109/ISEC.2015.7383488).
- 289 Y. Komura, M. Tanaka, S. Nagasawa, A. Bozbey, and A. Fujimaki, “Vortex transitional memory developed with Nb 4-layer, 10-kA/cm<sup>2</sup>; fabrication process,” in *2015 15th International Superconductive Electronics Conference (ISEC)*, 2015, doi: [10.1109/ISEC.2015.7383489](https://doi.org/10.1109/ISEC.2015.7383489).
- 290 S. Nagasawa and M. Hidaka, “Run-to-run yield evaluation of improved Nb 9-layer advanced process using single flux quantum shift register chip with 68,990 Josephson junctions,” *J. Phys.: Conf. Ser.*, vol. 871, no. 1, p. 012065, 2017, doi: [10.1088/1742-6596/871/1/012065](https://doi.org/10.1088/1742-6596/871/1/012065).

- 291 T. Ando *et al.*, “Three-dimensional adiabatic quantum-flux-parametron fabricated using a double-active-layered niobium process,” *Supercond. Sci. Technol.*, vol. 30, no. 7, p. 075003, Jul. 2017, doi: [10.1088/1361-6668/aa6ef4](https://doi.org/10.1088/1361-6668/aa6ef4).
- 292 S. K. Tolpygo *et al.*, “Advanced fabrication processes for superconducting very large-scale integrated circuits,” *IEEE Trans. Appl. Supercond.*, vol. 26, no. 3, p. 1100110, Apr. 2016, doi: [10.1109/TASC.2016.2519388](https://doi.org/10.1109/TASC.2016.2519388).
- 293 S. K. Tolpygo *et al.*, “Properties of unshunted and resistively shunted Nb/AlO<sub>x</sub>-Al/Nb Josephson junctions with critical current densities from 0.1 mA/μm<sup>2</sup> to 1 mA/μm<sup>2</sup>,” *IEEE Trans. Appl. Supercond.*, vol. 27, no. 4, p. 1100815, June 2017, doi: [10.1109/TASC.2017.2667403](https://doi.org/10.1109/TASC.2017.2667403).
- 294 S. K. Tolpygo *et al.*, “Advanced fabrication processes for superconductor electronics: Current status and new developments,” *IEEE Trans. Appl. Supercond.*, vol. 29, no. 5, p. 1102513, Aug. 2019, doi: [10.1109/TASC.2019.2904919](https://doi.org/10.1109/TASC.2019.2904919).
- 295 S. K. Tolpygo *et al.*, “Planarized fabrication process with two layers of SIS Josephson junctions and integration of SIS and SFS π-junctions,” *IEEE Trans. Appl. Supercond.*, vol. 29, no. 5, p. 1101208, Aug. 2019, doi: [10.1109/TASC.2019.2901709](https://doi.org/10.1109/TASC.2019.2901709).
- 296 S. K. Tolpygo *et al.*, “A 150-nm node of an eight-Nb-layer fully planarized process for superconductor electronics,” presented at the Applied Superconductivity Conference, Wk1EOr3B-01, Oct. 2020.
- 297 D. Olaya *et al.*, “Planarized process for single-flux-quantum circuits with self-shunted Nb/Nb<sub>x</sub>Si<sub>1-x</sub>/Nb Josephson junctions,” *IEEE Trans. Appl. Supercond.*, vol. 29, no. 6, p. 1101708, Sep. 2019, doi: [10.1109/TASC.2019.2900020](https://doi.org/10.1109/TASC.2019.2900020).
- 298 D. T. Yohannes *et al.*, “Planarized, extendible, multilayer fabrication process for superconducting electronics,” *IEEE Trans. Appl. Supercond.*, vol. 25, no. 3, p. 1100405, Oct. 2014, doi: [10.1109/TASC.2014.2365562](https://doi.org/10.1109/TASC.2014.2365562).
- 299 SeeQC Fabrication Services, “SeeQCSDesignRules\_S1.pdf,” <https://seeqc.com/innovation/fabrication-services/>, accessed 2020-01-14.
- 300 W. Xiong, L. Ying, Y. Wu, J. Ren, W. Peng, and Z. Wang, “Development of Nb/Al–AlO<sub>x</sub>/Nb tunnel junction for large-scale integrated digital circuits,” *IEEE Trans. Appl. Supercond.*, vol. 27, no. 4, p. 1100304, June 2017, doi: [10.1109/TASC.2016.2642056](https://doi.org/10.1109/TASC.2016.2642056).
- 301 W. Xiong *et al.*, “Measurement of specific capacitance for Nb/Al–AlO<sub>x</sub>/Nb Josephson junctions in single-flux quantum circuit applications,” *IEEE Trans. Appl. Supercond.*, vol. 28, no. 4, Art. no. 1300605, June 2018, doi: [10.1109/TASC.2018.2812737](https://doi.org/10.1109/TASC.2018.2812737).
- 302 L. Ying *et al.*, “Development of multi-layer fabrication process for SFQ large scale integrated digital circuits,” *IEEE Trans. Appl. Supercond.*, vol. 31, no. 5, Art. no. 1301504, Aug. 2021, doi: [10.1109/TASC.2021.3065277](https://doi.org/10.1109/TASC.2021.3065277).
- 303 S. S. Papa Rao *et al.*, “Materials and processes for superconducting qubits and superconducting electronic circuits on 300mm wafers,” *ECS Trans.*, vol. 85, no. 6, pp. 151–161, Apr. 2018, doi: [10.1149/08506.0151ecst](https://doi.org/10.1149/08506.0151ecst).
- 304 N. Foroozani *et al.*, “Development of transmon qubits solely from optical lithography on 300 mm wafers,” *Quantum Sci. Technol.*, vol. 4, no. 2, Art. no. 025012, Mar. 2019, doi: [10.1088/2058-9565/ab0ca8](https://doi.org/10.1088/2058-9565/ab0ca8).
- 305 D. Olaya, P. D. Dresselhaus, and S. P. Benz, “300-GHz operation of divider circuits using high- $J_c$  Nb/Nb<sub>x</sub>Si<sub>1-x</sub>/Nb Josephson junctions,” *IEEE Trans. Appl. Supercond.*, vol. 25, no. 3, Art. no. 1101005, June 2015, doi: [10.1109/TASC.2014.2373317](https://doi.org/10.1109/TASC.2014.2373317).
- 306 F. Müller, T. Scheller, R. Wendisch, R. Behr, O. Kieler, L. Palafox, and J. Kohlmann, “NbSi barrier junctions tuned for metrological applications up to 70 GHz: 20 V arrays for programmable Josephson voltage standards,” *IEEE Trans. Appl. Supercond.*, vol. 23, no. 5, Art. no. 1101005, June 2013, doi: [10.1109/TASC.2012.2235895](https://doi.org/10.1109/TASC.2012.2235895).
- 307 L. Wang *et al.*, “Effect of residual gas on structural, electrical and mechanical properties of niobium films deposited by magnetron sputtering deposition,” *Mater. Res. Express*, vol. 5, no. 4, p. 046410, 2018, doi: [10.1088/2053-1591/aab8c1](https://doi.org/10.1088/2053-1591/aab8c1).
- 308 K. Hinode, T. Satoh, S. Nagasawa, and M. Hidaka, “Origin of hydrogen-inclusion-induced critical current deviation in Nb/AlO<sub>x</sub>/Al/Nb Josephson junctions,” *J. Appl. Phys.*, vol. 107, no. 7, p. 073906, Apr. 2010, doi: [10.1063/1.3368660](https://doi.org/10.1063/1.3368660).
- 309 D. Amparo and S. K. Tolpygo, “Investigation of the role of H in fabrication-process-induced variations of Nb/Al/AlO<sub>x</sub>/Nb Josephson junctions,” *IEEE Trans. Appl. Supercond.*, vol. 21, no. 3, pp. 126–130, June 2011, doi: [10.1109/TASC.2010.2086990](https://doi.org/10.1109/TASC.2010.2086990).
- 310 M. D. Henry *et al.*, “Degradation of superconducting Nb/NbN films by atmospheric oxidation,” *IEEE Trans. Appl. Supercond.*, vol. 27, no. 4, Art. no. 1100505, June 2017, doi: [10.1109/TASC.2017.2669583](https://doi.org/10.1109/TASC.2017.2669583).



- 311 V. Yefremenko *et al.*, “Impact of electrical contacts design and materials on the stability of Ti superconducting transition shape,” *J. Low Temp. Phys.*, Aug. 2018, doi: [10.1007/s10909-018-2040-y](https://doi.org/10.1007/s10909-018-2040-y).
- 312 H. Kohlstedt, F. König, P. Henne, N. Thyssen, and P. Caputo, “The role of surface roughness in the fabrication of stacked Nb/Al–AlO<sub>x</sub>/Nb tunnel junctions,” *J. Appl. Phys.*, vol. 80, no. 9, pp. 5512–5514, Nov. 1996, doi: [10.1063/1.363459](https://doi.org/10.1063/1.363459).
- 313 Y. Wang, W. P. Pratt, and N. O. Birge, “Area-dependence of spin-triplet supercurrent in ferromagnetic Josephson junctions,” *Phys. Rev. B*, vol. 85, no. 21, p. 214522, June 2012, doi: [10.1103/PhysRevB.85.214522](https://doi.org/10.1103/PhysRevB.85.214522).
- 314 S. Kittiwatanakul, N. Anuniwat, N. Dao, S. A. Wolf, and J. Lu, “Surface morphology control of Nb thin films by biased target ion beam deposition,” *J. Vacuum Sci. Technol. A*, vol. 36, no. 3, p. 031507, Mar. 2018, doi: [10.1116/1.5023723](https://doi.org/10.1116/1.5023723).
- 315 S. Kempf, A. Ferring, A. Fleischmann, L. Gastaldo, and C. Enss, “Characterization of the reliability and uniformity of an anodization-free fabrication process for high-quality Nb/AlAlO<sub>x</sub>/Nb Josephson junctions,” *Supercond. Sci. Technol.*, vol. 26, no. 6, p. 065012, 2013, doi: [10.1088/0953-2048/26/6/065012](https://doi.org/10.1088/0953-2048/26/6/065012).
- 316 Y. Wu *et al.*, “Film stress influence on Nb/Al–AlO<sub>x</sub>/Nb Josephson junctions,” *IEEE Trans. Appl. Supercond.*, vol. 29, no. 5, p. 1102105, Aug. 2019, doi: [10.1109/TASC.2019.2904589](https://doi.org/10.1109/TASC.2019.2904589).
- 317 M. A. Gurvitch, “5.9 The Whole-Wafer Process: SNEP-SNAP,” in *Josephson Junctions: History, Devices, and Applications*, 1st ed., E. L. Wolf, G. B. Arnold, M. A. Gurvitch, and J. F. Zasadzinski, Eds. New York: Pan Stanford, 2017, pp. 127–133, doi: [10.1201/9781315364520-6](https://doi.org/10.1201/9781315364520-6).
- 318 M. Koberidze, M. J. Puska, and R. M. Nieminen, “Structural details of Al/Al<sub>2</sub>O<sub>3</sub> junctions and their role in the formation of electron tunnel barriers,” *Phys. Rev. B*, vol. 97, no. 19, p. 195406, May 2018, doi: [10.1103/PhysRevB.97.195406](https://doi.org/10.1103/PhysRevB.97.195406).
- 319 M. J. Cyster, J. S. Smith, J. A. Vaitkus, N. Vogt, S. P. Russo, and J. H. Cole, “Effect of atomic structure on the electrical response of aluminum oxide tunnel junctions,” *Phys. Rev. Research*, vol. 2, no. 1, p. 013110, Jan. 2020, doi: [10.1103/PhysRevResearch.2.013110](https://doi.org/10.1103/PhysRevResearch.2.013110).
- 320 C.-E. Kim, K. G. Ray, and V. Lordi, “A density-functional theory study of the Al/AlO<sub>x</sub>/Al tunnel junction,” *J. Appl. Phys.*, vol. 128, no. 15, p. 155102, Oct. 2020, doi: [10.1063/5.0020292](https://doi.org/10.1063/5.0020292).
- 321 M. J. Cyster, J. S. Smith, N. Vogt, G. Opletal, S. P. Russo, and J. H. Cole, “Simulating the fabrication of aluminium oxide tunnel junctions,” *npj Quantum Inf.*, vol. 7, no. 1, Art. no. 1, Jan. 2021, doi: [10.1038/s41534-020-00360-4](https://doi.org/10.1038/s41534-020-00360-4).
- 322 S. K. Tolpygo, A. Brinkman, A. A. Golubov, and M. Y. Kupriyanov, “Nb/AlO<sub>x</sub>/Al/AlO<sub>x</sub>/Nb double-barrier junctions with high critical current densities: influence of barrier asymmetry,” *IEEE Trans. Appl. Supercond.*, vol. 13, no. 2, pp. 138–141, June 2003, doi: [10.1109/TASC.2003.813665](https://doi.org/10.1109/TASC.2003.813665).
- 323 D. S. Holmes and J. McHenry, “Non-normal critical current distributions in Josephson junctions with aluminum oxide barriers,” *IEEE Trans. Appl. Supercond.*, vol. 27, no. 4, p. 1100605, 2017, doi: [10.1109/TASC.2016.2642053](https://doi.org/10.1109/TASC.2016.2642053).
- 324 J. Acharya, J. Wilt, B. Liu, and J. Wu, “Probing the dielectric properties of ultrathin Al/Al<sub>2</sub>O<sub>3</sub>/Al trilayers fabricated using in situ sputtering and atomic layer deposition,” *ACS Appl. Mater. Interfaces*, vol. 10, no. 3, pp. 3112–3120, Jan. 2018, doi: [10.1021/acsami.7b16506](https://doi.org/10.1021/acsami.7b16506).
- 325 R. Goul *et al.*, “Electron tunneling properties of Al<sub>2</sub>O<sub>3</sub> tunnel barrier made using atomic layer deposition in multilayer devices,” *AIP Adv.*, vol. 9, no. 2, p. 025018, Feb. 2019, doi: [10.1063/1.5052163](https://doi.org/10.1063/1.5052163).
- 326 J. Z. Wu, J. Acharya, and R. Goul, “In vacuo atomic layer deposition and electron tunneling characterization of ultrathin dielectric films for metal/insulator/metal tunnel junctions,” *J. Vacuum Sci. Technol. A*, vol. 38, no. 4, p. 040802, May 2020, doi: [10.1116/1.5141078](https://doi.org/10.1116/1.5141078).
- 327 M. Belogolovskii, E. Zhitlukhina, V. Lacquaniti, N. De Leo, M. Fretto, and A. Soso, “Intrinsically shunted Josephson junctions for electronics applications,” *Low Temp. Phys.*, vol. 43, no. 7, pp. 756–765, Jul. 2017, doi: [10.1063/1.4995622](https://doi.org/10.1063/1.4995622).
- 328 P. Febvre *et al.*, “Overdamped Josephson junctions for digital applications,” *Physica C*, vol. 484, pp. 175–178, 2013, doi: [10.1016/j.physc.2012.03.026](https://doi.org/10.1016/j.physc.2012.03.026).
- 329 B. Baek, P. D. Dresselhaus, and S. P. Benz, “Co-sputtered amorphous Nb<sub>x</sub>Si<sub>1-x</sub> barriers for Josephson-junction circuits,” *IEEE Trans. Appl. Supercond.*, vol. 16, no. 4, pp. 1966–1970, Dec. 2006, doi: [10.1109/TASC.2006.881816](https://doi.org/10.1109/TASC.2006.881816).
- 330 D. Olaya *et al.*, “Digital circuits using self-shunted Nb/Nb<sub>x</sub>Si<sub>1-x</sub>/Nb Josephson junctions,” *Appl. Phys. Lett.*, vol. 96, no. 21, p. 213510, 2010, doi: [10.1063/1.3432065](https://doi.org/10.1063/1.3432065).

- 331 B. Baek, P. D. Dresselhaus, and S. P. Benz, “Thermal stability of Nb/a-Nb<sub>x</sub>Si<sub>1-x</sub>/Nb Josephson junctions,” *Phys. Rev. B*, vol. 75, no. 5, p. 054514, Feb. 2007, doi: [10.1103/PhysRevB.75.054514](https://doi.org/10.1103/PhysRevB.75.054514).
- 332 I. W. Haygood *et al.*, “Characterization of Uniformity in Nb/Nb<sub>x</sub>Si<sub>1-x</sub>/Nb Josephson Junctions,” *IEEE Trans. Appl. Supercond.*, vol. 29, no. 8, p. 1103505, Dec. 2019, doi: [10.1109/TASC.2019.2922225](https://doi.org/10.1109/TASC.2019.2922225).
- 333 A. Gudkov, M. Kupriyanov, and A. Samus’, “Properties of planar Nb/ $\alpha$ -Si/Nb Josephson junctions with various degrees of doping of the  $\alpha$ -Si layer,” *J. Exp. Theor. Phys.*, vol. 114, no. 5, pp. 818–829, 2012, doi: [10.1134/S1063776112030144](https://doi.org/10.1134/S1063776112030144).
- 334 G. L. Kerber, A. W. Kleinsasser, and B. Bumble, “Fabrication of submicrometer high current density Nb/Al-AIN<sub>x</sub>/Nb junctions,” *IEEE Trans. Appl. Supercond.*, vol. 19, no. 3, pp. 159–166, June 2009, doi: [10.1109/TASC.2009.2017859](https://doi.org/10.1109/TASC.2009.2017859).
- 335 M. Huang, “Hafnium Oxide as an Alternative Barrier to Aluminum Oxide for Thermally Stable Niobium Tunnel Junctions,” Ph.D., Arizona State University, 2013. Available online: <http://hdl.handle.net/2286/R.A.125934>.
- 336 T. Li, J. Gallop, L. Hao, and E. Romans, “Ballistic Josephson junctions based on CVD graphene,” *Supercond. Sci. Technol.*, vol. 31, no. 4, p. 045004, Apr. 2018, doi: [10.1088/1361-6668/aaab81](https://doi.org/10.1088/1361-6668/aaab81).
- 337 Q.-Y. Xu *et al.*, “Fabrication of high-quality niobium superconducting tunnel junctions,” *Chinese Phys. Lett.*, vol. 28, no. 8, p. 087403, 2011, doi: [10.1088/0256-307X/28/8/087403](https://doi.org/10.1088/0256-307X/28/8/087403).
- 338 S. K. Tolpygo, V. Bolkhovskiy, T. J. Weir, L. M. Johnson, M. A. Gouker, and W. D. Oliver, “Fabrication process and properties of fully-planarized deep-submicron Nb/Al-AIOx/Nb Josephson junctions for VLSI circuits,” *IEEE Trans. Appl. Supercond.*, vol. 25, no. 3, pp. 1101312, June 2015, doi: [10.1109/TASC.2014.2374836](https://doi.org/10.1109/TASC.2014.2374836).
- 339 J. E. Hirsch, M. B. Maple, and F. Marsiglio, “Superconducting materials classes: Introduction and overview,” *Physica C*, vol. 514, pp. 1–8, Jul. 2015, doi: [10.1016/j.physc.2015.03.002](https://doi.org/10.1016/j.physc.2015.03.002).
- 340 A. Banerjee *et al.*, “Characterisation of amorphous molybdenum silicide (MoSi) superconducting thin films and nanowires,” *Supercond. Sci. Technol.*, vol. 30, no. 8, p. 084010, 2017, doi: [10.1088/1361-6668/aa76d8](https://doi.org/10.1088/1361-6668/aa76d8).
- 341 V. A. Seleznev *et al.*, “Deposition and characterization of few-nanometers-thick superconducting Mo–Re films,” *Supercond. Sci. Technol.*, vol. 21, no. 11, p. 115006, 2008, doi: [10.1088/0953-2048/21/11/115006](https://doi.org/10.1088/0953-2048/21/11/115006).
- 342 J. Zichi *et al.*, “Optimizing the stoichiometry of ultrathin NbTiN films for high-performance superconducting nanowire single-photon detectors,” *Opt. Express, OE*, vol. 27, no. 19, pp. 26579–26587, Sep. 2019, doi: [10.1364/OE.27.026579](https://doi.org/10.1364/OE.27.026579).
- 343 J. H. Goldsmith *et al.*, “Influence of nitride buffer layers on superconducting properties of niobium nitride,” *J. Vacuum Sci. Technol. A*, vol. 36, no. 6, p. 061502, Sep. 2018, doi: [10.1116/1.5044276](https://doi.org/10.1116/1.5044276).
- 344 H. Machhadani *et al.*, “Improvement of the critical temperature of NbTiN films on III-nitride substrates,” *Supercond. Sci. Technol.*, vol. 32, no. 3, p. 035008, Feb. 2019, doi: [10.1088/1361-6668/aaf99d](https://doi.org/10.1088/1361-6668/aaf99d).
- 345 L. Zhang, W. Peng, L. X. You, and Z. Wang, “Superconducting properties and chemical composition of NbTiN thin films with different thickness,” *Appl. Phys. Lett.*, vol. 107, no. 12, p. 122603, Sep. 2015, doi: [10.1063/1.4931943](https://doi.org/10.1063/1.4931943).
- 346 M. E. Cyberek *et al.*, “Growth and characterization of NbTiN films synthesized by reactive bias target ion beam deposition (RBTIBD),” *IEEE Trans. Appl. Supercond.*, vol. 29, no. 5, p. 1103405, Aug. 2019, doi: [10.1109/TASC.2019.2908254](https://doi.org/10.1109/TASC.2019.2908254).
- 347 Z. Wang *et al.*, “High-quality epitaxial NbN/AlN/NbN tunnel junctions with a wide range of current density,” *Appl. Phys. Lett.*, vol. 102, no. 14, p. 142604, Apr. 2013, doi: [10.1063/1.4801972](https://doi.org/10.1063/1.4801972).
- 348 K. Makise, H. Terai, S. Miki, T. Yamashita, and Z. Wang, “Design and fabrication of all-NbN SFQ circuits for SSPD signal processing,” *IEEE Trans. Appl. Supercond.*, vol. 23, no. 3, pp. 1100804, June 2013, doi: [10.1109/TASC.2012.2235504](https://doi.org/10.1109/TASC.2012.2235504).
- 349 R. Sun, K. Makise, L. Zhang, H. Terai, and Z. Wang, “Epitaxial NbN/AlN/NbN tunnel junctions on Si substrates with TiN buffer layers,” *AIP Adv.*, vol. 6, no. 6, p. 065119, June 2016, doi: [10.1063/1.4954743](https://doi.org/10.1063/1.4954743).
- 350 M. Cyberek, T. Farrahi, J. Lu, A. Kerr, R. M. Weikle, and A. W. Lichtenberger, “NbTiN/AlN/NbTiN SIS junctions realized by reactive bias target ion beam deposition,” *IEEE Trans. Appl. Supercond.*, vol. 29, no. 6, p. 1100306, Sep. 2019, doi: [10.1109/TASC.2018.2884967](https://doi.org/10.1109/TASC.2018.2884967).
- 351 H. Akaike, T. Funai, N. Naito, and A. Fujimaki, “Characterization of NbN tunnel junctions with radical-nitrided barriers,” *IEEE Trans. Appl. Supercond.*, vol. 23, no. 3, pp. 1101306–1101306, June 2013, doi: [10.1109/TASC.2013.2242511](https://doi.org/10.1109/TASC.2013.2242511).

- 352 H. Akaike, S. Sakamoto, K. Munemoto, and A. Fujimaki, "Fabrication of NbTiN/Al–AlN<sub>x</sub>/NbTiN Josephson junctions for superconducting circuits operating around 10 K," *IEEE Trans. Appl. Supercond.*, vol. 26, no. 5, pp. 1–5, Aug. 2016, doi: [10.1109/TASC.2016.2565613](https://doi.org/10.1109/TASC.2016.2565613).
- 353 M. Aoyagi, H. Nakagawa, I. Kurosawa, and S. Takada, "Submicron NbN/MgO/NbN Josephson tunnel junctions and their application to the logic circuit," *IEEE Trans. Appl. Supercond.*, vol. 2, no. 3, pp. 183–186, 1992, doi: [10.1109/77.160159](https://doi.org/10.1109/77.160159).
- 354 G. L. Kerber, L. A. Abelson, R. N. Elmadjian, G. Hanaya, and E. G. Ladizinsky, "An improved NbN integrated circuit process featuring thick NbN ground plane and lower parasitic circuit inductances," *IEEE Trans. Appl. Supercond.*, vol. 7, no. 2, pp. 2638–2643, June 1997, doi: [10.1109/77.621781](https://doi.org/10.1109/77.621781).
- 355 J.-C. Villegier, B. Delaet, V. Larrey, P. Febvre, J. W. Tao, and G. Angenieux, "Extraction of material parameters in NbN multilayer technology for RSFQ circuits," *Physica C*, vol. 326–327, pp. 133–143, Nov. 1999, doi: [10.1016/S0921-4534\(99\)00410-4](https://doi.org/10.1016/S0921-4534(99)00410-4).
- 356 J.-C. Villégier *et al.*, "NbN multilayer technology on R-plane sapphire," *IEEE Trans. Appl. Supercond.*, vol. 11, no. 1, pp. 68–71, Mar. 2001, doi: [10.1109/77.919286](https://doi.org/10.1109/77.919286).
- 357 A. Grimm *et al.*, "A self-aligned nano-fabrication process for vertical NbN–MgO–NbN Josephson junctions," *Supercond. Sci. Technol.*, vol. 30, no. 10, p. 105002, 2017, doi: [10.1088/1361-6668/aa8007](https://doi.org/10.1088/1361-6668/aa8007).
- 358 J.-C. Villégier, S. Bouat, M. Aurino, C. Socquet-Clerc, and D. Renaud, "Integration of planarized internally-shunted submicron NbN junctions," *IEEE Trans. Appl. Supercond.*, vol. 21, no. 3, pp. 102–106, June 2011, doi: [10.1109/TASC.2010.2090837](https://doi.org/10.1109/TASC.2010.2090837).
- 359 H. Akaike, K. Munemoto, Y. Sakakibara, and A. Fujimaki, "Fabrication of NbTiN Josephson junctions with thermally oxidized Hf tunnel barriers," *IEEE Trans. Appl. Supercond.*, vol. 29, no. 5, p. 1102605, Aug. 2019, doi: [10.1109/TASC.2019.2906278](https://doi.org/10.1109/TASC.2019.2906278).
- 360 H. Yamamori, T. Yamada, H. Sasaki, and A. Shoji, "Improved fabrication yield for 10-V programmable Josephson voltage standard circuit including 524288 NbN/TiN/NbN Josephson junctions," *IEEE Trans. Appl. Supercond.*, vol. 20, no. 2, pp. 71–75, Apr. 2010, doi: [10.1109/TASC.2010.2041349](https://doi.org/10.1109/TASC.2010.2041349).
- 361 A. B. Kaul, S. R. Whiteley, T. V. Duzer, L. Yu, N. Newman, and J. M. Rowell, "Internally shunted sputtered NbN Josephson junctions with a TaN<sub>x</sub> barrier for nonlatching logic applications," *Appl. Phys. Lett.*, vol. 78, no. 1, pp. 99–101, Jan. 2001, doi: [10.1063/1.1337630](https://doi.org/10.1063/1.1337630).
- 362 L. Yu *et al.*, "Internally shunted Josephson junctions with barriers tuned near the metal–insulator transition for RSFQ logic applications," *Supercond. Sci. Technol.*, vol. 19, no. 8, pp. 719–731, Aug. 2006, doi: [10.1088/0953-2048/19/8/006](https://doi.org/10.1088/0953-2048/19/8/006).
- 363 N. Missert *et al.*, "Materials study of NbN and TaxN thin films for SNS Josephson junctions," *IEEE Trans. Appl. Supercond.*, vol. 27, no. 4, p. 1100904, June 2017, doi: [10.1109/TASC.2017.2669582](https://doi.org/10.1109/TASC.2017.2669582).
- 364 M. A. Wolak *et al.*, "SNS Josephson Junctions With Tunable Ta–N Barriers," *IEEE Trans. Appl. Supercond.*, vol. 29, no. 5, p. 1102204, Aug. 2019, doi: [10.1109/TASC.2019.2904489](https://doi.org/10.1109/TASC.2019.2904489).
- 365 K. Munemoto, S. Sakamoto, H. Akaike, and A. Fujimaki, "Fabrication of NbTiN tunnel junctions using Hf overlayers," 15th International Superconductive Electronics Conference (ISEC), 2015, doi: [10.1109/ISEC.2015.7383458](https://doi.org/10.1109/ISEC.2015.7383458).
- 366 T. Yamashita, A. Kawakami, and H. Terai, "NbN-based ferromagnetic 0 and  $\pi$  Josephson junctions," *Phys. Rev. Appl.*, vol. 8, no. 5, p. 054028, Nov. 2017, doi: [10.1103/PhysRevApplied.8.054028](https://doi.org/10.1103/PhysRevApplied.8.054028).
- 367 F. Li, H. Zhang, L. Zhang, W. Peng, and Z. Wang, "Ferromagnetic Josephson junctions based on epitaxial NbN/Ni<sub>60</sub>Cu<sub>40</sub>/NbN trilayer," *AIP Adv.*, vol. 8, no. 5, p. 055007, May 2018, doi: [10.1063/1.5030348](https://doi.org/10.1063/1.5030348).
- 368 A. Pal, J. A. Ouassou, M. Eschrig, J. Linder, and M. G. Blamire, "Spectroscopic evidence of odd frequency superconducting order," *Sci. Rep.*, vol. 7, p. 40604, Jan. 2017, doi: [10.1038/srep40604](https://doi.org/10.1038/srep40604).
- 369 W. K. Withanage *et al.*, "Growth of magnesium diboride thin films on boron buffered Si and silicon-on-insulator substrates by hybrid physical chemical vapor deposition," *Supercond. Sci. Technol.*, vol. 31, no. 7, p. 075009, 2018, doi: [10.1088/1361-6668/aac6a0](https://doi.org/10.1088/1361-6668/aac6a0).
- 370 T. Melbourne, D. Cunnane, E. Galan, X. X. Xi, and K. Chen, "Study of MgB<sub>2</sub> Josephson junction arrays and sub-um junctions," *IEEE Trans. Appl. Supercond.*, vol. 25, no. 3, p. 1100604, June 2015, doi: [10.1109/TASC.2014.2366076](https://doi.org/10.1109/TASC.2014.2366076).
- 371 T. Melbourne, "Magnesium Diboride Devices and Applications," Ph.D., Temple University, Pennsylvania, USA, 2018. Available online: <https://pqdtopen.proquest.com/pubnum/10689307.html>.

- 372 L. Kasaei *et al.*, “MgB<sub>2</sub> Josephson junctions produced by focused helium ion beam irradiation,” *AIP Adv.*, vol. 8, no. 7, p. 075020, Jul. 2018, doi: [10.1063/1.5030751](https://doi.org/10.1063/1.5030751).
- 373 L. Kasaei *et al.*, “Reduced critical current spread in planar MgB<sub>2</sub> Josephson junction array made by focused helium ion beam,” *IEEE Trans. Appl. Supercond.*, vol. 29, no. 5, Art. no. 1102906, Aug. 2019, doi: [10.1109/TASC.2019.2903418](https://doi.org/10.1109/TASC.2019.2903418).
- 374 T. Jabbari, F. Shانهsazzadeh, H. Zandi, M. Banzet, J. Schubert, and M. Fardmanesh, “Effects of the design parameters on characteristics of the inductances and JJs in HTS RSFQ circuits,” *IEEE Trans. Appl. Supercond.*, vol. 28, no. 7, p. 1301304, Oct. 2018, doi: [10.1109/TASC.2018.2856850](https://doi.org/10.1109/TASC.2018.2856850).
- 375 E. E. Mitchell *et al.*, “2D SQIF arrays using 20 000 YBCO high R<sub>n</sub> Josephson junctions,” *Supercond. Sci. Technol.*, vol. 29, no. 6, p. 06LT01, 2016, doi: [10.1088/0953-2048/29/6/06LT01](https://doi.org/10.1088/0953-2048/29/6/06LT01).
- 376 B. Chesca, “Superconducting devices based on coherent operation of Josephson junction arrays above 77K,” *J. Phys.: Conf. Ser.*, vol. 1054, no. 1, p. 012057, 2018, doi: [10.1088/1742-6596/1054/1/012057](https://doi.org/10.1088/1742-6596/1054/1/012057).
- 377 X. Guang-Ming *et al.*, “Fabrication of rhenium Josephson junctions,” *Chinese Phys. B*, vol. 22, no. 9, p. 097401, 2013, doi: [10.1088/1674-1056/22/9/097401](https://doi.org/10.1088/1674-1056/22/9/097401).
- 378 V. E. Shaternik, A. P. Shapovalov, A. V. Suvorov, N. A. Skoryk, and M. A. Belogolovskii, “Tunneling through localized barrier states in superconducting heterostructures,” *Low Temp. Phys.*, vol. 42, no. 5, pp. 426–428, May 2016, doi: [10.1063/1.4951668](https://doi.org/10.1063/1.4951668).
- 379 V. Lacquaniti *et al.*, “Analysis of internally shunted Josephson junctions,” *IEEE Trans. Appl. Supercond.*, vol. 26, no. 3, p. 1100505, Apr. 2016, doi: [10.1109/TASC.2016.2535141](https://doi.org/10.1109/TASC.2016.2535141).
- 380 V. E. Shaternik, O. Y. Suvorov, A. P. Shapovalov, T. O. Prikhna, and T. B. Serbenyuk, “Improved design Josephson junctions with hybrid nanostructured barriers,” in *2017 IEEE 7th International Conference Nanomaterials: Application Properties (NAP)*, Odessa, Ukraine, 2017, pp. 04NESP07-1-04NESP07-4, doi: [10.1109/NAP.2017.8190295](https://doi.org/10.1109/NAP.2017.8190295).
- 381 A. Shapovalov, V. Shaternik, O. Suvorov, E. Zhitlukhina, and M. Belogolovskii, “Negative differential conductance in doped-silicon nanoscale devices with superconducting electrodes,” *Appl. Nanosci.*, vol. 8, no. 5, pp. 1025–1030, June 2018, doi: [10.1007/s13204-018-0687-y](https://doi.org/10.1007/s13204-018-0687-y).
- 382 V. E. Shaternik *et al.*, “Dissipation effects in superconducting heterostructures with tungsten nanorods as weak links,” *Low Temp. Phys.*, vol. 44, no. 3, pp. 252–256, Mar. 2018, doi: [10.1063/1.5024546](https://doi.org/10.1063/1.5024546).
- 383 A. Grib, S. Savich, R. Vovk, V. Shaternik, A. Shapovalov, and P. Seidel, “Electrical characteristics of long Josephson junctions based on tungsten nanorods as weak links: Effect of random critical-current distributions,” *IEEE Trans. Appl. Supercond.*, vol. 28, no. 7, p. 1801106, Oct. 2018, doi: [10.1109/TASC.2018.2865468](https://doi.org/10.1109/TASC.2018.2865468).
- 384 A. L. Kasatkin, V. E. Shaternik, O. Yu. Suvorov, A. A. Kalenyuk, and A. P. Shapovalov, “Josephson effect in superconducting junctions with a semiconducting barrier containing metallic nanoclusters,” *Physica C: Superconductivity*, vol. 566, p. 1353539, Nov. 2019, doi: [10.1016/j.physc.2019.1353539](https://doi.org/10.1016/j.physc.2019.1353539).
- 385 A. Kalenyuk *et al.*, “Submicron-sized MoRe-doped Si-MoRe Josephson junctions with a low specific capacitance,” in *J. Phys.: Conf. Ser.*, Glasgow, UK, June 2020, vol. 1559, p. 012005, doi: [10.1088/1742-6596/1559/1/012005](https://doi.org/10.1088/1742-6596/1559/1/012005).
- 386 A. W. Draelos *et al.*, “Supercurrent flow in multiterminal graphene Josephson junctions,” *Nano Lett.*, vol. 19, no. 2, pp. 1039–1043, Feb. 2019, doi: [10.1021/acs.nanolett.8b04330](https://doi.org/10.1021/acs.nanolett.8b04330).
- 387 T. Nakayama, M. Naruse, H. Myoren, and T. Taino, “Fabrication of TiN/AlN/TiN tunnel junctions,” *Physica C*, vol. 530, pp. 87–89, Nov. 2016, doi: [10.1016/j.physc.2016.04.005](https://doi.org/10.1016/j.physc.2016.04.005).
- 388 F. Giustino *et al.*, “The 2021 quantum materials roadmap,” *J. Phys. Mater.*, vol. 3, no. 4, p. 042006, Jan. 2021, doi: [10.1088/2515-7639/abb74e](https://doi.org/10.1088/2515-7639/abb74e).
- 389 IC Makers Maximize 300mm, 200mm Wafer Capacity. [Online] <https://anysilicon.com/ic-makers-maximize-300mm-200mm-wafer-capacity/>, accessed 2020-03-15.
- 390 “MRAM manufacturing equipment,” MRAM-Info. [Online]. Available: [https://www.mram-info.com/companies/manufacturing\\_equipment](https://www.mram-info.com/companies/manufacturing_equipment), accessed 2020-03-15.
- 391 C. J. Fourie, O. Wetzstein, T. Ortlev, and J. Kunert, “Three-dimensional multi-terminal superconductive integrated circuit inductance extraction,” *Supercond. Sci. Technol.*, vol. 24, no. 12, p. 125015, 2011, doi: [10.1088/0953-2048/24/12/125015](https://doi.org/10.1088/0953-2048/24/12/125015).

- 392 C. J. Fourie, “Full-gate verification of superconducting integrated circuit layouts with InductEx,” *IEEE Trans. Appl. Supercond.*, vol. 25, no. 1, p. 1300209, Feb. 2015, doi: [10.1109/TASC.2014.2360870](https://doi.org/10.1109/TASC.2014.2360870).
- 393 A. Inamdar, J. Ravi, S. Miller, S. S. Meher, M. E. Çelik, and D. Gupta, “Design of 64-Bit arithmetic logic unit using improved timing characterization methodology for RSFQ cell library,” *IEEE Trans. Appl. Supercond.*, vol. 31, no. 5, Art. no. 1301307, Aug. 2021, doi: [10.1109/TASC.2021.3061639](https://doi.org/10.1109/TASC.2021.3061639).
- 394 C. L. Ayala *et al.*, “A semi-custom design methodology and environment for implementing superconductor adiabatic quantum-flux-parametron microprocessors,” *Supercond. Sci. Technol.*, vol. 33, no. 5, p. 054006, Mar. 2020, doi: [10.1088/1361-6668/ab7ec3](https://doi.org/10.1088/1361-6668/ab7ec3).
- 395 R. Saito, C. L. Ayala, O. Chen, T. Tanaka, T. Tamura, and N. Yoshikawa, “Logic synthesis of sequential logic circuits for adiabatic quantum-flux-parametron logic,” *IEEE Trans. Appl. Supercond.*, vol. 31, no. 5, Art. no. 1301405, Aug. 2021, doi: [10.1109/TASC.2021.3061636](https://doi.org/10.1109/TASC.2021.3061636).
- 396 P. Sarangapani, A. Poudel, and L. Smith, “A physics-based TCAD simulator for superconducting electronics based on Josephson junctions,” *IEEE Trans. Appl. Supercond.*, vol. 30, no. 7, Art. no. 1301005, Oct. 2020, doi: [10.1109/TASC.2020.2991735](https://doi.org/10.1109/TASC.2020.2991735).
- 397 N. Pokhrel, T. A. Weingartner, M. Sulangi, E. Patrick, and M. Law, “Modeling the effect of fabrication process on grain boundary formation in Nb/Al-AlO<sub>x</sub>/Nb Josephson junction circuit,” *IEEE Trans. Appl. Supercond.*, 2021, doi: [10.1109/TASC.2021.3066533](https://doi.org/10.1109/TASC.2021.3066533).
- 398 K. Jackman and C. J. Fourie, “Flux trapping analysis in superconducting circuits,” *IEEE Trans. Appl. Supercond.*, vol. 27, no. 4, Art. no. 1300105, June 2017, doi: [10.1109/TASC.2016.2642590](https://doi.org/10.1109/TASC.2016.2642590).
- 399 C. J. Fourie and M. H. Volkmann, “Status of superconductor electronic circuit design software,” *IEEE Trans. Appl. Supercond.*, vol. 23, no. 3, pp. 1300205, June 2013, doi: [10.1109/TASC.2012.2228732](https://doi.org/10.1109/TASC.2012.2228732).
- 400 C. J. Fourie, “Digital superconducting electronics design tools – status and roadmap,” *IEEE Trans. Appl. Supercond.*, vol. 28, no. 5, p. 1300412, Aug. 2018, doi: [10.1109/TASC.2018.2797253](https://doi.org/10.1109/TASC.2018.2797253).
- 401 C. Fourie, “Single Flux Quantum Circuit Technology and CAD Overview,” in *Proceedings of the International Conference on Computer-Aided Design*, New York, NY, USA, 2018, pp. 109:1–109:6, doi: [10.1145/3240765.3243498](https://doi.org/10.1145/3240765.3243498).
- 402 N. Kito, K. Takagi, and N. Takagi, “Automatic wire-routing of SFQ digital circuits considering wire-length matching,” *IEEE Trans. Appl. Supercond.*, vol. 26, no. 3, p. 1300305, Apr. 2016, doi: [10.1109/TASC.2016.2521798](https://doi.org/10.1109/TASC.2016.2521798).
- 403 M. A. Karamuftuoglu *et al.*, “Development of an optimizer for vortex transitional memory using particle swarm optimization,” *IEEE Trans. Appl. Supercond.*, vol. 26, no. 8, p. 1301606, Dec. 2016, doi: [10.1109/TASC.2016.2598761](https://doi.org/10.1109/TASC.2016.2598761).
- 404 N. Katam, A. Shafaei, and M. Pedram, “Design of multiple fanout clock distribution network for rapid single flux quantum technology,” in *2017 22nd Asia and South Pacific Design Automation Conference (ASP-DAC)*, pp. 384–389, 2017, doi: [10.1109/ASPDAC.2017.7858353](https://doi.org/10.1109/ASPDAC.2017.7858353).
- 405 S. N. Shahsavani, T. R. Lin, A. Shafaei, C. J. Fourie, and M. Pedram, “An integrated row-based cell placement and interconnect synthesis tool for large SFQ logic circuits,” *IEEE Trans. Appl. Supercond.*, vol. 27, no. 4, p. 1302008, June 2017, doi: [10.1109/TASC.2017.2675889](https://doi.org/10.1109/TASC.2017.2675889).
- 406 C. Fourie, C. Ayala, L. Schindler, T. Tanaka, and N. Yoshikawa, “Design and characterization of track routing architecture for RSFQ and AQFP circuits in a multilayer process,” *IEEE Trans. Appl. Supercond.*, vol. 30, no. 6, p. 1301109, Sep. 2020, doi: [10.1109/TASC.2020.2988876](https://doi.org/10.1109/TASC.2020.2988876).
- 407 A. Inamdar *et al.*, “Development of superconductor advanced integrated circuit design flow using Synopsys tools,” *IEEE Trans. Appl. Supercond.*, 2021, doi: [10.1109/TASC.2021.3058088](https://doi.org/10.1109/TASC.2021.3058088).
- 408 IARPA SuperTools Program, <https://www.iarpa.gov/index.php/research-programs/supertools>, accessed 2020-03-15.
- 409 C. J. Fourie *et al.*, “ColdFlux superconducting EDA and TCAD tools project: Overview and progress,” *IEEE Trans. Appl. Supercond.*, vol. 29, no. 5, p. 1300407, Aug. 2019, doi: [10.1109/TASC.2019.2892115](https://doi.org/10.1109/TASC.2019.2892115).
- 410 C. J. Fourie, “Electronic design automation tools for superconducting circuits,” in *J. Phys.: Conf. Ser.*, Kyoto, Japan, Jul. 2020, vol. 1590, p. 012040, doi: [10.1088/1742-6596/1590/1/012040](https://doi.org/10.1088/1742-6596/1590/1/012040).
- 411 D. R. Gulevich, V. P. Koshelets, and F. V. Kusmartsev, “Josephson flux-flow oscillator: The microscopic tunneling approach,” *Phys. Rev. B*, vol. 96, no. 2, p. 024515, Jul. 2017, doi: [10.1103/PhysRevB.96.024515](https://doi.org/10.1103/PhysRevB.96.024515).
- 412 P. Shevchenko, “PSCAN2 superconductor circuit simulator.” [Online]. <http://pscan2sim.org/>, accessed 2020-03-15.

- 413 J. A. Delpert, K. Jackman, P. I Roux, and C. J. Fourie, “JoSIM—Superconductor SPICE Simulator,” *IEEE Trans. Appl. Supercond.*, vol. 29, no. 5, p. 1300905, Aug. 2019, doi: [10.1109/TASC.2019.2897312](https://doi.org/10.1109/TASC.2019.2897312).
- 414 Y. Hashimoto, S. Yorozu, and Y. Kameda, “Development of cryopackaging and I/O technologies for high-speed superconductive digital systems,” *IEICE Trans. Electron.*, vol. E91-C, no. 3, pp. 325–332, Mar. 2008, doi: [10.1093/ietele/e91-c.3.325](https://doi.org/10.1093/ietele/e91-c.3.325).
- 415 S. Narayana, V. K. Semenov, Y. A. Polyakov, V. Dotsenko, and S. K. Tolpygo, “Design and testing of high-speed interconnects for superconducting multi-chip modules,” *Supercond. Sci. Technol.*, vol. 25, no. 10, p. 105012, 2012, doi: [10.1088/0953-2048/25/10/105012](https://doi.org/10.1088/0953-2048/25/10/105012).
- 416 R. N. Das *et al.*, “Waferscale S-MCM for high performance computing,” in *Proc. 2020 IEEE 70th Electronic Components Tech. Conf. (ECTC)*, Orlando, FL, USA, June 2020, pp. 582–588, doi: [10.1109/ECTC32862.2020.00097](https://doi.org/10.1109/ECTC32862.2020.00097).
- 417 E. Bardalen, M. N. Akram, H. Malmbekk, and P. Ohlckers, “Review of devices, packaging, and materials for cryogenic optoelectronics,” *J. Microelectron. Electron. Packag.*, vol. 12, no. 4, pp. 189–204, Oct. 2015, doi: [10.4071/imaps.485](https://doi.org/10.4071/imaps.485).
- 418 R. Pillarisetty *et al.*, “High volume electrical characterization of semiconductor qubits,” in *2019 IEEE Int. Electron Devices Meeting (IEDM)*, San Francisco, USA, Dec. 2019, pp. 31.5.1-31.5.4, doi: [10.1109/IEDM19573.2019.8993587](https://doi.org/10.1109/IEDM19573.2019.8993587).
- 419 M. W. Jenkins *et al.*, “Ambient temperature thermally induced voltage alteration (TIVA) for identification of defects in superconducting electronics,” in *ISTFA 2018: Proceedings from the 44th International Symposium for Testing and Failure Analysis*, Phoenix, Arizona, USA, 2018, pp. 148–152.
- 420 N. A. Missert *et al.*, “Diagnosis of factors impacting yield in multilayer devices for superconducting electronics,” *IEEE Trans. Appl. Supercond.*, vol. 29, no. 5, Art. no. 1103004, Aug. 2019, doi: [10.1109/TASC.2019.2908052](https://doi.org/10.1109/TASC.2019.2908052).
- 421 N. Missert *et al.*, “Analysis of multilayer devices for superconducting electronics by high-resolution scanning transmission electron microscopy and energy dispersive spectroscopy,” *IEEE Trans. Appl. Supercond.*, vol. 27, no. 4, p. 1100704, June 2017, doi: [10.1109/TASC.2017.2669579](https://doi.org/10.1109/TASC.2017.2669579).
- 422 Y. Hashimoto, S. Yorozu, T. Satoh, and T. Miyazaki, “Demonstration of chip-to-chip transmission of single-flux-quantum pulses at throughputs beyond 100 Gbps,” *Appl. Phys. Lett.*, vol. 87, no. 2, p. 022502, 2005, doi: [10.1063/1.1993767](https://doi.org/10.1063/1.1993767).
- 423 Q. P. Herr, M. S. Wire, and A. D. Smith, “Ballistic SFQ signal propagation on-chip and chip-to-chip,” *IEEE Trans. Appl. Supercond.*, vol. 13, no. 2, pp. 463–466, June 2003, doi: [10.1109/TASC.2003.813901](https://doi.org/10.1109/TASC.2003.813901).
- 424 T. V. Filippov *et al.*, “Experimental Investigation of ERSFQ Circuit for Parallel Multibit Data Transmission,” in *2017 16th International Superconductive Electronics Conference (ISEC)*, June 2017, doi: [10.1109/ISEC.2017.8314191](https://doi.org/10.1109/ISEC.2017.8314191).
- 425 A. Kushino, Y. Teranishi, and S. Kasai, “Low temperature properties of a superconducting niobium coaxial cable,” *J. Supercond. Nov. Magn.*, vol. 26, no. 5, pp. 2085–2088, May 2013, doi: [10.1007/s10948-012-2053-8](https://doi.org/10.1007/s10948-012-2053-8).
- 426 D. B. Tuckerman *et al.*, “Flexible superconducting Nb transmission lines on thin film polyimide for quantum computing applications,” *Supercond. Sci. Technol.*, vol. 29, no. 8, p. 084007, 2016, doi: [10.1088/0953-2048/29/8/084007](https://doi.org/10.1088/0953-2048/29/8/084007).
- 427 A. Kushino, T. Okuyama, and S. Kasai, “Development of Semi-rigid Superconducting Coaxial Cables with Clad Central Conductor for Low-Noise Experiments,” *J. Low Temp. Phys.*, Jul. 2018, doi: [10.1007/s10909-018-2044-7](https://doi.org/10.1007/s10909-018-2044-7).
- 428 A. B. Walter, C. Bockstiegel, B. A. Mazin, and M. Daal, “Laminated NbTi-on-Kapton Microstrip Cables for Flexible Sub-Kelvin RF Electronics,” *IEEE Trans. Appl. Supercond.*, vol. 28, no. 1, pp. 1–5, Jan. 2018, doi: [10.1109/TASC.2017.2773836](https://doi.org/10.1109/TASC.2017.2773836).
- 429 D. P. Pappas *et al.*, “Enhanced superconducting transition temperature in electroplated rhenium,” *Appl. Phys. Lett.*, vol. 112, no. 18, p. 182601, Apr. 2018, doi: [10.1063/1.5027104](https://doi.org/10.1063/1.5027104).
- 430 M. Manheimer, “IARPA SuperCables program.” [Online]. Available: <https://www.iarpa.gov/index.php/research-programs/supercables>, accessed 2019-01-05.
- 431 D. Gupta, J. C. Bardin, A. Inamdar, A. Dayalu, S. Sarwana, P. Ravindran, Su-Wei Chang, A. H. Coskun, and M. Ghadiri Sadrabadi, “Low-power high-speed hybrid temperature heterogeneous technology digital data link,” *IEEE Trans. Appl. Supercond.*, vol. 23, no. 3, pp. 1701806, June 2013, doi: [10.1109/TASC.2013.2257231](https://doi.org/10.1109/TASC.2013.2257231).
- 432 P. Ravindran *et al.*, “Power-optimized temperature-distributed digital data link,” *IEEE Trans. Appl. Supercond.*, vol. 25, no. 3, p. 1300605, June 2015, doi: [10.1109/TASC.2014.2372339](https://doi.org/10.1109/TASC.2014.2372339).

- 433 P. Ravindran *et al.*, “Energy efficient digital data link,” *IEEE Trans. Appl. Supercond.*, vol. 27, pp. 1301105, June 2017, doi: [10.1109/TASC.2016.2636252](https://doi.org/10.1109/TASC.2016.2636252).
- 434 D. Gupta *et al.*, “Digital output data links from superconductor integrated circuits,” *IEEE Trans. Appl. Supercond.*, vol. 29, no. 5, Art. no. 1303208, Aug. 2019, doi: [10.1109/TASC.2019.2910469](https://doi.org/10.1109/TASC.2019.2910469).
- 435 O. A. Mukhanov *et al.*, “Development of Energy-efficient Cryogenic Optical (ECO) data link,” in *2013 IEEE 14th International Superconductive Electronics Conference (ISEC)*, Boston, MA, USA, 2013, doi: [10.1109/ISEC.2013.6604276](https://doi.org/10.1109/ISEC.2013.6604276).
- 436 A. N. Tait *et al.*, “Microresonator-enhanced, waveguide-coupled emission from silicon defect centers for superconducting optoelectronic networks,” in *Optical Fiber Comm. Conf. (OFC)*, Mar. 2020, p. M2K.6, doi: [10.1364/OFC.2020.M2K.6](https://doi.org/10.1364/OFC.2020.M2K.6).
- 437 I. V. Vernik, O. A. Mukhanov, A. M. Kadin, C. T. Phare, M. Lipson, and K. Bergman, “System and method for cryogenic optoelectronic data link,” US10097281B1, 2018-10-09.
- 438 K. Sakai, S. Kato, N. Yoshikawa, Y. Kokubun, and T. Arakawa, “Proposal of ultra-low voltage quantum well optical modulator for optical interconnection in superconducting integrated circuit systems,” *Jpn. J. Appl. Phys.*, vol. 59, no. SO, p. SOOB01, Apr. 2020, doi: [10.35848/1347-4065/ab8284](https://doi.org/10.35848/1347-4065/ab8284).
- 439 A. N. McCaughan *et al.*, “A superconducting thermal switch with ultrahigh impedance for interfacing superconductors to semiconductors,” *Nat. Electron.*, vol. 2, no. 10, pp. 451–456, Oct. 2019, doi: [10.1038/s41928-019-0300-8](https://doi.org/10.1038/s41928-019-0300-8).
- 440 R. Radebaugh, “Cryocoolers: The state of the art and recent developments,” *J. Phys.: Condens. Matter*, vol. 21, no. 16, p. 164219, Mar. 2009, doi: [10.1088/0953-8984/21/16/164219](https://doi.org/10.1088/0953-8984/21/16/164219).
- 441 J. W. Burgoyne and M. N. Cuthbert, “Rising to the challenges of changing liquid helium supply on cryogenic systems for the research market,” in: *The future of helium as a natural resource*, R. H. Clarke, B. A. Glowacki, and W. J. Nuttall, Eds. New York, NY: Routledge, 2012.
- 442 Y. Iwasa, “Cryogenics,” in *Case Studies in Superconducting Magnets*, 2nd ed., Boston, MA: Springer US, 2009, pp. 219–312. Available online: <https://link.springer.com/book/10.1007/b112047>. See: Discussion 4.1 A. Specific Cooling Powers at Specific Temperatures, p. 227.
- 443 M. A. Green, “The cost of coolers for cooling superconducting devices at temperatures at 4.2 K, 20 K, 40 K and 77 K,” *IOP Conf. Ser.: Mater. Sci. Eng.*, vol. 101, no. 1, p. 012001, 2015, doi: [10.1088/1757-899X/101/1/012001](https://doi.org/10.1088/1757-899X/101/1/012001).
- 444 G. Batey and G. Teleberg, “Principles of dilution refrigeration—A brief technology guide,” Oxford Instruments Nanoscience, 2015. Available online: [https://nanoscience.oxinst.com/assets/uploads/NanoScience/Brochures/Principles%20of%20dilution%20refrigeration\\_Sept15.pdf](https://nanoscience.oxinst.com/assets/uploads/NanoScience/Brochures/Principles%20of%20dilution%20refrigeration_Sept15.pdf), accessed 2020-03-15.
- 445 R. G. Ross Jr., “Chapter 6: Refrigeration Systems for Achieving Cryogenic Temperatures,” in *Low Temperature Materials and Mechanisms*, Y. Bar-Cohen, Ed. 2016, pp. 109–182. Available online: [https://www2.jpl.nasa.gov/adv\\_tech/coolers/Cool\\_ppr/Chap%206-Refrig%20Sys%20for%20Achiev%20Cryo%20Temps\\_2016.pdf](https://www2.jpl.nasa.gov/adv_tech/coolers/Cool_ppr/Chap%206-Refrig%20Sys%20for%20Achiev%20Cryo%20Temps_2016.pdf)
- 446 A. T. A. M. de Waele, “Basics of Joule–Thomson liquefaction and JT cooling,” *J. Low Temp. Phys.*, vol. 186, no. 5, pp. 385–403, Mar. 2017, doi: [10.1007/s10909-016-1733-3](https://doi.org/10.1007/s10909-016-1733-3).
- 447 A. T. A. M. de Waele, “Challenges in Cryocooling,” *IOP Conf. Ser.: Mater. Sci. Eng.*, vol. 502, p. 012001, Apr. 2019, doi: [10.1088/1757-899X/502/1/012001](https://doi.org/10.1088/1757-899X/502/1/012001).
- 448 D. E. Nikonov and I. A. Young, “Benchmarking of beyond-CMOS exploratory devices for logic integrated circuits,” *IEEE J. Explor. Solid-State Computat. Devices Circuits*, vol. 1, pp. 3–11, Dec. 2015, doi: [10.1109/JXCDC.2015.2418033](https://doi.org/10.1109/JXCDC.2015.2418033).
- 449 C. Pan and A. Naemi, “Interconnect design and benchmarking for charge-based beyond-CMOS device proposals,” *IEEE Electron Device Letters*, vol. 37, no. 4, pp. 508–511, Apr. 2016, doi: [10.1109/LED.2016.2532350](https://doi.org/10.1109/LED.2016.2532350).
- 450 C. Pan and A. Naemi, “Non-Boolean computing benchmarking for beyond-CMOS Devices based on cellular neural network,” *IEEE J. Explor. Solid-State Computat. Devices Circuits*, vol. 2, pp. 36–43, Dec. 2016, doi: [10.1109/JXCDC.2016.2633251](https://doi.org/10.1109/JXCDC.2016.2633251).
- 451 C. Pan and A. Naemi, “An Expanded Benchmarking of Beyond-CMOS Devices Based on Boolean and Neuromorphic Representative Circuits,” *IEEE J. Explor. Solid-State Computat. Devices Circuits*, vol. 3, pp. 101–110, Dec. 2017, doi: [10.1109/JXCDC.2018.2793536](https://doi.org/10.1109/JXCDC.2018.2793536).

- 452 R. Adam, M. Currie, C. Williams, R. Sobolewski, O. Harnack, and M. Darula, "Direct observation of subpicosecond single-flux-quantum generation in pulse-driven Y-Ba-Cu-O Josephson junctions," *Appl. Phys. Lett.*, vol. 76, no. 4, pp. 469–471, Jan. 2000, doi: [10.1063/1.125790](https://doi.org/10.1063/1.125790).
- 453 K. K. Likharev, "Ultrafast superconductor digital electronics: RSFQ technology roadmap," *Czechoslovak Journal of Physics*, vol. 46, no. S6, pp. 3331–3338, June 1996, doi: [10.1007/BF02548149](https://doi.org/10.1007/BF02548149).
- 454 M. Dorojevets, Z. Chen, C. L. Ayala, and A. K. Kasperek, "Towards 32-bit energy-efficient superconductor RQL processors: The cell-level design and analysis of key processing and on-chip storage units," *IEEE Trans. Appl. Supercond.*, vol. 25, no. 3, pp. 1–8, June 2015, doi: [10.1109/TASC.2014.2368354](https://doi.org/10.1109/TASC.2014.2368354).
- 455 N. Takeuchi, Y. Yamanashi, and N. Yoshikawa, "Adiabatic quantum-flux-parametron cell library adopting minimalist design," *J. Appl. Phys.*, vol. 117, no. 17, p. 173912, May 2015, doi: [10.1063/1.4919838](https://doi.org/10.1063/1.4919838).
- 456 D. S. Holmes, "Model-based fabrication technology roadmap for superconducting electronics," *2014 Applied Superconductivity Conference*, unpublished.
- 457 S. K. Tolpygo, "Superconductor digital electronics: Scalability and energy efficiency issues (Review Article)," *Low Temp. Phys.*, vol. 42, no. 5, pp. 361–379, May 2016, doi: [10.1063/1.4948618](https://doi.org/10.1063/1.4948618).
- 458 L. A. Abelson, Q. P. Herr, G. L. Kerber, M. Leung, and T. S. Tighe, "Full-scale integration of superconductor electronics for petaflops computing," *Supercond. Sci. Technol.*, vol. 12, no. 11, p. 904, 1999, doi: [10.1088/0953-2048/12/11/363](https://doi.org/10.1088/0953-2048/12/11/363).
- 459 S. Tahara *et al.*, "Superconducting digital electronics," *IEEE Trans. Appl. Supercond.*, vol. 11, no. 1, pp. 463–468, Mar. 2001, doi: [10.1109/77.919383](https://doi.org/10.1109/77.919383).
- 460 A. Silver *et al.*, "Development of superconductor electronics technology for high-end computing," *Supercond. Sci. Technol.*, vol. 16, no. 12, pp. 1368–1374, 2003, doi: [10.1088/0953-2048/16/12/010](https://doi.org/10.1088/0953-2048/16/12/010).
- 461 L. A. Abelson and G. L. Kerber, "Superconductor integrated circuit fabrication technology," *Proc. IEEE*, vol. 92, no. 10, pp. 1517–1533, Oct. 2004, doi: [10.1109/JPROC.2004.833652](https://doi.org/10.1109/JPROC.2004.833652).
- 462 A. Silver, P. Bunyk, A. Kleinsasser, and J. Spargo, "Vision for single flux quantum very large scale integrated technology," *Supercond. Sci. Technol.*, vol. 19, no. 5, pp. S307–S311, Mar. 2006, doi: [10.1088/0953-2048/19/5/S30](https://doi.org/10.1088/0953-2048/19/5/S30).
- 463 H. J. M. ter Brake *et al.*, "SCENET roadmap for superconductor digital electronics," *Physica C*, vol. 439, no. 1, pp. 1–41, June 2006, doi: [10.1016/j.physc.2005.10.017](https://doi.org/10.1016/j.physc.2005.10.017).
- 464 O. Tsukamoto, "Overview of superconductivity in Japan - Strategy road map and R&D status," *Physica C*, vol. 468, no. 15–20, pp. 1101–1111, Sep. 2008, doi: [10.1016/j.physc.2008.05.199](https://doi.org/10.1016/j.physc.2008.05.199).
- 465 IEEE Electronics Packaging Society, "Heterogeneous Integration Roadmap." Available online: <https://eps.ieee.org/technology/heterogeneous-integration-roadmap.html>, accessed 2020-03-15.
- 466 M. J. Ellsworth Jr., "The challenge of operating computers at ultra-low temperatures," *Electronics Cooling*, vol. 7, no. 3, Aug. 2001. Available online: <https://www.electronics-cooling.com/2001/08/the-challenge-of-operating-computers-at-ultra-low-temperatures/>
- 467 D. M. Carlson, D. C. Sullivan, R. E. Bach, and D. R. Resnick, "The ETA 10 liquid-nitrogen-cooled supercomputer system," *IEEE Trans. Electron Devices*, vol. 36, no. 8, pp. 1404–1413, 1989, doi: [10.1109/16.30952](https://doi.org/10.1109/16.30952).
- 468 E. D. Buchanan, D. J. Benford, J. B. Forgiione, S. Harvey Moseley, and E. J. Wollack, "Cryogenic applications of commercial electronic components," *Cryogenics*, vol. 52, no. 10, pp. 550–556, Oct. 2012, doi: [10.1016/j.cryogenics.2012.06.017](https://doi.org/10.1016/j.cryogenics.2012.06.017).
- 469 F. Balestra and G. Ghibaud, Eds., "Device and circuit cryogenic operation for low temperature," *Springer US*, 2001, doi: [10.1007/978-1-4757-3318-1](https://doi.org/10.1007/978-1-4757-3318-1).
- 470 A. R. Jha, "Cryogenic Electronics," *Encyclopedia of RF and Microwave Engineering*, Wiley Online Library, 2005, doi: [10.1002/0471654507.eme064](https://doi.org/10.1002/0471654507.eme064).
- 471 N. Valentine and P. McCluskey, "Chapter 12 Low Temperature Electronics," *Low Temperature Materials and Mechanisms*, Y. Bar-Cohen, Ed. CRC Press, 2016, pp. 395–420, doi: [10.1201/9781315371962-13](https://doi.org/10.1201/9781315371962-13).
- 472 K. Fogarty, "Pushing DRAM's Limits," *Semiconductor Engineering*, December 14, 2017. Available online: <https://semiengineering.com/pushing-drams-limits/>, accessed 2020-03-15.



- 473 A. Akturk, J. Allnutt, Z. Dilli, N. Goldsman, and M. Peckerar, "Device modeling at cryogenic temperatures: Effects of incomplete ionization," *IEEE Trans. Electron Devices*, vol. 54, no. 11, pp. 2984–2990, Nov. 2007, doi: [10.1109/TED.2007.906966](https://doi.org/10.1109/TED.2007.906966).
- 474 A. Akturk *et al.*, "Compact and distributed modeling of cryogenic bulk MOSFET operation," *IEEE Trans. Electron Devices*, vol. 57, no. 6, pp. 1334–1342, June 2010, doi: [10.1109/TED.2010.2046458](https://doi.org/10.1109/TED.2010.2046458).
- 475 A. Beckers, F. Jazaeri, and C. Enz, "Cryogenic MOS transistor model," *IEEE Trans. Electron Devices*, vol. 65, no. 9, pp. 3617–3625, Sep. 2018, doi: [10.1109/TED.2018.2854701](https://doi.org/10.1109/TED.2018.2854701).
- 476 C. Luo, Z. Li, T.-T. Lu, J. Xu, and G.-P. Guo, "MOSFET characterization and modeling at cryogenic temperatures," *Cryogenics*, vol. 98, pp. 12–17, Mar. 2019, doi: [10.1016/j.cryogenics.2018.12.009](https://doi.org/10.1016/j.cryogenics.2018.12.009).
- 477 H. Zhao and X. Liu, "Modeling of a standard 0.35  $\mu\text{m}$  CMOS technology operating from 77 K to 300 K," *Cryogenics*, vol. 59, pp. 49–59, Jan. 2014, doi: [10.1016/j.cryogenics.2013.10.003](https://doi.org/10.1016/j.cryogenics.2013.10.003).
- 478 Z. Chen, H. Wong, Y. Han, S. Dong, and B. L. Yang, "Temperature dependences of threshold voltage and drain-induced barrier lowering in 60 nm gate length MOS transistors," *Microelectron. Reliab.*, vol. 54, no. 6, pp. 1109–1114, June 2014, doi: [10.1016/j.microrel.2013.12.005](https://doi.org/10.1016/j.microrel.2013.12.005).
- 479 M. Shin *et al.*, "Low temperature characterization of mobility in 14 nm FD-SOI CMOS devices under interface coupling conditions," *Solid-State Electron.*, vol. 108, pp. 30–35, June 2015, doi: [10.1016/j.sse.2014.12.013](https://doi.org/10.1016/j.sse.2014.12.013).
- 480 A. H. Coskun and J. C. Bardin, "Cryogenic small-signal and noise performance of 32nm SOI CMOS," 2014 IEEE MTT-S International Microwave Symposium (IMS2014), 2014, pp. 1–4, doi: [10.1109/MWSYM.2014.6848614](https://doi.org/10.1109/MWSYM.2014.6848614).
- 481 A. Beckers, F. Jazaeri, A. Ruffino, C. Bruschini, A. Baschiroto, and C. Enz, "Cryogenic characterization of 28 nm bulk CMOS technology for quantum computing," in *2017 47th European Solid-State Device Research Conference (ESSDERC)*, 2017, pp. 62–65, doi: [10.1109/ESSDERC.2017.8066592](https://doi.org/10.1109/ESSDERC.2017.8066592).
- 482 H. Bohuslavskyi *et al.*, "28nm Fully-depleted SOI technology: Cryogenic control electronics for quantum computing," in 2017 Silicon Nanoelectronics Workshop (SNW), 2017, pp. 143–144, doi: [10.23919/SNW.2017.8242338](https://doi.org/10.23919/SNW.2017.8242338).
- 483 P. A. 't Hart, M. Babaie, E. Charbon, A. Vladimirescu, and F. Sebastiano, "Characterization and modeling of mismatch in cryo-CMOS," *IEEE J. Electron Devices Soc.*, vol. 8, pp. 263–273, 2020, doi: [10.1109/JEDS.2020.2976546](https://doi.org/10.1109/JEDS.2020.2976546).
- 484 R. M. Incandela, L. Song, H. Homulle, E. Charbon, A. Vladimirescu, and F. Sebastiano, "Characterization and compact modeling of nanometer CMOS transistors at deep-cryogenic temperatures," *IEEE J. Electron Devices Soc.*, vol. 6, pp. 996–1006, 2018, doi: [10.1109/JEDS.2018.2821763](https://doi.org/10.1109/JEDS.2018.2821763).
- 485 B. Patra, M. Mehrpoo, A. Ruffino, F. Sebastiano, E. Charbon, and M. Babaie, "Characterization and analysis of on-chip microwave passive components at cryogenic temperatures," *IEEE J. Electron Devices Soc.*, Apr. 2020, doi: [10.1109/JEDS.2020.2986722](https://doi.org/10.1109/JEDS.2020.2986722).
- 486 F. Balestra and G. Ghibaudo, "Physics and performance of nanoscale semiconductor devices at cryogenic temperatures," *Semicond. Sci. Technol.*, vol. 32, no. 2, p. 023002, 2017, doi: [10.1088/1361-6641/32/2/023002](https://doi.org/10.1088/1361-6641/32/2/023002).
- 487 S. Li, "Challenges for Future Cryogenic Electronics," presented at the *US Workshop for IC Design for High Energy Physics (HEPIC-2013)*, Lawrence Berkeley National Laboratory, 2013. Available online: [https://indico.physics.lbl.gov/indico/event/2/contributions/392/attachments/388/420/SLi\\_CryoElec.pdf](https://indico.physics.lbl.gov/indico/event/2/contributions/392/attachments/388/420/SLi_CryoElec.pdf)
- 488 A. Beckers, F. Jazaeri, and C. Enz, "Characterization and modeling of 28-nm bulk CMOS technology down to 4.2 K," *IEEE J. Electron Devices Soc.*, vol. 6, pp. 1007–1018, 2018, doi: [10.1109/JEDS.2018.2817458](https://doi.org/10.1109/JEDS.2018.2817458).
- 489 B. Cardoso Paz *et al.*, "Variability evaluation of 28nm FD-SOI technology at cryogenic temperatures down to 100mK for quantum computing," 2020 IEEE Symposium on VLSI Technology, June 2020, doi: [10.1109/VLSITechnology18217.2020.9265034](https://doi.org/10.1109/VLSITechnology18217.2020.9265034).
- 490 N. C. Dao, A. E. Kass, M. R. Azghadi, C. T. Jin, J. Scott, and P. H. W. Leong, "An enhanced MOSFET threshold voltage model for the 6–300K temperature range," *Microelectron. Reliab.*, vol. 69, pp. 36–39, Feb. 2017, doi: [10.1016/j.microrel.2016.12.007](https://doi.org/10.1016/j.microrel.2016.12.007).
- 491 A. Beckers, F. Jazaeri, H. Bohuslavskyi, L. Hutin, S. De Franceschi, and C. Enz, "Characterization and modeling of 28-nm FDSOI CMOS technology down to cryogenic temperatures," *Solid-State Electron.*, vol. 159, pp. 106–115 Sep. 2019, doi: [10.1016/j.sse.2019.03.033](https://doi.org/10.1016/j.sse.2019.03.033).

- 492 J. R. Hoff, G. W. Deptuch, G. Wu, and P. Gui, "Cryogenic lifetime studies of 130 nm and 65 nm nMOS transistors for high-energy physics experiments," *IEEE Trans. Nucl. Sci.*, vol. 62, no. 3, pp. 1255–1261, June 2015, doi: [10.1109/TNS.2015.2433793](https://doi.org/10.1109/TNS.2015.2433793).
- 493 W. H. Henkels *et al.*, "A low temperature 12 ns DRAM," in International Symposium on VLSI Technology, Systems and Applications, 1989, pp. 32–35, doi: [10.1109/VTSA.1989.68576](https://doi.org/10.1109/VTSA.1989.68576).
- 494 W. H. Henkels *et al.*, "Low temperature SER and noise in a high speed DRAM," in *Proceedings of the Workshop on Low Temperature Semiconductor Electronics*, 1989, pp. 5–9, doi: [10.1109/LTSE.1989.50171](https://doi.org/10.1109/LTSE.1989.50171).
- 495 F. Ware *et al.*, "Do superconducting processors really need cryogenic memories?: The case for cold DRAM," in *Proceedings of the International Symposium on Memory Systems*, New York, NY, USA, 2017, pp. 183–188, doi: [10.1145/3132402.3132424](https://doi.org/10.1145/3132402.3132424).
- 496 S. S. Tannu, D. M. Carmean, and M. K. Qureshi, "Cryogenic-DRAM based memory system for scalable quantum computers: A feasibility study," *Proceedings of the International Symposium on Memory Systems*, New York, NY, USA, 2017, pp. 189–195, doi: [10.1145/3132402.3132436](https://doi.org/10.1145/3132402.3132436).
- 497 F. Wang, T. Vogelsang, B. Haukness, and S. C. Magee, "DRAM retention at cryogenic temperatures," in *2018 IEEE Int. Memory Workshop (IMW)*, May 2018, doi: [10.1109/IMW.2018.8388826](https://doi.org/10.1109/IMW.2018.8388826).
- 498 D. Min, I. Byun, G.-H. Lee, S. Na, and J. Kim, "CryoCache: A fast, large, and cost-effective cache architecture for cryogenic computing," in *Proc. 25th Int. Conf. Architectural Support for Programming Languages and Operating Systems (ASPLOS)*, Lausanne, Switzerland, Mar. 2020, pp. 449–464, doi: [10.1145/3373376.3378513](https://doi.org/10.1145/3373376.3378513).
- 499 I. Byun, D. Min, G. Lee, S. Na, and J. Kim, "CryoCore: A fast and dense processor architecture for cryogenic computing," in *ACM/IEEE Proc. ISCA*, 2020, pp. 335–348, doi: [10.1109/ISCA45697.2020.00037](https://doi.org/10.1109/ISCA45697.2020.00037).
- 500 L.-J. Fan *et al.*, "Cryogenic characterisation of 55 nm SONOS charge-trapping memory in AC and DC modes," *Electron. Lett.*, vol. 56, no. 4, pp. 199–201, 2020, doi: [10.1049/el.2019.3229](https://doi.org/10.1049/el.2019.3229).
- 501 Y. Hibi *et al.*, "Cryogenic ultra-low power dissipation operational amplifiers with GaAs JFETs," *Cryogenics*, vol. 73, pp. 8–13, Jan. 2016, doi: [10.1016/j.cryogenics.2015.10.006](https://doi.org/10.1016/j.cryogenics.2015.10.006).
- 502 E. Charbon *et al.*, "Cryo-CMOS for quantum computing," in 2016 IEEE International Electron Devices Meeting (IEDM), 2016, doi: [10.1109/IEDM.2016.7838410](https://doi.org/10.1109/IEDM.2016.7838410).
- 503 F. Sebastiano *et al.*, "Cryogenic CMOS interfaces for quantum devices," in 2017 7th *IEEE International Workshop on Advances in Sensors and Interfaces (IWASI)*, 2017, pp. 59–62, doi: [10.1109/IWASI.2017.7974215](https://doi.org/10.1109/IWASI.2017.7974215).
- 504 I. D. Conway Lamb *et al.*, "An FPGA-based instrumentation platform for use at deep cryogenic temperatures," *Rev. Sci. Instrum.*, vol. 87, no. 1, p. 014701, Jan. 2016, doi: [10.1063/1.4939094](https://doi.org/10.1063/1.4939094).
- 505 H. Homulle, S. Visser, and E. Charbon, "A cryogenic 1 GSa/s, soft-core FPGA ADC for quantum computing applications," *IEEE Trans. Circuits Syst. I, Reg. Papers*, vol. 63, no. 11, pp. 1854–1865, Nov. 2016, doi: [10.1109/TCSI.2016.2599927](https://doi.org/10.1109/TCSI.2016.2599927).
- 506 H. Homulle *et al.*, "A reconfigurable cryogenic platform for the classical control of quantum processors," *Rev. Sci. Instrum.*, vol. 88, no. 4, p. 045103, Apr. 2017, doi: [10.1063/1.4979611](https://doi.org/10.1063/1.4979611).
- 507 B. Patra *et al.*, "Cryo-CMOS circuits and systems for quantum computing applications," *IEEE J. Solid-State Circuits*, vol. 53, no. 1, pp. 309–321, Jan. 2018, doi: [10.1109/JSSC.2017.2737549](https://doi.org/10.1109/JSSC.2017.2737549).
- 508 J. C. Bardin *et al.*, "Design and characterization of a 28-nm bulk-CMOS cryogenic quantum controller dissipating less than 2 mW at 3 K," *IEEE J. Solid-State Circuits*, vol. 54, no. 11, pp. 3043–3060, Nov. 2019, doi: [10.1109/JSSC.2019.2937234](https://doi.org/10.1109/JSSC.2019.2937234).
- 509 J. P. G. van Dijk *et al.*, "A scalable Cryo-CMOS controller for the wideband frequency-multiplexed control of spin qubits and transmons," *IEEE J. Solid-State Circuits*, vol. 55, no. 11, pp. 2930–2946, Nov. 2020, doi: [10.1109/JSSC.2020.3024678](https://doi.org/10.1109/JSSC.2020.3024678).
- 510 S. J. Pauka *et al.*, "Characterizing quantum devices at scale with custom cryo-CMOS," *Phys. Rev. Appl.*, vol. 13, no. 5, p. 054072, May 2020, doi: [10.1103/PhysRevApplied.13.054072](https://doi.org/10.1103/PhysRevApplied.13.054072).
- 511 S. J. Pauka *et al.*, "A cryogenic CMOS chip for generating control signals for multiple qubits," *Nat. Electron.*, vol. 4, no. 1, pp. 64–70, Jan. 2021, doi: [10.1038/s41928-020-00528-y](https://doi.org/10.1038/s41928-020-00528-y).

- 512 D. J. Reilly, "Challenges in Scaling-up the Control Interface of a Quantum Computer," in 2019 *IEEE International Electron Devices Meeting (IEDM)*, Dec. 2019, pp. 31.7.1-31.7.6, doi: [10.1109/IEDM19573.2019.8993497](https://doi.org/10.1109/IEDM19573.2019.8993497).
- 513 D. Gupta, B. Amrutur, E. Terzioglu, U. Ghoshal, M. R. Beasley, and M. Horowitz, "Optimization of hybrid JJ/CMOS memory operating temperatures," *IEEE Trans. Appl. Supercond.*, vol. 7, no. 2, pp. 3307-3310, June 1997, doi: [10.1109/77.622065](https://doi.org/10.1109/77.622065).
- 514 N. Yoshikawa *et al.*, "Characterization of 4 K CMOS devices and circuits for hybrid Josephson-CMOS systems," *IEEE Trans. Appl. Supercond.*, vol. 15, no. 2, pp. 267-271, 2005, doi: [10.1109/TASC.2005.849786](https://doi.org/10.1109/TASC.2005.849786).
- 515 T. Orllepp, S. R. Whiteley, and T. Van Duzer, "High-speed hybrid superconductor-to-semiconductor interface circuit with ultra-low power consumption," *IEEE Trans. Appl. Supercond.*, vol. 23, no. 3, pp. 1400104-1400104, June 2013, doi: [10.1109/TASC.2012.2227918](https://doi.org/10.1109/TASC.2012.2227918).
- 516 T. Van Duzer *et al.*, "64-kb hybrid Josephson-Josephson-Josephson-Josephson-Josephson-CMOS 4 kelvin RAM with 400 ps access time and 12 mW read power," *IEEE Trans. Appl. Supercond.*, vol. 23, no. 3, pp. 1700504, June 2013, doi: [10.1109/TASC.2012.2230294](https://doi.org/10.1109/TASC.2012.2230294).
- 517 G. Konno, Y. Yamanashi, and N. Yoshikawa, "Fully functional operation of low-power 64-kb Josephson-CMOS hybrid memories," *IEEE Trans. Appl. Supercond.*, vol. 27, no. 4, p. 1300607, June 2017, doi: [10.1109/TASC.2016.2646911](https://doi.org/10.1109/TASC.2016.2646911).
- 518 M. Tanaka, M. Suzuki, G. Konno, Y. Ito, A. Fujimaki, and N. Yoshikawa, "Josephson-CMOS hybrid memory with nanocryotrons," *IEEE Trans. Appl. Supercond.*, vol. 27, no. 4, p. 1800904, June 2017, doi: [10.1109/TASC.2016.2646929](https://doi.org/10.1109/TASC.2016.2646929).
- 519 G. De Simoni, F. Paolucci, P. Solinas, E. Strambini, and F. Giazotto, "Metallic supercurrent field-effect transistor," *Nat. Nanotechnol.*, vol. 13, no. 9, p. 802, Sep. 2018, doi: [10.1038/s41565-018-0190-3](https://doi.org/10.1038/s41565-018-0190-3).
- 520 S. Bouscher, D. Panna, and A. Hayat, "Semiconductor-superconductor optoelectronic devices," *J. Opt.*, vol. 19, no. 10, p. 103003, 2017, doi: [10.1088/2040-8986/aa8888](https://doi.org/10.1088/2040-8986/aa8888).
- 521 E. Bardalen, M. N. Akram, H. Malmbekk, and P. Ohlckers, "Review of devices, packaging, and materials for cryogenic optoelectronics," *J. Microelectron. Electron. Packag.*, vol. 12, no. 4, pp. 189-204, Oct. 2015, doi: [10.4071/imaps.485](https://doi.org/10.4071/imaps.485).
- 522 M. Shin *et al.*, "Low temperature characterization of mobility in 14 nm FD-SOI CMOS devices under interface coupling conditions," *Solid-State Electron.*, vol. 108, pp. 30-35, June 2015, doi: [10.1016/j.sse.2014.12.013](https://doi.org/10.1016/j.sse.2014.12.013).
- 523 R. Srivastava, I. Choi, and T. Cook, "The Commercial Prospects for Quantum Computing," NQIT User Engagement Team, UK, Dec. 2016. Available online: [http://qutip.org/news/Commercial\\_Prospects\\_for\\_Quantum\\_Computing\\_Dec\\_2016.pdf](http://qutip.org/news/Commercial_Prospects_for_Quantum_Computing_Dec_2016.pdf).
- 524 S. Gamble, "Quantum computing: What it is, why we want it, and how we're trying to get it," in *Frontiers of Engineering: Reports on Leading-Edge Engineering from the 2018 Symposium*, G. Metcalfe and J. Chow, Eds. Washington, DC, USA: National Academies Press, 2019, pp. 5-8. Available online: <https://www.ncbi.nlm.nih.gov/books/NBK538701/>
- 525 L. Gyongyos and S. Imre, "A Survey on quantum computing technology," *Comp. Sci. Rev.*, Vol. 31, pp. 51-71, Feb. 2019, doi: [10.1016/j.cosrev.2018.11.002](https://doi.org/10.1016/j.cosrev.2018.11.002).
- 526 S. Resch and U. R. Karpuzcu, "Quantum computing: An overview across the system stack," *arXiv:1905.07240 [quant-ph]*, Oct. 2019.
- 527 M. A. Nielsen and I. L. Chuang, *Quantum Computation and Quantum Information*, 10<sup>th</sup> Anniversary Ed., Cambridge University Press, 2011.
- 528 M. Loceff, A course in quantum computing (for the community college). Foothill College, 2015. Available online: [http://lapastillaroja.net/wp-content/uploads/2016/09/Intro\\_to\\_QC\\_Vol\\_1\\_Loceff.pdf](http://lapastillaroja.net/wp-content/uploads/2016/09/Intro_to_QC_Vol_1_Loceff.pdf), video lectures: [https://www.youtube.com/channel/UCsB0RuNjZeTRK2rVnZ-qs\\_g](https://www.youtube.com/channel/UCsB0RuNjZeTRK2rVnZ-qs_g), accessed 2020-03-15.
- 529 "Quantum computing models," [https://en.wikipedia.org/wiki/Quantum\\_computing#Quantum\\_computing\\_models](https://en.wikipedia.org/wiki/Quantum_computing#Quantum_computing_models), accessed 2021-04-05.
- 530 H. J. Briegel, D. E. Browne, W. Dür, R. Raussendorf, and M. V. den Nest, "Measurement-based quantum computation," *Nat. Phys.*, vol. 5, no. 1, pp. 19-26, Jan. 2009, doi: [10.1038/nphys1157](https://doi.org/10.1038/nphys1157).
- 531 "Quantum computing: Physical realizations," [https://en.wikipedia.org/wiki/Quantum\\_computing#Physical\\_realizations](https://en.wikipedia.org/wiki/Quantum_computing#Physical_realizations), accessed 2020-05-26.

- 532 National Academies of Sciences, Engineering, and Medicine, *Quantum Computing: Progress and Prospects*, Washington, DC, USA: The National Academies Press, 2019, doi: [10.17226/25196](https://doi.org/10.17226/25196).
- 533 "DiVincenzo's criteria," [https://en.wikipedia.org/wiki/DiVincenzo%27s\\_criteria](https://en.wikipedia.org/wiki/DiVincenzo%27s_criteria), accessed 2020-05-26.
- 534 M. W. Johnson *et al.*, "A scalable control system for a superconducting adiabatic quantum optimization processor," *Supercond. Sci. Technol.*, vol. 23, no. 6, p. 065004, June 2010, doi: [10.1088/0953-2048/23/6/065004](https://doi.org/10.1088/0953-2048/23/6/065004).  
<https://arxiv.org/abs/0907.3757>
- 535 C. C. McGeoch, "Theory versus practice in annealing-based quantum computing," *Theor. Comput. Sci.*, vol. 816, pp. 169–183, May 2020, doi: [10.1016/j.tcs.2020.01.024](https://doi.org/10.1016/j.tcs.2020.01.024).
- 536 M. Mariantoni *et al.*, "Implementing the quantum von Neumann architecture with superconducting circuits," *Science*, vol. 334, no. 6052, 2011, pp. 61–65, doi: [10.1126/science.1208517](https://doi.org/10.1126/science.1208517).
- 537 A. Blais, S. M. Girvin, and W. D. Oliver, "Quantum information processing and quantum optics with circuit quantum electrodynamics," *Nat. Phys.*, vol. 16, no. 3, Art. no. 3, Mar. 2020, doi: [10.1038/s41567-020-0806-z](https://doi.org/10.1038/s41567-020-0806-z).
- 538 H.-L. Huang, D. Wu, D. Fan and X. Zhu, "Superconducting quantum computing: a review", *Sci. China Inf. Sci.*, Vol. 63, 180501, July 2020, doi: [10.1007/s11432-020-2881-9](https://doi.org/10.1007/s11432-020-2881-9). <https://arxiv.org/abs/2006.10433>
- 539 J. Preskill, "Quantum computing in the NISQ era and beyond," *Quantum*, vol. 2, p. 79, Aug. 2018, doi: [10.22331/q-2018-08-06-79](https://doi.org/10.22331/q-2018-08-06-79).
- 540 F. Leymann and J. Barzen, "The bitter truth about gate-based quantum algorithms in the NISQ era," *Quantum Sci. Technol.*, vol. 5, no. 4, p. 044007, Sep. 2020, doi: [10.1088/2058-9565/abae7d](https://doi.org/10.1088/2058-9565/abae7d).
- 541 S. Bravyi, D. Gosset, and R. König, "Quantum advantage with shallow circuits," *Science*, vol. 362, no. 6412, pp. 308–311, Oct. 2018, doi: [10.1126/science.aar3106](https://doi.org/10.1126/science.aar3106).
- 542 Y. Alexeev *et al.*, "Quantum computer systems for scientific discovery," *PRX Quantum*, vol. 2, no. 1, p. 017001, Feb. 2021, doi: [10.1103/PRXQuantum.2.017001](https://doi.org/10.1103/PRXQuantum.2.017001).
- 543 T. Karzig *et al.*, "Scalable designs for quasiparticle-poisoning-protected topological quantum computation with Majorana zero modes," *Phys. Rev. B*, vol. 95, no. 23, p. 235305, June 2017, doi: [10.1103/PhysRevB.95.235305](https://doi.org/10.1103/PhysRevB.95.235305).
- 544 V. Lahtinen and J. Pachos, "A short introduction to topological quantum computation," *SciPost Phys.*, vol. 3, no. 3, p. 021, Sep. 2017, doi: [10.21468/SciPostPhys.3.3.021](https://doi.org/10.21468/SciPostPhys.3.3.021).
- 545 C. P. Knapp, "Topological Quantum Computing with Majorana Zero Modes and Beyond," Ph.D., UC Santa Barbara, Santa Barbara, CA, USA, 2019. Available online: <https://escholarship.org/uc/item/04305656>.
- 546 A. Conlon, D. Pellegrino, J. K. Slingerland, S. Dooley, and G. Kells, "Error generation and propagation in Majorana-based topological qubits," *Phys. Rev. B*, vol. 100, no. 13, p. 134307, Oct. 2019, doi: [10.1103/PhysRevB.100.134307](https://doi.org/10.1103/PhysRevB.100.134307).
- 547 O. Viyuela, S. Vijay, and L. Fu, "Scalable fermionic error correction in Majorana surface codes," *Phys. Rev. B*, vol. 99, no. 20, p. 205114, May 2019, doi: [10.1103/PhysRevB.99.205114](https://doi.org/10.1103/PhysRevB.99.205114).
- 548 T. Humble, "Consumer applications of quantum computing: A promising approach for secure computation, trusted data storage, and efficient applications," *IEEE Consum. Electron. Mag.*, vol. 7, no. 6, pp. 8–14, Nov. 2018, doi: [10.1109/MCE.2017.2755298](https://doi.org/10.1109/MCE.2017.2755298).
- 549 CSIRO Futures, "Growing Australia's Quantum Technology Industry," CSIRO, May 2020. [Online]. Available: <https://www.csiro.au/quantum>, accessed 2020-05-27.
- 550 P. W. Shor, "Polynomial-time algorithms for prime factorization and discrete logarithms on a quantum computer," *SIAM J. Comput.*, vol. 26, no. 5, pp. 1484–1509, Oct. 1997, doi: [10.1137/S0097539795293172](https://doi.org/10.1137/S0097539795293172).
- 551 L. K. Grover, "A fast quantum mechanical algorithm for database search," in *Proc. of the 28th Annual ACM Symposium on Theory of Computing*, New York, NY, USA, 1996, pp. 212–219, doi: [10.1145/237814.237866](https://doi.org/10.1145/237814.237866).
- 552 S. Jordan, "Quantum Algorithm Zoo," [Online]. Available: <http://quantumalgorithmzoo.org/>, accessed 2020-01-27.
- 553 J. Abhijith *et al.*, "Quantum algorithm implementations for beginners," *arXiv:1804.03719 [quant-ph]*, Mar. 2020.
- 554 A. Acín *et al.*, "The quantum technologies roadmap: A European community view," *New J. Phys.*, vol. 20, no. 8, p. 080201, 2018, doi: [10.1088/1367-2630/aad1ea](https://doi.org/10.1088/1367-2630/aad1ea).
- 555 R. Orús, S. Mugel, and E. Lizaso, "Quantum computing for finance: Overview and prospects," *Rev. Phys.*, vol. 4, p. 100028, Nov. 2019, doi: [10.1016/j.revip.2019.100028](https://doi.org/10.1016/j.revip.2019.100028).

- 556 D-Wave Systems Inc. Available online: [www.dwavesys.com](http://www.dwavesys.com), accessed 2020-02-17.
- 557 D-Wave Systems, [https://en.wikipedia.org/wiki/D-Wave\\_Systems](https://en.wikipedia.org/wiki/D-Wave_Systems), accessed 2020-01-26.
- 558 S. Aaronson, *Quantum Computing since Democritus*, Cambridge University Press, 2013.
- 559 A. Manzalini, “Quantum communications in future networks and services,” *Quantum Reports*, vol. 2, no. 1, pp. 221–232, Mar. 2020, doi: [10.3390/quantum2010014](https://doi.org/10.3390/quantum2010014).
- 560 T. H. Johnson, S. R. Clark, and D. Jaksch, “What is a quantum simulator?” *Eur. Phys. J. Quantum Technol.*, vol. 1, no. 1, p. 10, Dec. 2014, doi: [10.1140/epjqt10](https://doi.org/10.1140/epjqt10).
- 561 F. Tacchino, A. Chiesa, S. Carretta, and D. Gerace, “Quantum computers as universal quantum simulators: State-of-the-art and perspectives,” *Adv. Quantum Technol.*, vol. 3, no. 3, Art. no. 1900052, Mar. 2020, doi: [10.1002/qute.201900052](https://doi.org/10.1002/qute.201900052).
- 562 “Simulation Software Market by Component, Application, Vertical, Deployment Mode, and Region - Global Forecast to 2022,” Research and Markets, 4435888, Dec. 2017. Available online: <https://www.researchandmarkets.com/reports/4435888/simulation-software-market-by-component-software>
- 563 E. Altman *et al.*, “Quantum simulators: Architectures and opportunities,” *PRX Quantum*, vol. 2, no. 1, p. 017003, Feb. 2021, doi: [10.1103/PRXQuantum.2.017003](https://doi.org/10.1103/PRXQuantum.2.017003).
- 564 M. Reiher, N. Wiebe, K. M. Svore, D. Wecker, and M. Troyer, “Elucidating reaction mechanisms on quantum computers,” *Proc. Natl. Acad. Sci. U.S.A.*, p. 201619152, Jul. 2017, doi: [10.1073/pnas.1619152114](https://doi.org/10.1073/pnas.1619152114).
- 565 P.-L. Dallaire-Demers and F. K. Wilhelm, “Method to efficiently simulate the thermodynamic properties of the Fermi-Hubbard model on a quantum computer,” *Phys. Rev. A*, vol. 93, no. 3, p. 032303, Mar. 2016, doi: [10.1103/PhysRevA.93.032303](https://doi.org/10.1103/PhysRevA.93.032303).
- 566 N. Moll *et al.*, “Quantum optimization using variational algorithms on near-term quantum devices,” *Quantum Sci. Technol.*, vol. 3, no. 3, p. 030503, 2018, doi: [10.1088/2058-9565/aab822](https://doi.org/10.1088/2058-9565/aab822).
- 567 A. Kandala *et al.*, “Hardware-efficient variational quantum eigensolver for small molecules and quantum magnets,” *Nature*, vol. 549, no. 7671, pp. 242–246, Sep. 2017, doi: [10.1038/nature23879](https://doi.org/10.1038/nature23879).
- 568 P. J. J. O’Malley *et al.*, “Scalable quantum simulation of molecular energies,” *Phys. Rev. X*, vol. 6, no. 3, p. 031007, Jul. 2016, doi: [10.1103/PhysRevX.6.031007](https://doi.org/10.1103/PhysRevX.6.031007).
- 569 K. Bourzac, “Chemistry is quantum computing’s killer app,” *Chemical & Engineering News*, vol. 95, no. 43, Oct. 2017. <https://cen.acs.org/articles/95/i43/Chemistry-quantum-computings-killer-app.html>
- 570 R. Harris *et al.*, “Phase transitions in a programmable quantum spin glass simulator,” *Science*, vol. 361, no. 6398, pp. 162–165, Jul. 2018, doi: [10.1126/science.aat2025](https://doi.org/10.1126/science.aat2025).
- 571 A. D. King *et al.*, “Observation of topological phenomena in a programmable lattice of 1,800 qubits,” *Nature*, vol. 560, no. 7719, pp. 456–460, Aug. 2018, doi: [10.1038/s41586-018-0410-x](https://doi.org/10.1038/s41586-018-0410-x).
- 572 A. M. Childs, D. Maslov, Y. Nam, N. J. Ross, and Y. Su, “Toward the first quantum simulation with quantum speedup,” *Proc. Natl. Acad. Sci. U.S.A.*, vol. 115, no. 38, pp. 9456–9461, Sep. 2018, doi: [10.1073/pnas.1801723115](https://doi.org/10.1073/pnas.1801723115).
- 573 F. Ghafari, N. Tischler, C. D. Franco, J. Thompson, M. Gu, and G. J. Pryde, “Interfering trajectories in experimental quantum-enhanced stochastic simulation,” *Nat. Commun.*, vol. 10, no. 1, Art. no. 1630, Apr. 2019, doi: [10.1038/s41467-019-08951-2](https://doi.org/10.1038/s41467-019-08951-2).
- 574 A. Browaeys and T. Lahaye, “Many-body physics with individually controlled Rydberg atoms,” *Nat. Phys.*, vol. 16, no. 2, pp. 132–142, Feb. 2020, doi: [10.1038/s41567-019-0733-z](https://doi.org/10.1038/s41567-019-0733-z).
- 575 J. Zhang *et al.*, “Observation of a many-body dynamical phase transition with a 53-qubit quantum simulator,” *Nature*, vol. 551, no. 7682, pp. 601–604, Nov. 2017, doi: [10.1038/nature24654](https://doi.org/10.1038/nature24654).
- 576 U. Warring, F. Hakeberg, P. Kiefer, M. Wittemer, and T. Schaetz, “Trapped ion architecture for multi-dimensional quantum simulations,” *Adv. Quantum Tech.*, p. 1900137, 2020, doi: [10.1002/qute.201900137](https://doi.org/10.1002/qute.201900137).
- 577 J. Biamonte, P. Wittek, N. Pancotti, P. Rebentrost, N. Wiebe, and S. Lloyd, “Quantum machine learning,” *Nature*, vol. 549, no. 7671, p. 195, Sep. 2017, doi: [10.1038/nature23474](https://doi.org/10.1038/nature23474).
- 578 E. P. DeBenedictis, “A future with quantum machine learning,” *Computer*, vol. 51, no. 2, pp. 68–71, Feb. 2018, doi: [10.1109/MC.2018.1451646](https://doi.org/10.1109/MC.2018.1451646).

- 579 A. Perdomo-Ortiz, M. Benedetti, J. Realpe-Gómez, and R. Biswas, “Opportunities and challenges for quantum-assisted machine learning in near-term quantum computers,” *Quantum Sci. Technol.*, vol. 3, no. 3, p. 030502, 2018, doi: [10.1088/2058-9565/aab859](https://doi.org/10.1088/2058-9565/aab859).
- 580 V. Dunjko and H. J. Briegel, “Machine learning & artificial intelligence in the quantum domain: a review of recent progress,” *Rep. Prog. Phys.*, vol. 81, no. 7, p. 074001, June 2018, doi: [10.1088/1361-6633/aab406](https://doi.org/10.1088/1361-6633/aab406).
- 581 S. Greengard, “The algorithm that changed quantum machine learning,” *Commun. ACM*, vol. 62, no. 8, pp. 15–17, Jul. 2019, doi: [10.1145/3339458](https://doi.org/10.1145/3339458).
- 582 G. Acampora, “Quantum machine intelligence,” *Quantum Mach. Intell.*, vol. 1, no. 1, pp. 1–3, May 2019, doi: [10.1007/s42484-019-00006-5](https://doi.org/10.1007/s42484-019-00006-5).
- 583 “List of companies involved in quantum computing or communication,” Wikipedia, 2020. Available online: [https://en.wikipedia.org/w/index.php?title=List\\_of\\_companies\\_involved\\_in\\_quantum\\_computing\\_or\\_communication&lidid=937349289](https://en.wikipedia.org/w/index.php?title=List_of_companies_involved_in_quantum_computing_or_communication&lidid=937349289), accessed 2020-02-02.
- 584 D. Finke, “Qubit Technology,” *Quantum Computing Report*, 2020. <https://quantumcomputingreport.com/scorecards/qubit-technology/> (accessed 2020-05-07).
- 585 I. Mehta, “India finally commits to quantum computing, promises \$1.12B investment,” *The Next Web*, 2020-02-01. [Online]. Available: <https://thenextweb.com/in/2020/02/01/india-finally-commits-to-quantum-computing-promises-1-12b-investment/>, accessed 2020-02-01.
- 586 R. Zhao, “China is building a massive multi-location national-level quantum laboratory,” *TechNode*, 2018-09-05. <https://technode.com/2018/09/05/china-quantum-information-laboratory/>
- 587 M. Borak, “They lag behind Google, but Alibaba and Baidu are also fighting for quantum supremacy,” *Abacus News*, 2019-10-24. Available online: <https://www.abacusnews.com/tech/they-lag-behind-google-alibaba-and-baidu-are-also-fighting-quantum-supremacy/article/3034356>, accessed 2020-02-01.
- 588 “Quantum Information Processing and Communication (QIPC) Roadmap,” <http://quope.eu/content/qipc-roadmap>, accessed 2020-03-15.
- 589 M. F. Riedel, D. Binosi, R. Thew, and T. Calarco, “The European quantum technologies flagship programme,” *Quantum Sci. Technol.*, vol. 2, no. 3, p. 030501, 2017, doi: [10.1088/2058-9565/aa6aca](https://doi.org/10.1088/2058-9565/aa6aca).
- 590 J. Mlynek *et al.*, “Quantum Technologies Flagship Final Report,” June 2017. <https://ec.europa.eu/digital-single-market/en/news/quantum-flagship-high-level-expert-group-publishes-final-report>, accessed 2020-03-15.
- 591 D. Castelvecchi, “Europe shows first cards in €1-billion quantum bet,” *Nature*, vol. 563, no. 7729, pp. 14–15, Oct. 2018, doi: [10.1038/d41586-018-07216-0](https://doi.org/10.1038/d41586-018-07216-0).
- 592 BMBF-Internetredaktion, “Quantentechnologien - BMBF,” Bundesministerium für Bildung und Forschung - BMBF. Available online: <https://www.bmbf.de/de/quantentechnologien-7012.html>, accessed 2020-01-15.
- 593 “National Agenda on Quantum Technology,” The Dutch Research Council (NWO), Netherlands, TNO-2019-R11338, Sep. 2019. Available online: <https://www.qusoft.org/national-agenda-on-quantum-technology-the-netherlands-as-an-international-centre-for-quantum-technology/>, accessed 2020-01-15.
- 594 Full Committee Hearing to Examine DOE's Efforts in the Field of Quantum Information Science, 2018-09-25 10:00-12:00. Available online: <https://www.energy.senate.gov/public/index.cfm/hearings-and-business-meetings?ID=8C96E1A0-1272-45C9-ABEF-BF83C5A1107B>, go to 1:23:40 in the video, accessed 2020-03-15.
- 595 Quantum Economic Development Consortium (QED-C). Available online: <https://quantumconsortium.org/>, accessed 2020-03-15.
- 596 M.W. Johnson *et al.*, “Quantum annealing with manufactured spins,” *Nature*, vol. 473, no. 7346, 2011, pp. 194–198, doi: [10.1038/nature10012](https://doi.org/10.1038/nature10012).
- 597 P.I. Bunyk *et al.*, “Architectural considerations in the design of a superconducting quantum annealing processor,” *IEEE Trans. Appl. Supercond.*, vol. 24, no. 4, 2014, doi: [10.1109/TASC.2014.2318294](https://doi.org/10.1109/TASC.2014.2318294).
- 598 W. Tichy, “Is Quantum Computing for Real?: An Interview with Catherine McGeoch of D-Wave Systems,” *Ubiquity*, vol. 2017, no. July, pp. 2:1–2:20, Jul. 2017, doi: [10.1145/3084688](https://doi.org/10.1145/3084688).

- 599 M. W. Johnson, “Next generation quantum annealing system,” presented at Qubits North America, Newport, RI, USA, Sep. 24, 2019. [Online]. Available: [https://www.dwavesys.com/sites/default/files/13\\_DWJohnson.pdf](https://www.dwavesys.com/sites/default/files/13_DWJohnson.pdf), accessed: 2021-04-04.
- 600 K. Boothby, “Architectural considerations in the design of a novel superconducting quantum annealing processor,” presented at the Applied Superconductivity Conference, virtual, Nov. 06, 2020.
- 601 C. McGeoch and P. Farre, “The D-Wave Advantage System: An Overview,” D-Wave Systems, 14-1049A-A, Sep. 2020. [Online]. Available: [https://www.dwavesys.com/sites/default/files/14-1049A-A\\_The\\_D-Wave\\_Advantage\\_System\\_An\\_Overview\\_0.pdf](https://www.dwavesys.com/sites/default/files/14-1049A-A_The_D-Wave_Advantage_System_An_Overview_0.pdf).
- 602 S. E. Venegas-Andraca, W. Cruz-Santos, C. McGeoch, and M. Lanzagorta, “A cross-disciplinary introduction to quantum annealing-based algorithms,” *Contemp. Phys.*, vol. 59, pp. 174–197, Apr. 2018, doi: [10.1080/00107514.2018.1450720](https://doi.org/10.1080/00107514.2018.1450720).
- 603 T. Albash and D. A. Lidar, “Demonstration of a scaling advantage for a quantum annealer over simulated annealing,” *Phys. Rev. X*, vol. 8, no. 3, p. 031016, Jul. 2018, doi: [10.1103/PhysRevX.8.031016](https://doi.org/10.1103/PhysRevX.8.031016).
- 604 S. Jiang, K. A. Britt, A. J. McCaskey, T. S. Humble, and S. Kais, “Quantum annealing for prime factorization,” *Sci. Rep.*, vol. 8, no. 1, p. 17667, Dec. 2018, doi: [10.1038/s41598-018-36058-z](https://doi.org/10.1038/s41598-018-36058-z).
- 605 A. Pearson, A. Mishra, I. Hen, and D. A. Lidar, “Analog errors in quantum annealing: doom and hope,” *npj Quantum Inf.*, vol. 5, no. 1, p. Art. no. 107, Nov. 2019, doi: [10.1038/s41534-019-0210-7](https://doi.org/10.1038/s41534-019-0210-7).
- 606 E. Grant, T. S. Humble, and B. Stump, “Benchmarking quantum annealing controls with portfolio optimization,” *Phys. Rev. Applied*, vol. 15, no. 1, p. 014012, Jan. 2021, doi: [10.1103/PhysRevApplied.15.014012](https://doi.org/10.1103/PhysRevApplied.15.014012).
- 607 D. Aharonov, W. van Dam, J. Kempe, Z. Landau, S. Lloyd, and O. Regev, “Adiabatic quantum computation is equivalent to standard quantum computation,” *SIAM Rev.*, vol. 50, no. 4, pp. 755–787, Jan. 2008, doi: [10.1137/080734479](https://doi.org/10.1137/080734479).
- 608 H. Yu, Y. Huang, and B. Wu, “Exact equivalence between quantum adiabatic algorithm and quantum circuit algorithm,” *Chinese Phys. Lett.*, vol. 35, no. 11, p. 110303, Oct. 2018, doi: [10.1088/0256-307X/35/11/110303](https://doi.org/10.1088/0256-307X/35/11/110303).
- 609 K. C. Young, M. Sarovar, and R. Blume-Kohout, “Error suppression and error correction in adiabatic quantum computation: Techniques and challenges,” *Phys. Rev. X*, vol. 3, no. 4, p. 041013, 2013, doi: [10.1103/PhysRevX.3.041013](https://doi.org/10.1103/PhysRevX.3.041013).
- 610 H. Ushijima-Mwesigwa, C. F. A. Negre, and S. M. Mniszewski, “Graph partitioning using quantum annealing on the D-Wave system,” in *Proc. 2nd Int. Workshop Post Moore’s Era Supercomputing (PMES)*, Denver, CO, USA, Nov. 2017, pp. 22–29, doi: [10.1145/3149526.3149531](https://doi.org/10.1145/3149526.3149531).
- 611 J. King *et al.*, “Quantum annealing amid local ruggedness and global frustration,” *J. Phys. Soc. Jpn.*, vol. 88, no. 6, p. 061007, Mar. 2019, doi: [10.7566/JPSJ.88.061007](https://doi.org/10.7566/JPSJ.88.061007).
- 612 A. D. King *et al.*, “Scaling advantage over path-integral Monte Carlo in quantum simulation of geometrically frustrated magnets,” *Nat. Commun.*, vol. 12, no. 1, Art. no. 1113, Feb. 2021, doi: [10.1038/s41467-021-20901-5](https://doi.org/10.1038/s41467-021-20901-5).
- 613 F. K. Wilhelm *et al.*, “Status of quantum computer development v1.1,” Federal Office for Information Security, Germany, BSI Project Number 283, 2019-07. Available online: <https://www.bsi.bund.de/DE/Publikationen/Studien/Quantencomputer/quantencomputer.html>
- 614 T. S. Humble, H. Thapliyal, E. Muñoz-Coreas, F. A. Mohiyaddin, and R. S. Bennink, “Quantum Computing Circuits and Devices,” *IEEE Des. Test*, vol. 36, no. 3, pp. 69–94, June 2019, doi: [10.1109/MDAT.2019.2907130](https://doi.org/10.1109/MDAT.2019.2907130).
- 615 M. Erhard, M. Krenn, and A. Zeilinger, “Advances in high-dimensional quantum entanglement,” *Nat. Rev. Phys.*, vol. 2, no. 7, Art. no. 7, Jul. 2020, doi: [10.1038/s42254-020-0193-5](https://doi.org/10.1038/s42254-020-0193-5).
- 616 J. Roffe, “Quantum error correction: An introductory guide,” *Contemp. Phys.*, vol. 60, no. 3, pp. 226–245, July 2019, doi: [10.1080/00107514.2019.1667078](https://doi.org/10.1080/00107514.2019.1667078).
- 617 J. P. G. van Dijk *et al.*, “Impact of Classical Control Electronics on Qubit Fidelity,” *Phys. Rev. Applied*, vol. 12, no. 4, p. 044054, Oct. 2019, doi: [10.1103/PhysRevApplied.12.044054](https://doi.org/10.1103/PhysRevApplied.12.044054).
- 618 A. Butko *et al.*, “Understanding quantum control processor capabilities and limitations through circuit characterization,” *2020 ICRC*, Dec. 2020, pp. 66–75, doi: [10.1109/ICRC2020.2020.00011](https://doi.org/10.1109/ICRC2020.2020.00011).

- 
- 619 M. Kjaergaard *et al.*, “A quantum instruction set implemented on a superconducting quantum processor,” *arXiv:2001.08838 [quant-ph]*, Dec. 2020.
- 620 L. Riesebois *et al.*, “Quantum accelerated computer architectures,” in 2019 IEEE International Symposium on Circuits and Systems (ISCAS), Sapporo, Japan, May 2019, doi: [10.1109/ISCAS.2019.8702488](https://doi.org/10.1109/ISCAS.2019.8702488).
- 621 A. Holmes, S. Johri, G. G. Guerreschi, J. S. Clarke, and A. Y. Matsuura, “Impact of qubit connectivity on quantum algorithm performance,” *Quantum Sci. Technol.*, vol. 5, no. 2, p. 025009, Mar. 2020, doi: [10.1088/2058-9565/ab73e0](https://doi.org/10.1088/2058-9565/ab73e0).
- 622 R. LaRose, “Overview and Comparison of Gate Level Quantum Software Platforms,” *Quantum*, vol. 3, p. 130, Mar. 2019, doi: [10.22331/q-2019-03-25-130](https://doi.org/10.22331/q-2019-03-25-130).
- 623 R. LaRose, “Review of the Cirq Quantum Software Framework,” Quantum Computing Report, 2019. [Online]. Available: <https://quantumcomputingreport.com/scorecards/review-of-the-cirq-quantum-software-framework/>, accessed 2020-03-15.
- 624 F. Arute *et al.*, “Quantum supremacy using a programmable superconducting processor,” *Nature*, vol. 574, no. 7779, pp. 505–510, Oct. 2019, doi: [10.1038/s41586-019-1666-5](https://doi.org/10.1038/s41586-019-1666-5).
- 625 E. Pednault, J. A. Gunnels, G. Nannicini, L. Horesh, and R. Wisnieff, “Leveraging secondary storage to simulate deep 54-qubit Sycamore circuits,” *arXiv:1910.09534 [quant-ph]*, Oct. 2019.
- 626 E. Pednault, J. Gunnels, D. Maslov, and J. Gambetta, “On ‘Quantum Supremacy,’” IBM Research Blog, 2019-10-21. Available online: <https://www.ibm.com/blogs/research/2019/10/on-quantum-supremacy/>, accessed 2020-01-18.
- 627 Quantum volume, [https://en.wikipedia.org/wiki/Quantum\\_volume](https://en.wikipedia.org/wiki/Quantum_volume), accessed 2021-03-22.
- 628 P. Krantz, M. Kjaergaard, F. Yan, T. P. Orlando, S. Gustavsson, and W. D. Oliver, “A quantum engineer’s guide to superconducting qubits,” *Appl. Phys. Rev.*, vol. 6, no. 2, p. 021318, June 2019, doi: [10.1063/1.5089550](https://doi.org/10.1063/1.5089550).
- 629 O. Mukhanov *et al.*, “Scalable Quantum Computing Infrastructure Based on Superconducting Electronics,” in 2019 *IEEE Int. Electron Devices Meeting (IEDM)*, San Francisco, CA, USA, Dec. 2019, pp. 31.2.1–31.2.4, doi: [10.1109/IEDM19573.2019.8993634](https://doi.org/10.1109/IEDM19573.2019.8993634).
- 630 W. D. Oliver and P. B. Welander, “Materials in superconducting quantum bits,” *MRS Bull.*, vol. 38, no. 10, pp. 816–825, Oct. 2013, doi: [10.1557/mrs.2013.229](https://doi.org/10.1557/mrs.2013.229).
- 631 J. I.-J. Wang *et al.*, “Coherent control of a hybrid superconducting circuit made with graphene-based van der Waals heterostructures,” *Nat. Nanotechnol.*, Dec. 2018, doi: [10.1038/s41565-018-0329-2](https://doi.org/10.1038/s41565-018-0329-2).
- 632 L. Casparis *et al.*, “Superconducting gatemon qubit based on a proximitized two-dimensional electron gas,” *Nat. Nanotechnol.*, vol. 13, no. 10, pp. 915–919, Oct. 2018, doi: [10.1038/s41565-018-0207-y](https://doi.org/10.1038/s41565-018-0207-y).
- 633 L. Casparis *et al.*, “Voltage-controlled superconducting quantum bus,” *Phys. Rev. B*, vol. 99, no. 8, p. 085434, Feb. 2019, doi: [10.1103/PhysRevB.99.085434](https://doi.org/10.1103/PhysRevB.99.085434).
- 634 M. Kjaergaard *et al.*, “Superconducting qubits: Current state of play,” *Annu. Rev. Condens. Matter Phys.*, vol. 11, no. 1, Mar. 2020, doi: [10.1146/annurev-conmatphys-031119-050605](https://doi.org/10.1146/annurev-conmatphys-031119-050605).
- 635 J. H. Plantenberg, P. C. de Groot, C. J. P. M. Harmans, and J. E. Mooij, “Demonstration of controlled-NOT quantum gates on a pair of superconducting quantum bits,” *Nature*, vol. 447, no. 7146, pp. 836–839, June 2007, doi: [10.1038/nature05896](https://doi.org/10.1038/nature05896).
- 636 J. M. Chow *et al.*, “Implementing a strand of a scalable fault-tolerant quantum computing fabric,” *Nat. Commun.*, vol. 5, p. 4015, June 2014, doi: [10.1038/ncomms5015](https://doi.org/10.1038/ncomms5015).
- 637 M. H. Devoret and R. J. Schoelkopf, “Superconducting circuits for quantum information: An outlook,” *Science*, vol. 339, no. 6124, pp. 1169–1174, Mar. 2013, doi: [10.1126/science.1231930](https://doi.org/10.1126/science.1231930).
- 638 A. P. Vepsäläinen *et al.*, “Impact of ionizing radiation on superconducting qubit coherence,” *Nature*, vol. 584, no. 7822, Art. no. 7822, Aug. 2020, doi: [10.1038/s41586-020-2619-8](https://doi.org/10.1038/s41586-020-2619-8).
- 639 R. Van Meter and C. Horsman, “A blueprint for building a quantum computer,” *Commun. ACM*, vol. 56, no. 10, p. 84, Oct. 2013, doi: [10.1145/2494568](https://doi.org/10.1145/2494568).
- 640 E. A. Sete, W. J. Zeng, and C. T. Rigetti, “A functional architecture for scalable quantum computing,” in 2016 *IEEE International Conference on Rebooting Computing (ICRC)*, 2016, pp. 1–6, doi: [10.1109/ICRC.2016.7738703](https://doi.org/10.1109/ICRC.2016.7738703).
- 641 G. Wendin, “Quantum information processing with superconducting circuits: A review,” *Rep. Prog. Phys.*, vol. 80, no. 10, p. 106001, Oct. 2017, doi: [10.1088/1361-6633/aa7e1a](https://doi.org/10.1088/1361-6633/aa7e1a).



- 642 X. Fu et al., “A microarchitecture for a superconducting quantum processor,” *IEEE Micro*, vol. 38, no. 3, pp. 40–47, May 2018, doi: [10.1109/MM.2018.032271060](https://doi.org/10.1109/MM.2018.032271060).
- 643 H. Mukai et al., “Pseudo-2D superconducting quantum computing circuit for the surface code: proposal and preliminary tests,” *New J. Phys.*, vol. 22, no. 4, p. 043013, Apr. 2020, doi: [10.1088/1367-2630/ab7d7d](https://doi.org/10.1088/1367-2630/ab7d7d).
- 644 J. Gambetta, “IBM’s roadmap for scaling quantum technology,” *IBM Research Blog*, Sep. 15, 2020. <https://www.ibm.com/blogs/research/2020/09/ibm-quantum-roadmap/> (accessed 2021-03-07).
- 645 C. Chamberland et al., “Building a fault-tolerant quantum computer using concatenated cat codes,” *arXiv:2012.04108 [quant-ph]*, Dec. 2020.
- 646 P. Jurcevic et al., “Demonstration of quantum volume 64 on a superconducting quantum computing system,” *Quantum Sci. Technol.*, vol. 6, no. 2, p. 025020, Apr. 2021, doi: [10.1088/2058-9565/abe519](https://doi.org/10.1088/2058-9565/abe519).
- 647 A. Wallraff et al., “Strong coupling of a single photon to a superconducting qubit using circuit quantum electrodynamics,” *Nature*, vol. 431, no. 7005, p. 162, Sep. 2004, doi: [10.1038/nature02851](https://doi.org/10.1038/nature02851).
- 648 M. Göppl et al., “Coplanar waveguide resonators for circuit quantum electrodynamics,” *J. Appl. Phys.*, vol. 104, no. 11, p. 113904, Dec. 2008, doi: [10.1063/1.3010859](https://doi.org/10.1063/1.3010859).
- 649 A. Megrant et al., “Planar superconducting resonators with internal quality factors above one million,” *Appl. Phys. Lett.*, vol. 100, no. 11, p. 113510, Mar. 2012, doi: [10.1063/1.3693409](https://doi.org/10.1063/1.3693409).
- 650 D. C. McKay, S. Filipp, A. Mezzacapo, E. Magesan, J. M. Chow, and J. M. Gambetta, “Universal Gate for Fixed-Frequency Qubits via a Tunable Bus,” *Phys. Rev. Appl.*, vol. 6, no. 6, p. 064007, Dec. 2016, doi: [10.1103/PhysRevApplied.6.064007](https://doi.org/10.1103/PhysRevApplied.6.064007).
- 651 R. Barends et al., “Minimal resonator loss for circuit quantum electrodynamics,” *Appl. Phys. Lett.*, vol. 97, no. 2, p. 023508, Jul. 2010, doi: [10.1063/1.3458705](https://doi.org/10.1063/1.3458705).
- 652 B. Foxen et al., “Qubit compatible superconducting interconnects,” *Quantum Sci. Technol.*, vol. 3, no. 1, p. 014005, 2018, doi: [10.1088/2058-9565/aa94fc](https://doi.org/10.1088/2058-9565/aa94fc).
- 653 D. R. W. Yost et al., “Solid-state qubits integrated with superconducting through-silicon vias,” *npj Quantum Inf.*, vol. 6, no. 1, Art. no. 1, Jul. 2020, doi: [10.1038/s41534-020-00289-8](https://doi.org/10.1038/s41534-020-00289-8).
- 654 J. Gambetta, W. A. Braff, A. Wallraff, S. M. Girvin, and R. J. Schoelkopf, “Protocols for optimal readout of qubits using a continuous quantum nondemolition measurement,” *Phys. Rev. A*, vol. 76, no. 1, p. 012325, Jul. 2007, doi: [10.1103/PhysRevA.76.012325](https://doi.org/10.1103/PhysRevA.76.012325).
- 655 N. Bergeal et al., “Analog information processing at the quantum limit with a Josephson ring modulator,” *Nat. Phys.*, vol. 6, no. 4, pp. 296–302, Apr. 2010, doi: [10.1038/nphys1516](https://doi.org/10.1038/nphys1516).
- 656 T. Yamamoto et al., “Flux-driven Josephson parametric amplifier,” *Appl. Phys. Lett.*, vol. 93, no. 4, p. 042510, Jul. 2008, doi: [10.1063/1.2964182](https://doi.org/10.1063/1.2964182).
- 657 M. A. Castellanos-Beltran and K. W. Lehnert, “Widely tunable parametric amplifier based on a superconducting quantum interference device array resonator,” *Appl. Phys. Lett.*, vol. 91, no. 8, p. 083509, Aug. 2007, doi: [10.1063/1.2773988](https://doi.org/10.1063/1.2773988).
- 658 C. Macklin et al., “A near-quantum-limited Josephson traveling-wave parametric amplifier,” *Science*, vol. 350, no. 6258, pp. 307–310, Oct. 2015, doi: [10.1126/science.aaa8525](https://doi.org/10.1126/science.aaa8525).
- 659 A. Kamal, J. Clarke, and M. H. Devoret, “Noiseless non-reciprocity in a parametric active device,” *Nat. Phys.*, vol. 7, no. 4, pp. 311–315, Apr. 2011, doi: [10.1038/nphys1893](https://doi.org/10.1038/nphys1893).
- 660 Y.-F. Chen et al., “Microwave Photon Counter Based on Josephson Junctions,” *Phys. Rev. Lett.*, vol. 107, no. 21, p. 217401, Nov. 2011, doi: [10.1103/PhysRevLett.107.217401](https://doi.org/10.1103/PhysRevLett.107.217401).
- 661 A. Opremcak et al., “Measurement of a superconducting qubit with a microwave photon counter,” *Science*, vol. 361, no. 6408, pp. 1239–1242, Sep. 2018, doi: [10.1126/science.aat4625](https://doi.org/10.1126/science.aat4625).
- 662 R. McDermott et al., “Quantum–classical interface based on single flux quantum digital logic,” *Quantum Sci. Technol.*, vol. 3, no. 2, p. 024004, 2018, doi: [10.1088/2058-9565/aaa3a0](https://doi.org/10.1088/2058-9565/aaa3a0).
- 663 S. Sheldon, L. S. Bishop, E. Magesan, S. Filipp, J. M. Chow, and J. M. Gambetta, “Characterizing errors on qubit operations via iterative randomized benchmarking,” *Phys. Rev. A*, vol. 93, no. 1, p. 012301, Jan. 2016, doi: [10.1103/PhysRevA.93.012301](https://doi.org/10.1103/PhysRevA.93.012301).

- 664 R. McDermott and M. G. Vavilov, "Accurate qubit control with single flux quantum pulses," *Phys. Rev. Appl.*, vol. 2, no. 1, p. 014007, Jul. 2014, doi: [10.1103/PhysRevApplied.2.014007](https://doi.org/10.1103/PhysRevApplied.2.014007).
- 665 E. Leonard *et al.*, "Digital Coherent Control of a Superconducting Qubit," *Phys. Rev. Applied*, vol. 11, no. 1, p. 014009, Jan. 2019, doi: [10.1103/PhysRevApplied.11.014009](https://doi.org/10.1103/PhysRevApplied.11.014009).
- 666 N. Yoshikawa, "Superconducting digital electronics for controlling quantum computing systems," *IEICE Trans. Electron.*, vol. E102-C, no. 3, pp. 217–223, Mar. 2019, doi: [10.1587/transele.2018SDI0003](https://doi.org/10.1587/transele.2018SDI0003).
- 667 Y. Zhong *et al.*, "Deterministic multi-qubit entanglement in a quantum network," *Nature*, vol. 590, no. 7847, Art. no. 7847, Feb. 2021, doi: [10.1038/s41586-021-03288-7](https://doi.org/10.1038/s41586-021-03288-7). <https://arxiv.org/abs/2011.13108>
- 668 J.G. Bartholomew, J. Rochman, T. Xie, J.M. Kindem, A. Ruskuc, I. Craiciu, M. Lei and A. Faraon, "On-chip coherent microwave-to-optical transduction mediated by ytterbium in YVO<sub>4</sub>," *Nat. Comm.*, Vol. 11, 3266, June 2020, doi: [10.1038/s41467-020-16996-x](https://doi.org/10.1038/s41467-020-16996-x).
- 669 B. Kannan *et al.*, "Generating spatially entangled itinerant photons with waveguide quantum electrodynamics," *Sci. Adv.*, vol. 6, no. 41, p. eabb8780, Oct. 2020, doi: [10.1126/sciadv.abb8780](https://doi.org/10.1126/sciadv.abb8780).
- 670 M. Mirhosseini, A. Sipahigil, M. Kalaei, and O. Painter, "Superconducting qubit to optical photon transduction," *Nature*, vol. 588, no. 7839, Art. no. 7839, Dec. 2020, doi: [10.1038/s41586-020-3038-6](https://doi.org/10.1038/s41586-020-3038-6).
- 671 C. D. Bruzewicz, J. Chiaverini, R. McConnell, and J. M. Sage, "Trapped-ion quantum computing: Progress and challenges," *Appl. Phys. Rev.*, vol. 6, no. 2, p. 021314, May 2019, doi: [10.1063/1.5088164](https://doi.org/10.1063/1.5088164).
- 672 K. Wright *et al.*, "Benchmarking an 11-qubit quantum computer," *Nat. Commun.*, vol. 10, no. 1, p. Art. no. 5464, Nov. 2019, doi: [10.1038/s41467-019-13534-2](https://doi.org/10.1038/s41467-019-13534-2).
- 673 V. M. Schäfer *et al.*, "Fast quantum logic gates with trapped-ion qubits," *Nature*, vol. 555, no. 7694, pp. 75–78, Mar. 2018, doi: [10.1038/nature25737](https://doi.org/10.1038/nature25737).
- 674 Y. Wan *et al.*, "Quantum gate teleportation between separated qubits in a trapped-ion processor," *Science*, vol. 364, no. 6443, pp. 875–878, May 2019, doi: [10.1126/science.aaw9415](https://doi.org/10.1126/science.aaw9415).
- 675 P. Murali, D. M. Debroy, K. R. Brown, and M. Martonosi, "Architecting noisy intermediate-scale trapped ion quantum computers," in *ACM/IEEE Proc. ISCA*, May 2020, pp. 529–542, doi: [10.1109/ISCA45697.2020.00051](https://doi.org/10.1109/ISCA45697.2020.00051).
- 676 J. M. Pino *et al.*, "Demonstration of the QCCD trapped-ion quantum computer architecture," *arXiv:2003.01293 [quant-ph]*, Sep. 2020.
- 677 F. Jazaeri, A. Beckers, A. Tajalli, and J.-M. Sallese, "A review on quantum computing: From qubits to front-end electronics and cryogenic MOSFET physics," in *2019 MIXDES - 26th International Conference "Mixed Design of Integrated Circuits and Systems"*, Rzeszów, Poland, 2019, pp. 15–25, doi: [10.23919/MIXDES.2019.8787164](https://doi.org/10.23919/MIXDES.2019.8787164).
- 678 A. Chatterjee, P. Stevenson, S. De Franceschi, A. Morello, N. P. de Leon and F. Kuemmeth, "Semiconductor qubits in practice," *Nat. Rev. Phys.*, Feb. 2021, doi: [10.1038/s42254-021-00283-9](https://doi.org/10.1038/s42254-021-00283-9). <https://arxiv.org/abs/2005.06564>
- 679 B. Hensen *et al.*, "A silicon quantum-dot-coupled nuclear spin qubit," *Nat. Nanotechnol.*, vol. 15, no. 1, pp. 13–17, Jan. 2020, doi: [10.1038/s41565-019-0587-7](https://doi.org/10.1038/s41565-019-0587-7).
- 680 S. Asaad *et al.*, "Coherent electrical control of a single high-spin nucleus in silicon," *Nature*, vol. 579, no. 7798, pp. 205–209, Mar. 2020, doi: [10.1038/s41586-020-2057-7](https://doi.org/10.1038/s41586-020-2057-7).
- 681 D. Sabbagh *et al.*, "Quantum transport properties of industrial <sup>28</sup>Si/<sup>28</sup>SiO<sub>2</sub>," *Phys. Rev. Appl.*, vol. 12, no. 1, p. 014013, Jul. 2019, doi: [10.1103/PhysRevApplied.12.014013](https://doi.org/10.1103/PhysRevApplied.12.014013).
- 682 N. W. Hendrickx, D. P. Franke, A. Sammak, G. Scappucci, and M. Veldhorst, "Fast two-qubit logic with holes in germanium," *Nature*, vol. 577, no. 7791, pp. 487–491, Jan. 2020, doi: [10.1038/s41586-019-1919-3](https://doi.org/10.1038/s41586-019-1919-3).
- 683 W. I. L. Lawrie *et al.*, "Quantum dot arrays in silicon and germanium," *Appl. Phys. Lett.*, vol. 116, no. 8, p. 080501, Feb. 2020, doi: [10.1063/5.0002013](https://doi.org/10.1063/5.0002013).
- 684 D. Loss and D. P. DiVincenzo, "Quantum computation with quantum dots," *Phys. Rev. A*, vol. 57, no. 1, pp. 120–126, Jan. 1998, doi: [10.1103/PhysRevA.57.120](https://doi.org/10.1103/PhysRevA.57.120).
- 685 M. Veldhorst *et al.*, "A two-qubit logic gate in silicon," *Nature*, vol. 526, no. 7573, pp. 410–414, Oct. 2015, doi: [10.1038/nature15263](https://doi.org/10.1038/nature15263).
- 686 X. Xue *et al.*, "Benchmarking gate fidelities in a Si/SiGe two-qubit device," *Phys. Rev. X*, vol. 9, no. 2, p. 021011, Apr. 2019, doi: [10.1103/PhysRevX.9.021011](https://doi.org/10.1103/PhysRevX.9.021011).

- 687 W. Huang *et al.*, “Fidelity benchmarks for two-qubit gates in silicon,” *Nature*, vol. 569, no. 7757, pp. 532–536, May 2019, doi: [10.1038/s41586-019-1197-0](https://doi.org/10.1038/s41586-019-1197-0).
- 688 Y. He, S. K. Gorman, D. Keith, L. Kranz, J. G. Keizer, and M. Y. Simmons, “A two-qubit gate between phosphorus donor electrons in silicon,” *Nature*, vol. 571, no. 7765, pp. 371–375, Jul. 2019, doi: [10.1038/s41586-019-1381-2](https://doi.org/10.1038/s41586-019-1381-2).
- 689 T. Frey *et al.*, “Dipole coupling of a double quantum dot to a microwave resonator,” *Phys. Rev. Lett.*, vol. 108, no. 4, p. 046807, Jan. 2012, doi: [10.1103/PhysRevLett.108.046807](https://doi.org/10.1103/PhysRevLett.108.046807).
- 690 A. J. Landig *et al.*, “Virtual-photon-mediated spin-qubit–transmon coupling,” *Nat. Commun.*, vol. 10, no. 1, p. 5037, Nov. 2019, doi: [10.1038/s41467-019-13000-z](https://doi.org/10.1038/s41467-019-13000-z).
- 691 F. Borjans, X. G. Croot, X. Mi, M. J. Gullans, and J. R. Petta, “Resonant microwave-mediated interactions between distant electron spins,” *Nature*, vol. 577, pp. 195–198, Jan. 2020, doi: [10.1038/s41586-019-1867-y](https://doi.org/10.1038/s41586-019-1867-y).
- 692 T. Ito *et al.*, “Four single-spin Rabi oscillations in a quadruple quantum dot,” *Appl. Phys. Lett.*, vol. 113, no. 9, p. 093102, Aug. 2018, doi: [10.1063/1.5040280](https://doi.org/10.1063/1.5040280).
- 693 D. Rotta, F. Sebastiano, E. Charbon, and E. Prati, “Quantum information density scaling and qubit operation time constraints of CMOS silicon-based quantum computer architectures,” *npj Quantum Inf.*, vol. 3, no. 1, p. Art. no. 26, June 2017, doi: [10.1038/s41534-017-0023-5](https://doi.org/10.1038/s41534-017-0023-5).
- 694 M. Veldhorst, H. G. J. Eenink, C. H. Yang, and A. S. Dzurak, “Silicon CMOS architecture for a spin-based quantum computer,” *Nat. Commun.*, vol. 8, no. 1, p. 1766, Dec. 2017, doi: [10.1038/s41467-017-01905-6](https://doi.org/10.1038/s41467-017-01905-6).
- 695 C. Bäuerle *et al.*, “Coherent control of single electrons: a review of current progress,” *Rep. Prog. Phys.*, vol. 81, no. 5, p. 056503, Apr. 2018, doi: [10.1088/1361-6633/aaa98a](https://doi.org/10.1088/1361-6633/aaa98a).
- 696 X. Zhang, H.-O. Li, G. Cao, M. Xiao, G.-C. Guo, and G.-P. Guo, “Semiconductor quantum computation,” *Natl. Sci. Rev.*, vol. 6, no. 1, pp. 32–54, Jan. 2019, doi: [10.1093/nsr/nwy153](https://doi.org/10.1093/nsr/nwy153).
- 697 L. M. K. Vandersypen and M. A. Eriksson, “Quantum computing with semiconductor spins,” *Physics Today*, vol. 72, no. 8, pp. 38–45, Aug. 2019, doi: [10.1063/PT.3.4270](https://doi.org/10.1063/PT.3.4270).
- 698 E. Ferraro and E. Prati, “Is all-electrical silicon quantum computing feasible in the long term?” *Phys. Lett. A*, p. 126352, Mar. 2020, doi: [10.1016/j.physleta.2020.126352](https://doi.org/10.1016/j.physleta.2020.126352).
- 699 J. S. Clarke *et al.*, “Quantum computing within the framework of advanced semiconductor manufacturing,” *2016 IEEE International Electron Devices Meeting (IEDM)*, 2016, pp. 13.1.1–13.1.3, doi: [10.1109/IEDM.2016.7838406](https://doi.org/10.1109/IEDM.2016.7838406).
- 700 L. Petit *et al.*, “Universal quantum logic in hot silicon qubits,” *Nature*, vol. 580, no. 7803, pp. 355–359, Apr. 2020, doi: [10.1038/s41586-020-2170-7](https://doi.org/10.1038/s41586-020-2170-7).
- 701 L. M. K. Vandersypen *et al.*, “Interfacing spin qubits in quantum dots and donors—hot, dense, and coherent,” *npj Quantum Inf.*, vol. 3, no. 1, Art. no. 34, Sep. 2017, doi: [10.1038/s41534-017-0038-y](https://doi.org/10.1038/s41534-017-0038-y).
- 702 J. M. Boter *et al.*, “A sparse spin qubit array with integrated control electronics,” in *2019 IEEE International Electron Devices Meeting (IEDM)*, San Francisco, USA, Dec. 2019, pp. 31.4.1–31.4.4, doi: [10.1109/IEDM19573.2019.8993570](https://doi.org/10.1109/IEDM19573.2019.8993570).
- 703 L. Geck, A. Kruth, H. Bluhm, S. van Waasen, and S. Heinen, “Control electronics for semiconductor spin qubits,” *Quantum Sci. Technol.*, vol. 5, no. 1, p. 015004, Jan. 2020, doi: [10.1088/2058-9565/ab5e07](https://doi.org/10.1088/2058-9565/ab5e07).
- 704 S. Slussarenko and G. J. Pryde, “Photonic quantum information processing: A concise review,” *Appl. Phys. Rev.*, vol. 6, no. 4, p. 041303, Oct. 2019, doi: [10.1063/1.5115814](https://doi.org/10.1063/1.5115814).
- 705 D. Llewellyn *et al.*, “Chip-to-chip quantum teleportation and multi-photon entanglement in silicon,” *Nat. Phys.*, vol. 16, no. 2, pp. 148–153, Feb. 2020, doi: [10.1038/s41567-019-0727-x](https://doi.org/10.1038/s41567-019-0727-x).
- 706 J. Wang, F. Sciarrino, A. Laing, and M. G. Thompson, “Integrated photonic quantum technologies,” *Nat. Photonics*, vol. 14, no. 5, pp. 273–284, May 2020, doi: [10.1038/s41566-019-0532-1](https://doi.org/10.1038/s41566-019-0532-1).
- 707 J. M. Arrazola *et al.*, “Quantum circuits with many photons on a programmable nanophotonic chip,” *Nature*, vol. 591, no. 7848, Art. no. 7848, Mar. 2021, doi: [10.1038/s41586-021-03202-1](https://doi.org/10.1038/s41586-021-03202-1).
- 708 U. L. Andersen, “Photonic chip brings optical quantum computers a step closer,” *Nature*, vol. 591, no. 7848, Art. no. 7848, Mar. 2021, doi: [10.1038/d41586-021-00488-z](https://doi.org/10.1038/d41586-021-00488-z).
- 709 M. Leijnse and K. Flensberg, “Introduction to topological superconductivity and Majorana fermions,” *Semicond. Sci. Technol.*, vol. 27, no. 12, p. 124003, 2012, doi: [10.1088/0268-1242/27/12/124003](https://doi.org/10.1088/0268-1242/27/12/124003).

- 710 R. V. Mishmash, B. Bauer, F. von Oppen, and J. Alicea, “Dephasing and leakage dynamics of noisy Majorana-based qubits: Topological versus Andreev,” *Phys. Rev. B*, vol. 101, no. 7, p. 075404, Feb. 2020, doi: [10.1103/PhysRevB.101.075404](https://doi.org/10.1103/PhysRevB.101.075404).
- 711 B. Douçot and L. B. Ioffe, “Physical implementation of protected qubits,” *Rep. Prog. Phys.*, vol. 75, no. 7, p. 072001, 2012, doi: [10.1088/0034-4885/75/7/072001](https://doi.org/10.1088/0034-4885/75/7/072001).
- 712 P. Fan *et al.*, “Observation of magnetic adatom-induced Majorana vortex and its hybridization with field-induced Majorana vortex in an iron-based superconductor,” *Nat. Commun.*, vol. 12, no. 1, Art. no. 1348, Mar. 2021, doi: [10.1038/s41467-021-21646-x](https://doi.org/10.1038/s41467-021-21646-x).
- 713 N. Gisin and R. Thew, “Quantum communication,” *Nat. Photonics*, vol. 1, no. 3, pp. 165–171, Mar. 2007, doi: [10.1038/nphoton.2007.22](https://doi.org/10.1038/nphoton.2007.22).
- 714 C. J. Axline *et al.*, “On-demand quantum state transfer and entanglement between remote microwave cavity memories,” *Nat. Phys.*, vol. 14, no. 7, p. 705, Jul. 2018, doi: [10.1038/s41567-018-0115-y](https://doi.org/10.1038/s41567-018-0115-y).
- 715 R. H. Hadfield, “Single-photon detectors for optical quantum information applications,” *Nat. Photonics*, vol. 3, no. 12, pp. 696–705, Dec. 2009, doi: [10.1038/nphoton.2009.230](https://doi.org/10.1038/nphoton.2009.230).
- 716 M. Sanz, K. G. Fedorov, F. Deppe, and E. Solano, “Challenges in open-air microwave quantum communication and sensing,” in *2018 IEEE Conference on Antenna Measurements Applications (CAMA)*, Sep. 2018, doi: [10.1109/CAMA.2018.8530599](https://doi.org/10.1109/CAMA.2018.8530599).
- 717 S. J. Devitt, A. D. Greentree, A. M. Stephens, and R. Van Meter, “High-speed quantum networking by ship,” *Sci. Rep.*, vol. 6, p. 36163, Nov. 2016, doi: [10.1038/srep36163](https://doi.org/10.1038/srep36163).
- 718 D. Awschalom *et al.*, “Development of quantum interconnects (QuICs) for next-generation information technologies,” *PRX Quantum*, vol. 2, no. 1, p. 017002, Feb. 2021, doi: [10.1103/PRXQuantum.2.017002](https://doi.org/10.1103/PRXQuantum.2.017002).
- 719 M. Kutas, B. Haase, P. Bickert, F. Riexinger, D. Molter, and G. von Freymann, “Terahertz quantum sensing,” *Sci. Adv.*, vol. 6, no. 11, p. eaaz8065, Mar. 2020, doi: [10.1126/sciadv.aaz8065](https://doi.org/10.1126/sciadv.aaz8065).
- 720 “IBM Achieves Highest Quantum Volume to Date, Establishes Roadmap for Reaching Quantum Advantage,” March, 2019. Available online: <https://newsroom.ibm.com/2019-03-04-IBM-Achieves-Highest-Quantum-Volume-to-Date-Establishes-Roadmap-for-Reaching-Quantum-Advantage>, accessed 2020-01-18.
- 721 K. Michielsen, M. Nocon, D. Willsch, F. Jin, T. Lippert, and H. De Raedt, “Benchmarking gate-based quantum computers,” *Comput. Phys. Commun.*, vol. 220, pp. 44–55, Nov. 2017, doi: [10.1016/j.cpc.2017.06.011](https://doi.org/10.1016/j.cpc.2017.06.011).
- 722 A. K. Hashagen, S. T. Flammia, D. Gross, and J. J. Wallman, “Real Randomized Benchmarking,” *Quantum*, vol. 2, p. 85, Aug. 2018, doi: [10.22331/q-2018-08-22-85](https://doi.org/10.22331/q-2018-08-22-85).
- 723 G. Bai and G. Chiribella, “Test one to test many: A unified approach to quantum benchmarks,” *Phys. Rev. Lett.*, vol. 120, no. 15, p. 150502, Apr. 2018, doi: [10.1103/PhysRevLett.120.150502](https://doi.org/10.1103/PhysRevLett.120.150502).
- 724 J. R. Wootton, “Benchmarking of quantum processors with random circuits,” *arXiv:1806.02736 [quant-ph]*, June 2018.
- 725 J. King, S. Yarkoni, M. M. Nevisi, J. P. Hilton, and C. C. McGeoch, “Benchmarking a quantum annealing processor with the time-to-target metric,” *arXiv:1508.05087 [quant-ph]*, Aug. 2015.
- 726 N. M. Linke *et al.*, “Experimental comparison of two quantum computing architectures,” *Proc. Natl. Acad. Sci. U.S.A.*, vol. 114, no. 13, pp. 3305–3310, Mar. 2017, doi: [10.1073/pnas.1618020114](https://doi.org/10.1073/pnas.1618020114).
- 727 J. J. Burnett *et al.*, “Decoherence benchmarking of superconducting qubits,” *npj Quantum Inf.*, vol. 5, no. 1, Art. no. 54, June 2019, doi: [10.1038/s41534-019-0168-5](https://doi.org/10.1038/s41534-019-0168-5).
- 728 A. J. McCaskey *et al.*, “Quantum chemistry as a benchmark for near-term quantum computers,” *npj Quantum Inf.*, vol. 5, no. 1, Art. no. 99, Nov. 2019, doi: [10.1038/s41534-019-0209-0](https://doi.org/10.1038/s41534-019-0209-0).
- 729 A. Erhard *et al.*, “Characterizing large-scale quantum computers via cycle benchmarking,” *Nat. Commun.*, vol. 10, no. 1, Art. no. 5347, Nov. 2019, doi: [10.1038/s41467-019-13068-7](https://doi.org/10.1038/s41467-019-13068-7).
- 730 J. R. Wootton, “Benchmarking near-term devices with quantum error correction,” *Quantum Sci. Technol.*, vol. 5, no. 4, p. 044004, Aug. 2020, doi: [10.1088/2058-9565/aba038](https://doi.org/10.1088/2058-9565/aba038).
- 731 P7131 - Standard for Quantum Computing Performance Metrics & Performance Benchmarking, <https://standards.ieee.org/project/7131.html>.

- 
- 732 R. Kueng, D. M. Long, A. C. Doherty, and S. T. Flammia, “Comparing experiments to the fault-tolerance threshold,” *Phys. Rev. Lett.*, vol. 117, no. 17, p. Art. no. 170502, Oct. 2016, doi: [10.1103/PhysRevLett.117.170502](https://doi.org/10.1103/PhysRevLett.117.170502).
- 733 S. Mavadia *et al.*, “Experimental quantum verification in the presence of temporally correlated noise,” *npj Quantum Inf.*, vol. 4, no. 1, p. Art. no. 7, Feb. 2018, doi: [10.1038/s41534-017-0052-0](https://doi.org/10.1038/s41534-017-0052-0).
- 734 T. Brecht *et al.*, “Multilayer microwave integrated quantum circuits for scalable quantum computing,” *npj Quantum Information*, vol. 2, p. 16002, Feb. 2016, doi: [10.1038/npjqi.2016.2](https://doi.org/10.1038/npjqi.2016.2).